1-1-2012

Tunable Acellular Hyaluronic Acid Hydrogel Systems to Attenuate Left Ventricular Remodeling

Elena Tous
University of Pennsylvania, etous@seas.upenn.edu

Tunable Acellular Hyaluronic Acid Hydrogel Systems to Attenuate Left Ventricular Remodeling

Abstract
Following myocardial infarction (MI), left ventricular (LV) remodeling initiates a series of maladaptive events that may induce heart failure (HF). The use of injectable biomaterials is an attractive approach to attenuate negative remodeling; however, optimal properties for these systems have not been identified. The general hypothesis is that the properties of injectable hydrogels control the magnitude and duration of stabilization in the weakened myocardium and the ability to attenuate LV remodeling. To test this hypothesis, three specific aims were developed.

Increased stress due to geometric alterations is thought to exacerbate LV remodeling, causing infarct expansion. Aim 1 utilized methacrylated hyaluronic acid (MeHA) hydrogels to demonstrate ex vivo that macromer modification and oxidation-reduction (redox) initiator concentrations influence the mechanical properties of hydrogel/myocardium composites and their distribution in tissue. Experimental data incorporation into a finite element model of the dilated LV validated previous in vivo geometric outcomes and generally demonstrated the largest stress reduction with higher mechanics and larger volumes.

Aims 2 and 3 evaluated the influence of temporal mechanical support on LV remodeling in an in vivo MI model. Hydroxyethyl methacrylate groups were coupled to HA to produce hydrolytically degradable hydrogels (HeMA-HA) polymerized via redox reactions. In Aim 2, hydrogel gelation, mechanics, and degradation properties were varied by altering HeMA modification to yield low and high HeMA-HA with similar gelation and initial mechanics but accelerated degradation kinetics compared to previously studied low and high MeHA. High HeMA-HA was more effective than low HeMA-HA treatment in limiting remodeling; however, high HeMA-HA only limited LV dilation for 2 weeks, while its high MeHA counterpart sustained support up to 8 weeks. In Aim 3, a hydrogel/microsphere composite system was evaluated as an alternative approach to enhance temporal support via collagen bulking through controlled macrophage responses. The composite treatment increased myocardial thickness and decreased chamber volumes compared to hydrogel alone.

This work demonstrates the significance of the magnitude and duration of mechanical support in attenuating LV remodeling and provides insight on optimal material properties for injectable biomaterials to develop better therapies to prevent HF.

Degree Type
Dissertation

Degree Name
Doctor of Philosophy (PhD)

Graduate Group
Bioengineering

TUNABLE ACELLULAR HYALURONIC ACID HYDROGEL SYSTEMS TO ATTENUATE LEFT VENTRICULAR REMODELING

Elena Tous

A DISSERTATION

in

Bioengineering

Presented to the Faculties of the University of Pennsylvania

in

Partial Fulfillment of the Requirements for the

Degree of Doctor of Philosophy

2012

_____
Supervisor of Dissertation
Dr. Jason A. Burdick, Associate Professor of Bioengineering

_____
Graduate Group Chairperson
Dr. Beth A. Winkelstein, Professor of Bioengineering

Dissertation Committee
Dr. Robert L. Mauck (Chair), Associate Professor of Orthopaedic Surgery
Dr. Robert C. Gorman, Professor of Surgery
Dr. Daeyeon Lee, Assistant Professor of Chemical and Biomolecular Engineering

TUNABLE ACELLULAR HYALURONIC ACID HYDROGEL SYSTEMS TO ATTENUATE LEFT VENTRICULAR REMODELING

This dissertation is dedicated to my parents,

Guillermo and Lourdes Tous.

ACKNOWLEDGEMENTS

There are several people that deserve to be acknowledged for their help and support in completing this dissertation. Foremost, a special thank you to my advisor, Dr. Jason Burdick. I am grateful that Jason offered me a position in his laboratory and provided me with the opportunity and insight to perform research that I enjoyed. Over the past four years, I have learned so much from him, and have grown as a researcher and a professional under his guidance. I would also like to thank all of my committee members who took the time to provide me with the guidance needed to complete this work. They include Dr. Rob Mauck who was my chair, Dr. Daeyeon Lee who was also a collaborator and took the time (with his laboratory) to assist me in microsphere fabrication, and Dr. Rob Gorman who collaborated with us in the *in vivo* ovine work and provided a noteworthy clinical perspective. I also greatly appreciate the help of the surgeons in the Gorman Laboratory who worked long hours to perform all of the necessary surgeries. Additionally, Dr. Kenneth Margulies has been a valuable mentor throughout my graduate career. Finally, I am also thankful for my funding sources.

I am also grateful for the support of my other collaborators. This includes Dr. Jonathan Wenk who was a valuable resource in providing insight on finite element modeling and who performed all of the simulations in this dissertation, and Dr. Dawn Elliott's laboratory, especially Spencer Szczesny, who assisted me with biaxial testing.

I like to think that a better final product is produced when one enjoys her/his work environment, which is exemplified by the Burdick Laboratory. I would like to thank (past and present) members for being supportive throughout my graduate career and for making my time here so enjoyable. I would especially like to thank my good friends and

colleagues Dr. Jamie Ifkovits and Dr. Sudhir Khetan for being particularly helpful in providing me with input throughout my work. Additionally, I appreciate Heather Weber's assistance with the macrophage staining and analysis. In general, I am thankful for all of my friends for helping me balance all of the hard work with a lot of fun, and for making my graduate years a time I will always cherish.

I would next like to thank my family. I have dedicated this thesis to my mom and dad who have been the best role models for the past 27 years. Thank you for your hard work and for providing me with the opportunity to pursue all of my academic goals. Without your love and support I would not be as successful as I have been. You are both the smartest and strongest people that I know and true inspirations in my life. I would next like to thank my siblings, Nacho and Cristina, whom, despite being younger, I look up to (both figuratively and literally). Nachy for being not only a brother, but also a best friend; thanks for providing me with "life advice" and also fun memories. Cristina for always being positive and energetic; you always put a smile on my face and I cannot wait to see all of the great things you will accomplish.

Last but not least, I would like to thank another individual who has been a true inspiration to me: my fiancé and best friend, Derek. Derek has been tremendous in motivating me throughout my academic journey and particularly, while at the University of Pennsylvania. Thank you for listening and for always providing encouragement, and for even assisting me to troubleshoot! More importantly, thank you for making my time in graduate school so memorable; I do not know what I would have done without you.

ABSTRACT

TUNABLE ACELLULAR HYALURONIC ACID HYDROGEL SYSTEMS TO ATTENUATE LEFT VENTRICULAR REMODELING

Elena Tous

Jason A. Burdick, Ph.D.

Following myocardial infarction (MI), left ventricular (LV) remodeling initiates a series of maladaptive events that may induce heart failure (HF). The use of injectable biomaterials is an attractive approach to attenuate negative remodeling; however, optimal properties for these systems have not been identified. The general hypothesis is that the properties of injectable hydrogels control the magnitude and duration of stabilization in the weakened myocardium and the ability to attenuate LV remodeling. To test this hypothesis, three specific aims were developed.

Increased stress due to geometric alterations is thought to exacerbate LV remodeling, causing infarct expansion. Aim 1 utilized methacrylated hyaluronic acid (MeHA) hydrogels to demonstrate *ex vivo* that macromer modification and oxidation-reduction (redox) initiator concentrations influence the mechanical properties of hydrogel/myocardium composites and their distribution in tissue. Experimental data incorporation into a finite element model of the dilated LV validated previous *in vivo* geometric outcomes and generally demonstrated the largest stress reduction with higher mechanics and larger volumes.

Aims 2 and 3 evaluated the influence of temporal mechanical support on LV remodeling in an *in vivo* MI model. Hydroxyethyl methacrylate groups were coupled to HA to produce hydrolytically degradable hydrogels (HeMA-HA) polymerized via redox reactions. In Aim 2, hydrogel gelation, mechanics, and degradation properties were varied by altering HeMA modification to yield low and high HeMA-HA with similar gelation and initial mechanics but accelerated degradation kinetics compared to previously studied low and high MeHA. High HeMA-HA was more effective than low HeMA-HA treatment in limiting remodeling; however, high HeMA-HA only limited LV dilation for 2 weeks, while its high MeHA counterpart sustained support up to 8 weeks. In Aim 3, a hydrogel/microsphere composite system was evaluated as an alternative approach to enhance temporal support via collagen bulking through controlled macrophage responses. The composite treatment increased myocardial thickness and decreased chamber volumes compared to hydrogel alone.

This work demonstrates the significance of the magnitude and duration of mechanical support in attenuating LV remodeling and provides insight on optimal material properties for injectable biomaterials to develop better therapies to prevent HF.

TABLE OF CONTENTS

LIST OF TABLES

LIST OF FIGURES

CHAPTER 1

An Introduction to the Heart, Myocardial Infarction and Cardiac Tissue Engineering

1.1 The Heart

The heart is the muscular organ that is central to the cardiovascular system (e.g., the heart, blood vessels and blood); it serves the role of circulating oxygenated blood throughout the body by continuously beating (approximately 100,000 times daily) [1]. Due to the heart's crucial role in maintaining the body's overall physiological function, hindrance of its efficient pumping can lead to insufficient oxygenation of tissues, and in extreme cases, death. To prevent this and/or treat cardiac complications, it is important to understand the anatomy and physiology of the heart, both in healthy and diseased states; this will lead to the development of more specialized clinical treatments to better address pathological problems. To this end, this dissertation will focus on designing treatments to attenuate the negative outcomes of left ventricular (LV) remodeling after myocardial infarction (MI).

1.1.1 The Heart: Wall Structure and Function

The heart wall surrounding the outer portion of each cardiac chamber (right and left atria and ventricles) is responsible for executing contraction to facilitate transportation of oxygen and nutrients throughout the body [1, 2]. It is comprised of three tissue layers surrounded by a protective fibrous membrane (i.e., the pericardium) to prevent overextension [1]. The outermost layer is the epicardium and consists of both

connective and mesothelial tissue, the myocardium is the middle and thickest layer and is primarily made up of muscular tissue, and the inner most layer is the endocardium and is composed of endothelial tissue [1, 3]. All three layers play significant roles in maintaining the viability of the heart; however, the myocardium is the most relevant for controlling cardiac function. The myocardium is composed of two primary cell types: cardiac fibroblasts, which are responsible for producing and maintaining the cardiac extracellular matrix (ECM), and cardiomyocytes, which are the cardiac functional units and are responsible for initiating contraction [1-3].

1.1.2 The Heart: Myocardial Extracellular Matrix Structure and Function

The unique structure of the native myocardial ECM is a determining factor of its biological signaling, mechanical properties and contractile function [2, 4-6]. It is comprised of cardiomyocytes embedded in a matrix primarily composed of collagens I and III, which facilitate cell alignment and cell interconnection to form cardiac fibers to mediate contraction of the myocardium. Specifically, this fiber network allows cardiomyocytes to bear most of the wall load during systole (i.e., contraction), while collagen struts transmit force. In diastole (i.e., relaxation), as collagen fibers uncoil they resist further expansion, which prevents cardiomyocytes from overstretching [2].

On a macroscopic tissue scale, muscle fibers, oriented with their long axis, spiral around the heart, and meet at the apex in a vortex conformation (Figure 1.1) [7-9]. The distinct fiber orientation maintains the normal prolate elliptical geometry of heart, and is energy efficient in cardiac function, allowing for uniform stress and strain distributions throughout the heart [7-9]. This suggests that ECM structures both on micro (e.g., cellular/collagen fibril) and macro (e.g., tissue/fiber spiral) levels are essential to maintain

normal heart function. This will be discussed in more detail regarding myocardial injury in Section 1.2.

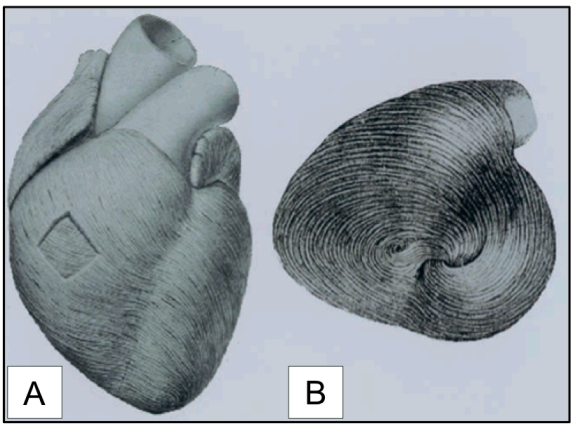

Figure 1.1 Muscle fiber spiral network of the heart (A) and apical view of the apical vortex (B). Adapted from Buckberg [7].

1.1.3 The Heart: Coronary Vessels

The myocardial wall, like any other living tissue, requires nutrients and oxygen to properly function. As blood enters the heart chambers during contraction, it is unable to diffuse efficiently through the endocardium to the cells in the myocardium. To compensate, the heart has its own vessel circuit (the coronary vessels), which feeds off the primary circulation system. Specifically, the coronary arteries branch from the aorta and the coronary veins empty into the right atrium [1]. Given that these vessels are crucial for delivery of nutrients and oxygen to the cardiomyocytes of the myocardium, their obstruction can have negative repercussions including cell necrosis, ECM disruption, and function (as discussed further below) [3, 4, 7, 10-13].

1.2 Cardiac Complications: Myocardial Infarction (MI)

Approximately 6 million Americans suffer from heart failure (HF); ~70% of these cases are associated with coronary artery disease (CAD), which causes MI [14, 15]. It is estimated that these numbers will increase with time with approximately 600,000 Americans suffering their first MI and ~300,000 others having a recurrent attack within the next year [15]. In general, MI triggers LV remodeling which involves a series of maladaptive events that alter the ECM structure of the myocardium and consequently the geometry of the heart, changing it from a prolate elliptical shape to a spherical (i.e., dilated) geometry (Figure 1.2) that is unable to recapitulate the function of the normal myocardium [3, 4, 10-13, 16, 17]. These changes, particularly geometric alterations, eventually may lead to significantly compromised function and HF [16]. This will be discussed in greater detail in the next section.

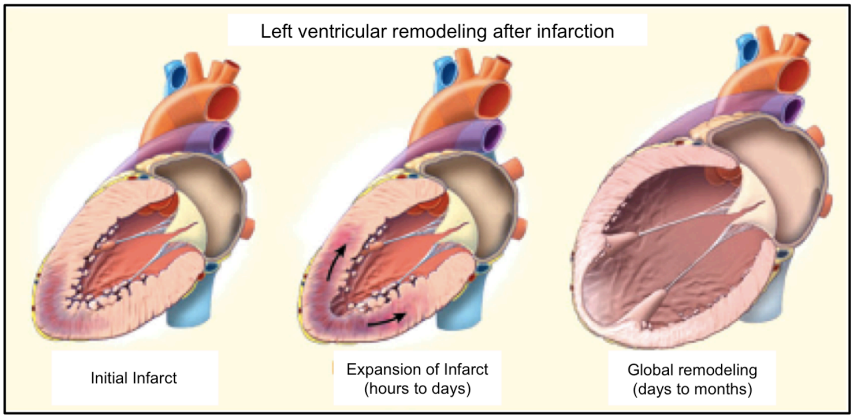

Figure 1.2 Schematic illustrating infarct expansion and geometric alterations that occur during LV remodeling. Adapted from Jessup et al. [17].

1.2.1 Left Ventricular (LV) Remodeling: Micro-Scale Alterations

MI occurs following the occlusion of a coronary vessel, which leads to the depletion of oxygen and nutrients to the myocardial tissue, cardiomyocyte necrosis and initiation of LV remodeling [3, 4, 10-13, 16]. LV remodeling is a dynamic process that involves both biological and mechanical changes and can be broken down into three main phases: 1) acute ischemia and necrosis, typically during the first week post-MI, 2) fibrosis generally ensuing the following 3 weeks, and 3) remodeling which can progress for months [16].

Generally, the first stage of remodeling (i.e., acute ischemia and necrosis) begins immediately after the onset of MI and is typically when the most dramatic alterations in the ECM composition occur [4, 10, 11, 16]. Cardiomyocyte necrosis initiates an inflammatory reaction in which cells infiltrate the infarct region to remove necrotic cardiomyocytes and debris and latent matrix metalloproteinases (MMPs) are activated [4, 10, 11, 16, 18]. MMP activation has been detected as early as 10 minutes post-MI (porcine model) [19] and results in an imbalance between MMPs and tissue inhibitors of metalloproteinases (TIMPs) (Figure 1.3). This imbalance precipitates a break down of ECM proteins, including the collagen network responsible for structural support of the aligned cardiomyocytes [4]. As will be discussed in more detail in Chapter 6, fragmentation of cardiac ECM proteins is not limited to collagen and also includes glycosaminoglycans such as hyaluronic acid (HA), which can facilitate the wound healing events that occur during this phase of remodeling [10, 11]. As the collagen network is disrupted, the cardiomyocytes that were embedded within slip out; ECM disruption and loss of cardiomyocytes weakens the myocardial wall and renders it susceptible to global geometric changes including chamber dilation and wall thinning.

These changes can then lead to expansion of the infarct, increased global stress, and ultimately HF, which will be discussed in more detail in Section 1.2.2 [3, 16, 20-22].

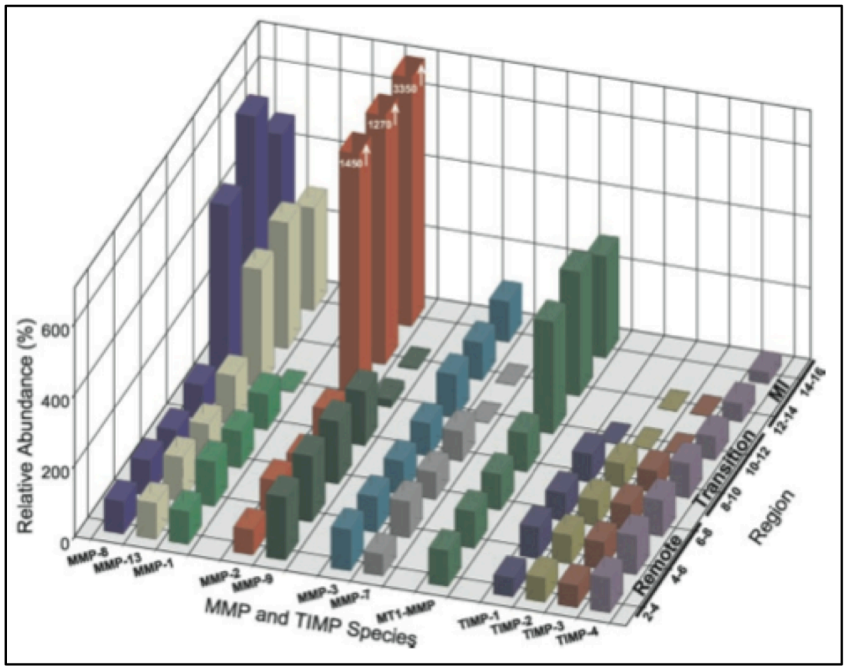

Figure 1.3 An imbalance of MMPs and TIMPs is present 8 weeks post-MI [18].

The fibrosis and remodeling stages comprise primarily the production and remodeling of collagen to counteract the break down that occurs in the initial phase. Fibrosis begins approximately 1 week after MI when the infarcted tissue is infiltrated by fibroblasts and myofibroblasts (i.e., differentiated fibroblasts that can also contract the scar) that initiate collagen production in an attempt to recover wall stability [4, 10, 11, 16]. Collagen deposition and stiffness of the infarct region increase in parallel during this period [16, 23]. Remodeling begins ~4 weeks after MI and involves the remodeling and crosslinking of collagen produced during fibrosis to generate a mature scare [4, 10, 11, 16]. There is no defined “end point” to this process as the “healing scar” is dynamic;

however, studies suggest that by this point a thin non-functional scar has replaced the once contractile healthy thick myocardium [4, 10, 11].

1.2.2 LV Remodeling: Macro-Scale Alterations

In addition to causing destructive alteration of the myocardial ECM at the micro/cellular scale, the disruption of the native ECM, as briefly discussed above, initiates global changes, including alterations in ventricular geometry and systolic and diastolic function [4, 7-11]. When the distinct fiber spiral that ensures a prolated elliptical geometry in the normal heart is disrupted, thinning of the myocardial wall into a spherical (dilated) geometry can occur, causing increased global stress and inefficient function [7, 20-22]. Geometric changes may decrease normal ejection fraction (EF) by 50% [7]. Additionally, contractile deficiencies caused by collagen scarring force the adjacent borderzone (BZ) region to compensate by increasing its workload, which can induce cardiomyocytes to hypertrophy, stretch and decrease their contractile function [16, 24, 25]. To counteract this, BZ expansion may ensue, causing the mechanical burden to extend to remote healthy regions of the heart [16, 24-26]. This process can propagate a positive feed back loop and result in further infarct expansion, geometric alterations, and increased stress until the onset of HF and heart function is severely compromised.

1.3 Current Treatments for MI

Current clinical treatments for MI are limited to either pharmacological interventions and/or invasive surgical approaches. Pharmacological approaches generally aim to either restore blood flow to the ischemic tissue (e.g., blood thinners, fibrinolytic drugs) or reduce the stress on the heart by decreasing blood pressure and/or heart rate (e.g., ACE inhibitors, beta blockers) [27, 28]. Surgical procedures, in cases

where the heart can still function, include bypass surgery and stent implantation to restore blood flow [29, 30]. In cases of end stage heart failure, cardiac transplantation still remains the gold-standard [31]. Due to a limited supply of donor hearts, left/ right ventricular assist devices can also be implanted to improve function of the failing left or right ventricle; however, their implantation is costly and requires an invasive implantation procedure [32, 33]. Most of these interventions fail to directly treat the altered structural state of the damaged myocardium; specifically, they do not replace the lost cardiomyocytes nor do they stabilize the weakened myocardial wall, both of which could assist in restoring cardiac function. Whole heart transplantation, the only one of the described interventions that does achieve these goals, suffers from the extremely limited donor supply, the need for invasive surgery, and life-long immunosuppressive therapy.

1.4 Tissue Engineering Approaches for LV Remodeling

Recent advances in tissue engineering (TE) are attempting to design better treatments to target specific aspects of damaged myocardium post-MI. There are two main TE approaches to treat MI: (1) cellular approaches that aim to replace the non-contractile scar with contractile tissue and (2) acellular mechanical strategies, which aim to stabilize the wall to limit the destructive geometric changes that ensue during remodeling.

1.4.1 Tissue Engineering: Cellular Strategies

Cardiomyocytes lack a regenerative capacity; this becomes a concern in MI when approximately 1 billion cardiomyocytes (~20% of cardiomyocytes in the myocardium) are lost, contributing to loss of contractile function [1, 34]. To address this, groups have aimed to restore contractility of the infarct region by delivering cells to

impart this function [3, 34, 35]. Endogenous cells have been homed to the injured myocardium via delivery of growth factors such as stromal derived growth factor (SDF-α) [36, 37]. Furthermore, a number of cell types including somatic cells (e.g., cardiomyocytes and skeletal cells) and stem cells (e.g., bone marrow-derived mesenchymal stem cells, hematopoietic stem cells, adipose-derived stem cells, embryonic stem cells) have been delivered via direct injection, seeding upon/within implanted scaffolds, and/or cellular grafts to restore cardiac function [34, 35, 38-51]. While some improvements (e.g., remodeling and/or function) have been observed with cellular approaches, it is unclear whether the source of improvement is due to the direct/intended activity of the delivered cells. Reports have suggested that cells may form a passive graft or induce paracrine signaling, leading to indirect cardiac benefits [52, 53]. Cellular approaches are also limited in that most studies report low viability, retention and engraftment of injected cells [3, 34, 35]. Although advances are being made to better address engraftment issues, overarching concerns of cellular therapies are the timing of their delivery, cell "dosage", and cell source. No phase of remodeling provides an ideal environment for cell survival due to high inflammation and limited vasculature. Additionally, regeneration takes time and several maladaptive changes that predispose the heart to HF occur early on in remodeling. To circumvent these limitations recent efforts have focused on developing acellular approaches to mechanically stabilize the disrupted injured myocardium to limit maladaptive geometric remodeling that occur post-MI.

It should be noted that cell approaches are not limited to direct delivery of cardiomyocytes and stem cells. Less direct approaches have also been investigated to restore blood flow to the infarct through growth factor delivery (e.g., vascular endothelial growth factor, VEGF, and platelet derived growth factor, PDGF) and cell delivery (e.g.,

fibroblasts and endothelial cells) and with the delivery of cardioprotective cytokines to decrease cell apoptosis (e.g., insulin-like growth factor, IGF-1) [45, 54-57]. These approaches, however, are subject to the same general limitations as current clinical treatments and the aforementioned cellular studies.

1.4.2 Tissue Engineering: Mechanical Strategies

Mechanical approaches to attenuate LV remodeling have recently gained interest because they do not focus on regeneration, which as described is limited in the infarct region. Instead they focus on providing mechanical stability to the weakened tissue to prevent geometric alterations and limit increases in stress immediately following MI, which are thought to be the primary cause of pathological processes that result in HF. Non-conventional approaches to achieve normal myocardial geometry include surgical procedures such as partial left ventriculectomy (the Batista procedure), which reconstructs the dilated ventricle into a more elliptical shape that better represents a healthy heart [58]. Data from FE modeling has demonstrated that removal of even dysfunctional myocardium is detrimental to heart function; in addition, the procedure is invasive and will probably not be performed in the United States again [59]. Polymeric restraints have also been designed for direct placement around (Figure 1.4A) or anchoring to a portion (Figure 1.4B) of the heart to physically prevent dilation (Figure 1.4C-E) by mechanically stabilizing and forcing it to maintain its original shape. Polypropylene Marlex [60, 61] and polyester Dacron (e.g., CorCap cardiac support device (CSD)) [62, 63] restraints have been employed in *in vivo* ovine MI models and were effective in limiting geometric changes. Furthermore, clinical trials of patients with HF demonstrated that treatment with the nitinol Paracor Medical Heart Net ventricular support system limited remodeling [64]; more recently, five-year follow up results from

the CorCap CSD “Acorn clinical trial” also showed that patients with HF treatment with the Corcap had decreased ventricle chamber dilation [65]. While restraint implementation has improved with time, they generally require an invasive surgery, which is particularly not ideal for older patients.

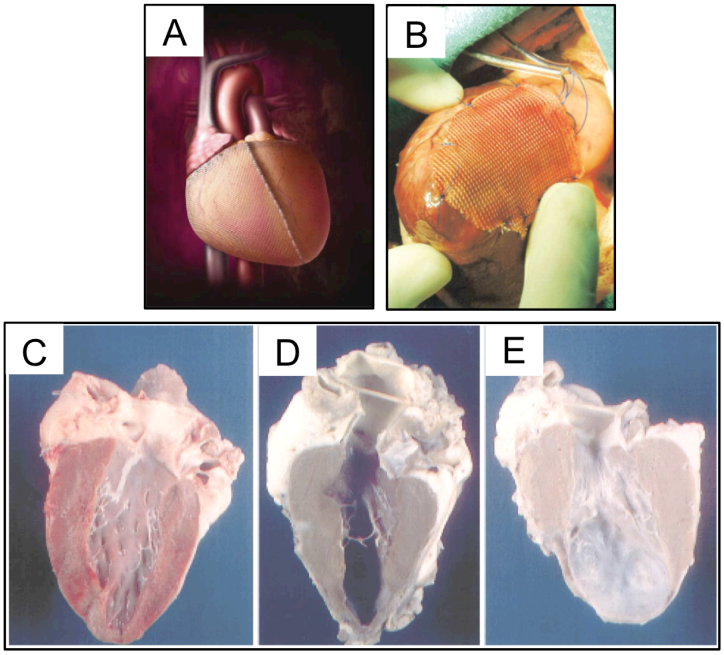

Figure 1.4 Corcap CSD restraint wrapped around modeled heart (A) [63]. Marlex patch placed over infarct region in ovine heart (B) [61]. Normal ovine heart (C), Marlex-treated infarcted heart (D), and control infarcted heart (E) [60]. Images adapted from their respective reference.

1.5 Summary

Motivated by the aforementioned studies, injectable biomaterials have recently become a more appealing TE treatment to attenuate LV remodeling via myocardial wall stabilization; their injectable nature allows for non-invasive delivery, potentially via

catheter. A variety of natural and synthetic hydrogels have been investigated to provide mechanical stability to the myocardium post-MI; a comprehensive review of these techniques can be found in Chapter 3 [66]. While several materials have been studied, there remains a lack of understanding of the mechanism involved in their success in limiting remodeling. As discussed, myocardial function is dependent on the physical properties of the myocardium, which are altered during dynamic remodeling; local changes to the ECM may lead to increased susceptibility of the myocardium to global geometric changes (e.g., dilation and thinning of the myocardial wall) making it difficult to maintain normal function. It is important to consider the alterations that occur throughout the progression of remodeling when engineering a treatment including: 1) the degree of mechanical support needed and 2) the duration of treatment to limit maladaptive alterations. This dissertation will focus on material design to fulfill these requirements by designing novel hydrogel systems with tunable mechanical and degradation properties, and investigating their efficacy in attenuating LV remodeling toward the prevention of maladaptive changes and HF following MI.

References:

[1] Tortora GJ ,Grabowski SR. The cardiovascular system: the heart. In: Roesch B, editor. Principles of Anatatomy and Physiology. Hoboken: John Wiley & Sons, Inc, 2003. p.659.

[2] Fomovsky GM, Thomopoulos S, Holmes JW. Contribution of extracellular matrix to the mechanical properties of the heart. J Mol Cell Cardiol 2010;48:490.

[3] Mukherjee S VJ, Ravichandran R, Ramakrishna S, Raghunath M. Multimodal biomaterial strategies for regeneration of infarcted myocardium. J Mater Chem 2010;20:8819.

[4] Cleutjens JP, Creemers EE. Integration of concepts: cardiac extracellular matrix remodeling after myocardial infarction. J Card Fail 2002;8:S344.

[5] Hein S, Schaper J. The extracellular matrix in normal and diseased myocardium. J Nucl Cardiol 2001;8:188.

[6] Ju H, Dixon IM. Extracellular matrix and cardiovascular diseases. Can J Cardiol 1996;12:1259.

[7] Buckberg GD. Basic science review: the helix and the heart. J Thorac Cardiovasc Surg 2002;124:863.

[8] Sengupta PP, Korinek J, Belohlavek M, Narula J, Vannan MA, Jahangir A, Khandheria BK. Left ventricular structure and function: basic science for cardiac imaging. J Am Coll Cardiol 2006;48:1988.

[9] Coghlan C, Hoffman J. Leonardo da vinci's flights of the mind must continue: cardiac architecture and the fundamental relation of form and function revisited. Eur J Cardiothorac Surg 2006;29S:S4.

[10] Dobaczewski M, Bujak M, Zymek P, Ren G, Entman ML, Frangogiannis NG. Extracellular matrix remodeling in canine and mouse myocardial infarcts. Cell Tissue Res 2006;324:475.

[11] Dobaczewski M, Gonzalez-Quesada C, Frangogiannis NG. The extracellular matrix as a modulator of the inflammatory and reparative response following myocardial infarction. J Mol Cell Cardiol 2010;48:504.

[12] Sun Y, Kiani MF, Postlethwaite AE, Weber KT. Infarct scar as living tissue. Basic Res Cardiol 2002;97:343.

[13] Sun Y, Weber KT. Infarct scar: a dynamic tissue. Cardiovasc Res 2000;46:250.

[14] Lloyd-Jones D, Adams RJ, Brown TM, Carnethon M, Dai S, De Simone G, Ferguson TB, Ford E, Furie K, Gillespie C, Go A, Greenlund K, Haase N, Hailpern S, Ho PM, Howard V, Kissela B, Kittner S, Lackland D, Lisabeth L, Marelli A, McDermott MM, Meigs J, Mozaffarian D, Mussolino M, Nichol G, Roger VL, Rosamond W, Sacco R, Sorlie P, Thom T, Wasserthiel-Smoller S, Wong ND, Wylie-Rosett J. Heart disease and stroke statistics--2010 update: a report from the american heart association. Circulation 2010;121:e46.

[15] Roger VL, Go AS, Lloyd-Jones DM, Adams RJ, Berry JD, Brown TM, Carnethon MR, Dai S, de Simone G, Ford ES, Fox CS, Fullerton HJ, Gillespie C, Greenlund KJ, Hailpern SM, Heit JA, Ho PM, Howard VJ, Kissela BM, Kittner SJ, Lackland DT, Lichtman JH, Lisabeth LD, Makuc DM, Marcus GM, Marelli A, Matchar DB, McDermott MM, Meigs JB, Moy CS, Mozaffarian D, Mussolino ME, Nichol G, Paynter NP, Rosamond WD, Sorlie PD, Stafford RS, Turan TN, Turner MB, Wong ND, Wylie-Rosett J. Heart disease and stroke statistics--2011 update: a report from the american heart association. Circulation 2011;123:e18.

[16] Holmes JW, Borg TK, Covell JW. Structure and mechanics of healing myocardial infarcts. Annu Rev Biomed Eng 2005;7:223.

[17] Jessup M, Brozena S. Heart failure. N Engl J Med 2003;348:2007.

[18] Wilson EM, Moainie SL, Baskin JM, Lowry AS, Deschamps AM, Mukherjee R, Guy TS, St John-Sutton MG, Gorman JH, 3rd, Edmunds LH, Jr., Gorman RC, Spinale FG. Region and type specific induction of matrix metalloproteinases in post-myocardial infarction remodeling. Circulation 2003;107:2857.

[19] Etoh T, Joffs C, Deschamps AM, Davis J, Dowdy K, Hendrick J, Baicu S, Mukherjee R, Manhaini M, Spinale FG. Myocardial and interstitial matrix metalloproteinase activity after acute myocardial infarction in pigs. Am J Physiol Heart Circ Physiol 2001;281:H987.

[20] Guccione JM, Costa KD, McCulloch AD. Finite element stress analysis of left ventricular mechanics in the beating dog heart. J Biomech 1995;28:1167.

[21] Wall ST, Walker JC, Healy KE, Ratcliffe MB, Guccione JM. Theoretical impact of the injection of material into the myocardium: a finite element model simulation. Circulation 2006;114:2627.

[22] Wenk JF, Wall ST, Peterson RC, Helgerson SL, Sabbah HN, Burger M, Stander N, Ratcliffe MB, Guccione JM. A method for automatically optimizing medical devices for treating heart failure: designing polymeric injection patterns. J Biomech Eng 2009;131:121011.

[23] Gupta KB, Ratcliffe MB, Fallert MA, Edmunds LH, Jr., Bogen DK. Changes in passive mechanical stiffness of myocardial tissue with aneurysm formation. Circulation 1994;89:2315.

[24] Ratcliffe MB. Non-ischemic infarct extension: a new type of infarct enlargement and a potential therapeutic target. J Am Coll Cardiol 2002;40:1168.

[25] Jackson BM, Gorman JH, 3rd, Salgo IS, Moainie SL, Plappert T, St John-Sutton M, Edmunds LH, Jr., Gorman RC. Border zone geometry increases wall stress after myocardial infarction: contrast echocardiographic assessment. Am J Physiol Heart Circ Physiol 2003;284:H475.

[26] Walker JC, Ratcliffe MB, Zhang P, Wallace AW, Hsu EW, Saloner DA, Guccione JM. Magnetic resonance imaging-based finite element stress analysis after linear repair of left ventricular aneurysm. J Thorac Cardiovasc Surg 2008;135:1094.

[27] Flather MD, Yusuf S, Kober L, Pfeffer M, Hall A, Murray G, Torp-Pedersen C, Ball S, Pogue J, Moye L, Braunwald E. Long-term ACE-inhibitor therapy in patients with heart failure or left-ventricular dysfunction: a systematic overview of data from individual patients. ACE-inhibitor myocardial infarction collaborative group. Lancet 2000;355:1575.

[28] van Zwieten PA. Current and newer approaches in the drug treatment of congestive heart failure. Cardiovasc Drugs Ther 1997;10:693.

[29] Hannan EL, Racz MJ, McCallister BD, Ryan TJ, Arani DT, Isom OW, Jones RH. A comparison of three-year survival after coronary artery bypass graft surgery and percutaneous transluminal coronary angioplasty. J Am Coll Cardiol 1999;33:63.

[30] Hannan EL, Racz MJ, Walford G, Jones RH, Ryan TJ, Bennett E, Culliford AT, Isom OW, Gold JP, Rose EA. Long-term outcomes of coronary-artery bypass grafting versus stent implantation. N Engl J Med 2005;352:2174.

[31] John R, Rajasinghe HA, Chen JM, Weinberg AD, Sinha P, Mancini DM, Naka Y, Oz MC, Smith CR, Rose EA, Edwards NM. Long-term outcomes after cardiac transplantation: an experience based on different eras of immunosuppressive therapy. Ann Thorac Surg 2001;72:440.

[32] Goldstein DJ, Oz MC, Rose EA. Implantable left ventricular assist devices. N Engl J Med 1998;339:1522.

[33] Padera RF, Jr., Schoen FJ. Cardiovascular medical devices. In: Ratner BD, Hoffman AS, Schoen FJ, Lemons JE, editor. Biomaterials Science, vol. 2. San Diego: Elsevier Academic Press, 2004. p.471.

[34] Zimmermann WH, Didie M, Doker S, Melnychenko I, Naito H, Rogge C, Tiburcy M, Eschenhagen T. Heart muscle engineering: an update on cardiac muscle replacement therapy. Cardiovasc Res 2006;71:419.

[35] Segers VF, Lee RT. Stem-cell therapy for cardiac disease. Nature 2008;451:937.

[36] Zhang G, Nakamura Y, Wang X, Hu Q, Suggs LJ, Zhang J. Controlled release of stromal cell-derived factor-1 alpha in situ increases c-kit+ cell homing to the infarcted heart. Tissue Eng 2007;13:2063.

[37] Abbott JD HY, Hickey R, Krasue DS, Gioedano FJ. Stromal cell-derived factor-1alpha plays a critical role in stem cell recruitment to the heart after myocardial infarction but is not sufficient to induce homing in the absence of injury. Circulation 2004;21:3300.

[38] Muller-Ehmsen J, Peterson KL, Kedes L, Whittaker P, Dow JS, Long TI, Laird PW, Kloner RA. Rebuilding a damaged heart: long-term survival of transplanted neonatal rat cardiomyocytes after myocardial infarction and effect on cardiac function. Circulation 2002;105:1720.

[39] Hagege AA, Marolleau JP, Vilquin JT, Alheritiere A, Peyrard S, Duboc D, Abergel E, Messas E, Mousseaux E, Schwartz K, Desnos M, Menasche P. Skeletal myoblast transplantation in ischemic heart failure: long-term follow-up of the first phase I cohort of patients. Circulation 2006;114:I108.

[40] Christman KL, Vardanian AJ, Fang Q, Sievers RE, Fok HH, Lee RJ. Injectable fibrin scaffold improves cell transplant survival, reduces infarct expansion, and induces neovasculature formation in ischemic myocardium. J Am Coll Cardiol 2004;44:654.

[41] Christman KL, Fok HH, Sievers RE, Fang Q, Lee RJ. Fibrin glue alone and skeletal myoblasts in a fibrin scaffold preserve cardiac function after myocardial infarction. Tissue Eng 2004;10:403.

[42] Jing D, Parikh A, Tzanakakis ES. Cardiac cell generation from encapsulated embryonic stem cells in static and scalable culture systems. Cell Transplant 2010;19:1397.

[43] Jing D, Parikh A, Canty JM, Jr., Tzanakakis ES. Stem cells for heart cell therapies. Tissue Eng Part B Rev 2008;14:393.

[44] Kawamoto A, Asahara T, Losordo DW. Transplantation of endothelial progenitor cells for therapeutic neovascularization. Cardiovasc Radiat Med 2002;3:221.

[45] Kawamoto A, Gwon HC, Iwaguro H, Yamaguchi JI, Uchida S, Masuda H, Silver M, Ma H, Kearney M, Isner JM, Asahara T. Therapeutic potential of ex vivo expanded endothelial progenitor cells for myocardial ischemia. Circulation 2001;103:634.

[46] Wang L DJ, Tian W, Xiang, B, Yang, T, Li G, Gruwel M, Kashour T, Rendell J, Glogowski M, Tomanek B, Freed D, Deslaurieres R, Arora RC, Tian G. Adipose-derived stem cells are an effective cell candidate for treatment of heart failure: an MR imaging study of rat hearts. Am J Physiol Heart Circ Physiol 2009;297:H1020.

[47] Balsam LB, Wagers AJ, Christensen JL, Kofidis T, Weissman IL, Robbins RC. Haematopoietic stem cells adopt mature haematopoietic fates in ischaemic myocardium. Nature 2004;428:668.

[48] Laflamme MA, Gold J, Xu C, Hassanipour M, Rosler E, Police S, Muskheli V, Murry CE. Formation of human myocardium in the rat heart from human embryonic stem cells. Am J Pathol 2005;167:663.

[49] Hodgson DM, Behfar A, Zingman LV, Kane GC, Perez-Terzic C, Alekseev AE, Puceat M, Terzic A. Stable benefit of embryonic stem cell therapy in myocardial infarction. Am J Physiol Heart Circ Physiol 2004;287:H471.

[50] Memon IA, Sawa Y, Fukushima N, Matsumiya G, Miyagawa S, Taketani S, Sakakida SK, Kondoh H, Aleshin AN, Shimizu T, Okano T, Matsuda H. Repair of impaired myocardium by means of implantation of engineered autologous myoblast sheets. J Thorac Cardiovasc Surg 2005;130:1333.

[51] Miyahara Y, Nagaya N, Kataoka M, Yanagawa B, Tanaka K, Hao H, Ishino K, Ishida H, Shimizu T, Kangawa K, Sano S, Okano T, Kitamura S, Mori H. Monolayered mesenchymal stem cells repair scarred myocardium after myocardial infarction. Nat Med 2006;12:459.

[52] Leri A, Kajstura J, Anversa P. Cardiac stem cells and mechanisms of myocardial regeneration. Physiol Rev 2005;85:1373.

[53] Passier R, van Laake LW, Mummery CL. Stem-cell-based therapy and lessons from the heart. Nature 2008;453:322.

[54] Davis ME, Hsieh PC, Takahashi T, Song Q, Zhang S, Kamm RD, Grodzinsky AJ, Anversa P, Lee RT. Local myocardial insulin-like growth factor 1 (IGF-1) delivery with biotinylated peptide nanofibers improves cell therapy for myocardial infarction. Proc Natl Acad Sci U S A 2006;103:8155.

[55] Kellar RS, Shepherd BR, Larson DF, Naughton GK, Williams SK. Cardiac patch constructed from human fibroblasts attenuates reduction in cardiac function after acute infarct. Tissue Eng 2005;11:1678.

[56] Maulik N, Thirunavukkarasu M. Growth factors and cell therapy in myocardial regeneration. J Mol Cell Cardiol 2008;44:219.

[57] Kinnaird T, Stabile E, Epstein SE, Fuchs S. Current perspectives in therapeutic myocardial angiogenesis. J Interv Cardiol 2003;16:289.

[58] Batista R. Partial left ventriculectomy--the Batista procedure. Eur J Cardiothorac Surg 1999;15 Suppl 1:S12.

[59] Ratcliffe MB, Hong J, Salahieh A, Ruch S, Wallace AW. The effect of ventricular volume reduction surgery in the dilated, poorly contractile left ventricle: a simple finite element analysis. J Thorac Cardiovasc Surg 1998;116:566.

[60] Kelley ST, Malekan R, Gorman JH, 3rd, Jackson BM, Gorman RC, Suzuki Y, Plappert T, Bogen DK, Sutton MG, Edmunds LH, Jr. Restraining infarct expansion preserves left ventricular geometry and function after acute anteroapical infarction. Circulation 1999;99:135.

[61] Moainie SL, Guy TS, Gorman JH, 3rd, Plappert T, Jackson BM, St John-Sutton MG, Edmunds LH, Jr., Gorman RC. Infarct restraint attenuates remodeling and reduces chronic ischemic mitral regurgitation after postero-lateral infarction. Ann Thorac Surg 2002;74:444.

[62] Pilla JJ, Blom AS, Brockman DJ, Ferrari VA, Yuan Q, Acker MA. Passive ventricular constraint to improve left ventricular function and mechanics in an ovine model of heart failure secondary to acute myocardial infarction. J Thorac Cardiovasc Surg 2003;126:1467.

[63] Blom AS, Pilla JJ, Gorman RC, 3rd, Gorman JH, Mukherjee R, Spinale FG, Acker MA. Infarct size reduction and attenuation of global left ventricular remodeling with the CorCap cardiac support device following acute myocardial infarction in sheep. Heart Fail Rev 2005;10:125.

[64] Klodell CT, Jr., Aranda JM, Jr., McGiffin DC, Rayburn BK, Sun B, Abraham WT, Pae WE, Jr., Boehmer JP, Klein H, Huth C. Worldwide surgical experience with the Paracor HeartNet cardiac restraint device. J Thorac Cardiovasc Surg 2008;135:188.

[65] Mann DL, Kubo SH, Sabbah HN, Starling RC, Jessup M, Oh JK, Acker MA. Beneficial effects of the CorCap cardiac support device: five-year results from the Acorn Trial. J Thorac Cardiovasc Surg 2012;143:1036.

[66] Tous E, Purcell B, Ifkovits JL, Burdick JA. Injectable acellular hydrogels for cardiac repair. J Cardiovasc Transl Res 2011;4:528.

CHAPTER 2

Research Overview

2.1 Specific Aims and Hypotheses

Heart disease continues to be the leading cause of death in the United States; approximately 82.6 million Americans suffer from cardiovascular disease with ~10% suffering from myocardial infarction (MI). MI leads to left ventricular (LV) remodeling, which involves a series of maladaptive events that can result in the onset of heart failure (HF). Geometric alterations resulting from LV remodeling, specifically myocardial wall thinning and dilation, are thought to be the root cause of exacerbated remodeling and eventual impairment of cardiac function. Despite advances in restraint technologies targeted to prevent these maladaptive changes, these approaches are invasive and have not been translated clinically.

To address this, there has been a recent focus in the development of acellular biomaterials to impart stability to the weakened myocardium with the goal of limiting geometric changes and subsequently decreasing global stress and maintaining heart function. Although a range of materials have been investigated towards this strategy, there is a lack of information on the specific material properties that lead to the best outcomes. Recently, a study was performed to independently evaluate the role of material properties in mitigating negative remodeling. Specifically, treatment with methacrylated hyaluronic acid (MeHA) hydrogels demonstrated that material mechanical properties play a critical role in stabilizing the infarcted myocardium as indicated by increased thickness, decreased ventricle dilation, and limited infarct area measurements

in an *in vivo* ovine MI model. This study initiated the work proposed and completed in this dissertation. To elaborate on these findings, the general goal of this dissertation is to further evaluate the role of material properties (including mechanics and degradation) on the efficacy of injectable agents in attenuating LV remodeling.

The *global hypothesis* encompassing the work of this dissertation is as follows: Engineered injectable hydrogels with tunable properties can provide enhanced control of both the magnitude (via tunability of material mechanics and distribution) and duration (via tunability of degradation) of stabilization in the weakened myocardium to provide insight on design criteria for targeted therapies to attenuate LV remodeling. This hypothesis will be systematically tested in the following three Specific Aims.

Specific Hypothesis 1: Stress reductions in the dilated LV are dependent on the mechanical properties and distribution of the injectable material.

Specific Aim 1: To theoretically examine different formulations of MeHA hydrogels with various mechanics and volume distributions to determine their influence on stress reduction in a finite element model of the dilated LV. Similar formulations (i.e., modification percent, initiator concentration) of MeHA hydrogels as those investigated in previous MI work will be formed via oxidation-reduction (redox) initiation reactions when injected into ovine cardiac explants to simulate *in vivo* injections and then characterized *in vitro* as hydrogel/tissue composites. Biaxial testing will be performed to assess the mechanics of each hydrogel/tissue composite formulation and magnetic resonance imaging (MRI) will be employed to examine their distribution within myocardial tissue. The mechanical and volume distribution data will be incorporated into a finite element (FE) model to assess their influence on stress in the dilated LV; previous

experimental geometric outcomes (e.g., increased thickness and decreased dilation) from MeHA treatment will be correlated to stress reduction data for validation. Similar studies will be performed with higher initiator concentrations to assess the influence of gelation on hydrogel distribution and mechanics, and consequently, on stress reduction, and will allow for relative comparisons between MeHA formulations.

Specific Hypothesis 2: The magnitude and duration of mechanical stabilization by injectable materials influences their efficacy in limiting LV remodeling.

Specific Aim 2: To synthesize and characterize hydrolytically degradable HA hydrogels and select formulations to assess the temporal role of mechanical support in attenuating LV remodeling in an *in vivo* ovine MI model. HA will be functionalized with varying amounts of the hydrolytically degradable functional group, hydroxyethyl methacrylate (HeMA), to yield HeMA-HA macromers with a range of modification efficiency. HeMA-HA hydrogels will be formed from these macromers by redox initiation and characterized for mechanics (via compressive testing), gelation (via rheometry) and hydrolytic degradation (via a uronic acid assay) to determine the tunability of material properties. Two formulations of hydrolytically degradable HeMA-HA hydrogels will be selected for investigation in an ovine *in vivo* MI model, and compared to the previously studied only enzymatically degradable MeHA hydrogels for their efficacy in attenuating LV remodeling. Each HeMA-HA formulation will be tuned to exhibit similar initial mechanics and gelation, but different degradation kinetics (based on modification percent and initiator concentration) relative to its respective MeHA counterpart. The influence of temporal mechanical support on LV remodeling will be measured by myocardial thickness, end diastolic volume, end systolic volume, and infarct area and compared to previous MeHA hydrogel results.

Specific Hypothesis 3: Collagen bulking, induced by stimulatory hydrogel/microsphere composites, to attenuate LV remodeling is dependent on the composite carrier and particle formulation.

Specific Aim 3: To design various hydrogel/microsphere composites to evaluate their influence on collagen production and macrophage response in a subcutaneous model, and to identify an optimal composite formulation to attenuate LV remodeling in an *in vivo* ovine MI model. Poly (DL-lactide-co-glycolide) (PLGA) microspheres will be fabricated via a glass microfluidic device to form microspheres that meet criteria to promote collagen production for constructive healing. The same candidate HeMA-HA formulations selected in Aim 2 will be employed as carriers for microspheres to form hydrogel/microsphere composites (via redox initiation) with varying concentrations of microspheres. Composites will be characterized for mechanics, gelation, and degradation, similar to Aim 2. *In vivo* evaluation of the tissue response to the composites will be performed in a murine subcutaneous model; the influence of macromer properties and microsphere concentrations on the temporal presentation of microspheres to the *in vivo* milieu and on the extent of bulking will be evaluated via histological (for temporal and spatial examination) and immunohistochemical (for spatial examination) assessments. A selected composite system (based on the timing and extent of collagen bulking from subcutaneous work) will be assessed in an *in vivo* ovine MI model to analyze its ability to induce *in situ* collagen bulking and attenuate ventricular remodeling with the same metrics as in Aim 2.

2.2 Research Overview

The motivation for improving the design of injectable materials to treat LV remodeling, specifically by optimizing their material properties, was already established in Chapter 1. Chapter 3 will review natural and synthetic injectable materials that have been evaluated to date in limiting LV remodeling and will introduce the described report by Ifkovits et al. that demonstrated the significance of injectate (e.g., MeHA) material properties (e.g., mechanics) on attenuating LV remodeling.

Chapters 4 and 5 will focus on *in vitro* data acquisition and FE modeling. Theoretical modeling will be performed 1) to elaborate on the *in vivo* findings from MeHA hydrogel treatment from the aforementioned study by translating experimental findings to stress reductions and 2) to assess treatment of two additional MeHA formulations with higher initiator concentration to examine stress between conditions of varied hydrogel mechanics and distribution. Specifically, Chapter 4 will explore imaging modalities (e.g., x-ray and MRI) to determine the optimal method to accurately assess hydrogel volume distribution in ovine myocardial explants. Radiopaque HA polymers will be synthesized by addition of an iodinated moiety and imaged with a fluoroscope to assess their radiopacity. MeHA hydrogels will be visualized via MRI with a contrast agent approach involving the addition of iron oxide nanoparticles to impart hydrogel contrast and a non-contrast agent approach involving the alteration of imaging parameters to enhance contrast. One optimized approach (i.e., non-contrast MRI) will be employed to quantify volume distributions for each MeHA formulation. Chapter 5 will describe the mechanical testing of MeHA hydrogel/tissue composites via compressive and biaxial techniques. Biaxial methods will be optimized for hydrogel/tissue composite testing and used to generate mechanical data that is physiologically representative of cardiac loading. Chapter 5 will conclude by incorporating both volume data from Chapter 4 and biaxial

mechanical data into an established FE model (collaboration with Dr. Jonathan Wenk at the University of Kentucky) to simulate injections of each MeHA formulation into a dilated LV and determine their respective influences on LV remodeling via stress simulations.

The next portion of this dissertation will investigate the influence of material temporal mechanical support (e.g., treatment duration) with respect to the evolving events of LV remodeling. An *in vivo* ovine MI model will be employed to assess the efficacy of treatment with two hydrogel systems: 1) a hydrolytically degradable HA hydrogel and 2) a hydrolytically degradable stimulatory HA/microsphere composite. Chapter 6 will introduce a hydrolytically degradable version of methacrylated HA (HeMA-HA) and detail macromer synthesis, purification, and hydrogel formation. The influence of HeMA addition on hydrogel material properties (e.g., mechanics, gelation, and degradation) will be assessed to determine the extent of system tunability. In Chapter 7 two HeMA-HA formulations will be selected for direct comparison to previously studied MeHA hydrogels (i.e., featuring similar initial mechanics and gelation, but different degradation profiles) to assess the importance of the duration of stabilization in attenuating LV remodeling in a clinically relevant *in vivo* ovine MI model via measurements for global ventricular geometry and infarct area.

Chapter 8 will describe an alternative material design to address the time sensitivity of LV remodeling, where the timing and extent of wall stabilization are dependent on the exposure and concentration of microsphere stimuli, respectively, which induce collagen production through an inflammatory response. PLGA microspheres will be incorporated within HeMA-HA formulations similar to those selected for Chapter 7 to form hydrogel/microsphere composites. These composites will be characterized *in vitro* to determine the influence of microspheres on properties including mechanics, gelation, and degradation, and implanted in an *in vivo* subcutaneous model

to examine the biological response elicited by each composite. Based on this characterization, a composite providing optimal bulking (e.g., timing and amount) will be selected for analysis in an *in vivo* ovine MI model; the efficacy of the stimulatory bulking agent in limiting LV remodeling will be assessed using similar metrics as in Aim 2.

Finally, Chapter 9 will summarize conclusions and major findings and discuss future directions and limitations of each Aim.

CHAPTER 3

Injectable Acellular Hydrogels for Cardiac Repair: A Review

(Adapted from: **E Tous**, B Purcell, JL Ifkovits, and JA Burdick, "Injectable Acellular Hydrogels for Cardiac Repair," J Cardiovasc Transl Res, 2011, 4:528–542.)

3.1 Introduction

As described in Chapter 1, early geometric alterations and infarct expansion due to extracellular matrix (ECM) break down have been associated with poor long-term prognosis and have been identified as the mechanical phenomena that initiate and sustain the process of adverse post-myocardial infarction (MI) left ventricular (LV) remodeling that may lead to heart failure (HF) [1-10]. These changes cause abnormal stress distributions in myocardial regions outside the infarction, especially in the adjacent borderzone (BZ) region, putting this region at a mechanical disadvantage and causing the infarct to further spread. With time, increased regional stress initiates a positive feedback loop, propagating and exacerbating maladaptive biologic and mechanical processes, which inherently alter the contractile properties of normally perfused myocardium [11, 12]. Once initiated, these processes lead to a HF phenotype that is difficult to reverse by medical or surgical means.

Over the past decade it has become clear that maladaptive mechanical alterations are vital to consider when developing post-MI therapies [13-16]. Globally, LV remodeling results in a change in the shape of the heart, shifting it from a prolated ellipsoidal geometry to a more spherical shape with reduced transmural wall thickness.

The Law of Laplace (Equation 3.1) illustrates how the resulting dilation (increased radius) and thinning of the myocardium post-MI leads to increased stress; where stress (T) is directly proportional to pressure (P) and the radius of curvature (R), and inversely to the thickness of the myocardial wall (h).

$$T = \frac{PR}{h} \tag{3.1}$$

As discussed in Chapter 1, previous work has demonstrated that the use of ventricular restraints reduces infarct expansion by mechanically stabilizing the heart and physically forcing it to maintain its normal shape [10, 17-20]. However, these approaches are limited by the invasive procedure in which they are applied and clinical adoption has not occurred. In order to circumvent the invasive surgical placement of restraining devices early post-MI, our group and others have begun to explore the use of injectable materials, and specifically hydrogels, to limit infarct geometric changes and normalize the regional stress distribution [21-37].

Hydrogels are water-swollen polymer networks that exhibit many tissue-like properties and have been explored for numerous tissue engineering applications [38-40]. Hydrogels can form through numerous techniques, including via self-assembly, through non-covalent interactions with ionic species, through covalent crosslinking via chemical reaction, and through thermal transitions that lead to gelation [38-40]. These methods are advantageous in that they may be applied in a non-invasive manner (liquid to solid transition) and can potentially translate to catheter delivery for minimally invasive, percutaneous therapies. This chapter will focus on common natural and synthetic hydrogels that have been investigated to mechanically stabilize the myocardial wall via

bulking (or thickening), as well as comment on the underlying mechanisms of therapy. The reader should refer to Table 3.1 throughout this chapter, which summarizes the various materials that have been investigated in animal models of MI.

Table 3.1 Summary of injectable hydrogels and their assessment in models of MI.

Hydrogel Type	Animal/Model	Inject Time	Gelation Mechanism	Injection Volume	End Point
Fibrin [21, 41, 71]	Rat: LAD ligation/ reperfusion	1 wk	Peptide-self assembly	50 μL	6 wks
Fibrin, collagen, matrigel [26]	Rat: LAD ligation/ reperfusion	1 wk	Peptide-self assembly/Thermal	50 μL	6 wks
Fibrin and Alginate [37]	Rat: LAD ligation/ reperfusion	5 wks	Peptide-self assembly/Ionic		10 wks
Alginate [44]	Rat: LAD ligation/ reperfusion	5 wks	Ionic		10 wks
Alginate [34]	Rat: Ligation of proximal left coronary artery	1 wk	Ionic	130 μL	9 wks
Alginate [29]	Rat: Ligation of proximal left coronary artery	1 wk and 2 months	Ionic	100 to 150 μL	2 and 4 months
Alginate [43]	Swine: Transient balloon occlusion of LAD	4 days	Ionic	1,2, and 4 mL	2 months
Alginate/fibrin composite [32]	Swine: Ligation of OM1 and OM2	1 week	Peptide-self assembly/Ionic	200 μL x 25	4 wks
Chitosan [61]	Rat: LAD ligation	1 wk	Thermal	100 μL	5 wks
Hyaluronic Acid [36]	Rat: Ligation of left circumflex arteries	2 wks	Michael-type addition	50 μL	6 wks
Hyaluronic Acid [54]	Sheep: LAD ligation and 2nd diagonal coronary artery	30 min	Redox initiation	300 μL x 20	2 months
Collagen [22]	Rat: Ligation of proximal left coronary artery	1 wk	Thermal	100 μL	6 wks
Matrigel [28]	Mouse: LAD ligation	Immediately	Thermal	50 μL	2 wks
Matrigel [55]	Rat: LAD ligation/ heterotopic transplant	Immediately	Thermal	125 μL	2 wks
Naturally Derived ECM [33]	Rat: no infarct	N/A	Thermal	90 μL	N/A
Naturally Derived ECM [56]	Rat: no infarct	N/A	Thermal	90 μL	N/A
Dex-PCL-HEMA/PNIPAAm [35]	Rabbit: Ligation of the proximal left coronary artery	4 Days	Thermal	50 μL x 4	34 days
poly(NIPAAm-*co*-AAc-*co*-HEMAPTMC) [25]	Rat: LAD ligation	2 wk	Thermal	100 μL x 5	10 wks
αCD-MPEG-PCL-MPEG [64]	Rat: LAD ligation	5 min	Self assembly	100 μL x 3	1 month
αCD-MPEG-PCL-MPEG [27]	Rabbit: LAD ligation	1 wk	Self assembly	200 μL	5 wks
PEG-VS [24]	Rat: LAD ligation	2 min	Redox reaction	100 μL (2 or 3)	13 wks

3.2 Natural Hydrogels

3.2.1 Fibrin

Christman and colleagues pioneered the field of acellular injectable biomaterials by exploring the effects of fibrin glue as a bulking agent [21, 26, 37, 41]. Fibrin has natural binding domains for soluble growth factors and cellular integrin receptors, motivating its use for wound healing applications. Although fibrin is commonly utilized for these biological properties, it can also be used as a mechanical support for the myocardium [21, 32, 37, 41]. Specifically, fibrin forms a crosslinked hydrogel in the myocardium upon injection with a dual-barreled syringe. One barrel contains fibrinogen and aprotinin, a fibrinolysis inhibitor, and the second barrel contains thrombin, factor XIIIa, and $CaCl_2$ [21, 26, 32, 41]. Following a similar mechanism to that involved in the normal clotting cascade *in vivo*, when fibrinogen and thrombin are mixed, fibrinogen is converted to fibrin which self assembles and is crosslinked via the factor XIIIa.

Christman et al. injected these fibrin hydrogels into the ischemic LV 1 week following induced MI in rats (reperfusion-MI model) and animals were sacrificed 5 weeks later. Echocardiograph and explant data showed that fibrin is capable of maintaining fractional shortening (FS) and preserving infarct scar thickness after the material was resorbed [21]. In later studies, using the same model, Christman et al. demonstrated the ability of fibrin to substantially decrease infarct size and increase arteriole density in the infarct area compared to control BSA injections [41]. These results imply that in addition to its bulking effects, fibrin may also elicit a bioactive response that influences LV remodeling. Significant increases in neovasculature formation (capillary density) following fibrin injection in rat models of MI were later confirmed by Huang et al. [26].

3.2.2 Alginate

Natural materials that are relatively bioinert such as alginate have also been explored as injectable hydrogels to treat MI. Alginate is a linear seaweed-derived copolymer consisting of linked β-D-mannuronate (M) and α-L-guluronate (G) residues and can be crosslinked into hydrogels with the addition of divalent cations [42]. Unlike fibrin, alginate must be modified with adhesive peptides to facilitate cell binding. Both non-modified alginate and alginate modified with adhesive peptides such as Arg-Gly-Asp (RGD) or Tyr-Ile-Gly-Ser-Arg (YIGSR) have been explored as bulking agents [29, 34, 37, 43, 44] and comparisons have been performed between the two [34, 44]. Yu et al. compared modified alginate to non-modified alginate using a rat reperfusion-MI model with injections 5 weeks post-MI, more indicative of a chronic response [44]. Five weeks after hydrogel injections, both alginate groups improved FS, reduced LV dimensions and significantly increased myocardial wall thickness compared to control BSA injections. Although both non-modified and modified groups also increased the number of arterioles in the infarct area, modified alginate resulted in higher densities, indicating the ability of adhesive peptide modifications to promote angiogenesis following MI. Tsur-Gang et al. also observed improved geometry and function following injection of non-modified alginate hydrogels; however, they observed conflicting data with modified alginate hydrogels [34]. Specifically, modified alginate showed a reduced benefit compared to non-modified alginate in terms of LV diastolic and systolic dimension (LVDD and LVSD), LV diastolic and systolic areas (LVDA and LVSA), FS, and fractional area change, although no significant differences in relative scar thickness or blood vessel densities were observed.

3.2.3 Fibrin and Alginate Composite

Utilizing a large animal swine model, Mukherjee et al. injected composite hydrogels containing both fibrin and alginate to prevent geometric LV remodeling [32]. One week post-MI, 200 μL injections (25 total) were applied to the infarct area via a double barreled injection device; one component was comprised of fibrinogen, fibronectin, factor XIII, plasminogen and gelatin-grafted alginate dissolved in an aprotinin solution, while the second consisted of thrombin and 40 mM $CaCl_2$. Therapeutic outcomes included increased posterior wall thickness 1 week post-injection and a reduction in infarct expansion 21 and 28 days post-MI; however, no functional improvements were observed. Other interesting findings included a significant reduction of soluble collagen in the treatment groups, suggesting that collagen was less vulnerable to protease degradation. This observation was supported by a significant decrease in protease levels (e.g., MMP-2) in the composite hydrogel injection group, which could favor infarct stiffening in the future.

3.2.4 Chitosan

Chitosan is a linear polysaccharide that is biocompatible and biodegradable and therefore has been used in a wide variety of tissue engineering applications [45]. Chitosan hydrogels can be formed upon mixing commercially produced chitosan with a glycerol phosphate and glyoxal solution. These gels exhibit a thermoresponsive gelation that is tuned to occur at 37 °C by changing the glyoxal concentration, while hydrogel degradation is controlled by the degree of deacetylation [46, 47]. In a rat infarct model, a thermally responsive chitosan was injected 1 week post-MI [31]. Four weeks after hydrogel injection, the myocardium thickness was significantly increased compared to

PBS controls, even though the amount of chitosan present in the myocardium after 4 weeks had substantially decreased due to hydrogel degradation. There were also significant improvements in infarct size, FS, ejection fraction (EF), end systolic diameter (ESD), end diastolic diameter (EDD), and microvessel density. Although the material was not completely degraded at the end of this study, like fibrin, this is an example of a degradable material that was effective in not only preserving thickness but also function.

3.2.5 Hyaluronic Acid

Hyaluronic acid (HA) is a polysaccharide that is abundant in the body and can play several biological roles that include angiogenesis, cell migration, and scar reduction depending on its molecular weight and the addition of function groups allows for tunability in material properties [48-53]. In one example, acrylated-HA was mixed with a thiol-terminated PEG crosslinker (PEG-SH_4) and crosslinked via Michael-type addition; the mixture was injected into a rat MI model 2 weeks post-MI [36]. Four weeks after treatment, heart function was evaluated; HA treatment led to significantly decreased infarct size, increased EF and increased arteriole and capillary density. Interestingly, results showed significant increases in infarct thickness while histology showed complete degradation of the HA gels. Improvements in this work were attributed to the biological role of HA, which like fibrin has proven to play a large role in wound healing applications. Additional work with engineered HA hydrogels [54] will be discussed in Section 3.8 on modulating hydrogel properties.

3.2.6 Collagen

Collagen is a natural ECM protein that has been applied for LV remodeling therapies due to the ability to inject as a liquid, which subsequently gels at 37 °C [22,

26]. Collagen injections in 1 week old rat infarcts substantially increased infarct thickness, stroke volume (SV) and EF compared to saline inject controls; there was also a trend for improved end systolic volume (ESV) [22]. While this study did not show any evidence of angiogenesis or cell infiltration, Huang et al, using a reperfused model, were able to demonstrate both increased angiogenesis and myofibroblast infiltration in the infarct zone compared to controls [26]. Contradicting results may be attributed to variables in methodology (Table 3.1) or differences in collagen types and concentrations used. Dai et al. used a mixture of collagen I (95%) and collagen III (5%) at 65 mg/mL, while Huang et al. used a collagen I at 1 mg/mL.

3.2.7 Matrigel

As an alternative to hydrogels composed solely of isolated collagen, Matrigel is commercially available hydrogel derived from the ECM that is primarily composed of collagen, but also contains numerous other molecules derived from the basement membrane. Studies with Matrigel alone in a mouse model showed trends towards increased scar thickening and improved function compared to infarct controls [28]; thickening and improved EDD were also observed in a rat model [55]. In addition, studies by Huang et al. showed significantly increased capillary density with Matrigel injection [26].

3.2.8 Extracellular Matrix Hydrogels

Extracellular matrix (ECM) components isolated from healthy myocardium have been recently explored to treat MI. Singelyn et al. decellularized and solubilized the ECM from porcine hearts for use as an injectable scaffold [33]. The isolated ECM material maintained a complex composition including collagen and glycosaminoglycan

content and exhibited a natural thermoresponsive behavior as it self-assembled into a nanofibrous gel at 37 °C from a liquid precursor at 25 °C. Interestingly, the cocktail of isolated ECM components stimulated the migration of human coronary artery endothelial cells (HCAEC) and rat aortic smooth muscle cells (RASMC) *in vitro.* For *in vivo* application, 90 μL hydrogels were successfully pushed through a catheter into the non-infarcted myocardium of rats where they induced a significant increase in arteriole formation 11 days post-injection. In later work, Seif-Narahi et al. isolated both porcine and human pericardial ECM (PPM and HPM respectively) to evaluate their potential as autologous scaffolds for treating MI [56]. Similarly, these gels polymerized under thermal stimulation and maintained native components of the pericardial ECM. While *in vitro* results demonstrated that PPM was more effective in promoting migration of HCAEC, RASMC, and rat epicardial cells (RECs) compared to HPM, *in vivo* data 2 weeks post-injection (90 μL) indicated that both PPM and HPM similarly promoted neovascularization (76 ± 13 arterioles per mm^2 and 51 ± 42 arterioles per mm^2, respectively). Interestingly, stem cell evaluation revealed that although very slight, c-kit+ cells were present within the injection regions, suggesting a role in endogenous homing of these materials. These studies demonstrate that providing cardiac-specific cues to the injured myocardium via decellularized ECM injectable hydrogels provides a useful strategy to promote cardiac-specific tissue formation.

3.3 Synthetic Hydrogels

Natural materials may provide numerous important cellular-interactive cues (e.g., adhesion and cell-mediated degradation), but are generally limited in the extent that their properties can be adjusted (i.e., mechanics, degradation, and viscosity). In contrast,

synthetic materials provide additional potential in engineering a variety of gelation mechanisms and physical properties.

3.3.1 Poly(N-isopropylacrylamide)

One synthetic thermosensitive polymer, comprised of dextran (Dex) grafted poly(caprolactone)-2-hydroxyethyl methacrylate (PCL-HEMA) and copolymerized with poly(N-isopropylacrylamide) (PNIPAAm) termed Dex-PCL-HEMA/PNIPAAm, was developed to gel *in situ*. Material injections were performed 4 days post-MI in a rabbit model and resulted in significant reductions in infarct scar and improvement in EF and LV end diastolic and systolic diameter (LVEDD and LVSD) compared to PBS control injections when assessed 30 days after injection [35]. Significant thickening was observed despite no histological evidence of material remaining.

Similarly, Fujimoto et al. synthesized a biodegradable, temperature responsive hydrogel composed of N-PNIPAAm, acrylic acid, and hydroxyethyl methacrylate-poly(trimethylene carbonate) (poly(NIPAAm-co-AAc-co-HEMAPTMC)) with slower degradation than the previously discussed polymer (Figure 3.1) [25]. Like Dex-PCL-HEMA/PNIPAAm, poly(NIPAAm-co-AAc-co-HEMAPTMC) was engineered to undergo gelation at body temperature. In this particular study, a hydrogel with a maximum tensile strength of 6.1 kPa and complete hydrogel degradation after 5 months was evaluated for its efficacy in preventing LV remodeling in a rat MI model. The polymer was injected 2 weeks post-MI; after 8 weeks the myocardium thickness, EDA and fractional area change were significantly improved compared to PBS injection controls.

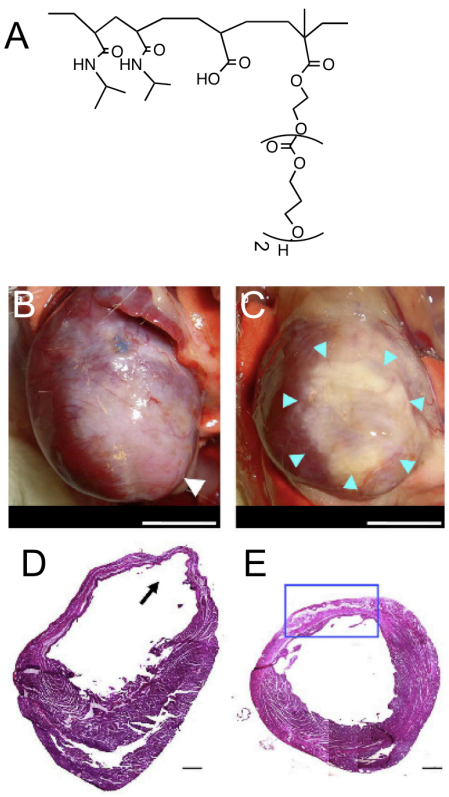

Figure 3.1 Chemical structure of poly(NIPAAm-co-AAc-co-HEMAPTMC) (A), representative images of PBS (B) and gel (C) injected hearts at 8 weeks, and hematoxylin and eosin stained section of PBS control (D) and gel treatment (E) hearts at 8 weeks. Scale bar: 5 mm in (B, C), 500 μm in (D, E). Figure adapted from [25].

3.3.2 α–Cyclodextrin

Another synthetic material consisting of α–cyclodextrin (α-CD) and poly(ethylene glycol) (MPEG-PCL-PEG) triblock polymer that has the ability to gel *in situ* has also demonstrated therapeutic benefits when injected to target LV remodeling [27, 35]. Degradation can be controlled by the PCL block and hydrogels were formed upon mixing the linear MPEG-PCL-MPEG polymer with α-CD. When injected 5 minutes post-MI in a rat model, the hydrogel-treated groups showed a significant reduction in infarct size,

LVEDD, LVESD, and an increase in FS compared to PBS inject controls. No increase in neovascularization was observed [35]. In 1 week old infarcts in a rabbit model, significant improvements in thickness, infarct size, LVEDD, LVESD, and EF were observed with no increase in microvessel density [27].

3.3.3 Poly(ethylene glycol)

The aforementioned synthetic materials have all been degradable. In contrast, a non-degradable vinyl sulfone derivatized poly(ethylene) glycol (PEG) (PEG-VS) has also been investigated to treat MI [24]. PEG-based hydrogels are bioinert and can be tailored to have high mechanical properties. PEG-VS was polymerized upon combination with dithiothreitol (DTT) and injected into a rat MI model 2 minutes post-MI. PEG-VS significantly increased the wall thickness at 4 weeks, and although no longer significant, was still thicker than saline controls at 13 weeks. Despite PEG-VS thickening the myocardial wall, echocardiograph analysis showed significant improvements in EDD only 4 weeks after MI; this was not maintained at 13 weeks. FS was also not improved in treatment groups. Here, in this small animal model, it is observed that prolonged material presence (or stabilization) is not sufficient to attenuate LV remodeling.

3.4 Biological Cues

3.4.1 Stimulatory Agents

Likewise, the biological activity of materials cannot be overlooked. A study by Ryan et al. injected a stimulatory dermal and soft tissue filler (Radiesse) composed of calcium hydroxyapatite microspheres suspended in an aqueous gel carrier of water, glycerin, and carboxymethylcellulose [57]. The uncrosslinked gel carrier allows endogenous cells to access the encapsulated microspheres to promote collagen

synthesis [57]. Radiesse was injected into the myocardium 45 minutes after ligation in an ovine MI model and analyzed at 4 weeks; injection resulted in a thickened myocardial wall, increased global EF and reduced LV end systolic volumes compared to controls. Unlike the previously mentioned hydrogel systems that directly bulk the myocardium through hydrogel crosslinking, this approach provides an effective means to induce tissue bulking by promoting the biological response to materials for attenuated LV remodeling and preserved cardiac function [58-63]. A similar approach to stabilize the infarcted myocardium will be discussed in more detail in Chapter 8.

3.5 Limitations of Experimental Assessment of Bulking Agents

From the above reviewed results, it is clear that bulking agents may attenuate remodeling post-MI; however, the mechanism involved in their success still remains to be elucidated. If anything, these results reveal the complexity in the material interaction with the myocardial tissue, including both the biological (e.g., material remodeling, inflammatory response) and mechanical (e.g., stress reduction) responses. Variable results from these studies indicate that myocardial thickness [24, 29, 32, 37], infarct size [37], and/or increased angiogenesis [22, 27, 64] do not necessarily correlate directly with improved heart function. However, discrepancies in results could be due to inconsistencies in methodology (Table 3.1) (e.g., animal models, infarct, amount of material injected, timing of injection) and material properties, and their importance should be considered when investigating LV remodeling. Specifically, several animal models have been used to study the efficacy of bulking agents. The most popular model is by far the rat model, possibly due to costs and ease of implementation; however, this model has several limitations. The most obvious is the lack of clinical relevance associated with a small animal model, as well as infarct consistency. In the clinical

setting, factors such as the LV volume and structure, material injection volume, and method for injection will be very different than in the rat.

Material injection of bulking studies has been performed as early as immediately post-MI [28] and as late as 8 weeks post-MI [29]. In separate studies with fibrin, injection at 1 week was more effective in improving myocardium function [21] versus injection 5 weeks post-MI [37]. Utilizing a permanent ligation rat model, Landa et al. directly compared injections into new (1 week post-MI) and old (2 months post-MI) infarcts and demonstrated the efficacy of alginate in both (although to different extents) [29]. Recent infarcts resulted in improvements in wall thickening and LV dilation; while older infarcts also showed improvements, results were less pronounced, implying that post-MI therapies are more effective when applied early in the LV remodeling process, potentially before irreversible processes have occurred. Similar to injection time, data collection time points are also important to consider. The longest study evaluated in this review was 3 months post-treatment [24] and 4 months post-MI [29].

3.6 Material Optimization: Theoretical Evaluation

Theoretical models have implied that material properties, specifically mechanics and volume, are important to consider when selecting the type of bulking agent to ameliorate dilation and increased stress in the myocardial wall [15, 65-67]. Using a finite element (FE) model to simulate the effects of injecting a non-contractile material into the myocardium, Wall et al. showed that bulking the myocardium was sufficient to decrease stress in the myocardial wall post-MI [15]. More specifically, they demonstrated that injections of 4.5% of the LV wall volume and 20% of the stiffness of the natural myocardium into the BZ were able to decrease the fiber stress by 20% compared to control simulations with no injections. Other approaches have validated the importance

of infarct compliance using FE, as well as lump-parameter models and results reveal similar overall beneficial outcomes [15, 65, 66]. FE models have also been employed to evaluate the effects of material volume and distribution in the myocardium and showed that they influence the extent of stress reduction (Figure 3.2) [15, 67]. After testing several injection patterns it was determined that the maximum number of injections leads to the highest reduction in fiber stress [67]. These simulations provide insight to the relevance of bulking material properties, specifically mechanics and volume distribution, and present more evidence to pursue injectable material therapies to control LV remodeling. FE modeling will be employed in this dissertation to further understand the role of injectable biomaterial treatment on attenuating LV remodeling; this will be discussed in more detail in Chapters 4 and 5.

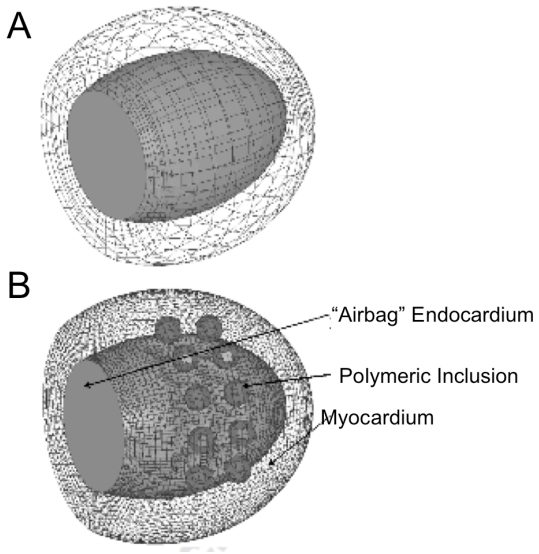

Figure 3.2 Reference FE model for infarcted canine heart (A) and modified FE model with polymeric inclusion injection pattern into dilated LV (B). Figure adapted from [67].

3.7 Material Optimization: Comparing Different Materials

Only two studies have directly compared different materials and their efficacy in preventing LV remodeling [26, 37]. Utilizing an infarct-reperfusion rat model, Yu et al. compared non-modified alginate to fibrin with injections applied 5 weeks post-MI [37]. Two days after injection, both materials were similarly effective in improving FS, LV dimensions and wall thickness. However, 5 weeks post injection, alginate demonstrated greater improvements than fibrin in FS, LV dimensions, and wall thickness. This could be attributed to the extended presence of alginate in the myocardium while fibrin was no longer detectable; however, fibrin treatment did result in thicker myocardial walls when compared to BSA control injections. Interestingly, while unable to promote cell adhesion, alginate, like fibrin, resulted in significantly higher arteriole density. Despite alginate's superiority in long-term functional outcomes, fibrin treatment groups had significantly smaller infarcts compared to controls. This comparison highlights potential differences in the efficacy of material stabilization in preventing LV remodeling, due to differences in material degradation and biological activity. In another study, Huang et al. compared the extent of angiogenesis between fibrin, collagen and Matrigel post-MI and determined that while all three polymers significantly increased capillary density, only collagen significantly increased the degree of myofibroblast infiltration [26].

3.8 Material Optimization: Comparing Properties

Few studies have experimentally evaluated the role of material properties (e.g., volume and mechanics) on LV remodeling. A review of injectable materials illustrates that a wide range of volumes have been injected as bulking agents (Table 3.1). As a single example of differences in injected volumes, Leor et al. injected an alginate-calcium solution into the LAD 4 days post-MI via a coronary catheter in swine [43].

During this time post-MI, the vasculature of the infarcted myocardium is leaky, allowing the alginate mixture to be delivered to the infarct site. Due to inadequate levels of calcium in the vasculature, the alginate solution does not crosslink until released into the myocardium where levels of calcium suffice to stimulate gelation. Various volumes of 1, 2 and 4 mL were injected; 2 and 4 mL injections led to superior LVDA and LVSA with 2 mL injections resulting in significant thickening (despite material degradation) and more pronounced trends for functional improvements. These findings illustrate the importance of injection volume in stabilizing the myocardial wall [67]. Other parameters, such as number and pattern of injections, although relevant through theoretical analysis [67], have yet to be investigated in a clinically relevant model.

The influence of material properties may also be an important parameter to control, yet few studies have investigated this, particularly in a controlled manner. This may be due to limitations in material systems where various important properties can be decoupled. For example, fibrin properties can be varied by adjusting the concentration of fibrinogen and thrombin [68] and Martens et al. adjusted these parameters to optimize fibrin viscosity and gelation for catheter delivery [69]. Similarly, alginate properties can be adjusted by varying weight percent and the ratio of M and G units [70]. However, in both of these systems viscosity may be changed during injection and lead to differences in not only final mechanics, but also material dispersion and biomaterial concentration.

A recent study by Ifkovits et al. was the first to explore how the mechanical properties of injectable materials influence LV remodeling (Figure 3.3) [54]. A highly modified HA polymer (methacrylated HA, MeHA) with a high compressive modulus (43 kPa) was directly compared to lower modified MeHA with a low compressive modulus (7.7 kPa) similar to that of native myocardium. This study demonstrated that although both materials similarly thickened, or bulked, the infarcted myocardial wall, high MeHA

was able to also decrease infarct size and dilation as well as improve function under stress compared to the infarct control.

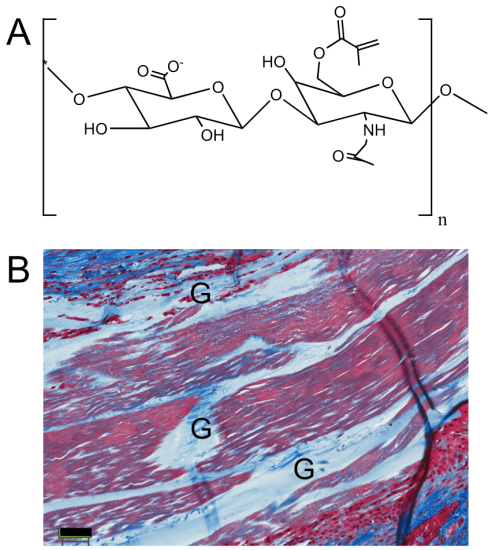

Figure 3.3 Chemical structure of methacrylated hyaluronic acid (A) and a representative Masson's Trichrome stain of the gel in myocardium 8 weeks post-MI (B). G= Gel. Scale Bar= 50 μm. Figure adapted from [54].

This provides evidence that the mechanical properties of the injectable material are important to consider for attenuating LV remodeling. Studies with tunable injectable materials will broaden the understanding of factors, such as mechanics and degradation that should be regarded to target LV remodeling via bulking agents. This dissertation will elaborate on the work of Ifkovits et al. [54], to further understand the optimal material properties for injectable materials to treat and limit LV remodeling.

3.9 Summary

Although only in its infancy, it is clear that the field of injectable hydrogels to treat the mechanical implications of LV remodeling has high potential as a translatable therapy. The lack of a cell source needed for transplantation will only accelerate development of percutaneous delivered hydrogels as tissue bulking agents. A wide range of both natural and synthetic materials have been investigated and each has unique properties, including mechanics, degradation, and cellular interactions. Due to the variety of materials and models employed, however, it is still unclear as to what type of material design is most effective in treating LV remodeling. Future work should further investigate the various mechanisms in which these materials act, both biologically and mechanically, and focus on clinically relevant parameters, such as the animal model and mode of delivery. Motivated by the advances and limitations of current injectable materials, the remainder of this dissertation will focus on furthering our knowledge on material design criteria to better treat patients with maladaptive remodeling due to MI. Chapters 4 and 5 will, specifically, elaborate on the work of Ifkovits et al. [54] (discussed in Section 3.8) and translate their *in vivo* outcomes to stress reduction data (as implied by the Law of Laplace) from FE model simulations.

References:

[1] Gheorghiade M, Bonow RO. Chronic heart failure in the United States: A manifestation of coronary artery disease. Circulation 1998;97:282.

[2] Eaton LW, Weiss JL, Bulkley BH, Garrison JB, Weisfeldt ML. Regional cardiac dilatation after acute myocardial infarction: recognition by 2-dimensional echocardiography. N Engl J Med 1979;300:57.

[3] Erlebacher JA, Weiss JL, Weisfeldt ML, Bulkley BH. Early dilation of the infarcted segment in acute transmural myocardial infarction: role of infarct expansion in acute left ventricular enlargement. J Am Coll Cardiol 1984;4:201.

[4] Weisman HF, Healy B. Myocardial infarct expansion, infarct extension, and eeinfarction: pathophysiologic concepts. Prog Cardiovasc Dis 1987;30:73.

[5] Epstein FH, Yang ZQ, Gilson WD, Berr SS, Kramer CM, French BA. MR tagging early after myocardial infarction in mice demonstrates contractile dysfunction in adjacent and remote regions. Magn Reson Med 2002;48:399.

[6] Jackson BM, Gorman JH, Moainie SL, Guy TS, Narula N, Narula J, John-Sutton MG, Edmunds LH, Gorman RC. Extension of borderzone myocardium in postinfarction dilated cardiomyopathy. J Am Coll Cardiol 2002;40:1160.

[7] Jackson BM, Gorman JH, Salgo IS, Moainie SL, Plappert T, St John-Sutton M, Edmunds LH, Gorman RC. Border zone geometry increases wall stress after myocardial infarction: contrast echocardiographic assessment. Am J Physiol Heart and Circ Physiol 2003;284:H475.

[8] Kramer CM, Lima JA, Reichek N, Ferrari VA, Llaneras MR, Palmon LC, Yeh IT, Tallant B, Axel L. Regional differences in function within noninfarcted myocardium during left-ventricular remodeling. Circulation 1993;88:1279.

[9] Lima JA, Becker LC, Melin JA, Lima S, Kallman CA, Weisfeldt ML, Weiss JL. Impaired thickening of nonischemic myocardium during acute regional ischemia in the dog. Circulation 1985;71:1048.

[10] Pilla JJ, Blom AS, Gorman JH, 3rd, Brockman DJ, Affuso J, Parish LM, Sakamoto H, Jackson BM, Acker MA, Gorman RC. Early postinfarction ventricular restraint improves borderzone wall thickening dynamics during remodeling. Ann Thorac Surg 2005;80:2257.

[11] Gorman RC, Jackson BM, Gorman JH. The potential role of ventricular compressive therapy. Surg Clin of North Am 2004;84:45.

[12] Mann DL. Mechanisms and models in heart failure: A combinatorial approach. Circulation 1999;100:999.

[13] Gupta KB, Ratcliffe MB, Fallert MA, Edmunds LH, Jr., Bogen DK. Changes in passive mechanical stiffness of myocardial tissue with aneurysm formation. Circulation 1994;89:2315.

[14] Holmes JW, Borg TK, Covell JW. Structure and mechanics of healing myocardial infarcts. Annu Rev Biomed Eng 2005;7:223.

[15] Wall ST, Walker JC, Healy KE, Ratcliffe MB, Guccione JM. Theoretical impact of the injection of material into the myocardium: a finite element model simulation. Circulation 2006;114:2627.

[16] Pfeffer MA, Pfeffer JM. Ventricular enlargement and reduced survival after myocardial infarction. Circulation 1987;75:IV93.

[17] Blom AS, Pilla JJ, Gorman RC, 3rd, Gorman JH, Mukherjee R, Spinale FG, Acker MA. Infarct size reduction and attenuation of global left ventricular remodeling with the CorCap cardiac support device following acute myocardial infarction in sheep. Heart Fail Rev 2005;10:125.

[18] Enomoto Y, Gorman JH, Moainie SL, Jackson BM, Parish LM, Plappert T, Zeeshan A, St John-Sutton MGS, Gorman RC. Early ventricular restraint after myocardial infarction: extent of the wrap determines the outcome of remodeling. Ann Thorac Surg 2005;79:881.

[19] Kelley ST, Malekan R, Gorman JH, 3rd, Jackson BM, Gorman RC, Suzuki Y, Plappert T, Bogen DK, Sutton MG, Edmunds LH, Jr. Restraining infarct expansion preserves left ventricular geometry and function after acute anteroapical infarction. Circulation 1999;99:135.

[20] Moainie SL, Guy S, Gorman JH, Plappert T, Jackson BM, St John-Sutton MG, Edmunds LH, Gorman RC. Infarct restraint attenuates remodeling and reduces chronic ischemic mitral regurgitation after postero-lateral infarction. Ann Thorac Surg 2002;74:444.

[21] Christman KL, Fok HH, Sievers RE, Fang QH, Lee RJ. Fibrin glue alone and skeletal myoblasts in a fibrin scaffold preserve cardiac function after myocardial infarction. Tissue Eng 2004;10:403.

[22] Dai W, Wold LE, Dow JS, Kloner RA. Thickening of the infarcted wall by collagen injection improves left ventricular function in rats. J Am Coll Cardiol 2005;46:714.

[23] Davis ME, Hsieh PCH, Takahashi T, Song Q, Zhang SG, Kamm RD, Grodzinsky AJ, Anversa P, Lee RT. Local myocardial insulin-like growth factor 1 (IGF-1) delivery with biotinylated peptide nanofibers improves cell therapy for myocardial infarction. Proc Natl Acad Sci USA 2006;103:8155.

[24] Dobner S, Bezuidenhout D, Govender P, Zilla P, Davies N. A synthetic non-degradable polyethylene glycol hydrogel retards adverse post-infarct left ventricular remodeling. J Card Fail 2009;15:629.

[25] Fujimoto KL, Ma ZW, Nelson DM, Hashizume R, Guan JJ, Tobita K, Wagner WR. Synthesis, characterization and therapeutic efficacy of a biodegradable, thermoresponsive hydrogel designed for application in chronic infarcted myocardium. Biomaterials 2009;30:4357.

[26] Huang NF, Yu J, Sievers R, Li S, Lee RJ. Injectable biopolymers enhance angiogenesis after myocardial infarction. Tissue Eng 2005;11:1860.

[27] Jiang XJ, Wang T, Li XY, Wu DQ, Zheng ZB, Zhang JF, Chen JL, Peng B, Jiang H, Huang C, Zhang XZ. Injection of a novel synthetic hydrogel preserves left ventricle function after myocardial infarction. J Biomed Mater Res A 2009;90:472.

[28] Kofidis T, Lebl DR, Martinez EC, Hoyt G, Tanaka M, Robbins RC. Novel injectable bioartificial tissue facilitates targeted, less invasive, large-scale tissue restoration on the beating heart after myocardial injury. Circulation 2005;112:I173.

[29] Landa N, Miller L, Feinberg MS, Holbova R, Shachar M, Freeman I, Cohen S, Leor J. Effect of injectable alginate implant on cardiac remodeling and function after recent and old infarcts in rat. Circulation 2008;117:1388.

[30] Leor J, Miller L, Feinberg MS, Shachar M, Landa N, Holbova R, Cohen S. A novel injectable alginate scaffold promotes angiogenesis and preserves left ventricular geometry and function after extensive myocardial infarction in rat. Circulation 2004;110:279.

[31] Lu WN, Lu SH, Wang HB, Li DX, Duan CM, Liu ZQ, Hao T, He WJ, Xu B, Fu Q, Song YC, Xie XH, Wang CY. Functional improvement of infarcted heart by co-injection of embryonic stem cells with temperature-responsive chitosan hydrogel. Tissue Eng Part A 2009;15:1437.

[32] Mukherjee R, Zavadzkas JA, Saunders SM, McLean JE, Jeffords LB, Beck C, Stroud RE, Leone AM, Koval CN, Rivers WT, Basu S, Sheehy A, Michal G, Spinale FG.

Targeted myocardial microinjections of a biocomposite material reduces infarct expansion in pigs. Ann Thorac Surg 2008;86:1268.

[33] Singelyn JM, DeQuach JA, Seif-Naraghi SB, Littlefield RB, Schup-Magoffin PJ, Christman KL. Naturally derived myocardial matrix as an injectable scaffold for cardiac tissue engineering. Biomaterials 2009;30:5409.

[34] Tsur-Gang O, Ruvinov E, Landa N, Holbova R, Feinberg MS, Leor J, Cohen S. The effects of peptide-based modification of alginate on left ventricular remodeling and function after myocardial infarction. Biomaterials 2009;30:189.

[35] Wang T, Wu DQ, Jiang XJ, Zhang XZ, Li XY, Zhang JF, Zheng ZB, Zhuo R, Jiang H, Huang C. Novel thermosensitive hydrogel injection inhibits post-infarct ventricle remodelling. Eur J Heart Fail 2009;11:14.

[36] Yoon SJ, Fang YH, Lim CH, Kim BS, Son HS, Park Y, Sun K. Regeneration of ischemic heart using hyaluronic acid-based injectable hydrogel. J Biomed Mater Res B Appl Biomater 2009;91:163.

[37] Yu J, Christman KL, Chin E, Sievers RE, Saeed M, Lee RJ. Restoration of left ventricular geometry and improvement of left ventricular function in a rodent model of chronic ischemic cardiomyopathy. J Thorac Cardiovasc Surg 2009;137:180.

[38] Lee KY, Mooney DJ. Hydrogels for tissue engineering. Chem Rev 2001;101:1869.

[39] Nguyen MK, Lee DS. Injectable biodegradable hydrogels. Macromol Biosci 2010;10:563.

[40] Yu L, Ding JD. Injectable hydrogels as unique biomedical materials. Chem Soc Rev 2008;37:1473.

[41] Christman KL, Vardanian AJ, Fang Q, Sievers RE, Fok HH, Lee RJ. Injectable fibrin scaffold improves cell transplant survival, reduces infarct expansion, and induces neovasculature formation in ischemic myocardium. J Am Coll Cardiol 2004;44:654.

[42] Rowley JA, Madlambayan G, Mooney DJ. Alginate hydrogels as synthetic extracellular matrix materials. Biomaterials 1999;20:45.

[43] Leor J, Tuvia S, Guetta V, Manczur F, Castel D, Willenz U, Petnehazy O, Landa N, Feinberg MS, Konen E, Goitein O, Tsur-Gang O, Shaul M, Klapper L, Cohen S. Intracoronary injection of in situ forming alginate hydrogel reverses left ventricular remodeling after myocardial infarction in Swine. J Am Coll Cardiol 2009;54:1014.

[44] Yu J, Gu Y, Du KT, Mihardja S, Sievers RE, Lee RJ. The effect of injected RGD modified alginate on angiogenesis and left ventricular function in a chronic rat infarct model. Biomaterials 2009;30:751.

[45] Kim IY, Seo SJ, Moon HS, Yoo MK, Park IY, Kim BC, Cho CS. Chitosan and its derivatives for tissue engineering applications. Biotechnol Adv 2008;26:1.

[46] Ruel-Gariepy E, Shive M, Bichara A, Berrada M, Le Garrec D, Chenite A, Leroux JC. A thermosensitive chitosan-based hydrogel for the local delivery of paclitaxel. Eur J Pharm Biopharm 2004;57:53.

[47] Chenite A, Chaput C, Wang D, Combes C, Buschmann MD, Hoemann CD, Leroux JC, Atkinson BL, Binette F, Selmani A. Novel injectable neutral solutions of chitosan form biodegradable gels in situ. Biomaterials 2000;21:2155.

[48] Chung C, Beecham M, Mauck RL, Burdick JA. The influence of degradation characteristics of hyaluronic acid hydrogels on in vitro neocartilage formation by mesenchymal stem cells. Biomaterials 2009;30:4287.

[49] Khetan S, Burdick J. Cellular encapsulation in 3D hydrogels for tissue engineering. J Vis Exp 2009;32:1590.

[50] Khetan S, Chung C, Burdick JA. Tuning hydrogel properties for applications in tissue engineering. Conf Proc IEEE Eng Med Biol Soc 2009;2009:2094-6.

[51] Laurent TC, Fraser JR. Hyaluronan. FASEB J 1992;6:2397.

[52] Sahoo S, Chung C, Khetan S, Burdick JA. Hydrolytically degradable hyaluronic acid hydrogels with controlled temporal structures. Biomacromolecules 2008;9:1088.

[53] Toole BP. Hyaluronan: from extracellular glue to pericellular cue. Nat Rev Cancer 2004;4:528.

[54] Ifkovits JL, Tous E, Minakawa M, Morita M, Robb JD, Koomalsingh KJ, Gorman JH, 3rd, Gorman RC, Burdick JA. Injectable hydrogel properties influence infarct expansion and extent of postinfarction left ventricular remodeling in an ovine model. Proc Natl Acad Sci U S A 2010;107:11507.

[55] Kofidis T, de Bruin JL, Hoyt G, Lebl DR, Tanaka M, Yamane T, Chang CP, Robbins RC. Injectable bioartificial myocardial tissue for large-scale intramural cell transfer and functional recovery of injured heart muscle. J Thorac Cardiovasc Surg 2004;128:571.

[56] Seif-Naraghi SB, Salvatore MA, Schup-Magoffin PJ, Hu DP, Christman KL. Design and characterization of an injectable pericardial matrix gel: a potentially autologous scaffold for cardiac tissue engineering. Tissue Eng Part A;16:2017.

[57] Ryan LP, Matsuzaki K, Noma M, Jackson BM, Eperjesi TJ, Plappert TJ, St. John-Sutton MG, Gorman JH, Gorman RC. Dermal filler injection: a novel approach for limiting infarct expansion. Ann Thorac Surg 2009;87:148.

[58] Anderson JM. Biological responses to materials. Annu Rev Mater Res 2001;31:20.

[59] Anderson JM, Rodriguez A, Chang DT. Foreign body reaction to biomaterials. Semin Immunol 2008;20:86.

[60] Badylak SF, Valentin JE, Ravindra AK, McCabe GP, Stewart-Akers AM. Macrophage phenotype as a determinant of biologic scaffold remodeling. Tissue Eng Part A 2008;14:1835.

[61] Brown BN, Valentin JE, Stewart-Akers AM, McCabe GP, Badylak SF. Macrophage phenotype and remodeling outcomes in response to biologic scaffolds with and without a cellular component. Biomaterials 2009;30:1482.

[62] Rodriguez A, Meyerson H, Anderson JM. Quantitative in vivo cytokine analysis at synthetic biomaterial implant sites. J Biomed Mater Res A 2009;89:152.

[63] Ziats NP, Miller KM, Anderson JM. In vitro and in vivo interactions of cells with biomaterials. Biomaterials 1988;9:5.

[64] Wang T, Jiang XJ, Lin T, Ren S, Li XY, Zhang XZ, Tang QZ. The inhibition of postinfarct ventricle remodeling without polycythaemia following local sustained intramyocardial delivery of erythropoietin within a supramolecular hydrogel. Biomaterials 2009;30:4161.

[65] Dang AB, Guccione JM, Mishell JM, Zhang P, Wallace AW, Gorman RC, Gorman JH, 3rd, Ratcliffe MB. Akinetic myocardial infarcts must contain contracting myocytes: finite-element model study. Am J Physiol Heart Circ Physiol 2005;288:H1844.

[66] Pilla JJ, Gorman JH, 3rd, Gorman RC. Theoretic impact of infarct compliance on left ventricular function. Ann Thorac Surg 2009;87:803.

[67] Wenk JF, Wall ST, Peterson RC, Helgerson SL, Sabbah HN, Burger M, Stander N, Ratcliffe MB, Guccione JM. A method for automatically optimizing medical devices for treating heart failure: designing polymeric injection patterns. J Biomech Eng 2009;131:121011.

[68] Sierra DH, Eberhardt AW, Lemons JE. Failure characteristics of multiple-component fibrin-based adhesives. J Biomed Mater Res 2002;59:1.

[69] Martens TP, Godier AF, Parks JJ, Wan LQ, Koeckert MS, Eng GM, Hudson BI, Sherman W, Vunjak-Novakovic G. Percutaneous cell delivery into the heart using hydrogels polymerizing in situ. Cell Transplant 2009;18:297.

[70] Augst AD, Kong HJ, Mooney DJ. Alginate hydrogels as biomaterials. Macromol Biosci 2006;6:623.

[71] Christman KL, Fang QZ, Yee MS, Johnson KR, Sievers RE, Lee RJ. Enhanced neovasculature formation in ischemic myocardium following delivery of pleiotrophin plasmid in a biopolymer. Biomaterials 2005;26:1139.

CHAPTER 4

Optimizing Imaging Modalities to Visualize Hyaluronic Acid Hydrogel Distribution in Cardiac Tissue

4.1 Introduction

The next two chapters will elaborate on the work of Ifkovits et al. (discussed in Section 3.8), which employed injectable methacrylated hyaluronic acid (MeHA) hydrogels as bulking agents to attenuate left ventricular (LV) remodeling [1]. Specifically, theoretical modeling based on data generated from different formulations of MeHA hydrogels will be performed to examine how alterations in material properties influence stress levels in the LV after infarct. This chapter will focus specifically on developing and optimizing imaging techniques to quantify hydrogel distribution in the LV.

4.1.1 Theoretical Models

As discussed in Chapter 3, several theoretical models have been developed to assess the extent of negative remodeling in the infarcted LV [2-6] and, more recently, to test the theoretical efficacy of injectable materials as therapies [7-9]. Using a finite element (FE) model to simulate the effects of injecting a non-contractile material into the myocardium, Wall et al. showed that bulking (i.e., thickening) the myocardium was sufficient to attenuate stress in the myocardial wall post-myocardial infarction (MI) [7]. Further investigation demonstrated the relevance of injectate properties such as volume, injection distribution within the LV, and mechanics on the degree of stress reduction [7, 8]. As previously discussed and shown in Figure 3.2, Wenk et al. developed a FE model

where inclusion (or injection) volume, geometry, and distribution in the LV could be adjusted and were determined to influence stress levels [8]. Additionally, as described in Chapter 3, passive material (e.g., mechanical) properties of injection regions can also be varied in FE modeling [3, 7]. This chapter will focus on the experimental generation of injection volume data in LV explants, while Chapter 5 will focus on the acquisition of mechanical properties of hydrogel/tissue composites. Volume distribution patterns will be used as previously reported [1]. This experimental information will then be employed for FE modeling to investigate stress levels based on experimentally derived, rather than theoretical input values.

4.1.2 Hyaluronic Acid (HA): Synthetic Versatility

Hyaluronic acid (HA) is a negatively charged non-sulfated glycosaminoglycan that has been extensively employed in the field of tissue engineering (TE) [10-23] due to its synthetic versatility and natural benefits *in vivo,* which will be discussed in more detail in Chapter 6 [24-28]. HA is readily functionalized with reactive moieties at the carboxyl and hydroxyl groups on each repeat unit for subsequent crosslinking into hydrogels [23, 29, 30]. Our group, as well as many others, have exploited this versatility to modify HA using a range of chemistries (e.g., thiols [31], aldehydes [32], dihydrazides [33, 34], and methacrylates and acrylates [1, 11, 22, 29]) to enable modulation of material properties towards specific applications. In addition to the type and degree of modification, the HA macromer molecular weight and weight percent can also be altered to achieve a wide range of hydrogel properties [1, 11, 22, 29]. This dissertation will, however, focus on evaluating the effects of the added reactive group; specifically, methacrylate and hydroxyethyl methacrylate chemistries will be added to HA to form a range of percent

modified MeHA and HeMA-HA macromers, respectively. Application of MeHA will be first discussed in the next two chapters, and HeMA-HA will be introduced in Chapter 6.

4.1.3 Hydrogel Crosslinking for Cardiac Applications

HA macromers can be chemically crosslinked to form hydrogels via numerous mechanisms (e.g., addition reactions and radical polymerization) that are defined by the added reactive groups [35]. Radical polymerization of MeHA into hydrogels has been a widely investigated system for both TE engineering applications and use in animal models [1, 10-15, 29, 35]. In these systems, initiators and a stimulus such as temperature, light, or oxidation-reduction (redox) forms radicals that propagate through the methacrylate vinyl groups to form kinetic chain crosslinks. The result is a hydrogel whose bulk properties are dependent on macromer properties including percent functionalization and macromer concentration and, also, on initiator efficiency. Several studies with MeHA hydrogels have shown that their mechanical properties can be controlled by altering the extent of methacrylate modification [1, 35], since an increase in reactive group concentration results in increased crosslinking and higher mechanics. Additionally, initiator concentration has been demonstrated to influence mechanics, as well as gel onset time based on the efficiency of crosslinking due to the availability of free radicals [1]. Photopolymerization is commonly used to form these hydrogels *ex vivo* for *in vivo* implantation or directly *in situ* where light can polymerize the macromer within the intended tissue; however, these approaches are not practical for delivery of material to the myocardium after MI [10, 11, 13, 29, 35]. To address this, hydrogels are formed from methacrylated HA macromers using redox chemical initiation [1, 36] to enable delivery of pre-polymer solutions with catheters and facilitate more controlled delivery, which is critical for dynamic organs such as the heart.

4.1.4 Experimental Versus Theoretical Work with HA Hydrogels

Ifkovits et al. employed two formulations (low and high percent modified) MeHA polymerized by the redox initiators ammonium persulfate (APS, A) and N,N,N,N',N'-tetramethylethylenediamine (TEMED, T) where hydrogel dispersion and degradation were the same and only hydrogel mechanics was varied [1]. This system was unique in that the influence of one variable (mechanics) on the attenuation of LV remodeling could be independently studied. The results concluded that mechanics did impact the extent of LV remodeling. Both MeHA formulations (7.7 kPa vs. 43.0 kPa) thickened the myocardial wall to a similar extent, but only high MeHA (43.0 kPa) treatment limited dilation of the ventricular wall (i.e., normalized end diastolic and normalized end systolic volume, NEDV and NESV, respectively) and decreased the expansion of the infarct area (Table 4.1) [1].

Table 4.1 Summary of hydrogel material properties and experimental outcomes from the work of Ifkovits et al. [1]. Values presented as mean ± SD.

	Low MeHA	High MeHA
Compressive Modulus	7.7 ± 1.0 kPa	43.0 ± 12.3 kPa
Gel Onset	Same (~4-5 minutes)	Same (~4-5 minutes)
Degradation Time	Same (Stable)	Same (Stable)
Myocardial Thickness	Same (6.54 mm)	Same (7.02 mm)
NEDV and NESV	Similar to Infarct Control	Improved
Infarct Size	Similar to Infarct Control	Improved

While Ifkovits et al. used *in vivo* experimental outcomes to demonstrate that a hydrogel with higher mechanics provided the most benefits in attenuating LV remodeling

[1], theoretical modeling can also be used to correlate this data with stress levels in the heart wall [8]. In addition to those used in the described report [1], two additional formulations crosslinked with higher concentrations of redox initiators will also be studied to further examine the influence of crosslinking parameters on stress reductions; past work has shown that increasing initiator concentration both increases mechanics and accelerates the gel onset, influencing the hydrogel distribution in explants [1].

4.1.5 Imaging HA Hydrogels

While our group has previously shown that in MeHA hydrogels, redox initiator concentrations influence gel onset (evaluated with rheometry) and distribution (assessed in explants) [1], the employed technique was not adequate to acquire data for FE analysis. Distribution was analyzed in a non-quantitative manner (on the bench); explants were simply sliced in half and rhodamine labeled HA (methacrylated rhodamine attached to HA could be grossly visualized in explanted tissue) was macroscopically distinguished and traced [1]. However, this is not an optimal technique to directly compare hydrogel distribution between groups, since hydrogel/tissue samples would need to be collected, prepared for histology, and sequentially sliced to construct a representative three-dimensional (3-D) image. Other imaging techniques can address these drawbacks. Specifically, x-ray and magnetic resonance imaging (MRI) modalities will be compared for their ability to assess MeHA hydrogel distribution in the myocardium and generate FE model inputs.

4.1.6 X-Ray Imaging

X-ray imaging can be utilized to acquire two-dimensional (via standard x-ray) and 3-D images (via x-ray computed tomography, CT); it is commonly used in the clinic as a

diagnostic tool and has recently been used to image polymers [37-44]. In general, x-ray generation occurs after high voltage is applied to accelerate electrons from the cathode portion of the x-ray tube to the anode; it is here that x-rays are formed as high voltage electrons strike. After filtration, the x-rays are delivered to the object to be visualized. Image generation is dependent on the amount of x-rays that exit the object (Equation 4.1), where I is the number of x-rays exiting, I_0 is the number entering, t is the thickness of the object, and μ is the mass attenuation coefficient (an intrinsic property of the material). Image contrast (C) is dependent on the differences between the exiting rays of the area of interest and the background as defined in Equation 4.2 [40, 41].

$$I = I_0 e^{-\mu t} \tag{4.1}$$

$$C = 1 - e^{-\Delta\mu\Delta t} \tag{4.2}$$

The mass attenuation coefficient is important in determining the radiopacity of an object. While it is dependent on several properties (coherent scattering, photoelectron scattering, and Compton scattering), the photoelectron scattering is of most significance in this work [40].

Photoelectric scattering is primarily dependent on both the atomic number (Z) of the elements that comprise the tissue and on the photon energy (E) used to image. Specifically, it is proportional to the cube of Z and inversely proportional to the cube of E [40, 41]. In general, a higher atomic number results in more rapid electron absorption for a given density and, thus, results in a brighter signal [40, 41]. Most soft tissues, however, are comprised of smaller atoms (hydrogen, nitrogen, oxygen, and carbon), thus larger atoms are typically used as agents to enhance contrast between the

background tissue and region of interest [45]. For best contrast with these agents, it is also important to consider the photon energy that is employed to image. The targeted atom's K edge energy, which is the energy above the binding energy of the K shell electrons interacting with the photon (i.e., where mass attenuation is optimal) should be accounted for when selecting a photon energy range for imaging [41].

X-ray detectability of conventional polymers is limited by their atomic make up, or density, which is similar to that of soft tissue [46]. In order to distinguish polymers from tissue, contrast agents with higher atomic number are often incorporated into the system [40, 45, 46]. While contrast agents can be integrated into polymer systems by simply mixing them in or via chelation, covalently binding the radiopaque entity enhances control and eliminates concerns of leaching.

Iodinated agents have an atomic number of 53, which is much higher than any natural element found in tissue; they have consequently become particularly popular as a contrast agent [40, 45, 46] and been covalently bound to polymer backbones to introduce intrinsic radiopaque material properties [37-39]. Blakley et al. conjugated PEG-acrylate with 4-iodobenzene chloride to form the radiopaque moiety (IPEGA). This was incorporated into the polymerization reaction with pentaerythritol tetrakis 3-mercaptopropionate (QT) thiols and poly(propylene glycol) diacrylate where gels were formed and the agent was introduced via Michael-Type Addition [37]. X-ray imaging of gel samples revealed that radiopacity was achieved at 10% IPEGA. Others have introduced more dense iodinated functional groups into polymers to increase their sensitivity in x-ray. Leon et al. modified N-isopropylacrylamide (NIPAAm) with 2,3,5-triiodobenzoic acid (TIBA) with three times the amount of iodine used by Blakely et al. [37, 39]. Their work successfully showed conjugation that resulted in radiopacity. These studies demonstrated the ability to tune material radiopacity by altering the amount of

iodinated substrate bound to the polymer as well as the type of radiopaque molecule used. Motivated by these studies, for x-ray assessment to visualize HA, an iodinated contrast molecule will be added for contrast.

4.1.7 Magnetic Resonance Imaging (MRI)

Due to its high temporal and spatial resolution, MRI is widely used in the clinic and has also been a useful tool to experimentally assess LV remodeling [47, 48]. MRI exploits the permanent magnetic moment of atomic nuclei or protons. In the absence of a magnetic field, protons are naturally randomly organized, transitioning the orientation of their spin (known as precession). To obtain an MR image of an object, the object is placed in a constant (static) magnetic field $\mathbf{B_0}$, causing the protons to align in the direction of the magnetic field; the protons precess about $\mathbf{B_0}$ at a frequency (ω_0) proportional to the applied field of strength, where ω_0 is the Larmor frequency and γ is the gyromagnetic ratio (Equation 4.3).

$$\omega_0 = \gamma B_0 \tag{4.3}$$

This alignment creates a macroscopic magnetic moment that is referred to as magnetization (**M)**. In the MR scanner, the imaged object is surrounded by a radiofrequency coil (RF coil) that is tuned to the natural resonance frequency of the protons so they can be specifically energized. The RF coil applies a series of $\mathbf{B_1}$ pulses perpendicular to $\mathbf{B_0}$ that cause the protons to change orientation away from alignment with $\mathbf{B_0}$. When the RF signal is removed, the protons realign such that their net magnetization **M** is again parallel with $\mathbf{B_0}$, in a process referred to as relaxation. During

relaxation, protons lose energy and emit a signal in the form of a free-induction decay (FID), which is detected and reconstructed to obtain 3-D MR images [47].

In order to generate a 3-D image, the FID signal must be encoded in three dimensions. While the RF pulse is running, gradient coils embedded within the bore of the MR scanner turn on to control the portion of the material that is analyzed. These gradients encode phase and frequency information within each slice, resulting in data that is generated in a series of slices to provide optimal spatial resolution and enable reconstruction of a 3-D image. Mathematical data from the MRI signal are later converted to images by a Fourier Transform for interpretation by the user [47].

The MRI scanner interface controls parameters (e.g., the type of pulse sequence and length of the pulse), which influence the magnetized protons and hence, the tissue contrast generated by MRI. Specifically, the type (e.g., spin echo, gradient echo) of pulse sequence influences proton orientation, echo time (T_E) determines the time until a signal or echo is generated, and repetition time (T_R) is the time for a pulse to complete. In combination with these parameters, MRI contrast also depends on the composition of the imaged tissue, specifically its proton density and intrinsic relaxation properties. These innate properties include the material's longitudinal (T_1) and transverse (T_2) relaxation times, which are the time required for protons to return to equilibrium or rephase, respectively, after the application of a RF pulse; differences in proton density and relaxation between different tissues differentiates them from one another. The dependence of magnetization **M** on these intrinsic properties and the gyromagnetic ratio is illustrated by the Bloch equation (Equation 4.4), where M_{xy} is the transverse magnetization and M_z is the longitudinal magnetization [47].

$$\frac{d\mathrm{M}}{dt} = \gamma \mathrm{M} \times \mathrm{B} - \frac{\mathrm{M}_{xy}}{T_2} - \frac{\mathrm{M}_z - \mathrm{M}_0}{T_1} \quad (4.4)$$

A major advantage to MRI is its sensitivity; the RF pulse is required to influence the precession of only a few protons to successfully produce a 3-D image. However, contrast agents can also be applied in small amounts to alter the intrinsic relaxation properties (T_1 and T_2) of the imaged tissue or polymer [49-54]. Typical contrast agents (e.g., gadolinium and iron oxide particles) possess paramagnetic properties that influence surrounding protons and shorten their relaxation times to enhance contrast with surrounding tissue [50-53]. Iron oxide nanoparticles are a particularly attractive contrast agent in that they are superparamagnetic (e.g., elicit stronger effects on surrounding protons) and can readily be chemically modified with functional groups, including amines and carboxylic acids [45, 49, 54]. Iron oxide nanoparticle addition leads to a shortened T_2 relaxation time due to the accelerated dephasing of protons; consequently, areas with iron oxide particles can be easily distinguished from those without [45, 49, 54]. Additionally, chemical functionalization of iron oxide nanoparticles provides a means to potentially facilitate binding with other polymers either through electrostatic or covalent interactions. This dissertation will exploit the electrostatic interactions between positively charged aminated iron oxide particles with negatively charged HA.

In addition to directly altering the proton makeup of the imaged object with the incorporation of contrast agents, imaging parameters such as the type of pulse sequence and length of pulse (e.g., T_E and T_R) can be adjusted. Tailoring these properties can vary the manner by which protons reorient and, thus, can be used to

enhance differences in intrinsic relaxation material properties without the addition of an exogenous contrast agent [45, 55]. A non-contrast approach is attractive in that it does not add the extra variable of using a contrast agent.

This chapter will examine both x-ray and MRI as options to analyze distribution and volumes of four MeHA formulations with low or high percent modification and low or high initiator concentration (A/T) in ovine LV explants: low MeHA, low A/T and high MeHA, low A/T (used by Ifkovits et al.) and low MeHA, high A/T and high MeHA high A/T (Table 4.2) [1]. The technique that best represents hydrogel volume and distribution in explants will be used to generate data that will be input into a FE model to evaluate stress in Chapter 5.

4.2 Materials and Methodology

4.2.1 Synthesis of Methacrylated HA (MeHA) Macromer

MeHA was synthesized as previously discussed and is illustrated in Figure 4.1 [29]. Briefly, methacrylic anhydride (MA) (Sigma) at ~20 fold excess was added to a 1 wt% solution of HA sodium salt (Lifecore, 66kDa) in deionized water on ice. The solution was titrated to maintain a pH of 8 by adding concentrated sodium hydroxide (NaOH) for ~6 hours or until the pH stabilized. The reaction was stirred overnight at 4 °C and on day 2 half the amount of MA was added again and reacted by similarly maintaining a pH of 8 on ice for ~ 4 hours, or until pH stabilization. Excess unreacted MA was removed by dialysis (MW cutoff 5-8 kDa) against deionized water at room temperature (RT) for at least 3 days with repeated water changes. The final product was frozen and lyophilized and stored in powder form at 20 °C until further use. Methacrylate coupling to HA and macromer purity was assessed via ^{1}H NMR (Bruker, 360 MHz).

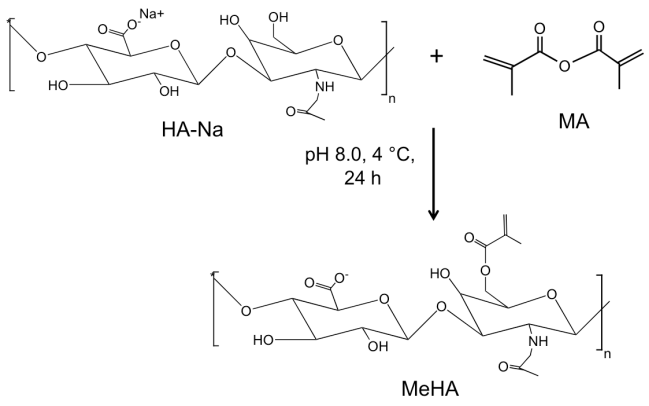

Figure 4.1 Reaction schematic for MeHA synthesis.

4.2.2 Formation and Characterization of MeHA Hydrogels

MeHA hydrogels employed for experimental work were characterized as previously discussed [1]; gel onset, mechanics, and degradation were assessed in two formulations of MeHA (~30% and ~60% modified). Macromers were mixed and crosslinked at two concentrations of the redox chemical initiators APS (A) (Sigma) and TEMED (T) (Sigma) (low A/T: 5 mM A and 5 mM T or high A/T: 12.5 mM A and 6.25 mM T) to form the following formulations of 4 wt% hydrogels: (1) low MeHA, low A/T, (2) high MeHA, low A/T, (3) low MeHA, high A/T, and (4) high MeHA, high A/T. Gelation was evaluated by monitoring the storage (G') and loss (G'') modulus using an AR2000ex Rheometer (TA Instruments) at 37 °C under 1% strain and a frequency of 1 Hz in a cone and plate geometry (1°, 20 mm diameter). To evaluate mechanics and degradation, hydrogels were formed between two glass slides within a teflon mold sealed with vacuum grease by mixing macromer solutions with APS and TEMED and incubating at 37 °C for 30 minutes. Compressive moduli were determined with a Dynamic Mechanical Analyzer (DMA) (Q800 TA Instruments) at a strain rate of 10%/ min and moduli were calculated at a strain from 10-20%. For degradation, samples were incubated at 37 °C

for 8 weeks with phosphate buffered saline (PBS) changes at weeks 1, 2, and 4. Degradation was assessed by collecting samples in PBS after 1, 2, 4, and 8 weeks and performing a uronic acid assay to measure HA content [56].

4.2.3 Imaging HA via X-Ray

4.2.3.1 Synthesis of Radiopaque HA

A schematic depicting the reaction to couple a radiopaque molecule to HA is illustrated in Figure 4.2.

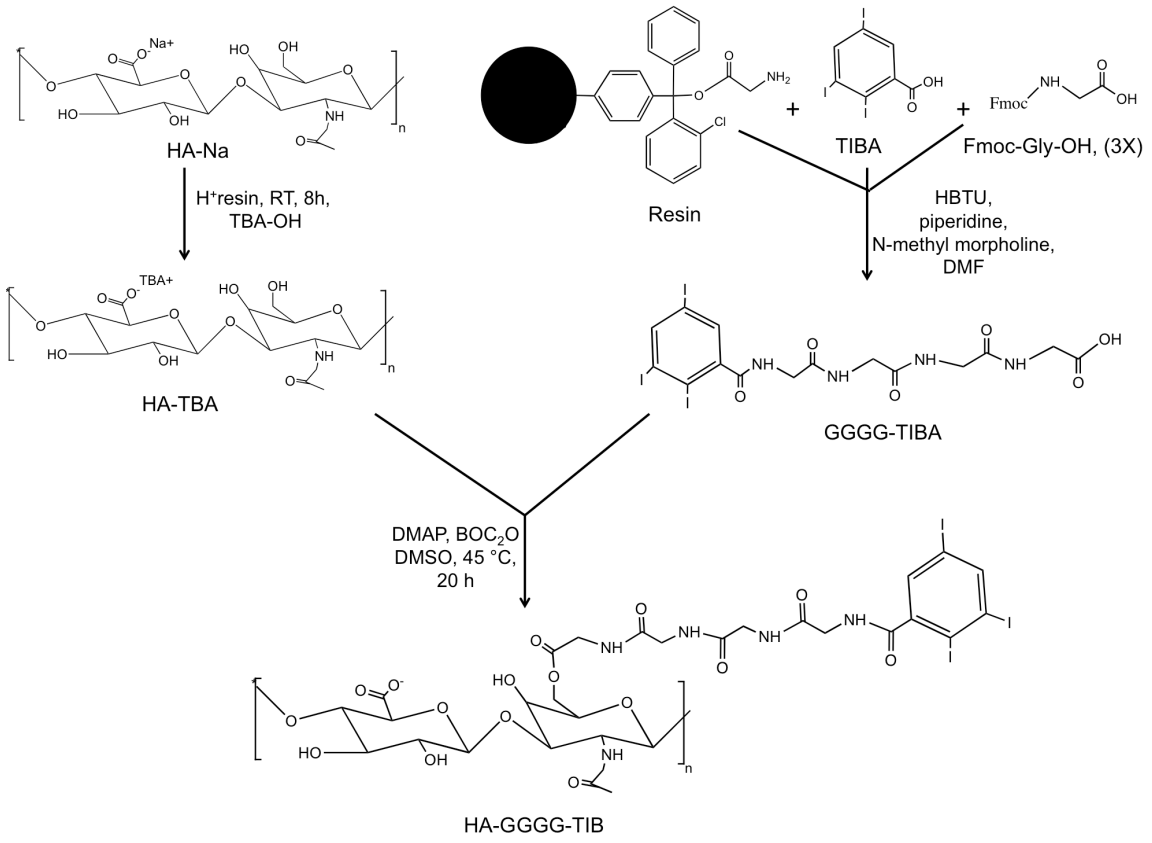

Figure 4.2 Chemical synthesis of HA-GGGG-TIB and intermediate products (GGGG-TIBA and HA-TBA).

Synthesis of Radiopaque Spacer

A spacer group consisting of 4 glycine amino acids (Fmoc-Gly-OH) (Sigma) (including the resin) was added to 2,3,5, triiodobenzoic acid (TIBA) (Sigma) to limit steric hindrance and facilitate the attachment of the radiopaque entity to HA. A 0.25 mmol reaction was run on a peptide synthesizer (Protein Technologies, Inc., PS3) with 4X excess of the reagents (TIBA and Gly, G) and the coupling agent o-benzotriazole-N,N,N',N'-tetramethyl-uronium-hexafluoro-phosphate (HBTU) (Sigma) to the H-Gly-2-ClTrt resin (AnaSpec, Inc.) in dimethylformamide (DMF) (Fisher). A 0.4 M N-methyl morpholine (Fisher) solution in DMF was used for activation and a 20% piperidine (Fisher) solution in DMF was used for deprotection. Residual DMF was removed from the resin by vacuum filtration and was rinsed with dichloromethane (DCM) (Fisher). The resin was cleaved with DCM and hexafluoroisopropanol (HFIP) (Sigma) (4:1) for 2 hours and separated from the synthesized peptide by vacuum filtration. Most of the DCM was removed by rotovap and the final product was precipitated in cold ether (Fisher). Ether was removed and the peptide was collected, dissolved in deionized water, and frozen for lyophilization. The final powder was stored at -20 °C until further use. Confirmation of the final radiopaque spacer (GGGG-TIBA) was assessed via ^{1}H NMR and mass spectrometry (Waters SQD with an Acquity UPLC).

Synthesis of HA-TBA

HA-sodium salt (Lifecore, 66 kDa) was converted into a tetrabutylammonium (TBA) salt by performing an acidic ion exchange with the ion exchange resin (Dowex, 50W x 8-200) (Sigma) at RT for 8 hours. After filtration for resin removal, the solution was neutralized by titrating with tetrabutylammonium hydroxide (Sigma) until the desired equivalent coupling of TBA to HA was reached (pH: 7.02-7.05) [30]. Final products were

lyophilized and stored at -20 °C until further use. ^{1}H NMR was performed to assess TBA coupling.

Synthesis of Radiopaque HA

The radiopaque spacer was coupled to HA-TBA via an esterification reaction with the catalyst dimethylaminopyridine (DMAP) (Sigma) and the coupling agent di-*tert*-butyl dicarbonate (BOC_2O) (Sigma) in anhydrous di-methyl sulfoxide (DMSO) (Acros) at 45 °C for 20 hours. GGGG-TIBA and BOC_2O were added at a 1:1 ratio to HA-TBA and trace amounts of hydroquinone were added to the reaction to limit free reaction during storage.

The synthesis product was dialyzed against deionized water (MW cutoff 5-8 kDa) at RT overnight. Sodium chloride (NaCl) was added to the solution for exchange of TBA with Na to facilitate precipitation in acetone. The final precipitate was collected, dissolved in water and dialyzed against deionized water at RT for 3 more days. Final products were lyophilized and stored at -20 °C until further use. ^{1}H NMR was performed to assess the degree of GGGG-TIB coupling to HA. (An extensive elaboration on the optimization of this purification process can be found in Chapter 6).

4.2.3.2 Imaging of Radiopaque HA

The radiopacity of HA was assessed by imaging 4 wt% and 10 wt% solutions of coupled HA-GGGG-TIB and non-coupled HA with a fluoroscope (Fluoroscan III Imaging System) at a range of voltages (40-75 kVp). Radiopaque macromer solutions were compared to control HA solution (4 and 10 wt %) and a TIBA control.

4.2.4 Imaging HA via MRI

4.2.4.1 Sample Preparation

Hydrogel distribution and volume within the myocardium was assessed using explanted ovine myocardial tissue from the LV portion of the heart and simulating the injection protocol as Ifkovits et al. performed in their experimental *in vivo* work [1]. In general, 0.3 mL of the four hydrogel formulations (low or high modified MeHA, with low (5/5 mM A/T) or high (12.5/ 6.25 mM A/T) initiators) were injected 3 minutes after initiator addition. After 30 minutes, hydrogel/tissue samples were collected from the LV and included the transmural injection region from the epicardium to endocardium.

4.2.4.2 MRI with Contrast Agents

Iron oxide nanoparticles (~40 nm, provided by Dr. Andrew Tsourkas and his lab [53]) were used for preliminary imaging of HA. Electrostatic interactions between iron oxide nanoparticles and MeHA macromers were confirmed with dynamic light scattering (DLS) (Malvern Instruments). Nanoparticles (100 μg/mL) were mixed with 4 wt% solutions of low and high MeHA macromers for 30 seconds and diluted 1:100 in deionized water for DLS. Nanoparticle/MeHA samples were compared to iron oxide (100 μg/mL, 1:100 dilution) and MeHA controls (4 wt%, 1:100 dilution).

Nanoparticles were mixed with MeHA macromer solutions prior to the addition of A (5 mM) and T (5 mM) initiators at a range of concentrations (10-200 μg/mL) and injected into LV explants to determine the optimal range needed to accurately represent hydrogel distribution. (Note: A different high modified version of MeHA (~66% modified) was used for the pilot nanoparticle concentration study). MR imaging was performed using a 9.4 Tesla 31 cm horizontal bore MR Spectrometer (Varian) with the following

parameters: echo time= 5 ms, repetition time= 308 ms, matrix= 256 x 256 x 24, field of view= 30 x 30 mm^2, voxel size= 0.117 x 0.117 x 1.00 mm^3. A concentration of 100 μg/mL nanoparticles was selected to image the four hydrogel formulations and a gradient echo pulse sequence was used to visualize injected explants (n=2/formulation) with the following parameters: echo time= 5 ms, repetition time= 308 ms, matrix= 256 x 256 x 32, field of view= 40 x 40 mm^2, voxel size= 0.156 x 0.156 x 1.00 mm^3. Images were processed with ImageJ software and hydrogel/tissue volumes were calculated using ITK-SNAP segmentation software [57].

4.2.4.3 MRI without Contrast Agents

Injected explants were imaged without contrast agents by adjusting image parameters to exploit intrinsic material properties; a spin echo pulse sequence was employed and the echo time (30-60 ms) was adjusted for optimal contrast. Voxel size was also altered (0.234 x 0.234 x 1.00 mm^3 vs. 0.234 x 0.234 x 0.234 mm^3) to optimize resolution. After optimization, final settings used for non-contrast imaging were as follows: echo time= 40 ms, repetition time= 5.8 s, matrix= 128 x 128 x 128, field of view= 30 x 30 mm^2, voxel size = 0.234 x 0.234 x 0.234 mm^3.

Prior to testing the hydrogel formulations, the non-crosslinked MeHA macromer (n=3) was injected into myocardial explants to determine whether it could be visualized at the selected imaging parameters. Non-crosslinked MeHA was injected into explants identically to hydrogel forming macromers, but the solutions did not contain initiator. Samples were imaged at days 0, 1, 2, 3, 4, and 5 to examine contrast differences between the HA injection and background tissue. Explant samples were rinsed 6X at RT with 50 mL of sterile PBS (1% penicillin streptomycin (P/S)) and overnight at 4 °C in 200 mL of sterile PBS for 2 days; samples were rinsed the final 3 days at 4 °C in 200 mL of

sterile PBS with daily PBS changes. Images were converted into NIFTI files using imageJ software and converted to their correct dimensions with convert3D (c3D software). Contrast was quantified using ITK-SNAP after MRI bias correction was performed with an N4 algorithm [58, 59]; the percent change in intensity between injected HA and background tissue was quantified over the course of 6 days (i.e., days 0-5). Five slices in 3 regions of the explant were evaluated (near the epicardium, myocardium, and the endocardium).

Crosslinked samples (n=4/formulation) were imaged at day 3 (when the average percent change in intensity between non-crosslinked HA and tissue was ~5%); samples were washed 6X with 50 mL sterile PBS (1% (P/S)) for 2 days (i.e., day 0 and 1) at RT and overnight in 200 mL at 4 °C, and 1 day (i.e., day 2) at 4 °C in 200 mL of sterile PBS. Images were converted to NIFTI files with the correct dimensions and a MRI bias correction was performed as discussed. Automatic segmentation was performed using Atropos (an ITK-based multivariate *n*-class open source segmentation algorithm distributed with ANTs) [60, 61] to distinguish hydrogel from the background tissue and for initial segmentation. The input domain component included only the tissue portion of images, and N4 images were segmented using a smoothing factor of 0.1 (mrf 1.0, 1x1x1) and defining 3 tissues (i.e., 3 distinct regions of segmentation). A manual segmentation for hydrogel was subsequently performed; Atropos results were employed as initial detection criterion and hydrogel was defined as a percent change in intensity between HA and tissue above 7% (i.e., one standard deviation (SD) above the average change in intensity at day 3 in non-crosslinked studies).

4.2.5 Statistical Analysis

Data is presented as mean ± SD or mean ± SEM (standard error of the mean) as indicated in the figure captions. Differences in composite volumes were assessed using a one-way ANOVA with Tukey's post hoc evaluation. For all comparisons $p<0.05$ was considered to be statistically significant.

4.3 Results and Discussion

4.3.1 MeHA Hydrogel Formation and Characterization

Two formulations of MeHA (~30% and ~60% modified) were synthesized as previously described and as shown in Figure 4.1 [1]; their degree of functionalization was determined via ^{1}H NMR by integrating the acrylate peaks resonating at δ ~6.20 ppm and δ ~5.80 ppm with respect to the HA backbone (Figure 4.3A). As discussed by Ifkovits et al., material properties such as gelation time and mechanics can be tuned by varying the percentage methacrylation [1]. Additionally, initiator concentrations also influence hydrogel properties; here, the redox initiators APS (A) and TEMED (T) were employed for hydrogel generation (Figure 4.3B) where bulk properties (e.g., mechanics and gelation) were altered by the extent of crosslinking. In this chapter we focus on four formulations in total with low or high percentage modification and low or high A/T to explore the influence of initiator parameters on MeHA gelation and distribution and ultimately stress reduction in the infarcted myocardium. Gelation was assessed by performing a time sweep upon mixing of the component solutions, where gel onset was defined as the intersection of the storage (G') and loss (G'') moduli (Figure 4.3C). Gel onset results for all four formulations are summarized in Table 4.2.

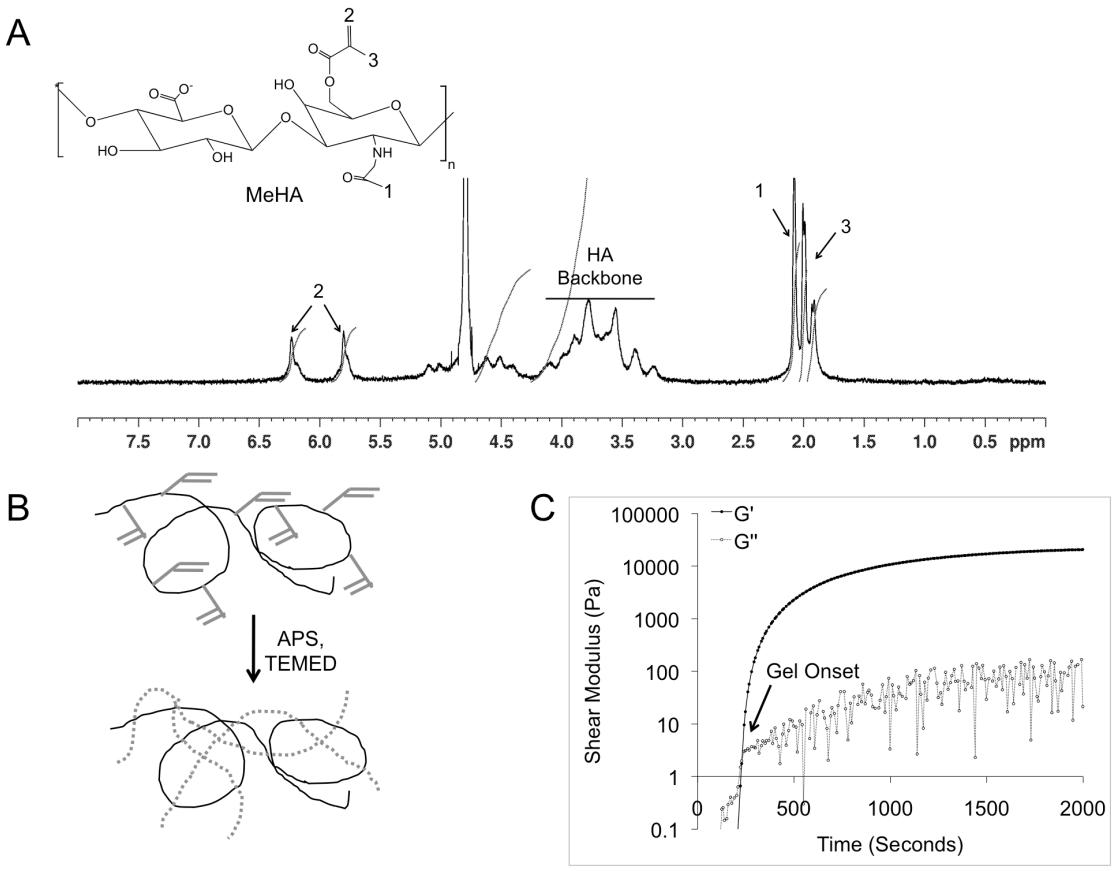

Figure 4.3 ^{1}H NMR spectrum (D_2O) of representative MeHA macromer (A). Schematic of hydrogel formation via redox initiation (B). Representative rheological time sweep, where the intersection of the storage and loss moduli is defined as the gel onset (C). In panel A, peak 1= protons on N-acetyl group on HA, peak 2= protons on alkene of methacrylate group, and peak 3= protons on methyl group on methacrylate.

Table 4.2 Summary of methacrylate modification, initiator concentration and gel onset time for all four hydrogels formulations investigated. *= formulations investigated by Ifkovits et al. [1]. Values presented as mean ± SD.

Formulation	Modification	A/T Concentration	Gel Onset (Seconds)
Low MeHA, Low A/T *	~30%	5 mM A, 5mM T	312 ± 12
High MeHA, Low A/T *	~60%	5 mM A, 5mM T	234 ± 6
Low MeHA, High A/T	~30%	12.5 mM A, 6.25 mM T	128 ± 9
High MeHA, High A/T	~60%	12.5 mM A, 6.25 mM T	105 ± 2

4.3.2 Imaging HA via X-Ray

4.3.2.1 Synthesis of Radiopaque HA

As discussed in the introduction of this chapter, x-ray visibility is contingent on the mass attenuation coefficient of the imaged object; thus, groups have incorporated additional radiopaque chemistries into materials to enhance this property for visualization [40, 41, 45]. Motivated by the work of Leon et al., we sought to generate a radiopaque version of HA by covalently attaching an iodinated entity in a similar fashion (Figure 4.2) where addition should enhance hydrogel contrast.

A spacer group was synthesized to limit steric hindrance between the targeted acid and the bulky iodinated benzene ring to encourage binding to HA. As described in Methods, formation of the spacer groups entailed the addition of 4 Gly amino acids to TIBA and was performed on a peptide synthesizer. ^{1}H NMR was used to confirm the successful production of GGGG-TIBA, where protons on the benzene rings (*) resonate at δ ~7.62 and δ ~8.25 ppm (Figure 4.4A). Mass spectrometry was also performed with a detected peak of 728.97 g/mol at 720 m/z corresponding to the molecular weight of GGGG-TIBA (Figure 4.4B).

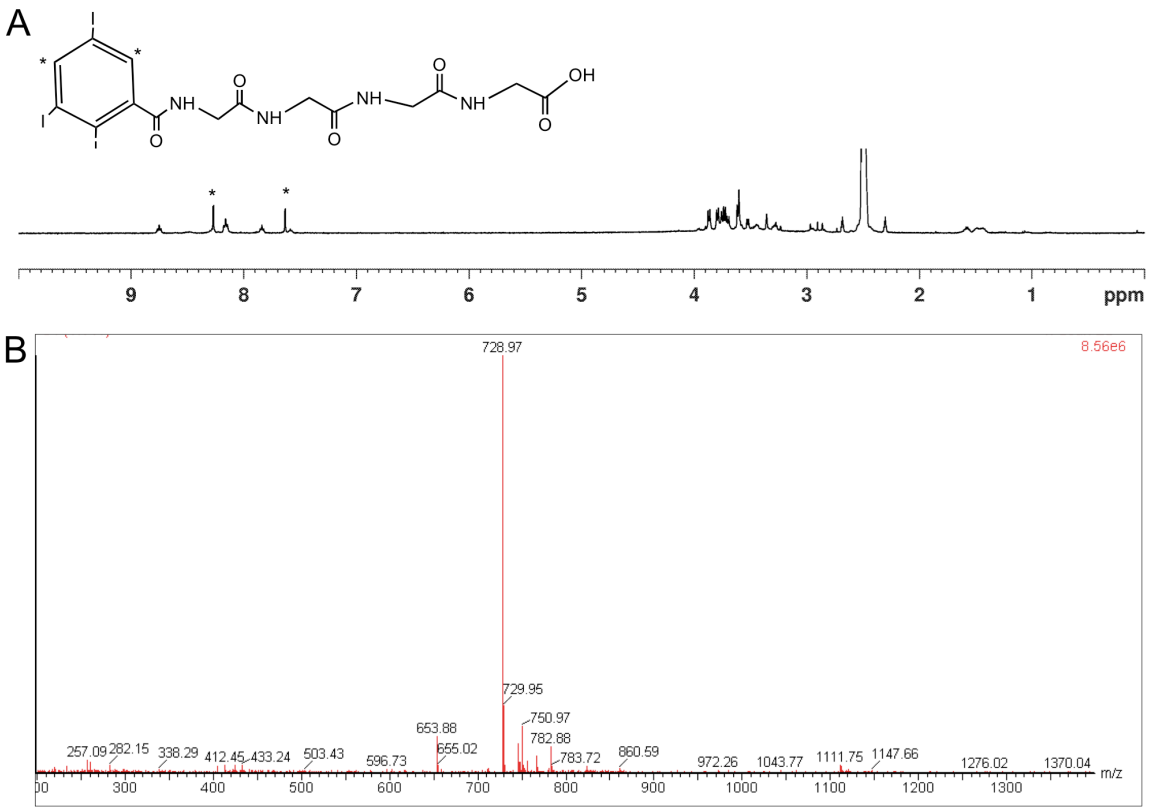

Figure 4.4 Chemical structure and ^{1}H NMR spectrum (DMSO) of GGGG-TIBA with labeled peaks (*) corresponding to the protons on the benzene ring (A). Mass spectrum confirming the production of GGGG-TIBA (~728 g/mol) at the mass to charge ratio of ~720 m/z (B).

The solubility of the HA sodium salt (Figure 4.5A) is limited to aqueous solvents; thus, to render it soluble in DMSO for functionalization, the sodium salt was converted to a TBA salt. TBA addition to HA was confirmed with ^{1}H NMR by the presence of additional peaks corresponding to the protons on 4 butyl groups at resonances of δ ~3.24 ppm, δ ~1.67 ppm, δ ~1.42 ppm, and δ ~0.98 ppm (corresponding to peaks, 2, 3, 4, and 5, respectively Figure 4.5B). The degree of TBA addition (~1.4 TBA molecules

per HA repeat unit) was assessed by integrating with respect to the N-acetyl group corresponding to the HA backbone (resonance of δ ~ 2.10 ppm).

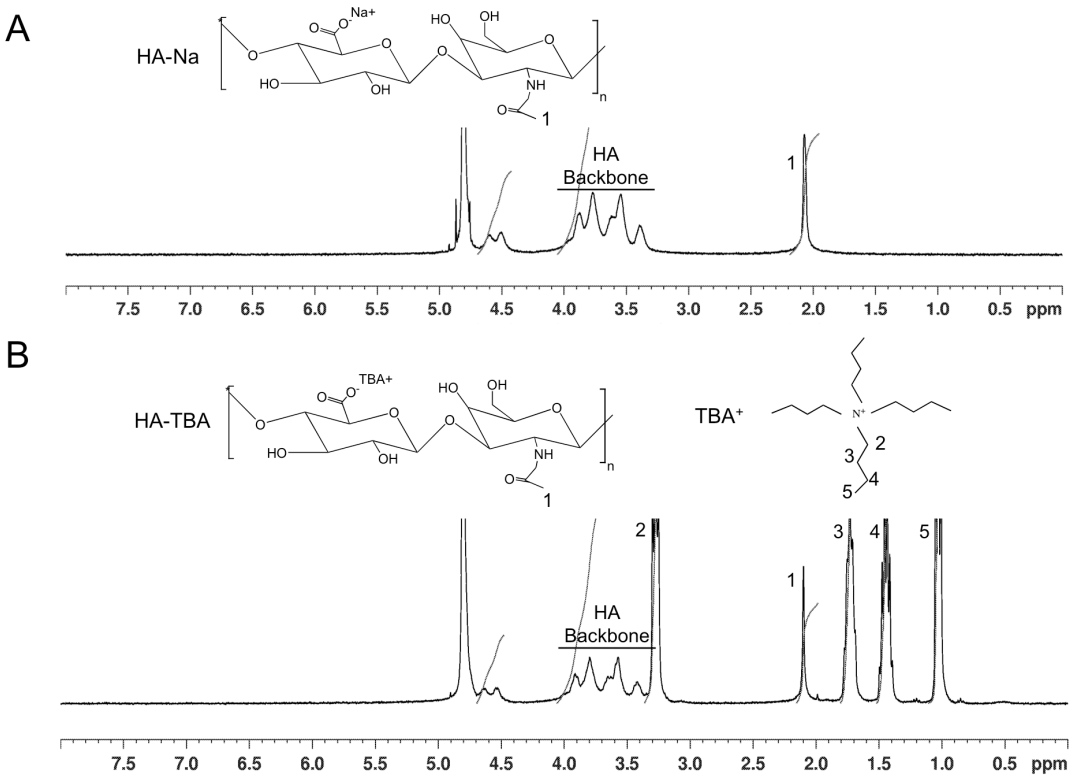

Figure 4.5 Chemical structure and ^{1}H NMR spectrum (D_2O) of HA sodium salt (A) and HA-TBA salt (B). Peak 1= protons on the N-acetyl group on HA. Peaks 2, 3, 4, 5= protons on butyl groups of TBA.

HA-TBA was reacted with GGGG-TIBA in DMSO and purified by dialysis and acetone precipitation. Coupling of GGGG-TIBA to HA was assessed with ^{1}H NMR where the protons corresponding to the benzene ring (*) were integrated with respect to the N-acetyl group corresponding to the HA backbone (peak 1) (Figure 4.6) to confirm ~12% modification.

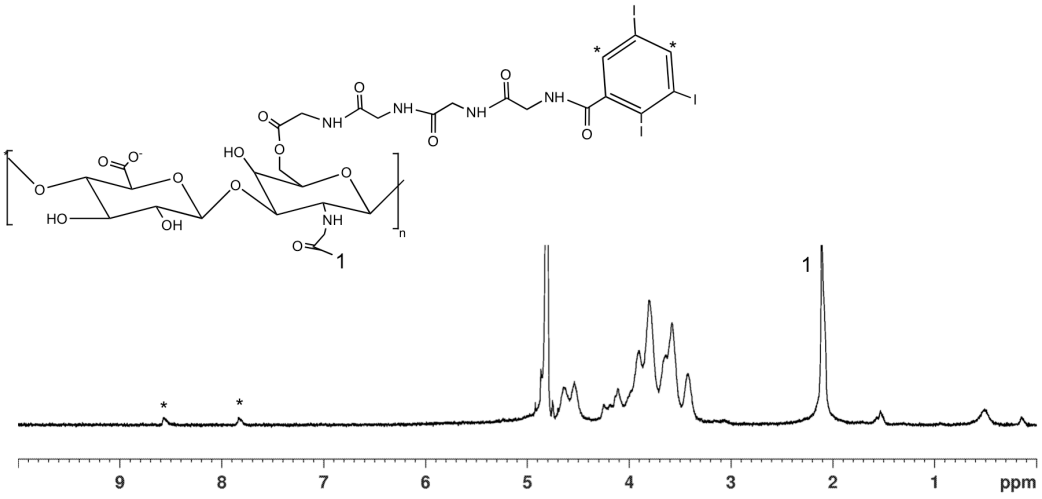

Figure 4.6 Chemical structure and ^{1}H NMR spectrum (D_2O) for representative HA-GGGG-TIB. Peak 1= protons on the N-acetyl group on HA. *= protons on the benzene ring of GGGG-TIBA.

4.3.2.2 Imaging of Radiopaque HA

After successful coupling of GGGG-TIBA to HA, HA-GGGG-TIB solutions were imaged and compared to non-coupled HA with a fluoroscope to evaluate their radiopacity (Figure 4.7). 4 wt% solutions (coupled and non-coupled) were made to simulate the concentration of hydrogels used in the work by Ifkovits et al. [1]; 10 wt% solutions (coupled and non-coupled) were also evaluated to increase the concentration of the groups. Imaging was performed at a range of voltages to best account for iodine's K-edge energy. Visually, HA-GGGG-TIB solutions lacked contrast and appeared similar to non-coupled HA solutions and the PBS control (Figure 4.7B). Whereas, positive TIB powder was clearly visible (Figure 4.7A). It is important to note that these images are positive images rather than the negative images typically produced in an x-ray film. Fluoroscopes commonly convert the transmitted radiation from x-ray into light for real

time imaging [62]. Overall, these data suggest that 12% modification is not sufficient to impart radiopaque properties to HA.

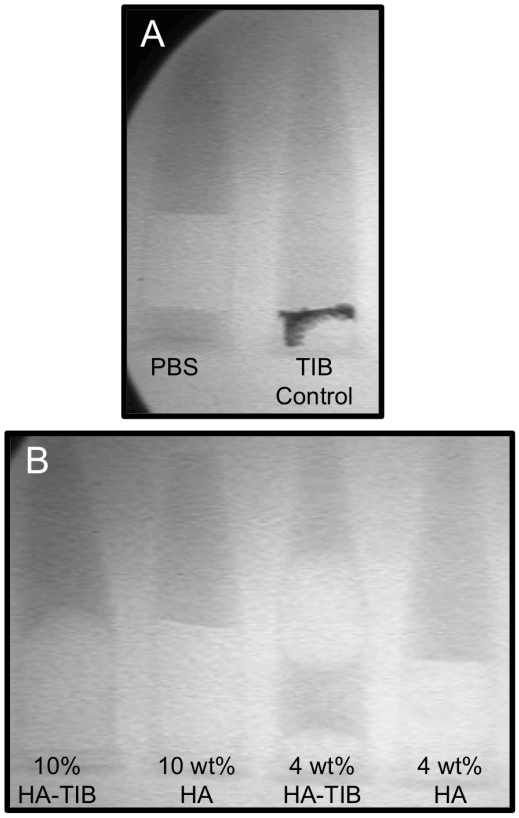

Figure 4.7 Representative fluoroscopic images (56 kVp and 0.023 mA) of PBS and TIBA controls (A) and HA controls and HA-GGGG-TIB at 4 wt% and 10 wt% (B).

Past work suggests that higher concentrations (wt% and modification of the contrast agent) are needed to enhance contrast in radiopaque agents [37, 39, 63]. However, this is not desirable since too much GGGG-TIBA addition could alter the properties of MeHA hydrogels. For example, excessive addition of GGGG-TIBA could limit MeHA modification since the methacrylate is also added to the hydroxyl group of the HA backbone. In this investigation, our goal was to keep material properties of

MeHA hydrogels consistent with the work of Ifkovits et al. [1]. This work indicated that x-ray imaging is insufficient for HA detection for purposes of the current studies and was not further explored. Specifically, to circumvent this problem, a different imaging modality with less dependence on contrast agent concentration was explored.

4.3.3 Imaging HA via MRI

4.3.3.1 MRI with Contrast Agents

Aminated iron oxide nanoparticles are particularly attractive for HA imaging due to their ability to bind to HA [64]. DLS assessment revealed that positively changed aminated nanoparticles formed electrostatic interactions with negatively charged HA (Figure 4.8); for example, the addition of MeHA macromer to iron oxide nanoparticles resulted in a shift in both the iron oxide and MeHA control curves, corresponding to increases in particle diameters.

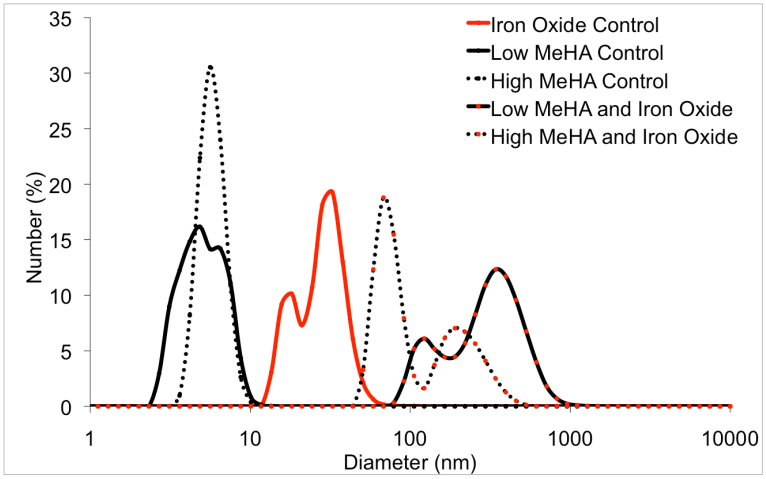

Figure 4.8 DLS plot evaluating electrostatic interactions between iron oxide particles and MeHA macromers.

As discussed in Methods, for explant work, nanoparticles and initiators were mixed with MeHA macromers and 0.3 mL of the precursor solution was then injected into the LV portion of ovine explants 3 minutes after initiator addition. Initial studies entailed performing a particle concentration (10-200 μg/mL) sweep to determine the optimal concentration for hydrogel imaging. Hydrogels (with iron oxide nanoparticles) were imaged with MRI, and volumes were quantified. Hydrogel visualization was particle concentration dependent (Figure 4.9); a drop in signal and detected hydrogel volume was observed at concentrations lower than 100 μg/mL. At concentrations greater than 100 μg/mL, the detected volumes were comparable, suggesting that they were accurately representing the entire injection volume. Thus, for the next study, a nanoparticle density of 100 μg/mL was selected to examine volume and distribution of the four hydrogel formulations (Figure 4.10). These preliminary results (n= 2/condition) indicate that addition of iron oxide nanoparticles in a small quantity is an effective method to detect hydrogel volume and distribution differences between hydrogel formulations. While effective, as trends will be confirmed and discussed in more detail in non-contrast agent studies, the incorporation of particles into hydrogels could potentially alter their properties; thus, a non-contrast agent approach where image parameters could be altered without influencing hydrogel properties was explored.

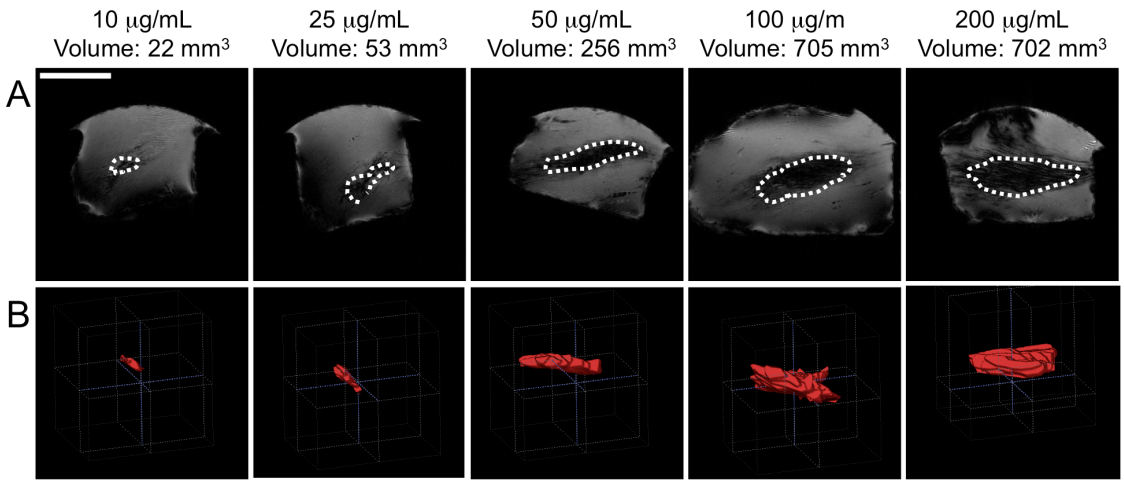

Figure 4.9 Representative MRI slice after injection of 66% modified MeHA, low A/T mixed with a range of iron oxide particles (10-200 μg/mL) into the myocardium (A) and their respective 3-D construction of the injection region (B). Scale bar= 1 cm.

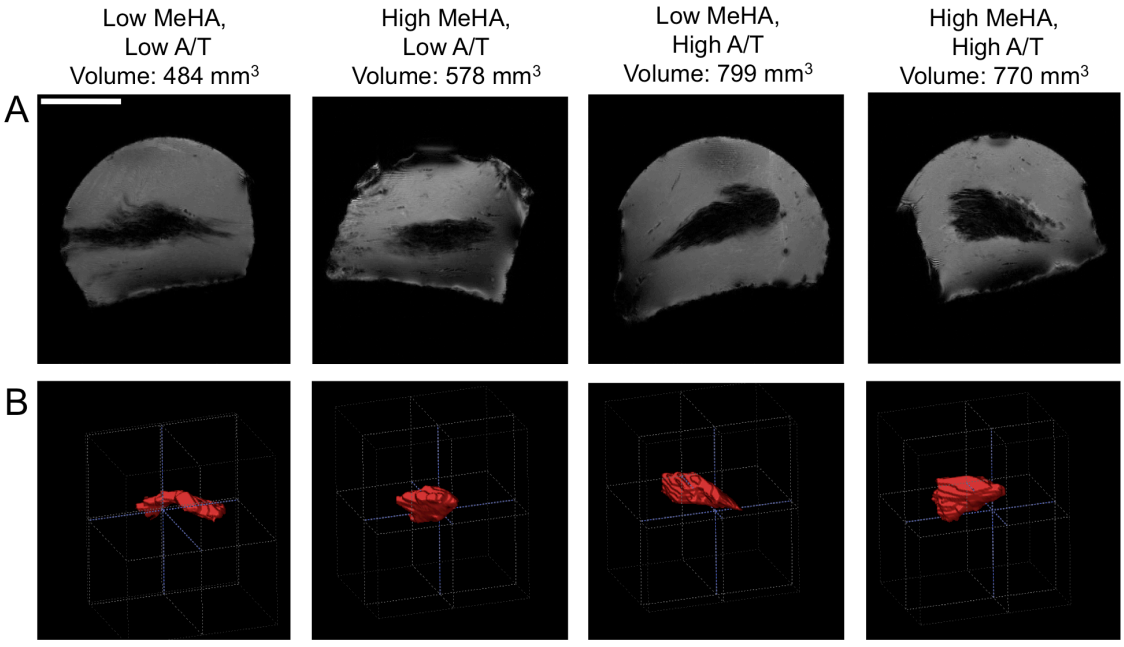

Figure 4.10 Representative MRI slice after injection of each hydrogel formulation mixed with iron oxide particles (100 μg/mL) into the myocardium (A) and the respective 3-D constructions of the injection region (B). Scale bar= 1 cm.

4.3.3.2 MRI without Contrast Agents

The proton makeup of a water swollen HA hydrogel is different than that of tissue; thus, when injected into an explant, the endogenous properties of the composite hydrogel/tissue region are different than tissue alone. It is not completely understood how much of this is due to changes in proton density or relaxation times, yet hydrogels should be detectable without the inclusion of contrast agents. However, the extent of detectability is dependent on the imaging parameters. For example, when implementing the imaging parameters used in Section 4.3.3.1, only sporadic detection of portions of more highly crosslinked networks were observed. However, by varying image parameters (type and time of pulse) we were able to more clearly detect and image all hydrogel formulations. Specifically, a spin echo pulse was implemented and the T_E was altered (Figure 4.11). Images became darker with higher T_E (60ms) and lighter with lower T_E (30 ms); for optimal contrast an intermediate T_E (40 ms) was selected for hydrogel imaging.

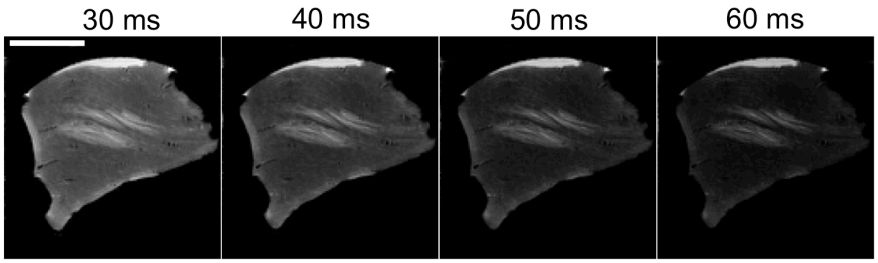

Figure 4.11 Representative MRI slices of high MeHA, low A/T injections into the myocardium without contrast agent at various T_E (30-60 ms). Scale bar= 1 cm.

In addition to altering acquisition parameters to better visualize the hydrogel within the explant, resolution was also adjusted by altering the voxel size, where a

smaller voxel size corresponded to thinner slices and better hydrogel image resolution relative to larger voxels (Figure 4.12). When quantified, volume size decreased with the smaller voxel size, suggesting that larger voxels overestimated volumes. Based on this data, a smaller isotropic voxel size (0.234 x 0.234 x 0.234 mm^3, Figure 4.12) was selected for further imaging.

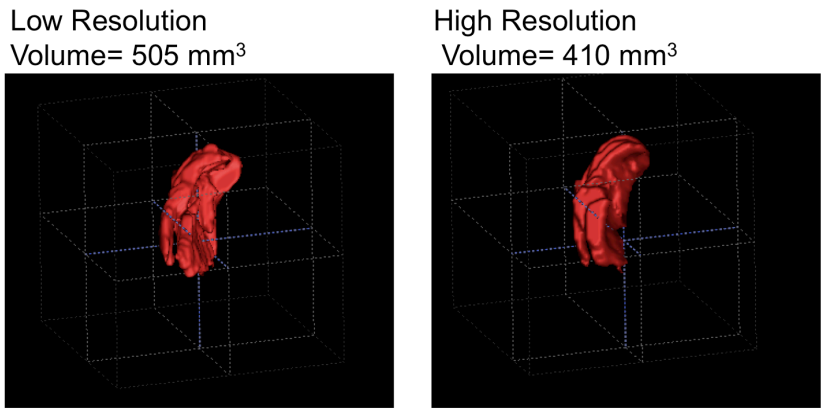

Figure 4.12 Representative 3-D construction of high MeHA, low A/T injection into the myocardium imaged at different voxel sizes (low resolution: 0.234 x 0.234 x 1 mm^3 and high resolution: 0.234 x 0.234 x 0.234 mm^3) to assess resolution effects.

Before beginning non-contrast imaging with MRI on hydrogels, initial studies were performed to better understand what portion of the original injected MeHA solution (i.e., crosslinked vs. non-crosslinked MeHA) could be visualized using the selected imaging parameters. To address this, non-crosslinked MeHA was injected into explants, and the contrast between HA and the tissue was assessed at days 0-5 both visually (Figure 4.13A) and quantitatively (Figure 4.13B) by calculating the percent change in intensity between the injection area and background tissue. Visual and quantitative assessment revealed that non-crosslinked MeHA could clearly be discerned at day 0 (1-

4 hours following injection). During the following 5 day time course, the intensity difference between the non-crosslinked injection and tissue decreased with time with differences reaching a plateau by day 3 as un-crosslinked material diffused from the tissue. Thus, this time point was chosen for imaging of hydrogel formulations.

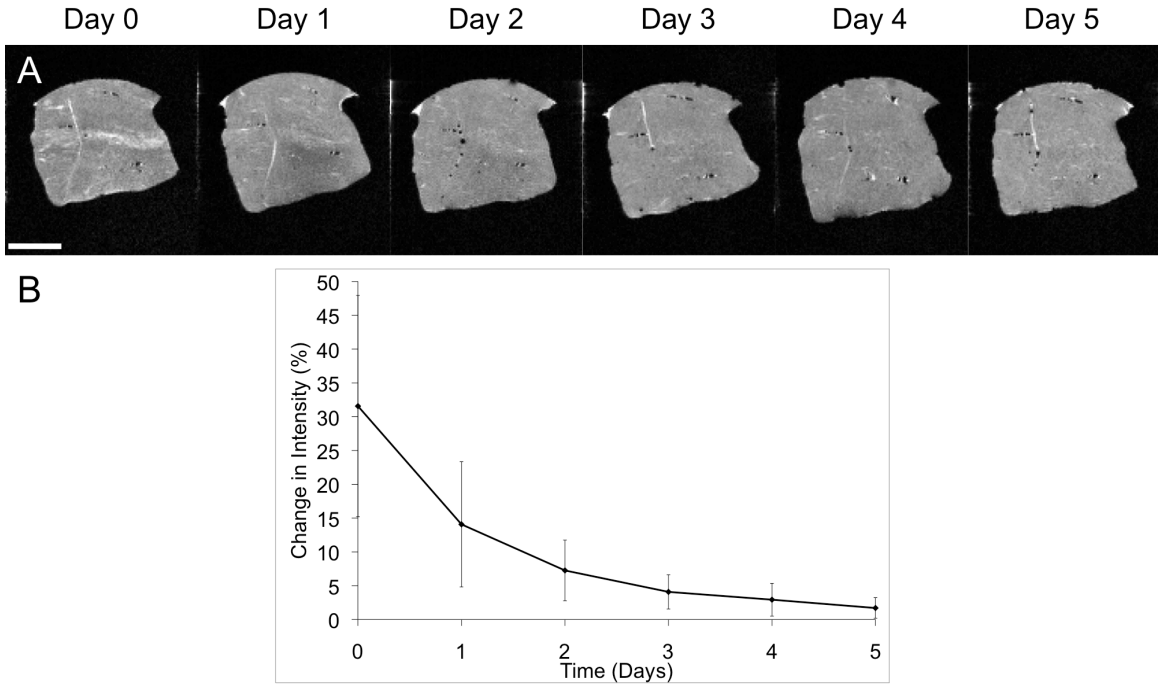

Figure 4.13 MRI slice of non-crosslinked MeHA macromer without contrast agent injected into myocardium and tracked 5 days after injection (day 0) (A). Quantified percent change in intensity between non-crosslinked MeHA (n=3) portion and tissue background over the course of 5 days (B). Data are presented as mean ± SD.
Scale bar= 1 cm.

A summary of volume distributions for low and high MeHA at low and high initiator concentrations is shown in Figure 4.14. Figure 4.14A illustrates that compared to minimal contrast observed in control myocardial tissue, all four tissue-embedded

MeHA formulations were clearly distinguishable. While the geometry of injections varied both within and between formulations, most injections took on an ellipsoidal shape with the major axis matching the fiber direction (Figure 4.14A, B). As alluded to in Section 4.3.3.1, the results also revealed a trend in detected volume differences between groups that were dependent on macromer modification and initiator concentration (Figure 4.14C). Macromer modification had a pronounced influence only at the lower initiator concentration; in this case lower macromer modification led to smaller volumes. Volume differences were, however, not significantly different as Ifkovits et al. concluded from their rheology assessment for gel onset [1]. Furthermore, lower A/T resulted in smaller volumes compared to higher A/T and was most pronounced in the lower macromer case where the difference was statistically significant.

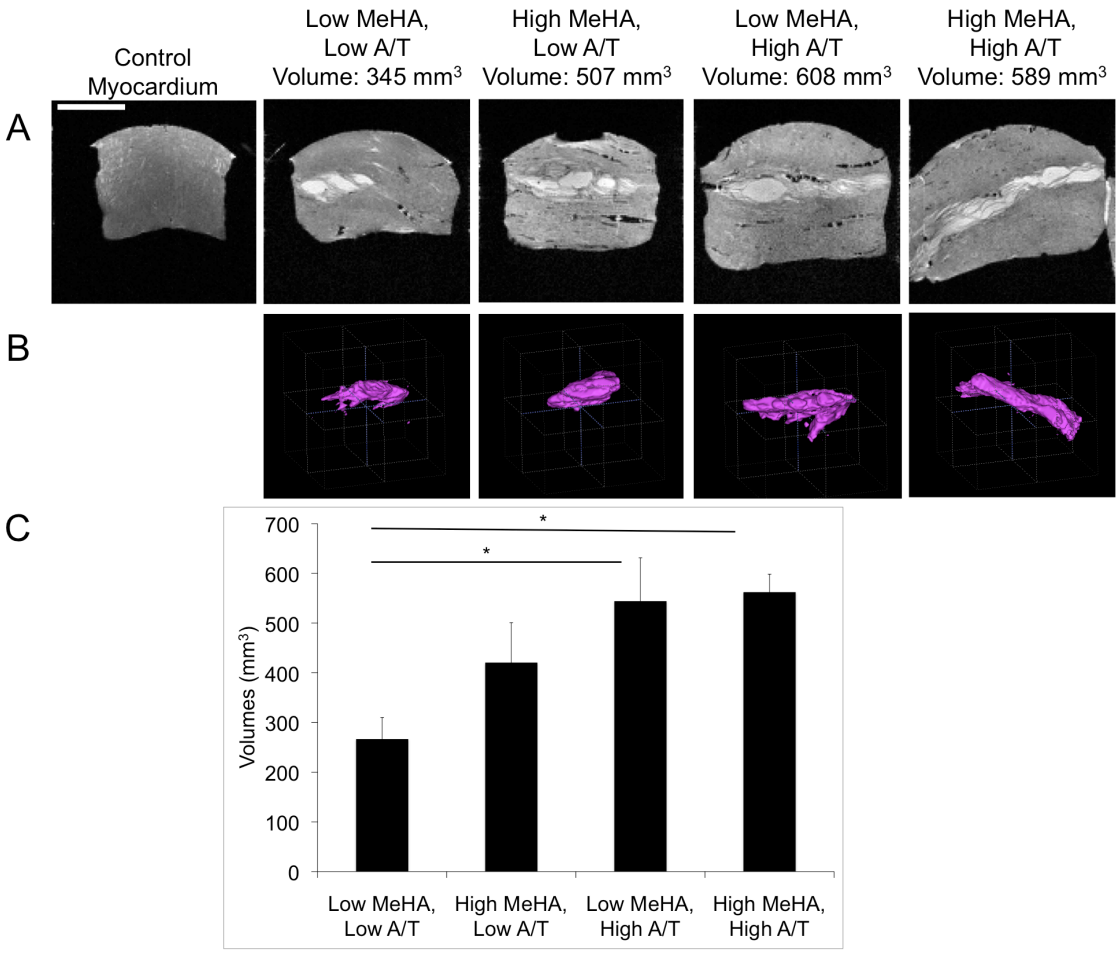

Figure 4.14 Representative MRI slice of each hydrogel formulation without contrast agent injected into the myocardium (A) and the respective 3-D constructions of the injection region (B). Quantified volume of the injection region for each MeHA formulation (n=4) injected into LV explants (C). In panel A, scale bar= 1 cm. In panel C, data are presented as mean ± SEM. *p<0.05 compared to low MeHA, low A/T.

The smaller volumes observed with low macromer modification and initiator concentration can be attributed to the lower number of reactive groups and radical initiators relative to the high groups. When injected into tissue, it is probable that the precursor solutions of the low macromer/initiator formulations are more susceptible to

dilution by the fluids within the tissue, leading to inefficient reaction and lower hydrogel volume relative to the high formulations. It is also important to note that differences were observed in the distribution of the hydrogel within the myocardial fibers. While hydrogels formed with low initiators did at times form small hydrogel "plugs" (areas of mostly hydrogel), these formulations generally dispersed more evenly within the fibers. Hydrogels formed with higher initiators exhibited more frequent "plugs" in addition to considerable dispersion. While plugs were observed to an extent in all formulations, in most cases the calculated volumes were larger than the original 0.3 mL that was injected, suggesting that the hydrogel is dispersing within the tissue rather than only forming a plug that displaces the tissue.

4.4 Conclusions

Two imaging techniques (x-ray and MRI) were examined as options to image MeHA hydrogels and quantify their volume; specifically, four MeHA formulations with low or high macromer modification and low or high initiator concentration were investigated to determine the influence of each on hydrogel volume. For x-ray imaging, an iodinated benzene molecule was successfully added to HA; however, the degree of modification (~12%) was insufficient to provide radiopacity. Due to its enhanced sensitivity and high spatial resolution, MRI was explored as an alternative to x-ray for hydrogel imaging both with and without contrast agents. While applying iron oxide nanoparticles to MeHA hydrogel formulations resulted in similar trends as non-contrast approaches, the latter approach to generate data for FE modeling was pursued further due to similar concerns regarding the potentially detrimental effects of agent incorporation on hydrogel properties. Non-contrast MR imaging was performed by adjusting image parameters to achieve high resolution images of hydrogel dispersion without contrast agent.

Interestingly, hydrogel volume was influenced by both macromer and initiator concentration, with significant differences observed with different initiator concentrations. Smaller volumes in formulations with low A/T were observed and attributed to inefficient formation of kinetic chains due to the limited presence of free radicals and reactive groups (in low MeHA), resulting in loss of precursor solution before crosslinking. The final volumes quantified with non-contrast MR imaging will be applied in Chapter 5.

References:

[1] Ifkovits JL, Tous E, Minakawa M, Morita M, Robb JD, Koomalsingh KJ, Gorman JH, 3rd, Gorman RC, Burdick JA. Injectable hydrogel properties influence infarct expansion and extent of postinfarction left ventricular remodeling in an ovine model. Proc Natl Acad Sci U S A 2010;107:11507.

[2] Pilla JJ, Gorman JH, 3rd, Gorman RC. Theoretic impact of infarct compliance on left ventricular function. Ann Thorac Surg 2009;87:803.

[3] Wenk JF, Klepach D, Lee LC, Zhang Z, Ge L, Tseng EE, Martin A, Kozerke S, Gorman JH, 3rd, Gorman RC, Guccione JM. First evidence of depressed contractility in the border zone of a human myocardial infarction. Ann Thorac Surg 2012;93:1188.

[4] Kerckhoffs RC, Neal ML, Gu Q, Bassingthwaighte JB, Omens JH, McCulloch AD. Coupling of a 3D finite element model of cardiac ventricular mechanics to lumped systems models of the systemic and pulmonic circulation. Ann Biomed Eng 2007;35:1.

[5] Walker JC, Ratcliffe MB, Zhang P, Wallace AW, Hsu EW, Saloner DA, Guccione JM. Magnetic resonance imaging-based finite element stress analysis after linear repair of left ventricular aneurysm. J Thorac Cardiovasc Surg 2008;135:1094.

[6] Dang AB, Guccione JM, Mishell JM, Zhang P, Wallace AW, Gorman RC, Gorman JH, 3rd, Ratcliffe MB. Akinetic myocardial infarcts must contain contracting myocytes: finite-element model study. Am J Physiol Heart Circ Physiol 2005;288:H1844.

[7] Wall ST, Walker JC, Healy KE, Ratcliffe MB, Guccione JM. Theoretical impact of the injection of material into the myocardium: a finite element model simulation. Circulation 2006;114:2627.

[8] Wenk JF, Wall ST, Peterson RC, Helgerson SL, Sabbah HN, Burger M, Stander N, Ratcliffe MB, Guccione JM. A method for automatically optimizing medical devices for

treating heart failure: designing polymeric injection patterns. J Biomech Eng 2009;131:121011.

[9] Jhun CS, Wenk JF, Zhang Z, Wall ST, Sun K, Sabbah HN, Ratcliffe MB, Guccione JM. Effect of adjustable passive constraint on the failing left ventricle: a finite-element model study. Ann Thorac Surg 2010;89:132.

[10] Chung C, Mesa J, Miller GJ, Randolph MA, Gill TJ, Burdick JA. Effects of auricular chondrocyte expansion on neocartilage formation in photocrosslinked hyaluronic acid networks. Tissue Eng 2006;12:2665.

[11] Chung C, Mesa J, Randolph MA, Yaremchuk M, Burdick JA. Influence of gel properties on neocartilage formation by auricular chondrocytes photoencapsulated in hyaluronic acid networks. J Biomed Mater Res A 2006;77:518.

[12] Chung C, Burdick JA. Influence of three-dimensional hyaluronic acid microenvironments on mesenchymal stem cell chondrogenesis. Tissue Eng Part A 2009;15:243.

[13] Chung C, Erickson IE, Mauck RL, Burdick JA. Differential behavior of auricular and articular chondrocytes in hyaluronic acid hydrogels. Tissue Eng Part A 2008;14:1121.

[14] Bian L, Zhai DY, Tous E, Rai R, Mauck RL, Burdick JA. Enhanced MSC chondrogenesis following delivery of TGF-β3 from alginate microspheres within hyaluronic acid hydrogels in vitro and in vivo. Biomaterials 2011;32:6425.

[15] Erickson IE, Huang AH, Chung C, Li RT, Burdick JA, Mauck RL. Differential maturation and structure-function relationships in mesenchymal stem cell- and chondrocyte-seeded hydrogels. Tissue Eng Part A 2009;15:1041.

[16] Marklein RA, Burdick JA. Controlling stem cell fate with material design. Adv Mater 2010;22:175.

[17] Masters KS, Shah DN, Leinwand LA, Anseth KS. Crosslinked hyaluronan scaffolds as a biologically active carrier for valvular interstitial cells. Biomaterials 2005;26:2517.

[18] Rodriguez KJ, Piechura LM, Masters KS. Regulation of valvular interstitial cell phenotype and function by hyaluronic acid in 2-D and 3-D culture environments. Matrix Biol 2011;30:70.

[19] Tous E, Ifkovits JL, Koomalsingh KJ, Shuto T, Soeda T, Kondo N, Gorman JH, 3rd, Gorman RC, Burdick JA. Influence of injectable hyaluronic acid hydrogel degradation behavior on infarction-induced ventricular remodeling. Biomacromolecules 2011;12:4127.

[20] Tous E, Purcell B, Ifkovits JL, Burdick JA. Injectable acellular hydrogels for cardiac repair. J Cardiovasc Transl Res 2011;4:528.

[21] Khetan S, Burdick J. Cellular encapsulation in 3D hydrogels for tissue engineering. J Vis Exp 2009;32:1590.

[22] Khetan S, Burdick JA. Patterning network structure to spatially control cellular remodeling and stem cell fate within 3-dimensional hydrogels. Biomaterials 2010;31:8228.

[23] Khetan S, Chung C, Burdick JA. Tuning hydrogel properties for applications in tissue engineering. Conf Proc IEEE Eng Med Biol Soc 2009;2009:2094-6.

[24] Toole BP. Hyaluronan: from extracellular glue to pericellular cue. Nat Rev Cancer 2004;4:528.

[25] Chen WY, Abatangelo G. Functions of hyaluronan in wound repair. Wound Repair Regen 1999;7:79.

[26] Fraser JR, Laurent TC, Laurent UB. Hyaluronan: its nature, distribution, functions and turnover. J Intern Med 1997;242:27.

[27] Laurent TC, Fraser JR. Hyaluronan. FASEB J 1992;6:2397.

[28] Volpi N, Schiller J, Stern R, Soltes L. Role, metabolism, chemical modifications and applications of hyaluronan. Curr Med Chem 2009;16:1718.

[29] Burdick JA, Chung C, Jia X, Randolph MA, Langer R. Controlled degradation and mechanical behavior of photopolymerized hyaluronic acid networks. Biomacromolecules 2005;6:386.

[30] Sahoo S, Chung C, Khetan S, Burdick JA. Hydrolytically degradable hyaluronic acid hydrogels with controlled temporal structures. Biomacromolecules 2008;9:1088.

[31] Shu XZ, Liu Y, Luo Y, Roberts MC, Prestwich GD. Disulfide cross-linked hyaluronan hydrogels. Biomacromolecules 2002;3:1304.

[32] Jha AK, Hule RA, Jiao T, Teller SS, Clifton RJ, Duncan RL, Pochan DJ, Jia X. Structural analysis and mechanical characterization of hyaluronic acid-based doubly cross-linked networks. Macromolecules 2009;42:537.

[33] Pouyani T, Prestwich GD. Functionalized derivatives of hyaluronic acid oligosaccharides: drug carriers and novel biomaterials. Bioconjug Chem 1994;5:339.

[34] Vercruysse KP, Marecak DM, Marecek JF, Prestwich GD. Synthesis and in vitro degradation of new polyvalent hydrazide cross-linked hydrogels of hyaluronic acid. Bioconjug Chem 1997;8:686.

[35] Burdick JA, Prestwich GD. Hyaluronic acid hydrogels for biomedical applications. Adv Mater 2011;23:H41.

[36] Temenoff JS, Kasper FK, Mikos AG. Fumarate-based macromers as scaffolds for tissue engineering. Top Tissue Eng 2007;3:16.

[37] Blakely B, Hoon Lee B, Riley C, McLemore R, Pathak CP, Vernon BL. Formulation and characterization of radio-opaque conjugated in situ gelling materials. J Biomed Mater Res B Appl Biomater 2010;93:9.

[38] Lee BH, Leon C, McLemore R, Macias JV, Vernon BL. Synthesis and characterization of thermo-sensitive radio-opaque poly(N-Isopropylacrylamide-co- PEG-2-Iodobenzoate). J Biomater Sci Polym Ed 2011;22:2357.

[39] CM Leon BL, M Preul, R McLemore. Synthesis and characterization of radio-opaque thermosensitive poly[N-isopropylacrylamide-2,2'-(ethylenedioxy)bis(ethylamine)-2,3,5-triiodobenzaminde. Polym Int 2009;58:847.

[40] Yu SB, Watson AD. Metal-based x-ray contrast media. Chem Rev 1999;99:2353.

[41] Maidment ADA. X-rays. In: Bryan RN, editor. Introduction to the Science of Medical Imaging. NY: Cambridge University Press, 2010. p.133.

[42] James NR, Philip J, Jayakrishnan A. Polyurethanes with radiopaque properties. Biomaterials 2006;27:160.

[43] Mottu F, Rufenacht DA, Laurent A, Doelker E. Iodine-containing cellulose mixed esters as radiopaque polymers for direct embolization of cerebral aneurysms and arteriovenous malformations. Biomaterials 2002;23:121.

[44] Davy KW, Anseau MR, Berry C. Iodinated methacrylate copolymers as X-ray opaque denture base acrylics. J Dent 1997;25:499.

[45] Joseph PM. Exogenous contrast agents: Contrast agents for x-ray and MR imaging. In: Bryan RN, editor. Introduction to the Science of Medical Imaging. NY: Cambridge University Press, 2010. p.183.

[46] Mottu F, Rufenacht DA, Doelker E. Radiopaque polymeric materials for medical applications. Current aspects of biomaterial research. Invest Radiol 1999;34:323.

[47] Wehrli FW. Magnetic resonance imaging. In: Byran RN, editor. Introduction to the Science of Medical Imaging. NY: Cambridge University Press, 2010. p.160.

[48] Dixon JA, Spinale FG. Large animal models of heart failure: a critical link in the translation of basic science to clinical practice. Circ Heart Fail 2009;2:262.

[49] Thorek DL, Chen AK, Czupryna J, Tsourkas A. Superparamagnetic iron oxide nanoparticle probes for molecular imaging. Ann Biomed Eng 2006;34:23.

[50] Cheng Z, Thorek DL, Tsourkas A. Gadolinium-conjugated dendrimer nanoclusters as a tumor-targeted T1 magnetic resonance imaging contrast agent. Angew Chem Int Ed Engl 2010;49:346.

[51] Frullano L, Meade TJ. Multimodal MRI contrast agents. J Biol Inorg Chem 2007;12:939.

[52] Xu Q, Zhu L, Yu M, Feng F, An L, Xing C, Wang S. Gadolinium(III) chelated conjugated polymer as a potential MRI contrast agent. Poymer 2010;51:1336.

[53] Elias DR, Cheng Z, Tsourkas A. An intein-mediated site-specific click conjugation strategy for improved tumor targeting of nanoparticle systems. Small 2010;6:2460.

[54] Neuberger T, Schopf B, Hofmann H, Hofmann M, von Rechenberg B. Superparamagnetic nanoparticles for biomedical applications: Possibilities and limitations of a new drug delivery system. J Magn and Magn Mater 2005;293:483.

[55] Springer F, Martirosian P, Schwenzer NF, Szimtenings M, Kreisler P, Claussen CD, Schick F. Three-dimensional ultrashort echo time imaging of solid polymers on a 3-Tesla whole-body MRI scanner. Invest Radiol 2008;43:802.

[56] Platzer M, Ozegowski JH, Neubert RH. Quantification of hyaluronan in pharmaceutical formulations using high performance capillary electrophoresis and the modified uronic acid carbazole reaction. J Pharm Biomed Anal 1999;21:491.

[57] Yushkevich PA, Piven J, Hazlett HC, Smith RG, Ho S, Gee JC, Gerig G. User-guided 3D active contour segmentation of anatomical structures: significantly improved efficiency and reliability. Neuroimage 2006;31:1116.

[58] Sled JG, Zijdenbos AP, Evans AC. A nonparametric method for automatic correction of intensity nonuniformity in MRI data. IEEE Trans Med Imaging 1998;17:87.

[59] Tustison NJ, Avants BB, Cook PA, Zheng Y, Egan A, Yushkevich PA, Gee JC. N4ITK: improved N3 bias correction. IEEE Trans Med Imaging 2010;29:1310.

[60] Avants BB, Tustison NJ, Wu J, Cook PA, Gee JC. An open source multivariate framework for n-tissue segmentation with evaluation on public data. Neuroinformatics 2011;9:381.

[61] Vannier MW, Butterfield RL, Jordan D, Murphy WA, Levitt RG, Gado M. Multispectral analysis of magnetic resonance images. Radiology 1985;154:221.

[62] Raj B, Jayakumar T, Thavasimuthu M. Real time radiography. Practical Non-Destructive Testing. New Delhi: Woodhead Publishing 2002.

[63] Hainfeld JF, Slatkin DN, Smilowitz HM. The use of gold nanoparticles to enhance radiotherapy in mice. Phys. Med. Biol. 2004;49:N309.

[64] Manju S, Sreenivasan K. Enhanced drug loading on magnetic nanoparticles by layer-by-layer assembly using drug conjugates: blood compatibility evaluation and targeted drug delivery in cancer cells. Langmuir 2011;27:14489.

CHAPTER 5

A Mechanical and Finite Element Assessment of Methacrylated Hyaluronic Acid Hydrogels in Treating Left Ventricular Remodeling

5.1 Introduction

In Chapter 4, we employed non-contrast magnetic resonance imaging (MRI) to visualize methacrylated hyaluronic acid (MeHA) hydrogels in myocardial explants. Volume data demonstrated that all hydrogels (to a degree) distributed with tissue fibers; thus, these regions will be referred to as hydrogel/tissue composites for the remainder of this chapter. As discussed in Section 4.1.1, finite element (FE) models can incorporate material volume, injection distribution, and mechanical data to generate representative injections and theoretically assess their influence on stress levels in left ventricular (LV) remodeling [1, 2]. Here, the goal is to continue acquiring data for FE modeling; specifically, the same four hydrogel formulations (low MeHA, low A/T, high MeHA, low A/T, low MeHA, high A/T, and high MeHA, high A/T, where A= ammonium persulfate (APS) and T= N,N,N,N',N'-tetramethylethylenediamine (TEMED)) will similarly be injected into explants and mechanically tested (e.g., compressive and biaxial) to investigate the mechanical properties of the hydrogel/tissue composites.

With this data and information on composite volumes (from Chapter 4) and injection distribution (previously reported [3]), the efficacy of each treatment to limit LV remodeling will be theoretically evaluated in a FE model and compared to no treatment by quantifying subsequent stress reductions. As discussed in Chapter 1, increased stress due to geometric alterations induces a positive feedback loop exacerbating

remodeling and eventually the potential for heart failure (HF); this work will ultimately provide more insight on how material treatment specifically mitigates increased stresses.

5.1.1 Mechanical Testing of Myocardial Tissue

The material properties of the myocardium are an important determinant in its global function. Specifically, studies have demonstrated that both the amount and type of stiffening (e.g., isotropic, anisotropic), both due to pathological processes and injection to treat these processes, influence stress and functional outcomes [1, 2, 4-6]. In order to accurately assess these properties in myocardial tissue it is important to select a model that is representative of the loads that the heart experiences *in vivo*. To date, myocardial mechanics have been reported using a variety of techniques including atomic force microscopy (AFM) [7, 8], compressive testing [3], uniaxial testing [3, 9], and biaxial testing [9-14]. While methods such as AFM and one-dimensional compressive and uniaxial testing have contributed to our understanding of fundamental cardiac mechanics, they are limited in that they only provide information on local (AFM) or unidirectional mechanics (compressive and uniaxial). Like many soft tissues, the myocardium is mechanically anisotropic [10-12, 14-18], being stiffer in the fiber direction (circumferential) compared to the cross-fiber direction (longitudinal) and is referred to as transversely isotropic. Hence, the described unidirectional methods to assess mechanics are insufficient to evaluate the myocardium's multiaxial properties. The anisotropic nature of the myocardium has been implicated in LV remodeling where studies have shown that the infarct can heal both in an isotropic and anisoptropic manner depending on the animal model [4, 6, 10, 13]. Interestingly, in a recent theoretical study, Fomovsky et al. altered the mechanics of the infarcted myocardium in an isotropic and anisotropic manner (e.g., increasing the stiffness in either the

circumferential or longitudinal direction) and demonstrated that directional stiffening influences the extent of myocardial function with an optimal stroke volume occurring with longitudinal stiffening [5]. Biaxial testing provides us with the ability to simulate the multiaxial loading experienced physiologically by the heart so that we can accurately assess the influence of material injection on its mechanical properties.

5.1.2 Biaxial Testing: Sample and Test Design

Biaxial testing is a versatile technique that has been employed to test numerous biological tissues [10-14, 19-27]. Sample preparation is generally consistent across applications; thin tissues (usually 1 mm and no larger than 3 mm in thickness) are typically tested under strain control (instead of load control) that is optically tracked to avoid mechanical interferences [17, 18]. Strain control entails optically tracking the displacement of markers on the tissue (or grips) at a predefined strain rate and range of strain (or until a maximum load is reached). This will be discussed in more detail later in this section.

Myocardial tissue is generally tested in trampoline-like fashion, where sutures are hooked directly through the tissue edge and threads tied on their free ends attach to motors that apply load to the tissue [11, 12, 17, 18]. Markers to optically control strain are secured directly onto the center of the tissue (away from the hooks) where the stress and strain fields are generally considered to be homogenous. This approach is advantageous for myocardium testing because it allows for all edges of the sample to freely expand while accurately controlling the applied strain [17, 18]. In cases where tissues are heterogeneous, however, markers for protocol optical tracking cannot be placed on the tissue due to influences on predefined strain control parameters from variations in the tissue strain.

As reported in Chapter 4, MeHA hydrogels dispersed throughout myocardial tissue in an initiator concentration and macromer percent modification (at low initiator) dependent manner. While trends were observed in hydrogel volumes and most samples took on an ellipsoidal geometry, observed variations in the distributions could potentially influence sample testing if tested in the typical trampoline-like manner that is employed for tissue with homogenous strain fields. Furthermore, hydrogel incorporation made it difficult to secure sutures onto composites due to the inability of the suture to hook onto regions where there was prominent hydrogel present. To circumvent these concerns and ensure that testing of hydrogel/tissue composites was consistent for all groups, alternative biaxial testing techniques were explored for this investigation.

We specifically explored clamp-like grips that could be directly secured (e.g., glued) to the tissue, so that markers could be attached to the grip to provide optimal strain control. These types of grips also offered an alternative point of attachment, obviating concerns of sutures ripping through the hydrogel portion of the composite. However, while clamp-like grips could overcome problems such as testing heterogeneous tissues and those susceptible to ripping, they also had drawbacks that needed to be considered.

A major disadvantage in typical clamp-like grips is that due to their tab-like geometry, they restrict free expansion of samples edges [28, 29]. To avoid this problem, a finger-like grip design (developed by Dr. Dawn Elliott's group at the University of Pennsylvania) was employed [30]. Typical grip tabs were converted into "fingers" to allow edges to freely expand at the loads that would be applied to this system. Additionally, while grip-to-grip strains (i.e., optically computed strain from the markers on the grips) could be used to provide consistent strain conditions for test protocols, they do not necessarily represent the strain experienced by the tested tissue. To overcome this,

we computed tissue strains by performing post-test strain analysis with image correlation on samples that were speckle coated before testing [20]. Specifically, tissues were tested by optically tracking markers on grips (grip-to-grip strains); after testing, the images were analyzed to measure displacements of speckled regions, which were then used to compute a deformation gradient tensor **F** for that image [15, 17, 18]. **F** can then be used to compute strains, which will be discussed in more detail in Section 5.1.3.

5.1.3 Biaxial Testing: Kinematics and Stresses

*In this section capital letters in bold will be used to define tensors and vectors and scalars will be represented as normal text.

The computation of strain for biaxial testing is based on the displacement of the tracked markers and tissue deformation is generally described by the deformation gradient tensor **F**. In general, the bidirectional components for displacements are described by Equations 5.1 and 5.2 where **x** and **X** are the position vectors at the deformed and reference states, respectively, and λ_i and κ_i are components of **F** that correspond to the axial stretch ratio and measure of in-plane shear, respectively [17, 18, 21].

$$x_1 = \lambda_1 X_1 + \kappa_1 X_2 \tag{5.1}$$

$$x_2 = \lambda_2 X_2 + \kappa_2 X_1 \tag{5.2}$$

The deformation gradient tensor **F** is dependent on these displacements as shown in Equation 5.3.

$$\mathrm{F} = \begin{bmatrix} \frac{\partial x_1}{\partial X_1} & \frac{\partial x_1}{\partial X_2} \\ \frac{\partial x_2}{\partial X_1} & \frac{\partial x_2}{\partial X_2} \end{bmatrix} = \begin{bmatrix} \lambda_1 & \kappa_1 \\ \kappa_2 & \lambda_2 \end{bmatrix} \tag{5.3}$$

The right Cauchy-Green deformation tensor can be calculated from **F** and is defined as $\mathbf{C}=\mathbf{F}^{\mathrm{T}}\bullet\mathbf{F}$. It can be used to calculate the Green-Lagrange strain tensor **E**, which is the most common finite strain measure used to analyze soft biological tissues due to its simple incorporation in constitutive models (**E**= ½ (**C**-**I**), where **I** is the identity tensor) [17, 18]. **E** can also be derived directly from the components of **F** as shown by the two-dimensional (2-D) Green-Lagrange strain components in Equations 5.4, 5.5, and 5.6 [17, 18, 21].

$$\mathrm{E}_{11} = \frac{1}{2}\left(\lambda_1^2 + \kappa_2^2 - 1\right) \tag{5.4}$$

$$\mathrm{E}_{22} = \frac{1}{2}\left(\lambda_2^2 + \kappa_1^2 - 1\right) \tag{5.5}$$

$$\mathrm{E}_{12} = \frac{1}{2}\left(\lambda_1\kappa_1 + \lambda_2\kappa_2\right) \tag{5.6}$$

To experimentally gain information on the stiffness of the tested specimen, the first Piola-Kirchhoff stress tensor **T** can be computed directly from the initial tissue dimensions (cross-sectional area of each loaded side) and measured axial forces **P**

acquired from biaxial testing. The components of **T** are defined in Equations 5.7 and 5.8, where h is the thickness and L_i is the tissue length [17, 18, 21].

$$T_{11} = \frac{P_1}{hL_2} \tag{5.7}$$

$$T_{22} = \frac{P_2}{hL_1} \tag{5.8}$$

Due to load application being normal to the specimen edges, T_{12} and T_{21} are zero. **T** can later be employed with **F** to determine second Piola-Kirchhoff stress **S** (**S=TF**$^{-1}$), which will be discussed in more detail in the next section where it is implemented in the development of constitutive models [17, 18].

A similar concept as described in this section is generally applied to calculate tissue strains; rather than representing displacements from the tracked markers, initial displacements are computed from speckled regions [20].

5.1.4 Constitutive Modeling of Biological Tissues

In 1974, Lanir and Fung pioneered the field of biaxial testing by performing the first experimental studies on biological tissues [22, 23]; shortly after, these findings were employed to develop a constitutive model [31]. From their experimental findings (e.g., strain rate independent hysteresis and curve geometry), they determined that a strain-energy function W could be developed to model the stress-strain relationship for biological tissues [18, 32]. The same group later proposed a simplified exponential form of W that adequately fits experimental data (Equation 5.9), where C is a constant

(defined in the next section in terms of the passive myocardium) and Q is a non-linear function of the Green-Lagrange strain components [17, 18, 33].

$$W = \frac{C}{2}\left(\exp(Q) - 1\right) \tag{5.9}$$

5.1.4.1 Constitutive Modeling of the Myocardium

Passive Myocardium

Early biaxial testing on the ventricular myocardium by Yin et al. confirmed that the passive (i.e., diastolic, non-contracting) myocardium displayed a similar stress-strain relationship, anisotropy, and strain-rate independence to characteristic biological tissues described in the previous section [14, 32]. Modeling the myocardium as transversely isotropic with respect to the fiber direction (anisotropic), nearly incompressible and hyperelastic, Guccione et al. later applied these findings to the work of Fung et al. to derive a version Q to input into the simplified form of W (Equation 5.9). With the incorporation of the newly derived Q, the final derivation of W was optimal to represent the mechanical properties of the three-dimensional (3-D) passive myocardium [32]. The commonly applied form of Q for recent FE modeling of the passive myocardium [1, 2, 34-36] is depicted in Equation 5.10, where E_{11} is circumferential strain, E_{22} is longitudinal in-plane strain, E_{33} is radial strain, and the remaining strain components are shear strains. The variables b_f, b_t, and b_{fs} are diastolic myocardial material parameters; specifically, b_f and b_t are associated with stiffness in the circumferential and longitudinal directions, respectively (i.e., material stiffness is directionally increased by increasing b_f or b_t) and b_{fs} is directly related to the rigidity of the material under shear.

$$Q = b_f E_{11}^2 + b_t (E_{22}^2 + E_{33}^2 + E_{23}^2 + E_{32}^2) + b_{fs} (E_{12}^2 + E_{21}^2 + E_{13}^2 + E_{31}^2) \quad (5.10)$$

When Equations 5.9 and 5.10 are combined, the constitutive model W can be employed to describe the passive myocardium where C is also a diastolic material property that scales the stresses (Equation 5.11) [32, 34].

$$W = \frac{C}{2}(\exp(b_f E_{11}^2 + b_t (E_{22}^2 + E_{33}^2 + E_{23}^2 + E_{32}^2) + b_{fs} (E_{12}^2 + E_{21}^2 + E_{13}^2 + E_{31}^2)) - 1) \quad (5.11)$$

Active Myocardium

The active myocardium (i.e., systolic, contracting) is generally modeled as nearly incompressible, transversely isotropic (anisotropic with respect to the fiber direction) and hyperelastic [1, 2, 35-38]. The commonly applied constitutive laws for modeling of the active myocardium also stem from the work of Guccione et al. [37, 38]. Their work led to a derivation for systolic contraction, which was modeled as the sum of the passive stress derived from W (Equation 5.11) and an active fiber directional component T_0 and is defined in Equation 5.12. In the developed model, T_0 is a function of time, t, peak intracellular calcium concentration, Ca_0, sarcomere length, l, and the maximum isometric tension achieved at the longest sarcomere length T_{max}. The additional variables in the equation are as follows: **S** is the second Piola-Kirchhoff stress tensor (introduced in Section 5.1.3), p is the hydrostatic pressure as the Lagrange multiplier to ensure incompressibility, J is the Jacobian of the deformation gradient tensor, **C** is the right Cauchy-Green deformation tensor (introduced in Section 5.1.3), Dev is the deviatoric projection operator, and $\hat{W}$ is the deviatoric contribution of W.

$$\mathrm{S} = pJ\mathrm{C}^{-1} + 2J^{-2/3}\mathrm{Dev}\left(\frac{\partial \tilde{W}}{\partial \mathrm{C}}\right) + T_0\left\{t, Ca_0, l, T_{\max}\right\} \quad (5.12)$$

Altering Passive and Active Myocardium Material Properties

As previously described, the constitutive laws for the passive (Equation 5.11) and active (Equation 5.12) myocardium can be applied to examine the influence of alterations in mechanical and contractile properties, respectively, on outcomes such as stress in the myocardium. Colleagues have varied the diastolic myocardial material parameters C, b_t, b_f, and b_{fs} to simulate adjustments in myocardium stiffness [1]. Systolic parameters have also been altered to model variations in contraction due to both the physiological state of the heart (i.e., normal vs. weakened) or volume additions to the wall [1, 35, 36]. In 2009, Wenk et al. developed a model that incorporated polymer inclusions; in addition to their mechanical properties and volume, the number and distribution of inclusions could also be altered (refer to Chapter 3, Figure 3.2) [2]. This advanced model furthered the field of myocardial modeling by providing control over more variables to better study the influence of injectable biomaterials.

In this chapter, we will first report the outcomes of mechanical testing (compressive and biaxial) of MeHA hydrogel/tissue composites. While compressive testing has been employed in the past to assess the mechanics of tissue composites [3], to our knowledge, this is the first study to perform multiaxial testing to evaluate the influence of an injectable biomaterial on myocardium mechanics. After assessing the general influence of hydrogel incorporation on moduli, this data will be applied to

compute the diastolic myocardial material parameters (C, b_f, and b_t) for each composite formulation for their theoretical assessment.

The theoretical portion of this chapter will be two-fold. Both portions will employ a modified version of the already established FE model by Wenk et al. [2], where hydrogel/tissue composite mechanical parameters, volumes and their distribution [3] can all be adjusted to better model the influence of MeHA hydrogel treatments on stress levels in the dilated LV. First, treatment of the MeHA formulations (low and high MeHA, low A/T) previously studied by Ifkovits et al. will be theoretically modeled to correlate their influence on stress to their *in vivo* geometric outcomes [3]. Many studies in the field assume that experimental outcomes such as decreases in ventricle dilation and increases in wall thickness directly correlate to reduction in myocardial stress (as per the Law of Laplace discussed in Chapter 3). Here, we further investigate this paradigm by evaluating the benefits of two MeHA hydrogel formulations both experimentally (i.e., *in vivo*) and theoretically. The second portion of the theoretical assessment in this chapter will provide more insight on injectable biomaterial design criteria; two additional MeHA hydrogel formulations with faster gelation (low and high MeHA, high A/T) will be modeled to further assess the influence of hydrogel mechanics and also distribution on myocardial stress (limitations in this theoretical model will be discussed in both Methods and Chapter 9). Here, we demonstrate an innovative approach that incorporates *in vitro* hydrogel/tissue composite data into a theoretical model to validate and better understand the outcomes of *in vivo* models such as that by Ifkovits et al. [3]. Furthermore, this technique can be employed as a tool to optimize material design, specifically material properties, for development of better therapies to treat LV remodeling.

5.2 Materials and Methodology

5.2.1 Methacrylated Hyaluronic Acid (MeHA) Synthesis, Hydrogel Formation and Characterization

Two MeHA macromers were synthesized as described in Chapter 4 [39] and their percent modification (~30% and ~60%) was assessed by ^{1}H NMR (Bruker, 360 MHz). Macromers were crosslinked with the same oxidation-reduction (redox) initiators introduced in Chapter 4 (APS (A) and TEMED (T)) at either a low or high concentration (low A/T, 5/5 mM and high A/T 12.5/6.25 mM). Similar to Chapter 4, initial compressive testing on MeHA hydrogels was performed at a strain rate of 10%/min, and moduli were calculated as the slope of the stress-strain curve at 10-20% strain.

5.2.2 In Vitro Assessment of Hydrogel/Tissue Composite Mechanics

The influence of hydrogel delivery and addition on the mechanical properties of myocardium was assessed in explanted ovine myocardial tissue from the LV. Similar to imaging work, 0.3 mL of precursor solutions were injected in explants 3 minutes after initiator addition. Thirty minutes after injection, samples were collected for compressive and biaxial testing.

5.2.2.1 Compressive Testing

For compressive testing, cylindrical (~5 mm diameter) composite samples (n=3-4/group) were collected via a biopsy punch. Testing was performed with the same protocol as non-composite hydrogels as described in Section 5.2.1.

5.2.2.2 Biaxial Testing

Sample Preparation

For biaxial testing, a total of 5 samples (maximum of 2 per injection) were tested per group: (1) control myocardium, (2) low MeHA, low A/T, (3) high MeHA, low A/T, (4) low MeHA, high A/T, and (5) high MeHA, high A/T. Samples were collected from the myocardial region and trimmed to ~7 X 7 mm^2 with a thickness ~2 mm. Average thickness values were calculated to compute cross-sectional areas to later determine the first Piola-Kirchhoff stresses (discussed in more detail in the Experimental Data Analysis portion of this section). The surface of each sample was speckle-coated with Verhoeff's stain for post-test tissue strain analysis with digital image correlation (Figure 5.1A). As a point of attachment for mechanical testing, finger-like grips were made out of waterproof sandpaper (T214 Norton) (~75x5 mm^2) to allow for free expansion of sample edges. Slabs were folded in half, and 3, 25x1 mm "fingers" were excised at the free end so that 6 "fingers" in total (3 on the top and 3 on the bottom) were formed. Grips were painted white to enhance contrast and glued (Locite 454) onto the bottom and top of each side of the tissue samples with about 1 mm overlap between the grip and tissue. Brass 0.5 mm markers (Small Parts) were painted black for contrast and placed on the middle "finger" of each group (4 markers in total) (Figures 5.1A and 5.1B). Before testing, samples were equilibrated for ~1 hour in phosphate buffered saline (PBS) at room temperature (RT).

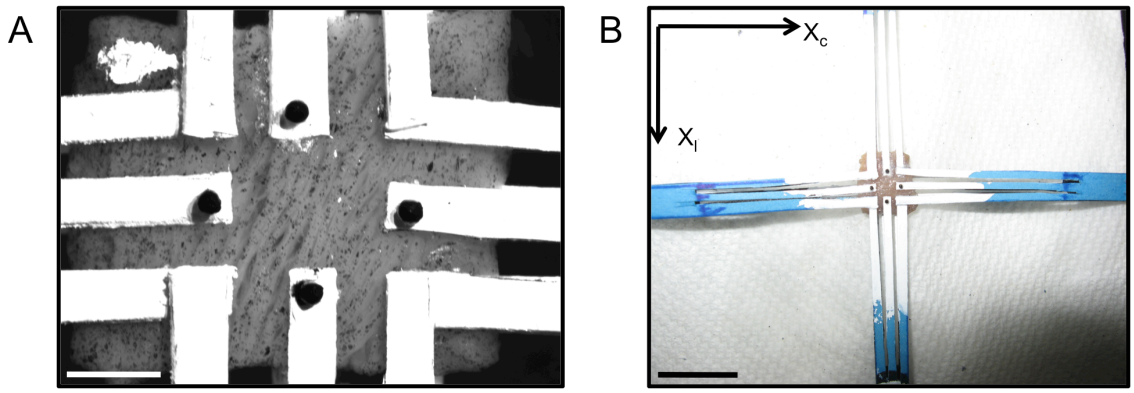

Figure 5.1 Representative images of biaxial sample preparation. Speckle-coated hydrogel/tissue composite (with finger-like grips and tracking markers) mounted on a biaxial apparatus at 0 grip-to-grip strain (A). Zoomed out view of specimen ready for biaxial mounting (B). Scale bar= 1.5 mm (A) and scale bar= 10 mm (B). Representative sample= low MeHA, high A/T formulation.

Biaxial Testing

In general, grip-to-grip strains were optically tracked by following the 4 markers and provided consistent strain conditions for testing. Tissue strains were acquired by tracking the speckle-coat on the tissue surface after biaxial testing. Samples were all tested in PBS at RT and placed in the same orthogonal (longitudinal and circumferential) orientation with respect to the myocardium for all testing.

For testing, silk (2-0) sutures were folded in half and secured through the free end of each sandpaper grip by metal hooks. The looped ends of the sutures were then hooked around the pulleys attached to the motors of the custom biaxial device [19]. Four independent motors (controlled by LabVIEW software) applied strain to the myocardial samples in both the circumferential and longitudinal directions, while a high-resolution digital camera with a telecentric lens (NT63-730, Edmund Optics) tracked the

black markers on the middle tabs to track strains. Testing was performed by grip-to-grip strain control; all samples were preconditioned, exposed to a 1 hour hold, and then tested. Each sample was preconditioned by pre-straining to 0.01 equibiaxial strain and then equibiaxially straining to 0.20 for 5 cycles at 0.10 strain/min. Immediately after preconditioning, samples were subjected to a 1 hour hold where no load was applied and samples were allowed to freely contract in both directions. The test protocol was identical to the preconditioning parameters; data and images from the final loading curve of each test were used for experimental data analysis.

Experimental Data Analysis

All moduli calculations were based on orienting samples for tests according to their original orthogonal orientation in the myocardium. For most samples, this corresponded to the expected fiber direction (e.g., against fibers for longitudinal and with fibers for circumferential).

Grip-to-grip stress-strain curves were formed from the optically tracked data collected from the labVIEW interface. Curves and moduli in both the longitudinal and circumferential directions were determined for three ranges of Green-Lagrange strains (0.05-0.10, 0.10-0.15, and 0.15-0.20). First Piola-Kirchhoff stresses were determined by dividing the cross-sectional areas of each sample length by the load values calculated by labVIEW in the corresponding direction.

To calculate tissue strains, 2-D displacement maps (Figure 5.2) were first developed using the speckle-coated surface via digital image correlation (Vic2D 2009, Correlated Solutions). A single deformation gradient tensor **F** was calculated from the displacement map of each image by finding the least-squares solution to the system of equations with a Matlab algorithm developed and described by Szczesny et al. [20]. The

deformation gradient tensor **F** for each image was used to compute the tissue Green-Lagrange strains (as discussed in Introduction) in both the longitudinal and circumferential directions at that specific grip-to-grip strain. Stress-tissue strain curves and moduli were again obtained in three ranges of strains (0.05-0.10, 0.10-0.15, and 0.15-0.20). Stress-tissue strain raw data was applied to derive the parameters for FE modeling.

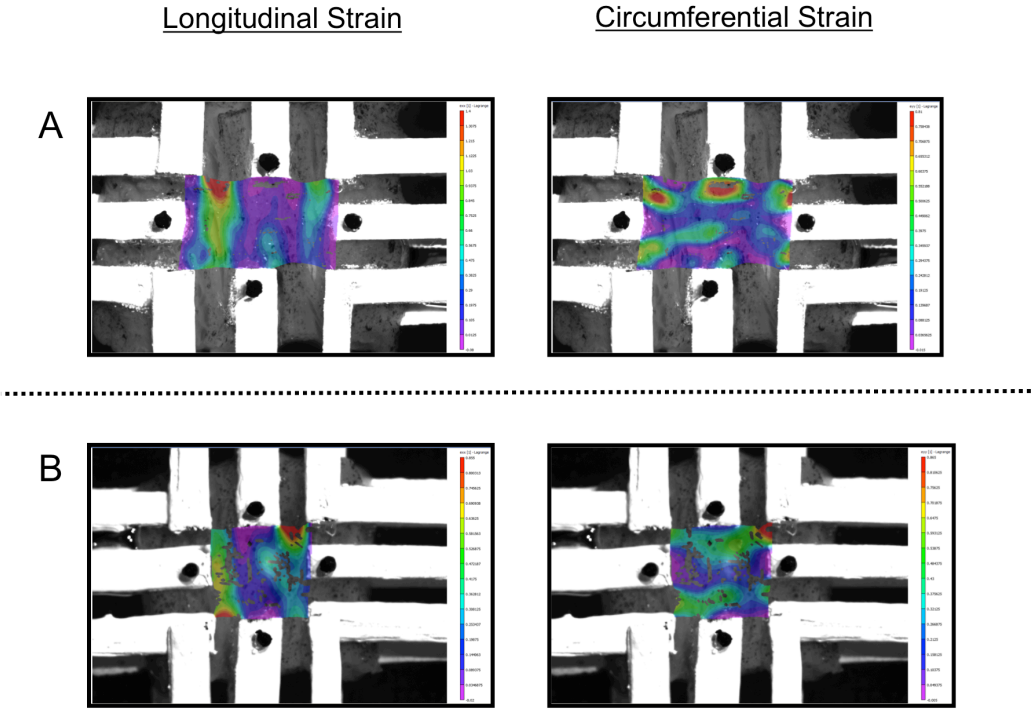

Figure 5.2 Representative two-dimensional displacement maps at 0.20 grip-to-grip strain for control myocardium (A) and hydrogel/tissue composites (low MeHA, high A/T) (B).

5.2.3 Theoretical Assessment of Hydrogel/Tissue Composites

5.2.3.1 Application and Derivation of Material Parameters

The constitutive model for the passive myocardium (Equation 5.11) was modified for curve fitting with 2-D data provided from biaxial tests; the E_{33} term was included due to incompressibility; however, shear strains were out of the plane of deformation and therefore these terms were removed. Iterations were performed to determine the most suitable diastolic myocardial material parameters (C, b_f, and b_t) for each MeHA hydrogel/tissue formulation and control myocardium (Table 5.1). The remaining terms in the original constitutive model (Equation 5.11) were obtained from previous reports [40]. These material properties were assigned as the material parameters for each component of the LV model (i.e., either composite injections or myocardial tissue).

Table 5.1 Summary of diastolic myocardial material parameters derived from biaxial data for FE modeling. *= formulations investigated by Ifkovits et al. [3].

Formulation	C (kPa)	b_f	b_t
Control Myocardium	0.51 ± 0.11	22.84 ± 6.26	3.46 ± 1.03
Low MeHA, Low A/T*	0.67 ± 0.31	13.06 ± 8.27	4.67 ± 3.89
High MeHA, Low A/T*	0.66 ± 0.24	18.59 ± 8.67	7.45 ± 1.53
Low MeHA, High A/T	0.81 ± 0.42	17.30 ± 4.70	4.69 ± 3.04
High MeHA, High A/T	1.05 ± 0.63	16.26 ± 5.22	9.48 ± 9.27

The systolic myocardial material parameters employed in this model were previously defined by Wenk et al. [2]. Tested myocardium was normal (not infarcted) and therefore (to ensure consistency with diastolic myocardial material parameters) selected systolic parameters assumed that all portions of the modeled heart (i.e., injection sites

and myocardium) had normal myocardium contractile properties. This limitation will be described more in Chapter 9 of this dissertation.

5.2.3.2 Finite Element (FE) Model

A 3-D FE model of the dilated LV was generated using a modified version of the model from Wenk et al. [2]. The injections were modeled as ellipsoidal, rather than spherical, based on composite geometries obtained from MRI data (Chapter 4) and the material properties in these regions were assumed to behave as a composite (i.e., the injection sites are a combination of myocardium and the hydrogel) (Figure 5.3A). A distribution pattern similar to that employed in previous *in vivo* studies by Ifkovits et al. was used (Figure 5.3B) [3]; specifically, there were 20 injection sites, with a pattern of 5 circumferential by 4 longitudinal (Figure 5.3C). Due to the incompressibility of the myocardium, to conserve volume with each injection the endocardial wall was thickened into the LV cavity.

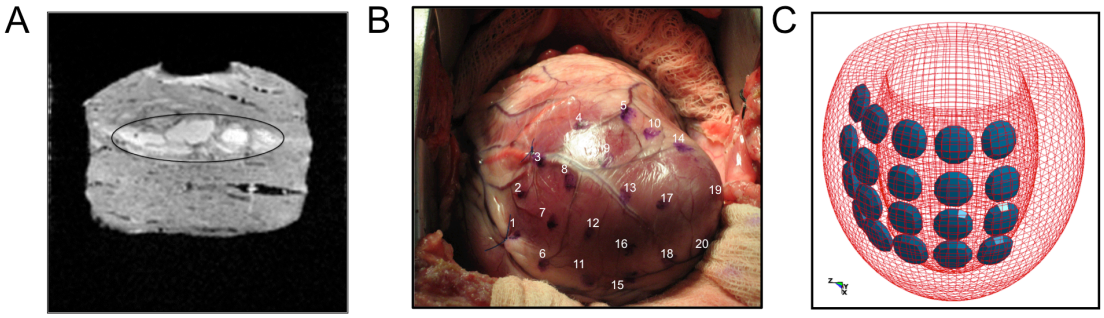

Figure 5.3 Representative cross-sectional view of a high MeHA, low A/T composite injection site in myocardium (A). Representative distribution of 20 injections from *in vivo* work by Ifkovits et al. [3] (B) and transparent view of modeled dilated LV with 20 injections (blue) for FE assessment (C).

Hydrogel/tissue composite volumes were based on the MRI data; however, due to limitations in the FE model, 20 injections with the calculated average volume of the high MeHA, low A/T and low and high MeHA, high A/T formulations could not be achieved. While the FE model mesh will be adjusted to accommodate these volumes for future analysis, in the context of this dissertation, volumes were adjusted for modeling. The following cases were considered:

1) For theoretical evaluation of the formulations assessed in the *in vivo* work of Ifkovits et al. (i.e., low and high MeHA, low A/T) [3], reported average volumes from Chapter 4 were decreased by half a standard deviation (SD) for their simulation. While this adjustment is not ideal, these volumes are still representative of the volumes injected *in vivo* and provide applicable information on the influence of their injection on stress reduction in the dilated LV. Adjusted volumes are reported in Table 5.2.

Table 5.2 Summary of injection volumes used to validate *in vivo* work of Ifkovits et al. [3]. Injection volumes equal each formulation's average volume minus half its SD.

Formulation	Volume (mm^3)
Low MeHA, Low A/T	220.0
High MeHA, Low A/T	339.0

2) The aforementioned solution could not be applied to assess the high initiator formulations due to their larger volumes. To gain a general idea on the relative differences between all four formulations, all cases were simulated with volumes equal to 60% of the average values (Table 5.3).

Table 5.3 Summary of injection volumes for relative comparisons between all groups. Injection volumes are equal to 60% of each formulation's average volume.

Formulation	Volume (mm^3)
Low MeHA, Low A/T	159.6
High MeHA, Low A/T	251.9
Low MeHA, High A/T	326.2
High MeHA, High A/T	337.0

5.2.3.3 Stress Assessment

All cases were run on either a 12-core or 32-core computer node. Stress in each formulation was assessed in the fiber and cross-fiber directions at end-diastole (ED) or end-systole (ES) and compared to a control simulation of a dilated LV with no treatment. For all cases, the volume average of these stress components was calculated in the following regions:

1) Global average over the entire LV, including injection sites.

2) Transmural average of a single injection site at the equator (Figure 5.4A, B).

3) Mid-wall average in a row of injections at the equator (Figure 5.4A, C).

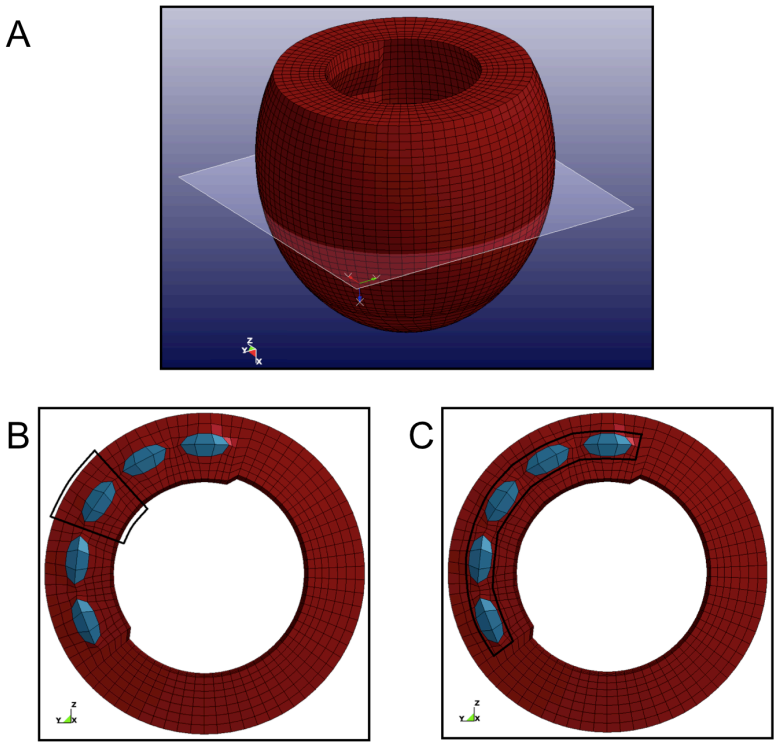

Figure 5.4 Plane near the equator where transmural and mid-wall stresses were calculated (A). Representative set of elements where transmural (B) and mid-wall (C) stresses were calculated.

5.2.4 Statistical Analysis

Data is presented as mean ± SD or mean ± SEM (standard error of the mean) as indicated in each figure legend. Changes in moduli (for compressive and biaxial testing) were assessed using a one-way ANOVA with Tukey's post hoc evaluation. For all comparisons, $p \leq 0.05$ was considered to be statistically significant.

5.3 Results and Discussion

5.3.1 Compressive Testing of MeHA Hydrogels and MeHA Hydrogel/Tissue Composites

Similar to the previous studies by Ifkovits et al., compressive testing on non-composite hydrogels and hydrogel/tissue composites was performed to provide information on MeHA hydrogel behavior in tissue [3]. Non-composite MeHA hydrogels displayed expected trends, where higher macromer percent modification and initiator concentration led to higher compressive moduli (Figure 5.5). Specifically, higher macromer modification at both low and high A/T resulted in higher mechanics compared to both low MeHA formulations, indicating that compressive mechanics in these hydrogels are more dependent on macromer functionalization. Compared to control myocardial explant tissue, significant differences were observed in all formulations except for low MeHA, low A/T, which displayed a comparable compressive modulus. As described in Chapter 4, macromer modification and initiator concentration both influence the formation of kinetic chains and, consequently, the bulk properties (e.g., mechanics) of the resulting hydrogels [41, 42]. Increasing either parameter results in more efficient crosslinking and subsequently higher mechanics [3, 41, 43]. Similar trends were observed in mechanical testing of composite tissue, but to a lesser degree (Figure 5.5). Increasing both macromer modification and initiator concentration resulted in higher mechanics, with higher moduli observed in high MeHA macromers. However, these differences were less pronounced relative to the MeHA alone groups; a statistically significant increase in modulus compared to myocardial explant tissue was only observed in the high MeHA, high A/T formulation. Overall, this work demonstrates that the addition of MeHA hydrogels to myocardial tissue results in a hydrogel/tissue composite with its own set of unique mechanical properties.

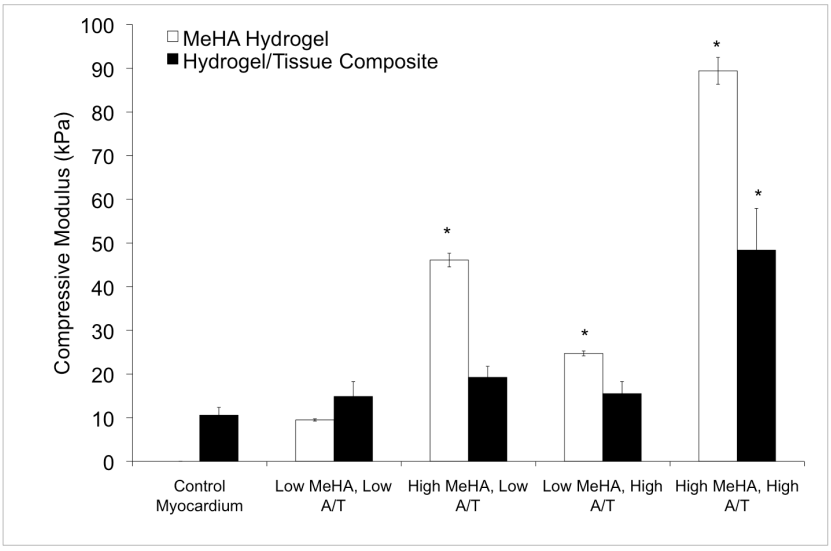

Figure 5.5 Compressive moduli for non-composite MeHA hydrogels and composite formulations compared to control myocardium. Data presented as mean ± SD. *p<0.05 vs. control myocardium.

5.3.2 Biaxial Testing of MeHA Hydrogel/Tissue Composites

5.3.2.1 Optimization of Biaxial Testing Parameters

Biaxial testing was performed as a means to acquire more physiologically relevant mechanical data for hydrogel/tissue composites. As discussed in Methods, composites were preconditioned, subjected to a 1 hour hold to allow for sample recovery, and then tested. To determine the required sample recovery time, samples were unloaded immediately after preconditioning and the strain was monitored in both directions while samples contracted (Figure 5.6A). A 1 hour hold was selected for recovery time, since by this time point following unloading, the sample strain reached equilibrium in both directions. As described in Methods, for preconditioning and testing,

samples were loaded based on strain (i.e., grip-to-grip strain), which was optically tracked. As specified by the labVIEW test protocol, samples were always strained to a reported grip-to-grip Green-Lagrange strain of 0.20 as indicated by the representative stress-strain curves in Figure 5.6B.

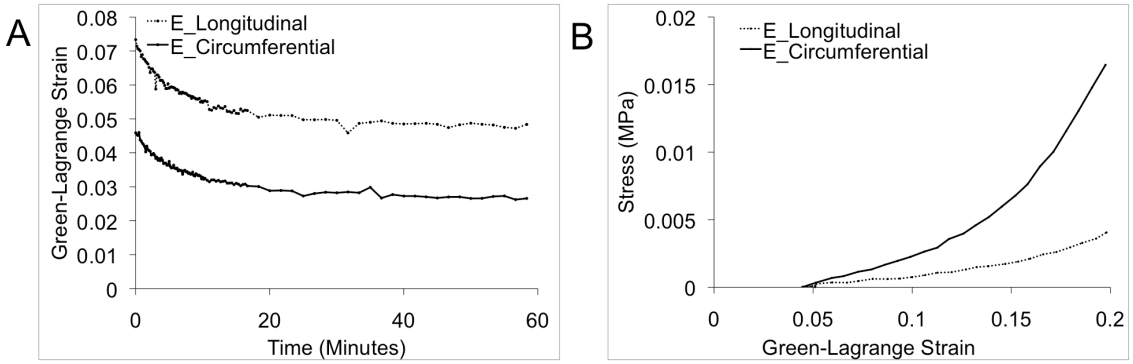

Figure 5.6 Representative time sweep of sample recovery (control myocardium) (A) and representative stress-strain curve for grip-to-grip strains (control myocardium) (B).

5.3.2.2 Grip-to-Grip Strain Analysis

Physiological strain has been reported to range from 0.10 to 0.15 [44-47]; to account for the lower and higher ends, a mechanical assessment was performed between 0.05 and 0.10 (Figure 5.7A) and between 0.10 and 0.15 (Figure 5.7B) Green-Lagrange strain, where 0.05-0.10 corresponded to the linear toe region in stress-strain curves. A strain range of 0.15-0.20 (Figure 5.7C), which generally corresponded to the second linear portion in stress-strain curves, was analyzed as an extreme case that could potentially simulate a hypertrophied borderzone. Mechanics were most influenced in the longitudinal direction for all strain ranges (Figure 5.7); in this direction, increases in macromer percent modification and initiator concentration (particularly at the two lower strain ranges) resulted in higher moduli compared to control myocardium. Statistically

significant differences compared to control myocardium were observed in the high MeHA, high A/T formulations between 0.05-0.10 (high MeHA, high A/T: 32.16 kPa vs. control myocardium: 11.75 kPa) and 0.10-0.15 (high MeHA, high A/T: 49.32 kPa vs.control myocardium: 15.10 kPa) strain. Differences in the circumferential direction were less pronounced; however, similar trends were observed in all groups except low MeHA, low A/T. The reported decreased modulus (in the circumferential direction) in the low MeHA, low A/T formulation is not completely understood; however, it may be a result of the decrease in anisotropy.

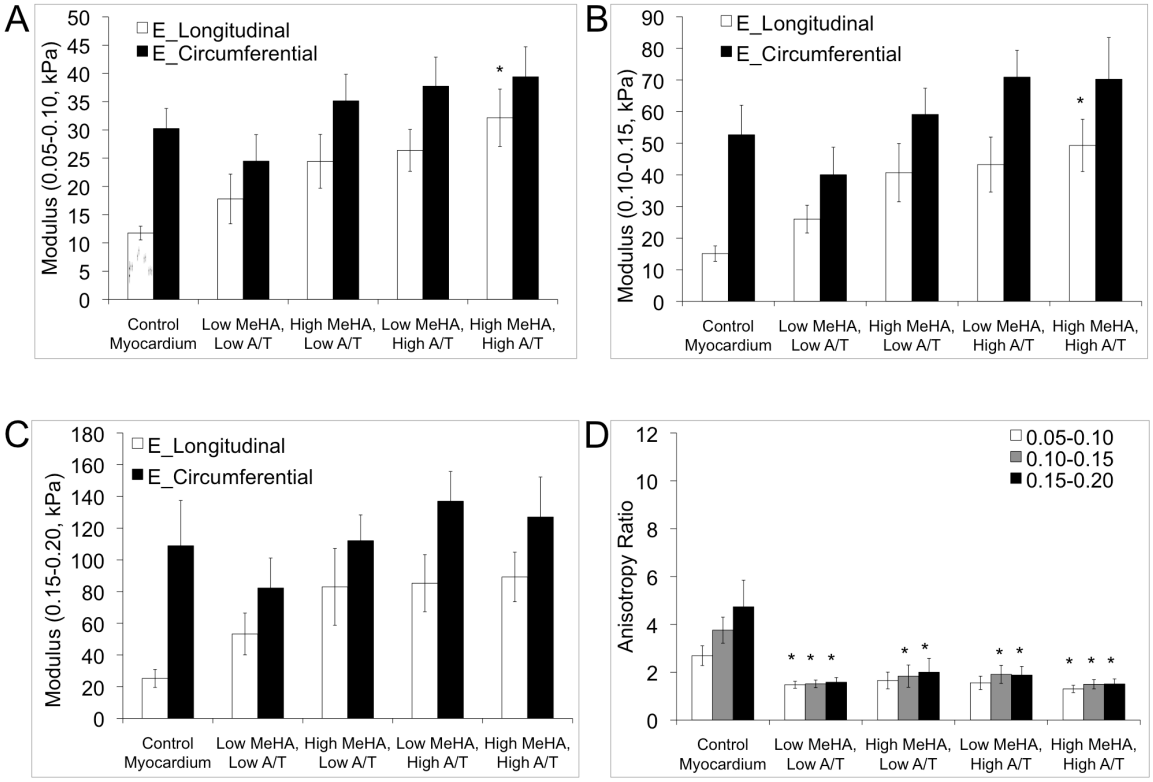

Figure 5.7 Calculated moduli from grip-to-grip strains in three strain ranges 0.05-0.10 (A), 0.10-0.15 (B), 0.15-0.20 (C), and the calculated anisotropic ratio (D). Data are presented as mean ± SEM. *p<0.05 vs. control myocardium.

Interestingly, the hydrogel formulations collectively had a pronounced effect on the anisotropic nature of myocardial tissue. As discussed in the introduction, healthy normal myocardial tissue is anisotropic; stiffness in one direction (circumferential) is higher than the other (longitudinal) direction [14, 32, 46]. The results reported in Figure 5.7 support this trend for normal myocardial tissue; however, when compared to control myocardium, hydrogel incorporation at all formulations resulted in a larger increase in the modulus in the longitudinal direction than circumferential direction. Consequently, this led to a statistically significant decreased anisotropy in all composite groups (at most strain ranges) compared to control myocardium (Figure 5.7D). As hydrogels exhibit isotropic properties alone, this is not entirely unexpected as the composite consists of both cardiac tissue and hydrogel. Yet, this is interesting considering the recent findings of Fomovsky et al., which indicated that anisotropic stiffening may be beneficial in cardiac function [5]. Morita et al. observed a similar trend where treatment with an injectable dermal filler led to increased stiffening in the longitudinal direction [13]. It should be noted, however, that both of the aforementioned studies were performed in an infarct model, while this work was performed in normal myocardial tissue and this could influence the final outcomes. Regardless, this is an exciting finding and provides insight on the influence of injectable biomaterials on the mechanical properties (i.e., directional stiffening) of the myocardium.

5.3.2.3 Tissue Strain Analysis

Tissue strains were quantified as discussed in Introduction and Methods by computing the deformation gradient tensor **F** from the local displacements (Figure 5.2) of each image acquired from grip-to-grip strain analysis. While strains were consistent between groups due to optical tracking, there was some variability observed as indicated

by the stress-strain curves in Figure 5.8. Generally, tissue strains remained close to equiaxial, but some inconsistency in strains within and between conditions were observed, which could be attributed to sample heterogeneity. For example, local displacements in composite samples are dependent on hydrogel distributions, which (as discussed in Chapter 4) were variable between groups. Another cause of sample heterogeneity may be the relatively thick samples used for testing; in thicker samples the fiber orientation is more likely to change transmurally. While sectioning techniques could be used to produce thinner samples, this option was not explored due to the potentially detrimental effects of processing on the properties of embedded hydrogels.

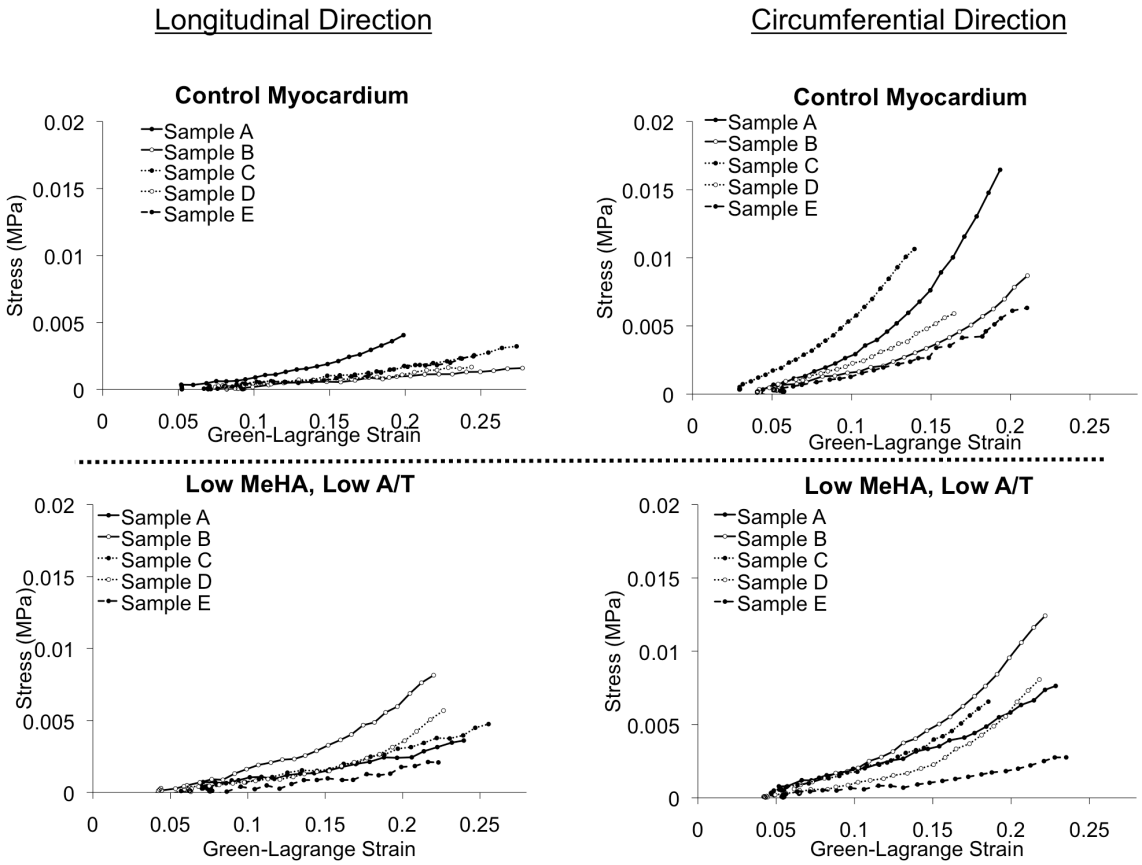

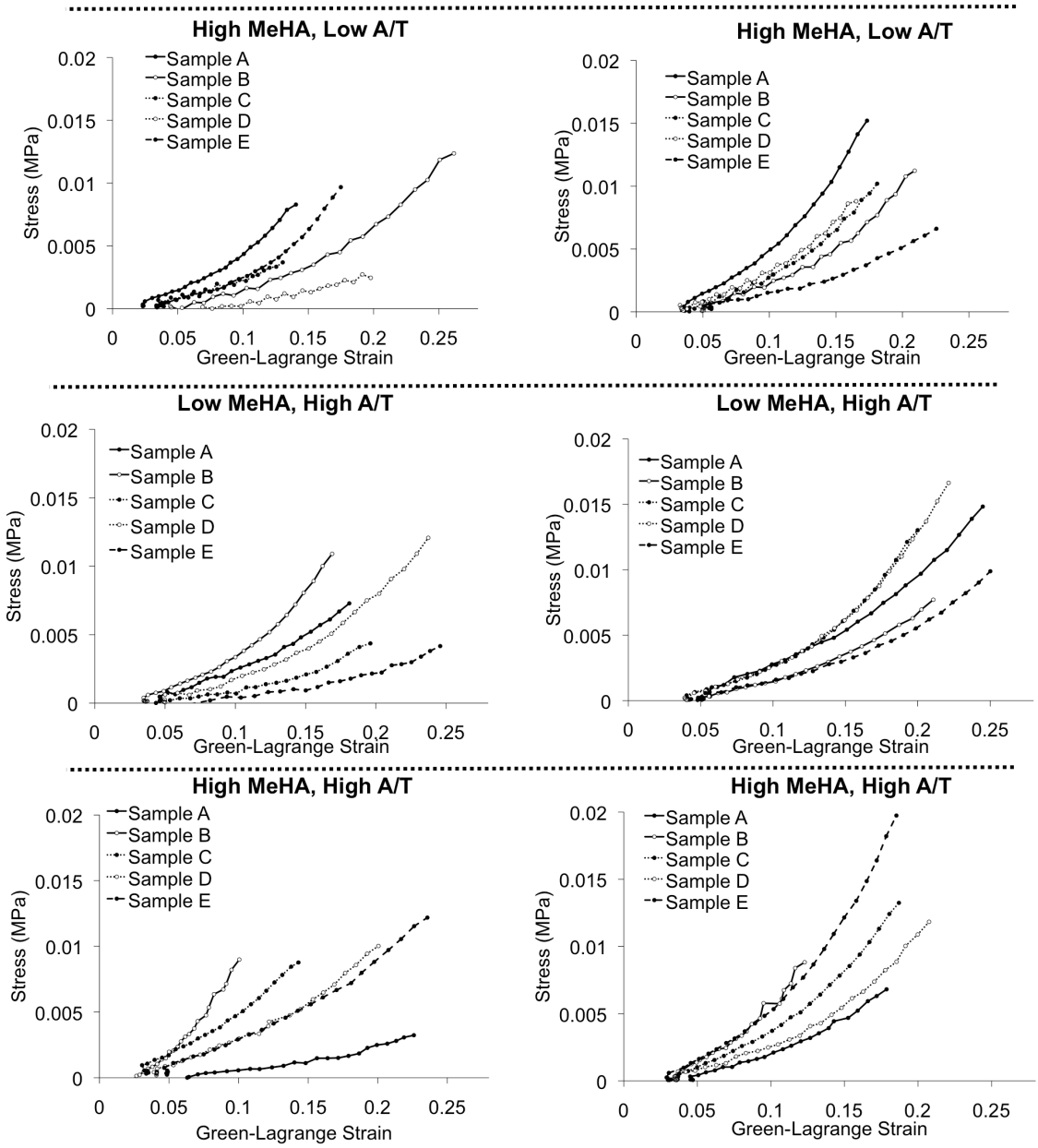

Figure 5.8 Stress-strain curves for tissue strains for all tested formulations. This data was applied to derive the diastolic myocardial material parameters for FE modeling.

Tissue strains were analyzed in a similar manner as grip-to-grip analysis where moduli were calculated in three ranges of strain from stress-strain curves (Figure 5.9). Overall, when compared to control myocardium, a directionally dependent trend was

observed where moduli were influenced most in the longitudinal direction. Data in Figure 5.9A indicates that from 0.05-0.10 strain, moduli in the longitudinal direction were higher than control myocardium groups, with more significant increases as the macromer percent modification and initiator concentration increased. While similar trends were observed at 0.10-0.15 and 0.15-0.20 strains, increases in moduli were limited to low macromer modification and initiator concentration (Figure 5.9B, C). In the circumferential direction, the modulus of high MeHA, high A/T increased most compared to control myocardium (Figure 5.9A, B, C). While only high macromer conditions resulted in mechanical increases relative to control myocardium in the circumferential direction, a trend was observed between composite groups that mimicked those of compressive testing. Specifically, macromer percent modification had a larger influence on mechanics than initiators did on low percent modified MeHA (Figure 5.9A, B, C). Overall, tissue strain analysis data indicates that hydrogel incorporation does influence the stiffness of myocardial tissue. Specifically, high macromer percent modification and initiator concentration generally lead to higher mechanics compared to control myocardium in the longitudinal direction and within composites in the circumferential direction. As with grip-to-grip strain analysis, there was generally a larger mechanical influence in the longitudinal direction than circumferential direction compared to control myocardium. Consequently, the anisotropy of all hydrogel formulations compared to control myocardium was decreased as indicated in Figure 5.9D. Section 5.3.2.2 should be referred to for a more thorough discussion on this trend.

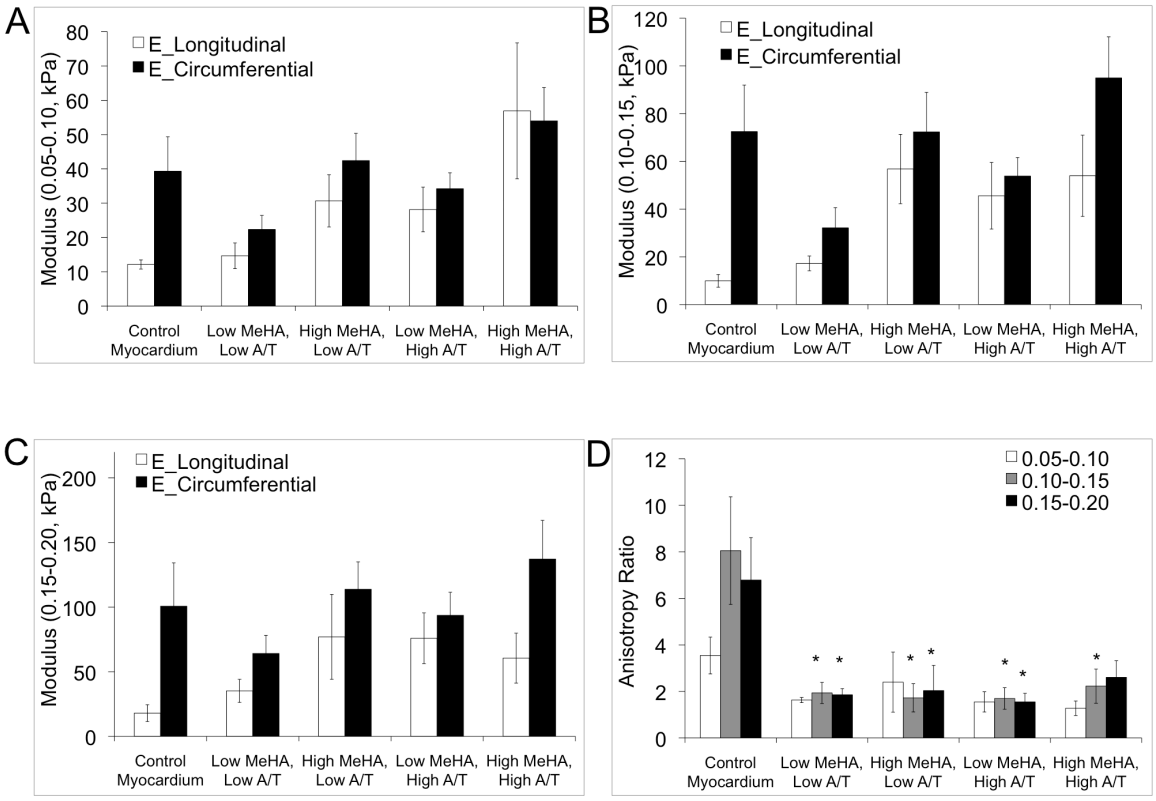

Figure 5.9 Calculated moduli from tissue strains in three strain ranges 0.05-0.10 (A), 0.10-0.15 (B), 0.15-0.20 (C), and the calculated anisotropic ratio (D). Data are presented as mean ± SEM. *p<0.05 vs. control myocardium.

Tissue strain analysis data was chosen for FE modeling instead of grip-to-grip data because it provided more representative values for strain experienced by composite formulations, regardless of differences in hydrogel distribution. As discussed in Methods (Section 5.2.3.1) using a curve fitting scheme with raw stress-strain curves (Figure 5.8), iterations of the constitutive law for the passive myocardium were performed to determine the optimal diastolic myocardial material parameters to represent composite injections and control myocardium. These parameters were assigned to represent either injection sites or control myocardium in the FE model.

5.3.3 Stress Assessment with FE Modeling

. As discussed in Methods, FE modeling was performed on two sets of injections and resulting stresses were assessed in three ways: globally, transmurally, and at the mid-wall. The first set of simulations was performed on the low initiator formulations to further elaborate on the work of Ifkovits et al. [3] and, specifically, to determine if stress data between treatments and no treatment control led to similar trends as observed in *in vivo* outcomes. Simulation results demonstrated that both treatments generally resulted in lower stress levels compared to no treatment at ED and ES in the fiber direction; moreover, high MeHA, low A/T generally resulted in the largest stress reductions compared to low MeHA, low A/T (Figure 5.10A, B). Both treatments resulted in stress reductions in the cross-fiber direction with more variability in trends between groups; however, relative to stress levels in the fiber direction, stress values in the cross-fiber direction were much lower (Figure 5.10C, D). Overall, these data supported the *in vivo* findings since both techniques indicate that high MeHA, low A/T is more effective in limiting LV remodeling compared to low MeHA, low A/T.

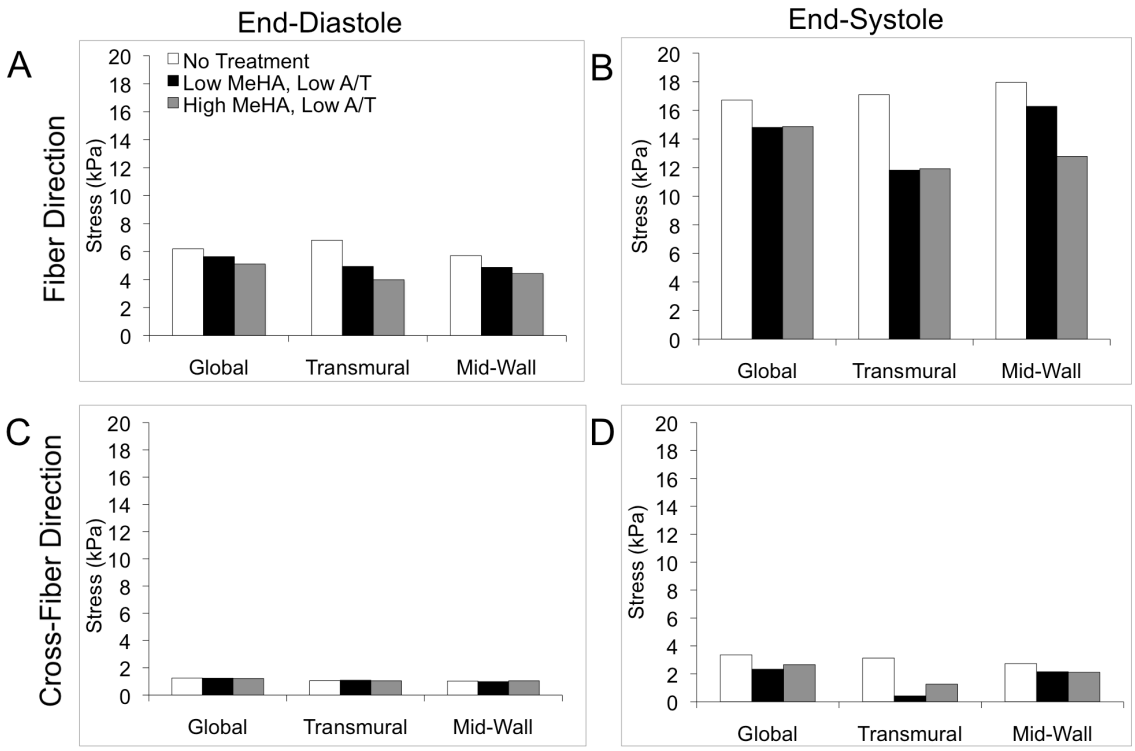

Figure 5.10 Stress values for low and high MeHA, low A/T treatment and no treatment control. Global, transmural, and mid-wall stresses at end-diastole (ED) and end-systole (ES) in the fiber (A, B) and cross-fiber (C, D) directions.

For the second set of simulations, treatment with all four formulations were simulated and stresses were compared between groups and no treatment control; the goal here was to assess relative differences between treatments and to assess how injection mechanical properties and distribution influence reductions in stress. Similar to the aforementioned simulations, all treatments resulted in lower stresses compared to no treatment control at ED and ES in the fiber direction (Figure 5.11A, B). Additionally, treatment with formulations with higher mechanics and larger volume distributions generally resulted in the largest stress reductions. While treatment generally resulted in lower stress compared to no treatment controls, trends in stress at ED and ES in the

cross-fiber direction were more variable and much lower than the fiber direction (Figure 5.11C, D).

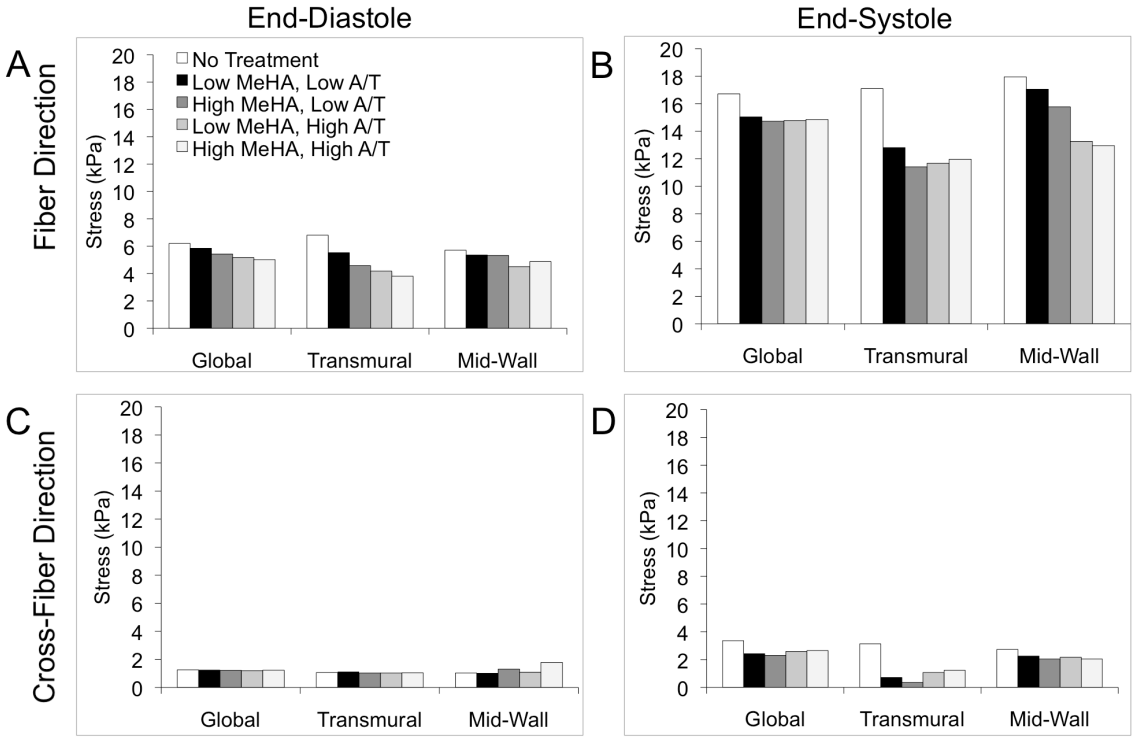

Figure 5.11 Calculated stresses for all treatments (volume estimated as 60% of measured mean values) and no treatment control. Global, transmural, and mid-wall stresses at end-diastole (ED) and end-systole (ES) in the fiber (A, B) and cross-fiber (C, D) directions.

5.4 Conclusions

To our knowledge this is the first study to a) perform biaxial testing on hydrogel/tissue composites and b) to apply these data to derive passive myocardial material parameters to simulate injections to treat a dilated LV. By performing compressive and biaxial testing on composites and control myocardium, we

demonstrated that MeHA hydrogel incorporation into myocardial tissue resulted in composites with mechanical properties that were dependent on macromer percent modification and initiator concentration; overall increases in both led to higher moduli. Interestingly, in biaxial testing, this trend was more pronounced in the longitudinal direction, suggesting that composite formation directionally influences mechanical properties of myocardial tissue. Consequently, anisotropy of all composites was decreased compared to myocardial control tissue. Biaxial data was used to derive diastolic myocardial material properties for control myocardium and composite formulations. Theoretical outcomes validated previous *in vivo* findings by Ifkovits et al. particularly at ED and ES in the fiber direction [3]; treatment with high MeHA, low A/T was more effective than the low MeHA, low A/T both *in vivo* (resulting in less dilation) and in theoretical simulations (resulting in larger stress reductions). Additionally, comparisons between all treatments (low or high MeHA and low or high A/T) demonstrated that higher hydrogel mechanics and greater distribution typically resulted in larger reductions in stress at ED and ES in the fiber direction. Overall, these data indicate that FE modeling is an effective technique to employ material properties of hydrogel/tissue formulations to predict their performance *in vivo* via stress outputs that can be correlated to experimental outcomes. Moreover, these data demonstrate that the magnitude of mechanical support provided by injectable biomaterials influences myocardial stress (a major contributor in the progression of LV remodeling) and should be considered when developing materials to treat LV remodeling.

References:

[1] Wall ST, Walker JC, Healy KE, Ratcliffe MB, Guccione JM. Theoretical impact of the injection of material into the myocardium: a finite element model simulation. Circulation 2006;114:2627.

[2] Wenk JF, Wall ST, Peterson RC, Helgerson SL, Sabbah HN, Burger M, Stander N, Ratcliffe MB, Guccione JM. A method for automatically optimizing medical devices for treating heart failure: designing polymeric injection patterns. J Biomech Eng 2009;131:121011.

[3] Ifkovits JL, Tous E, Minakawa M, Morita M, Robb JD, Koomalsingh KJ, Gorman JH, 3rd, Gorman RC, Burdick JA. Injectable hydrogel properties influence infarct expansion and extent of postinfarction left ventricular remodeling in an ovine model. Proc Natl Acad Sci U S A 2010;107:11507.

[4] Fomovsky GM, Holmes JW. Evolution of scar structure, mechanics, and ventricular function after myocardial infarction in the rat. Am J Physiol Heart Circ Physiol 2010;298:H221.

[5] Fomovsky GM, Macadangdang JR, Ailawadi G, Holmes JW. Model-based design of mechanical therapies for myocardial infarction. J Cardiovasc Transl Res 2011;4:82.

[6] Holmes JW, Nunez JA, Covell JW. Functional implications of myocardial scar structure. Am J Physiol 1997;272:H2123.

[7] Berry MF, Engler AJ, Woo YJ, Pirolli TJ, Bish LT, Jayasankar V, Morine KJ, Gardner TJ, Discher DE, Sweeney HL. Mesenchymal stem cell injection after myocardial infarction improves myocardial compliance. Am J Physiol Heart Circ Physiol 2006;290:H2196.

[8] Hiesinger W, Brukman MJ, McCormick RC, Fitzpatrick JR, 3rd, Frederick JR, Yang EC, Muenzer JR, Marotta NA, Berry MF, Atluri P, Woo YJ. Myocardial tissue

elastic properties determined by atomic force microscopy after stromal cell-derived factor 1alpha angiogenic therapy for acute myocardial infarction in a murine model. J Thorac Cardiovasc Surg 2012;143:962.

[9] Ghaemi H, Behdinan K, Spence AD. In vitro technique in estimation of passive mechanical properties of bovine heart part I. Experimental techniques and data. Med Eng Phys 2009;31:76.

[10] Gupta KB, Ratcliffe MB, Fallert MA, Edmunds LH, Jr., Bogen DK. Changes in passive mechanical stiffness of myocardial tissue with aneurysm formation. Circulation 1994;89:2315.

[11] Sacks MS, Chuong CJ. Biaxial mechanical properties of passive right ventricular free wall myocardium. J Biomech Eng 1993;115:202.

[12] Demer LL, Yin FC. Passive biaxial mechanical properties of isolated canine myocardium. J Physiol 1983;339:615.

[13] Morita M, Eckert CE, Matsuzaki K, Noma M, Ryan LP, Burdick JA, Jackson BM, Gorman JH, 3rd, Sacks MS, Gorman RC. Modification of infarct material properties limits adverse ventricular remodeling. Ann Thorac Surg 2011;92:617.

[14] Yin FC, Strumpf RK, Chew PH, Zeger SL. Quantification of the mechanical properties of noncontracting canine myocardium under simultaneous biaxial loading. J Biomech 1987;20:577.

[15] Humphrey JD, Strumpf RK, Yin FC. Determination of a constitutive relation for passive myocardium: II. Parameter estimation. J Biomech Eng 1990;112:340.

[16] Humphrey JD, Strumpf RK, Yin FC. Determination of a constitutive relation for passive myocardium: I. A new functional form. J Biomech Eng 1990;112:333.

[17] Sacks M. Biaxial mechanical evaluation of planar and biological materials. J Elast 2001;61:199.

[18] Sacks MS, Sun W. Multiaxial mechanical behavior of biological materials. Annu Rev Biomed Eng 2003;5:251.

[19] O'Connell GD, Sen S, Elliott DM. Human annulus fibrosus material properties from biaxial testing and constitutive modeling are altered with degeneration. Biomech Model Mechanobiol 2012;11:493.

[20] Szczesny SE, Peloquin JM, Cortes DH, Kadlowec JA, Soslowsky LJ, Elliott DM. Biaxial tensile testing and constitutive modeling of human supraspinatus tendon. J Biomech Eng 2012;134:021004.

[21] Humphrey JD, Strumpf RK, Yin FC. Biaxial mechanical behavior of excised ventricular epicardium. Am J Physiol 1990;259:H101.

[22] Lanir Y, Fung YC. Two-dimensional mechanical properties of rabbit skin. II. Experimental results. J Biomech 1974;7:171.

[23] Lanir Y, Fung YC. Two-dimensional mechanical properties of rabbit skin. I. Experimental system. J Biomech 1974;7:29.

[24] Billiar KL, Sacks MS. Biaxial mechanical properties of the natural and glutaraldehyde treated aortic valve cusp--Part I: Experimental results. J Biomech Eng 2000;122:23.

[25] Debes JC, Fung YC. Biaxial mechanics of excised canine pulmonary arteries. Am J Physiol 1995;269:H433.

[26] Ghaemi H, Behdinan K, Spence AD. In vitro technique in estimation of passive mechanical properties of bovine heart part II. Constitutive relation and finite element analysis. Med Eng Phys 2009;31:83.

[27] Choi HS, Vito RP. Two-dimensional stress-strain relationship for canine pericardium. J Biomech Eng 1990;112:153.

[28] Waldman SD, Sacks, MS, Lee JM. Boundary conditions during biaxial testing of planar connective tissues. Part II: fiber orientation. J Mater Sci Lett 2002;21:1215.

[29] Waldman SD, Lee JM. Boundary conditions during biaxial testing of planar connective tissues. Part 1: dynamic behavior. J Mater Sci Mater Med 2002;13:933.

[30] Jacobs NT, Cortes DH, Szczesny SE, Vresilovic EJ, Elliott DM. Effect of boundary conditions on stress-strain uniformity in biaxial tension of annulus fibrosus. The 56th Annual Meeting Orth Res Soc. Long Beach, CA, 2011;21:125.

[31] Tong P, Fung YC. The stress-strain relationship for the skin. J Biomech 1976;9:649.

[32] Guccione JM, McCulloch AD, Waldman LK. Passive material properties of intact ventricular myocardium determined from a cylindrical model. J Biomech Eng 1991;113:42.

[33] Choung CJ, Fung YC. Residual stress in the arteries. In: Schmid-Schonbein GW, Woo SL-Y, Zweifach BW, editor. Frontiers in Biomechanics. New York: Springer, 1986. p.117.

[34] Guccione JM, Costa KD, McCulloch AD. Finite element stress analysis of left ventricular mechanics in the beating dog heart. J Biomech 1995;28:1167.

[35] Walker JC, Ratcliffe MB, Zhang P, Wallace AW, Hsu EW, Saloner DA, Guccione JM. Magnetic resonance imaging-based finite element stress analysis after linear repair of left ventricular aneurysm. J Thorac Cardiovasc Surg 2008;135:1094.

[36] Jhun CS, Wenk JF, Zhang Z, Wall ST, Sun K, Sabbah HN, Ratcliffe MB, Guccione JM. Effect of adjustable passive constraint on the failing left ventricle: a finite-element model study. Ann Thorac Surg 2010;89:132.

[37] Guccione JM, Waldman LK, McCulloch AD. Mechanics of active contraction in cardiac muscle: Part II--Cylindrical models of the systolic left ventricle. J Biomech Eng 1993;115:82.

[38] Guccione JM, McCulloch AD. Mechanics of active contraction in cardiac muscle: Part I--Constitutive relations for fiber stress that describe deactivation. J Biomech Eng 1993;115:72.

[39] Burdick JA, Chung C, Jia X, Randolph MA, Langer R. Controlled degradation and mechanical behavior of photopolymerized hyaluronic acid networks. Biomacromolecules 2005;6:386.

[40] Walker JC, Ratcliffe MB, Zhang P, Wallace AW, Fata B, Hsu EW, Saloner D, Guccione JM. MRI-based finite-element analysis of left ventricular aneurysm. Am J Physiol Heart Circ Physiol 2005;289:H692.

[41] Burdick JA, Prestwich GD. Hyaluronic acid hydrogels for biomedical applications. Adv Mater 2011;23:H41.

[42] Temenoff JS, Kasper FK, Mikos AG. Fumarate-based macromers as scaffolds for tissue engineering. Top Tissue Eng 2007;3:16.

[43] Chung C, Mesa J, Randolph MA, Yaremchuk M, Burdick JA. Influence of gel properties on neocartilage formation by auricular chondrocytes photoencapsulated in hyaluronic acid networks. J Biomed Mater Res A 2006;77:518.

[44] Gupta V, Grande-Allen KJ. Effects of static and cyclic loading in regulating extracellular matrix synthesis by cardiovascular cells. Cardiovasc Res 2006;72:375.

[45] Lee AA, McCulloch AD. Multiaxial myocardial mechanics and extracellular matrix remodeling: mechanochemical regulation of cardiac fibroblast function. Adv Exp Med Biol 1997;430:227.

[46] Engelmayr GC, Jr., Cheng M, Bettinger CJ, Borenstein JT, Langer R, Freed LE. Accordion-like honeycombs for tissue engineering of cardiac anisotropy. Nat Mater 2008;7:1003.

[47] Rappaport D, Adam D, Lysyansky P, Riesner S. Assessment of myocardial regional strain and strain rate by tissue tracking in B-mode echocardiograms. Ultrasound Med Biol 2006;32:1181.

CHAPTER 6

Synthesis, Purification, and Characterization of Hydrolytically Degradable Hyaluronic Acid Hydrogels

(Adapted from: **E Tous**, JL Ifkovits, KJ Koomalsingh, T Shuto, T Soeda, N Kondo, JH Gorman, III, RC Gorman, JA Burdick, "Influence of Injectable Hyaluronic Acid Hydrogel Degradation Behavior on Infarction Induced Ventricular Remodeling," Biomacromolecules, 2011, 12:4127-4135.)

6.1 Introduction

The previous three chapters applied methacrylated hyaluronic acid (MeHA) hydrogels to demonstrate that mechanics (via experimental/ *in vivo* [1] and theoretical assessment) and hydrogel distribution (via theoretical assessment) influence left ventricular (LV) remodeling. Here, we introduce hydrolytically degradable hyaluronic acid (HA) hydrogels to address the time sensitivity of remodeling by investigating the temporal considerations in material design. Specifically, these hydrogels are used to examine the temporal role of mechanical support during this process; this will provide insight to the duration of stability that is required to effectively attenuate LV remodeling. This chapter will focus on material synthesis and characterization, while Chapters 7 and 8 will apply iterations of these materials to assess their efficacy in limiting these maladaptive changes in an *in vivo* ovine MI model. Overall, the goal is a better understanding of material design toward the development of more targeted therapies (injectable biomaterials) to attenuate LV remodeling

6.1.1 Hyaluronic Acid (HA): Tissue Engineering

As briefly discussed in Chapter 4, HA is a biocompatible linear polysaccharide comprised of alternating D-glucuronic and β-N-acetyl-D-glucosamine disaccharide repeat units that is found abundantly throughout the body [2]. HA plays both cellular and mechanical functions that are essential in maintaining our homeostasis [2-7]. Specifically, HA provides biomechanical integrity by facilitating extracellular matrix (ECM) organization and also mediates biological processes such as cell proliferation, morphogenesis, inflammation, and wound healing through three main types of cell surface receptors: CD44, CD54 (intracellular adhesion molecule-1, ICAM-1), and CD168 (receptor for hyaluronan mediated motility, RHAMM) [2, 4-7]. These attractive qualities make HA a good candidate for a range of tissue engineering (TE) applications including cartilage [8-13], valve [3, 14], and cardiac [1, 15, 16] tissues and in controlling stem cell fate [17-20].

6.1.2 HA: Cardiac Engineering

HA is particularly appealing as a material for cardiac engineering because of its role in cardiac development and ECM homeostasis [21, 22]. During cardiac embryogenesis, HA mediates the expansion of the endocardial cushions, which develop into the valvular and septal portion of the heart by organizing the ECM and hydrating the cardiac jelly [21]. Experimental work has verified the significance of HA in morphogenesis; Camenisch et al. reported cardiac abnormalities in mice deficient in HA synthase 2 (a prominent contributor to HA production) [23]. Additionally, HA-based scaffolds have been implemented *in vitro* to investigate their utility in valvular engineering, where seeded valvular interstitial cells (VICs) demonstrated effective adherence and proliferation capabilities [3]. The role of HA has also been investigated

with respect to negative remodeling after MI; the concentration of low molecular weight (LMW) HA was observed to be greater compared to pre-MI where high molecular weight (HMW) presence was more dominant [22]. After MI, proteases not only break down collagen, but can also degrade HMW-HA to LMW-HA, which plays a "wound healing" role in mediating cell migration and inflammation after MI [24]. Additionally, when compared to fetal tissues, adult tissues express higher amounts of hyaluronidases that facilitate the enzymatic break down of HA, rendering HMW-HA in adults more susceptible to break down into LMW fragments [25]. Overall, these reports demonstrate the relevance of HA in maintaining a functional myocardium and suggest that HMW-HA is more relevant in the development and maintenance of ECM structures [21, 22]. Reports also suggest a role of LMW-HA in wound healing applications, mediating inflammatory activities post-MI and upregulating vascular endothelial growth factor (VEGF) and promoting angiogenesis and cell proliferation [3, 7], which can be attractive for treating ischemic tissues such as in the infarct region.

6.1.3 HA: Hydrolytically Degradable Hydrogels

As discussed in Section 4.1.2, HA is readily modified at its carboxyl and hydroxyl groups with a range of chemistries, including methacrylates [1, 11, 12, 20, 26]. These groups can undergo radical polymerization at the vinyl group via initiation techniques to form hydrogels with bulk properties (e.g., mechanics and gelation) that are varied based on the extent of crosslinking, which can be influenced by extent of macromer modification, macromer concentration, and initiator efficiency [1, 27]. In addition to their tunability due to alterations in crosslinking, MeHA hydrogels are generally attractive for TE applications due to their natural enzymatic degradation.

Most degradable scaffolds applied in TE are designed so that they leave after providing their structural purpose; however, HA degradable scaffolds are unique in that their degradation products may also be biologically active. HA is enzymatically degradable at its backbone by hyaluronidases naturally found in the body and is broken down to yield oligosaccharides [2, 4, 6, 7]. Studies with MeHA hydrogels (formed via photopolymerization) have shown that their degradation kinetics by exogenous hyaluronidases can be tailored [26]. However, these systems are limited in that they are only enzymatically degradable; thus, degradation at physiological hyaluronidase concentrations can take months to years and is dependent on the amount of hyaluronidases present *in vivo*. To circumvent these drawbacks, our group has modified HA with methacrylate-based reactive groups that also introduce hydrolytically degradable moieties to provide more controlled degradation for TE applications [28, 29].

Like MeHA, these macromers can be crosslinked at the vinyl portion of the methacrylate to control bulk properties dependent on the efficiency of crosslinking and are still enzymatically degradable [28, 29]. In addition to these qualities, however, the inclusion of ester bonds between the HA backbone and the reactive groups provides enhanced control over hydrogel degradation. Chung, Sahoo and colleagues were the first to synthesize and characterize these types of HA hydrogels; they achieved this by including α-hydroxy ester-based chemistries (lactic acid, LA and caprolactone, CL) between the HA backbone and methacrylate [28, 29]. Using photopolymerization, they formed hydrogels and demonstrated that, as expected, LA-containing hydrogels degraded more quickly than CL-containing hydrogels, due to a greater susceptibility to hydrolysis, and that both degraded much faster than MeHA hydrogels. In general, hydrolytic degradation was tailored by either adjusting the number of repeat units within each added group or the amount added to the HA backbone [28, 29]. While these

hydrolytically degradable HA hydrogels were successfully synthesized, their synthesis was tedious and inefficient and they are highly hydrophobic, limiting functionalization and hydrogel concentrations; hence, here we explore an alternative synthesis and purification scheme.

In this dissertation, we functionalize HA at the hydroxyl group with a hydroxyethyl methacrylate (HeMA) group, which is more easily synthesized and results in more efficient macromer yield. This chapter will summarize the optimized synthesis and purification for HeMA-HA macromers of varying extents of modification. While past work employed photopolymerization techniques to form hydrogels, as discussed in Chapter 4 and as employed by Ifkovits et al. [1], oxidation-reduction (redox) initiation with ammonium persulfate (APS, A) and N,N,N,N',N'-tetramethylethylenediamine (TEMED, T) will be used to initiate hydrogel polymerization in this work [30]. This method of polymerization facilitates further control of crosslink efficiency and also provides a more practical means to deliver hydrogels for MI application. Here, HeMA-HA homopolymer and copolymer (HeMA-HA and MeHA) hydrogels are formed and characterized to evaluate the influence of the amount of HeMA (percent modification) and type of copolymer (ratio) on material parameters including gel onset, mechanics, and degradation. In general, this work provides insight into the design and material properties of HeMA-HA hydrogels. Understanding degradation kinetics, in particular, will allow for the optimal application of this class of materials to treat the evolving progression of LV remodeling.

6.2 Materials and Methodology

6.2.1 Synthesis of Hydroxyethyl Methacrylated Hyaluronic Acid (HeMA-HA) Macromer

The reaction scheme for HeMA-HA synthesis is summarized in Figure 6.1. 2-hydroxyethyl methacrylate (HeMA) (Acros) was reacted with succinic anhydride (SA) (Sigma) at 1:1.1 molar ratio via a ring opening reaction that was catalyzed by N-methylimidazole (NMI) (Sigma) in dichloroethane (DCE) (Fisher) at 65 °C for 16 hours. A small amount of hydroquinone (Acros) was added to scavenge free radicals and inhibit their polymerization of the methacrylate groups during storage. The end product of this reaction was a mixture containing a carboxylic acid terminated HeMA (HeMA-COOH). HeMA-COOH was purified and isolated from impurities by undergoing several washes with aqueous hydrochloric acid to remove excess SA and with deionized water to remove water-soluble impurities. The mixture was dried by adding magnesium sulfate ($MgSO_4$) (Fisher) and filtration was performed to remove $MgSO_4$. The filtered solution was rotovapped to concentrate the final product by minimizing the volume of DCE and stored at 4 °C. ^1H NMR (Bruker, 360 MHz) was performed to confirm HeMA-COOH formation and purity.

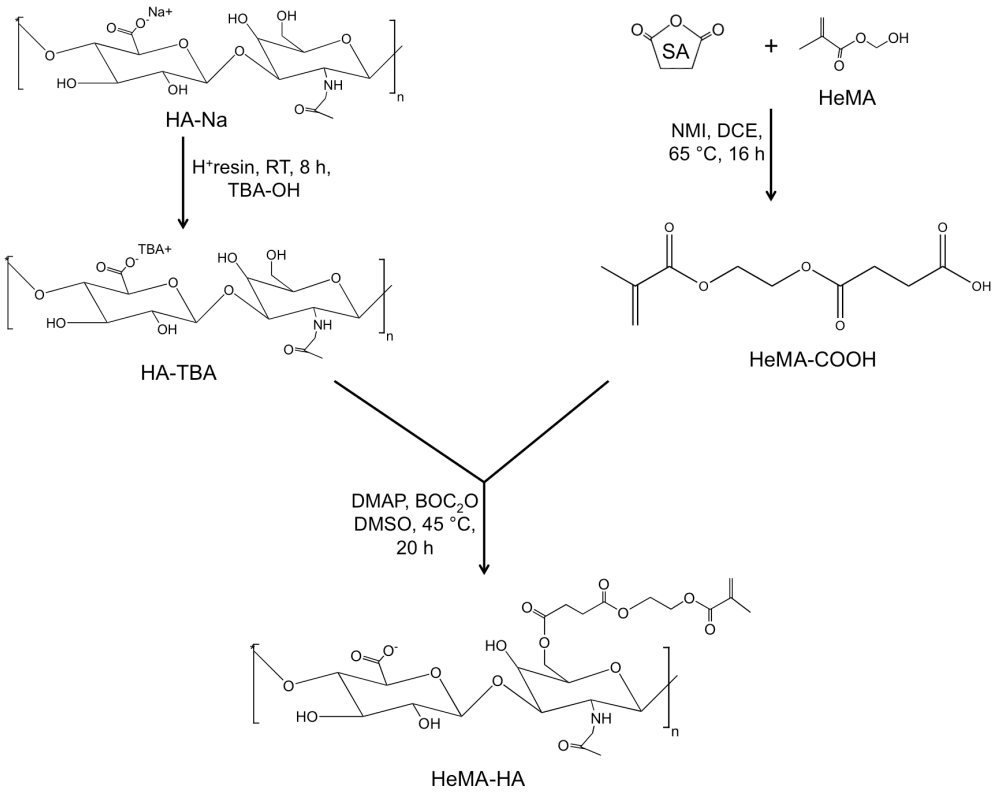

Figure 6.1 Chemical synthesis of HeMA-HA intermediate products (HeMA-COOH and HA-TBA) and final product (HeMA-HA).

HA-tetrabutylammonium salt (HA-TBA) was synthesized as described in Section 4.2.3.1 where HA-sodium salt (Lifecore, 66 kDa) was converted into a tetrabutylammonium (TBA) salt by performing an acidic ion exchange followed by titration [29].

HeMA-COOH was coupled to HA-TBA via an esterification reaction where dimethylaminopyridine (DMAP) (Sigma) activated the carboxylic acid on HeMA-COOH and the coupling agent di-*tert*-butyl dicarbonate (BOC_2O) (Sigma) mediated the attachment of HeMA-COOH to HA-TBA in anhydrous di-methyl sulfoxide (DMSO) (Acros) at 45 °C for 20 hours. Trace amounts of hydroquinone were added to the

reaction to prevent free radical polymerization. HeMA addition to the HA backbone was altered by adjusting the concentration and molar ratios of HeMA-COOH and the coupling agent BOC_2O and confirmed via ^1H NMR.

6.2.2 Purification of HeMA-HA Macromer

A variety of purification techniques were explored to obtain a pure form of HeMA-HA from the reaction mixture. Three specific approaches were examined (all dialysis was performed against deionized water at 4 °C and a MW cutoff 5-8 kDa): 1) only dialysis for 1 and 5 days, 2) acetone precipitation followed by overnight dialysis, and 3) 1 or 5 days of dialysis followed by acetone precipitation and dialysis again. After all forms of purification, the HeMA-HA final products were lyophilized and stored at -20 °C prior to use. The degree of purification was assessed via ^1H NMR.

6.2.3 Synthesis of Methacrylated HA (MeHA) Macromer

Methacrylated HA was synthesized as discussed in Methods of Chapter 4 (Section 4.2.1) [26] where methacrylic anhydride (MA) (Sigma) was reacted in excess with HA sodium salt (Lifecore, 66kDa) and modification was assessed via ^1H NMR.

6.2.4 Formation and Characterization of Hydrogels

Gelation, mechanics and degradation were evaluated to assess hydrogel tunability based on HeMA-HA modification (~10%, ~30%, and ~60%) and MeHA inclusion at 5 ratios (100:0, 75:25, 50:50, 25:75, 0:100, HeMA-HA (~20% modified): MeHA (~100% modified)). Macromers were crosslinked through radical initiation with APS (5 mM) (Sigma) and TEMED (5 mM) (Sigma) to form 4 wt% hydrogels. Gel onset and compressive moduli were generally assessed as in Section 4.2.2. Gelation was

assessed by monitoring the intersection of the storage (G') and loss (G'') moduli using an AR2000ex Rheometer (TA Instruments) at 37 °C under 1% strain and a frequency of 1 Hz in a cone and plate geometry (1°, 20 mm diameter). To examine mechanics and degradation, hydrogels (~50 μL) were formed between two glass slides within a teflon mold sealed with vacuum grease by mixing macromer solutions with APS and TEMED and incubating at 37 °C for 30 minutes. Compression testing was performed on samples immediately after gelation with a Dynamic Mechanical Analyzer (DMA) (Q800 TA Instruments) at a strain rate of 10%/ min and moduli were calculated at a strain from 10-20%. For HeMA-HA homopolymers, degradation was assessed by incubating hydrogels in phosphate buffered saline (PBS) at 37 °C and changing solutions at 1, 7, 14, 28, 56, 63, 70, 77, and 84 days or until hydrogels were completely degraded. Degradation assessment was performed for copolymers by incubating hydrogels in PBS at 37 °C, collecting samples at 1, 7, 14, 28, 42, 49, and 56, and quantifying percent (%) HA release using a uronic acid assay [31]. Hyaluronidases (Sigma) were added to PBS solutions to completely enzymatically degrade hydrogels after 8 weeks if necessary.

6.2.5 Statistical Analysis

Data is presented as mean ± SD (standard deviation). Differences in gel onset, moduli, and percent mass loss were assessed using a one-way ANOVA with Tukey's post hoc evaluation. Differences in mass loss between copolymer and MeHA at 8 weeks were assessed using the Student's T-Test. For all comparisons, $p<0.05$ was considered to be statistically significant.

6.3 Results and Discussion

A hydrolytically degradable HeMA-COOH group was added to the enzymatically degradable HA backbone to provide more precise control of degradation. While our group has previously designed hydrolytically degradable hydrogels with the inclusion of α-hydroxy esters (e.g., lactic acid and caprolactone) [28, 29], the macromer synthesis employed was time consuming and inefficient. Instead of performing two reactions to obtain a hydrolytically degradable carboxylic acid terminated moiety, the HeMA-HA synthesis combines these two steps by directly converting the HeMA hydroxyl group into a carboxylic acid via the ring opening reaction with SA (Figure 6.1). This new synthesis allows for a more convenient and efficient synthesis of tunable hydrolytically degradable HA-based macromers.

6.3.1 Synthesis of HeMA-HA Macromer

The hydroxyl groups of HeMA were first converted to carboxylic acids as described in Methods. The conversion from hydroxyl to carboxyl terminated chemistry was confirmed with ^{1}H NMR with the detection of a peak at δ ~2.70 ppm corresponding to the protons added from the addition of SA (4, 5, Figure 6.2). The presence of minimal impurities is also supported by the relatively clean ^{1}H NMR spectrum.

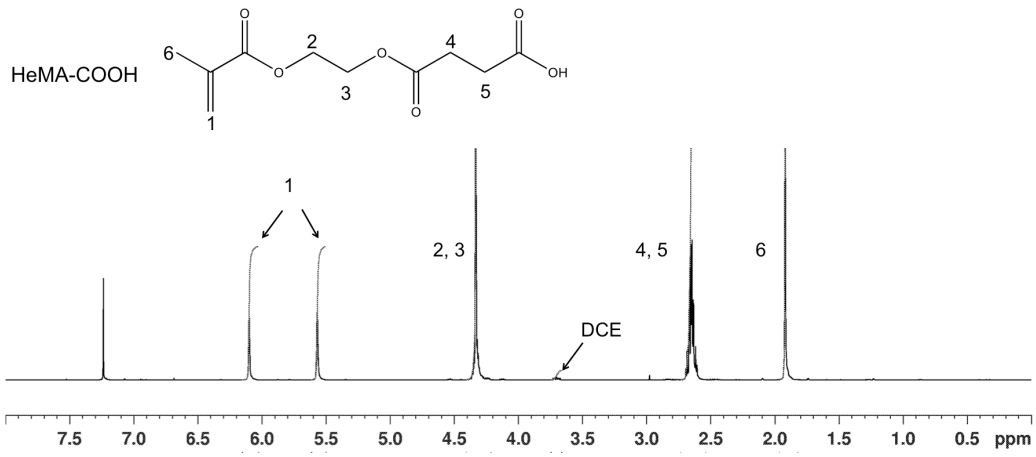

Figure 6.2 Chemical structure and representative ^{1}H NMR spectrum ($CDCL_3$) for HeMA-COOH with labeled peaks corresponding to the protons on the intermediate product. Peak 1= protons on alkene group. Peak 2, 3= protons corresponding to portion from HeMA. Peak 4, 5= protons corresponding to SA addition. Peak 6= protons on methyl group.

HA-TBA (characterization described in Chapter 4, Section 4.3.2.1) was reacted as discussed in Methods with HeMA-COOH to synthesize HeMA-HA (Figure 6.1). HeMA-HA was purified via several techniques to evaluate the most efficient and effective method for pure HeMA-HA Figure 6.6.

6.3.2 Purification of HeMA-HA Macromer

As briefly discussed in Methods, HeMA-HA purification was analyzed in three primary ways. In all cases, dialysis against deionized water was performed at 4 °C to minimize hydrolytic degradation of the HeMA groups; purification optimization indicated that dialysis at 4 °C did not influence the modification (Figure 6.5). Acetone precipitation entailed the addition of NaCl to the reaction solution for exchange of TBA with Na so that

TBA salts dissolved in the organic acetone solvent, while the Na and HA products precipitated. The NaCl mixture was dripped into a solution of stirring acetone on ice that was 10X the reaction volume to ensure efficient precipitation. Reaction solutions were precipitated no more than 100 mL at a time to prevent crosslinking; precipitating large amounts of HA at once resulted in unwanted polymerization, possibly due to the close proximity of HA macromers in the polar acetone solvent. The HA-based precipitate was collected, dissolved in water and then dialyzed to remove soluble impurities.

At day 1 the extent of purification by dialysis alone could not be assessed because of the high content of impurities, likely due to high levels of DMSO; this prevented lyophilization and salvage of the macromer. Immediate acetone precipitation followed by overnight dialysis decreased the impurities (e.g., cloudiness of the solution); however, ^{1}H NMR revealed that DMSO and excess TBA salts were still present (Figure 6.3A). Dialysis, followed by acetone precipitation and further dialysis produced the purest product at day 1, with minimal DMSO and TBA (Figure 6.3B). These results suggest that initial dialysis is important for DMSO removal; excess DMSO may hinder precipitation as suggested by data from immediate acetone precipitation studies.

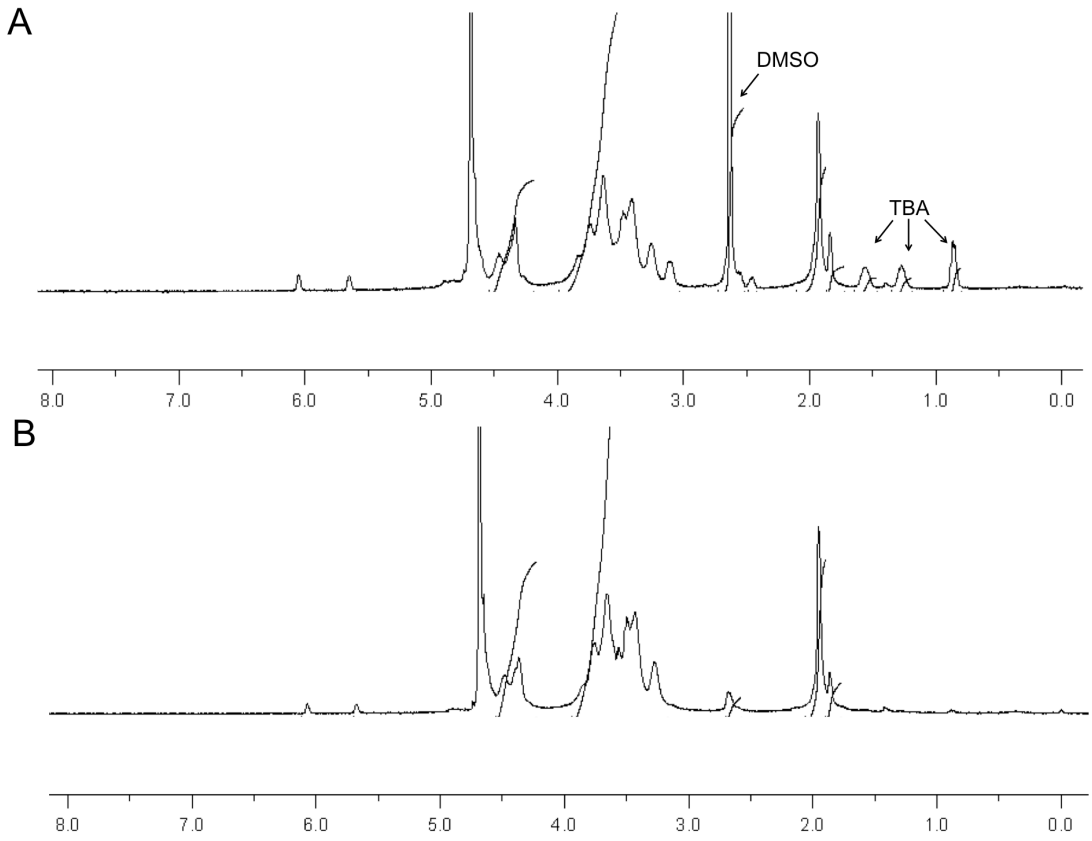

Figure 6.3 Representative ^{1}H NMR spectrum (D_2O) for HeMA-HA macromer after 1 day of purification. Acetone precipitation followed by overnight dialysis (A) or overnight dialysis followed by acetone precipitation and further dialysis (B).

At day 5, groups 1 (dialysis alone) and 3 (5 days of dialysis, acetone precipitation, and further dialysis) were evaluated. After 5 days of dialysis, DMSO was no longer present; however, TBA salts (although in smaller quantities then in group 2 at day 1) remained (Figure 6.4A). In contrast, significant reduction of DMSO and TBA salt impurities were observed in group 3 at day 5 (Figure 6.4B). While impurities were significantly minimized, several macromers after acetone precipitation followed by an overnight dialysis displayed an abnormal HA backbone as shown in Figure 6.4B. This may be due to residual acetone remaining in the final product after precipitation. A

normal HA backbone was restored after an additional 3 days of dialysis following acetone precipitation (Figure 6.5A and 6.5B). Also, prolonged dialysis at 4 °C did not alter the macromer modification (~30%) (Figure 6.5).

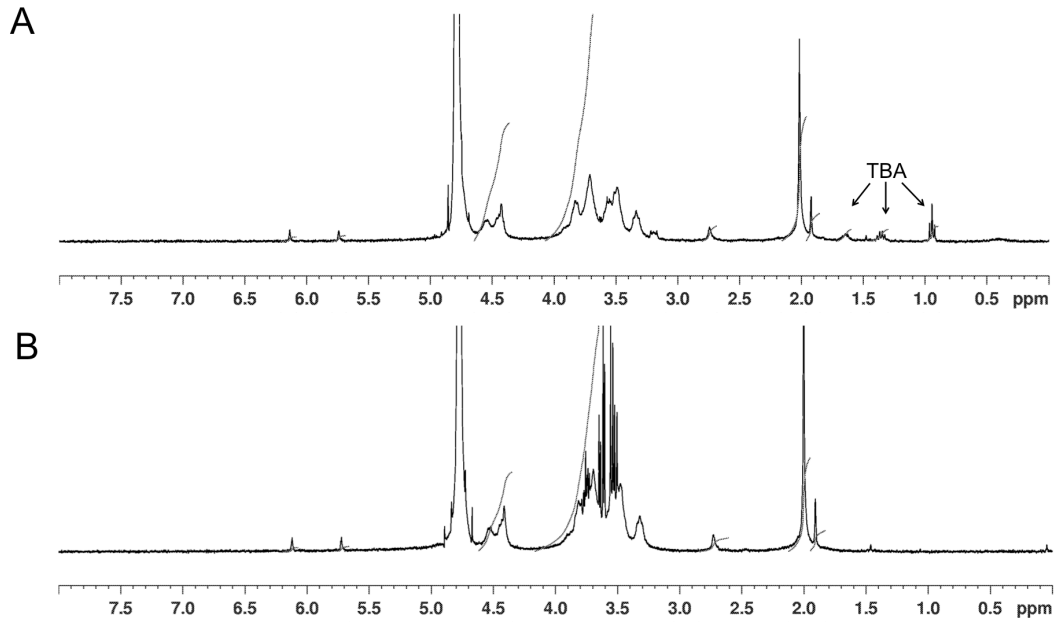

Figure 6.4 Representative ^{1}H NMR spectrum (D_2O) for HeMA-HA macromer after 5 days of purification. 5 days of dialysis alone (A) or 5 days of dialysis followed by acetone precipitation and further dialysis (B).

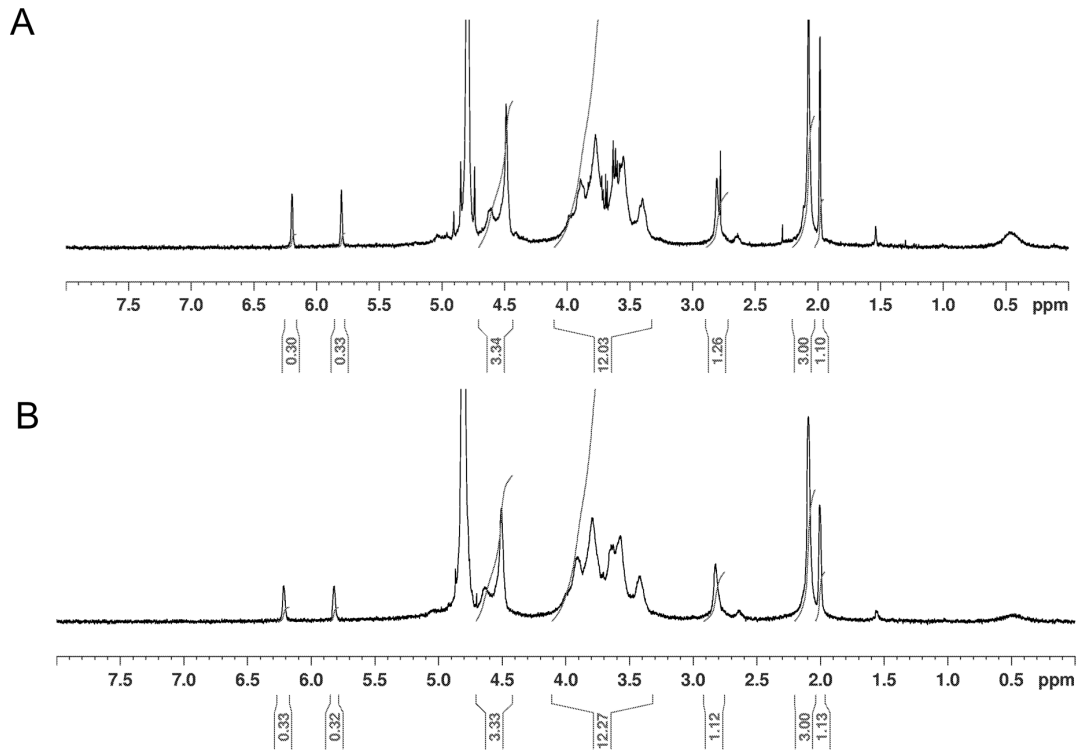

Figure 6.5 Representative ^{1}H NMR spectrum (D_2O) for HeMA-HA macromer assessing its purity immediately after acetone precipitation (A) or 3 days of dialysis after acetone precipitation (B).

Taking into consideration the aforementioned studies, the purification protocol was finalized as follows: a 1 day dialysis to remove DMSO for precipitation, acetone precipitation to remove most of the TBA salts, and a 3 day dialysis to remove leftover salts and acetone impurities to ensure a normal HA backbone after precipitation. Employing this purification technique resulted in a pure HeMA-HA macromer (Figure 6.6).

6.3.3 Alteration of HeMA-HA Functionalization

The amount of HeMA added to the HA backbone (e.g., percent modification/ methacrylation) was tuned by varying the concentration of HeMA-COOH and BOC_2O in the same ratio (1.4: 1.2, HeMA-COOH: BOC_2O) with excess HeMA-COOH (Figure 6.6B). Syntheses performed with the same or excess amounts of BOC_2O to HeMA were prone to crosslinking both within the reaction vessel and during acetone precipitation. Modification was assessed by ^1H NMR; percent methacrylation was determined by integrating the methacrylate peaks on the HeMA (peaks 2, δ ~6.20 ppm and δ ~5.80 ppm) with respect to the N-acetyl group on HA, or peak 1 at a resonance of δ ~2.10 ppm (Figure 6.6A, C).

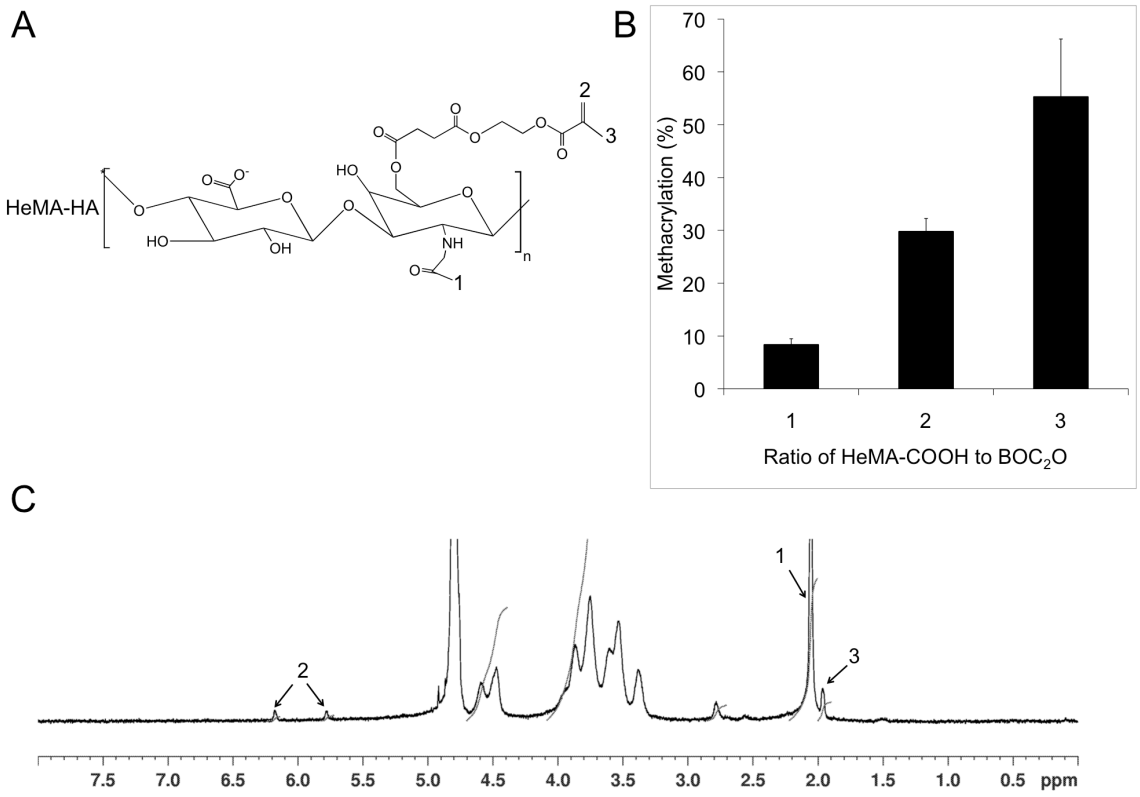

Figure 6.6 Chemical structure for HeMA-HA (A), the relationship between final methacrylation (modification) and HeMA-COOH to BOC_2O ratio during synthesis, n=4 (B), and representative ^1H NMR spectrum (D_2O) of HeMA-HA macromer (~10% modification) after finalized purification method (C). Peak 1= protons on the N-acetyl group on HA. Peak 2= protons of alkene on methacrylate group. Peak 3= protons of methyl group on HeMA moiety. Data presented as mean ± SD.

6.3.4 Formation of HeMA-HA and Copolymer Hydrogels

APS and TEMED redox reaction initiation was employed to polymerize macromers into hydrogels. As discussed in Section 4.1.3, this type of polymerization is most practical to facilitate delivery of the pre-polymer solution (ideally via catheter) to the

heart for MI repair. Furthermore, gelation times can be adjusted by altering initiator concentrations, providing enhanced control for delivery [1].

Specifically, either HeMA-HA alone or HeMA-HA/MeHA macromer solutions were mixed with APS and TEMED initiators to form homopolymer or copolymer hydrogels, respectively. Kinetic chains form through the reactive methacrylate groups to generate a network where bulk properties are dependent on the macromer percent modification, macromer concentration, and initiator concentration. In addition to the similar mechanical tunability and enzymatic degradation of MeHA hydrogels, HeMA-HA hydrogels are also susceptible to hydrolysis of the HeMA side groups, which break down into poly(methacrylic acid) kinetic chains and HA fragments. Here, we investigate the influence of the degree (i.e., HeMA percent modification) and type (i.e., HeMA/MeHA macromer ratio) of modification on gelation, mechanics, and degradation of HeMA-HA and copolymer hydrogels.

6.3.5 Characterization of HeMA-HA and Copolymer Hydrogels

HeMA-HA hydrogel characterization was performed to evaluate the influence of HeMA modification (~10%, ~30%, ~60%) on material properties including gelation, mechanics and degradation. Gelation was examined as described in Section 4.3.1 by performing a time sweep and defining the gel onset time as the intersection of the storage (G') and loss (G'') moduli. Increases in HeMA-HA methacrylation led to significantly shortened gel onset times (Figure 6.7A), potentially due to changes in reactive group concentration with HeMA-HA modification. As expected, increased methacrylation led to significantly increased compressive moduli and degradation time due to the greater crosslink density and number of bonds needing to hydrolyze for complete hydrogel degradation (Figure 6.7B).

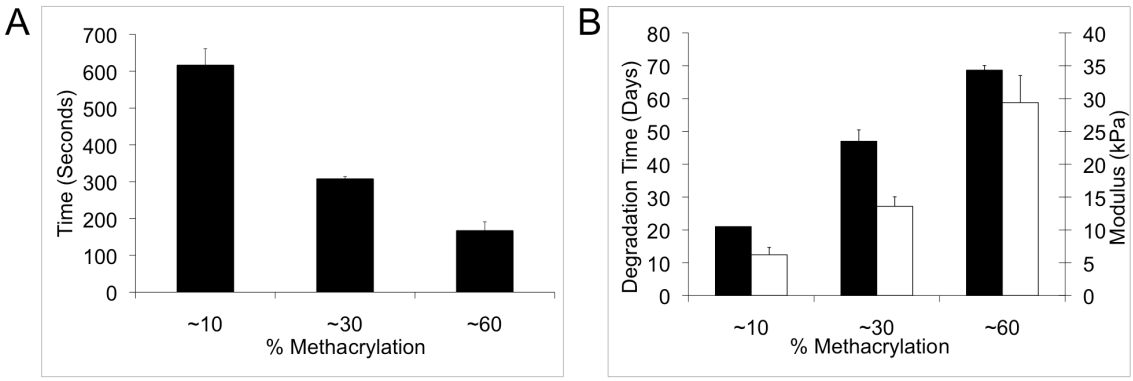

Figure 6.7 Gel onset, n=3-4, (A) and degradation time (black) and compressive modulus (white), n=3-4, (B) as a function of HeMA-HA modification, gelled at 5 mM APS/TEMED. Data are presented as mean ± SD. All groups are statistically significant ($p<0.05$).

Past work by our group with MeHA and α-hydroxy ester block copolymers has demonstrated that material properties such as mechanics and degradation can be tailored by adjusting the ratio of the MeHA block to the hydrolytically degradable block [28]. Here, we performed similar characterization with HeMA-HA (~20% modified) and MeHA (~100% modified) hydrogels formed at 5 copolymer ratios (HeMA-HA:MeHA, 100:0. 75:25, 50:50, 25:75, and 0:100) and a constant concentration (4 wt%). MeHA alone (0:100) displayed higher mechanics compared to HeMA-HA alone (100:0) and for copolymer groups the mechanics also increased with increased MeHA amount (Figure 6.8A). One copolymer formulation was selected for additional characterization (e.g., HeMA-HA:MeHA, 75:25); this formulation contained the greatest number of hydrolytically degradable groups, allowing for the most thorough assessment of degradation (via hydrolysis) on hydrogels.

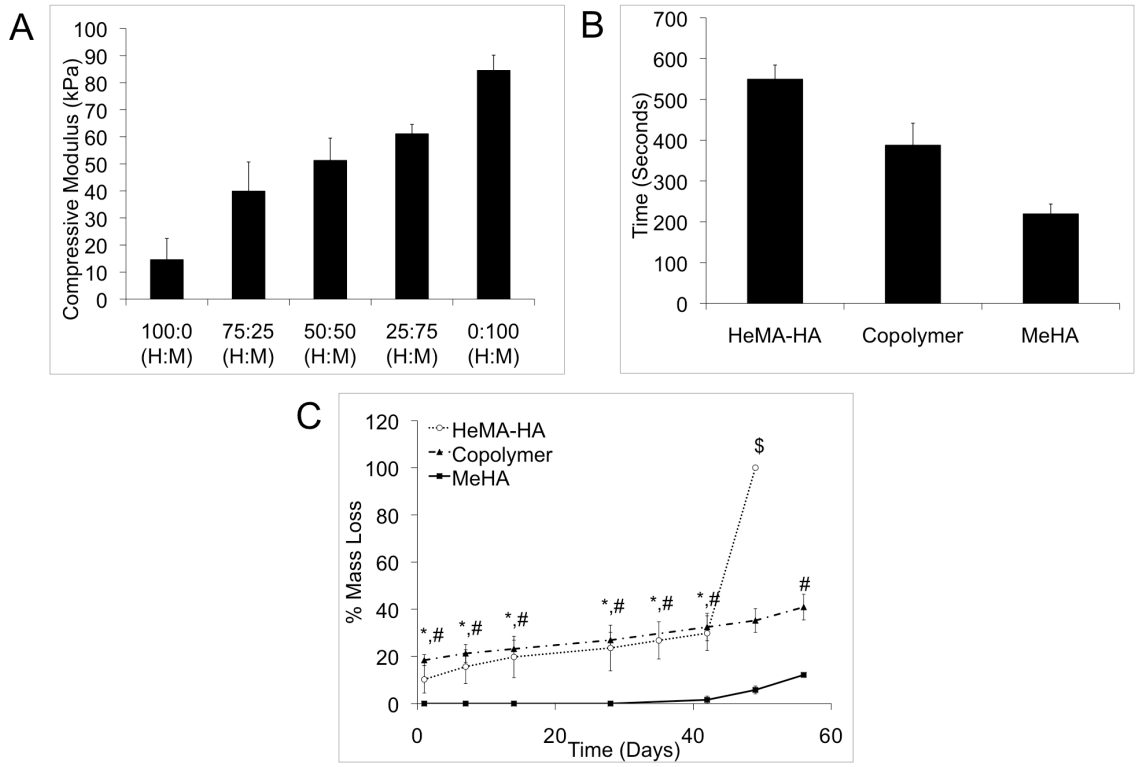

Figure 6.8 Compressive moduli of hydrogels formed from HeMA-HA:MeHA (H:M) copolymers at various ratios (n=4-5) (A). Gel onset times (n=4-5) (B) and degradation (n=3) (C) of HeMA-HA, selected copolymer (75:25, H:M), and MeHA. Data are presented as mean ± SD. For A, all groups are statistically different from each other except for 50:50 compared to 25:75 and 75:25 ($p<0.05$). All groups are statistically significant in B ($p<0.05$). For C: *$p<0.05$ HeMA-HA vs. MeHA, #$p<0.05$ copolymer vs. MeHA, \$$p<0.05$ between all groups.

Gel onset time for copolymer hydrogels was assessed as in homopolymer studies and results indicate that increased MeHA addition relative to HeMA-HA corresponds to accelerated gelation times (Figure 6.8B). Due to the extensive amount of time required for MeHA degradation, degradation for copolymer studies was evaluated with a uronic acid assay for 8 weeks, at which point hydrogels were degraded

via the addition of exogenous hyaluronidases. Figure 6.8C demonstrates that HA release from MeHA alone hydrogels was minimal throughout the 8 weeks and statistically lower than the copolymer and HeMA-HA hydrogels at all time points. Conversely, percent mass loss and degradation rate between the copolymer and HeMA-HA alone hydrogels were similar for about 6 weeks until a burst of HA release was observed in HeMA-HA hydrogels; this observation is likely due to the bulk degradation exhibited by hydrolytically degradable hydrogels, which is dependent on hydrogel swelling, where once a threshold of broken crosslinks is reached an exponential increase in mass loss follows. Copolymer degradation by 8 weeks was still comparatively low; however, a similar burst release as observed in HeMA-HA alone hydrogels may have been observed in a prolonged study since the copolymer is composed of primarily HeMA-HA compared to MeHA.

6.4 Conclusions

In this section, the synthesis and purification of a hydrolytically degradable HA macromer (HeMA-HA) with tunable functionality was achieved. Various hydrogels of varying composition were formed via redox chemical initiation by altering the amount of HeMA on the HA backbone and/or by forming copolymers with MeHA. Characterization of HeMA-HA hydrogels was performed for gel onset, initial mechanics and degradation. Altering the HeMA addition influenced all these parameters, confirming the tunability of hydrogel properties based on HeMA modification. Copolymers were also evaluated as an alternative approach to form hydrogels with tunable properties. This chapter illustrates the versatility of HeMA-HA hydrogels; by altering both functionalization and incorporating MeHA macromers, several combinations of initial mechanics and degradation can be achieved depending on the desired application. While the use of

copolymers was also effective in tuning degradation properties, the remainder of this dissertation will employ solely HeMA-HA homopolymers for simplicity in experimental design and the desire for accelerated degradation behavior. The next chapter will explore the application and influence of temporal degradation of HeMA-HA hydrogels to attenuate LV remodeling.

References:

[1] Ifkovits JL, Tous E, Minakawa M, Morita M, Robb JD, Koomalsingh KJ, Gorman JH, 3rd, Gorman RC, Burdick JA. Injectable hydrogel properties influence infarct expansion and extent of postinfarction left ventricular remodeling in an ovine model. Proc Natl Acad Sci U S A 2010;107:11507.

[2] Toole BP. Hyaluronan: from extracellular glue to pericellular cue. Nat Rev Cancer 2004;4:528.

[3] Masters KS, Shah DN, Leinwand LA, Anseth KS. Crosslinked hyaluronan scaffolds as a biologically active carrier for valvular interstitial cells. Biomaterials 2005;26:2517.

[4] Fraser JR, Laurent TC, Laurent UB. Hyaluronan: its nature, distribution, functions and turnover. J Intern Med 1997;242:27.

[5] Laurent TC, Fraser JR. Hyaluronan. FASEB J 1992;6:2397.

[6] Volpi N, Schiller J, Stern R, Soltes L. Role, metabolism, chemical modifications and applications of hyaluronan. Curr Med Chem 2009;16:1718.

[7] Chen WY, Abatangelo G. Functions of hyaluronan in wound repair. Wound Repair Regen 1999;7:79.

[8] Chung C, Burdick JA. Influence of three-dimensional hyaluronic acid microenvironments on mesenchymal stem cell chondrogenesis. Tissue Eng Part A 2009;15:243.

[9] Chung C, Erickson IE, Mauck RL, Burdick JA. Differential behavior of auricular and articular chondrocytes in hyaluronic acid hydrogels. Tissue Eng Part A 2008;14:1121.

[10] Erickson IE, Huang AH, Chung C, Li RT, Burdick JA, Mauck RL. Differential maturation and structure-function relationships in mesenchymal stem cell- and chondrocyte-seeded hydrogels. Tissue Eng Part A 2009;15:1041.

[11] Chung C, Mesa J, Randolph MA, Yaremchuk M, Burdick JA. Influence of gel properties on neocartilage formation by auricular chondrocytes photoencapsulated in hyaluronic acid networks. J Biomed Mater Res A 2006;77:518.

[12] Chung C, Mesa J, Miller GJ, Randolph MA, Gill TJ, Burdick JA. Effects of auricular chondrocyte expansion on neocartilage formation in photocrosslinked hyaluronic acid networks. Tissue Eng 2006;12:2665.

[13] Bian L, Zhai DY, Tous E, Rai R, Mauck RL, Burdick JA. Enhanced MSC chondrogenesis following delivery of TGF-β3 from alginate microspheres within hyaluronic acid hydrogels in vitro and in vivo. Biomaterials 2011;32:6425.

[14] Rodriguez KJ, Piechura LM, Masters KS. Regulation of valvular interstitial cell phenotype and function by hyaluronic acid in 2-D and 3-D culture environments. Matrix Biol 2011;30:70.

[15] Tous E, Ifkovits JL, Koomalsingh KJ, Shuto T, Soeda T, Kondo N, Gorman JH, 3rd, Gorman RC, Burdick JA. Influence of injectable hyaluronic acid hydrogel degradation behavior on infarction-induced ventricular remodeling. Biomacromolecules 2011;12:4127.

[16] Tous E, Purcell B, Ifkovits JL, Burdick JA. Injectable acellular hydrogels for cardiac repair. J Cardiovasc Transl Res 2011;4:528.

[17] Khetan S, Burdick JA. Patterning network structure to spatially control cellular remodeling and stem cell fate within 3-dimensional hydrogels. Biomaterials 2010;31:8228.

[18] Khetan S, Chung C, Burdick JA. Tuning hydrogel properties for applications in tissue engineering. Conf Proc IEEE Eng Med Biol Soc 2009;2009:2094-6.

[19] Khetan S, Burdick J. Cellular encapsulation in 3D hydrogels for tissue engineering. J Vis Exp 2009;32:1590.

[20] Marklein RA, Burdick JA. Controlling stem cell fate with material design. Adv Mater 2010;22:175.

[21] Rodgers LS, Lalani S, Hardy KM, Xiang X, Broka D, Antin PB, Camenisch TD. Depolymerized hyaluronan induces vascular endothelial growth factor, a negative regulator of developmental epithelial-to-mesenchymal transformation. Circ Res 2006;99:583.

[22] Mataveli FD, Han SW, Nader HB, Mendes A, Kanishiro R, Tucci P, Lopes AC, Baptista-Silva JC, Marolla AP, de Carvalho LP, Denapoli PM, Pinhal MA. Long-term effects for acute phase myocardial infarct VEGF165 gene transfer cardiac extracellular matrix remodeling. Growth Factors 2009;27:22.

[23] Camenisch TD, Spicer AP, Brehm-Gibson T, Biesterfeldt J, Augustine ML, Calabro A, Jr., Kubalak S, Klewer SE, McDonald JA. Disruption of hyaluronan synthase-2 abrogates normal cardiac morphogenesis and hyaluronan-mediated transformation of epithelium to mesenchyme. J Clin Invest 2000;106:349.

[24] Dobaczewski M, Gonzalez-Quesada C, Frangogiannis NG. The extracellular matrix as a modulator of the inflammatory and reparative response following myocardial infarction. J Mol Cell Cardiol 2010;48:504.

[25] West DC, Shaw DM, Lorenz P, Adzick NS, Longaker MT. Fibrotic healing of adult and late gestation fetal wounds correlates with increased hyaluronidase activity and removal of hyaluronan. Int J Biochem Cell Biol 1997;29:201.

[26] Burdick JA, Chung C, Jia X, Randolph MA, Langer R. Controlled degradation and mechanical behavior of photopolymerized hyaluronic acid networks. Biomacromolecules 2005;6:386.

[27] Burdick JA, Prestwich GD. Hyaluronic acid hydrogels for biomedical applications. Adv Mater 2011;23:H41.

[28] Chung C, Beecham M, Mauck RL, Burdick JA. The influence of degradation characteristics of hyaluronic acid hydrogels on in vitro neocartilage formation by mesenchymal stem cells. Biomaterials 2009;30:4287.

[29] Sahoo S, Chung C, Khetan S, Burdick JA. Hydrolytically degradable hyaluronic acid hydrogels with controlled temporal structures. Biomacromolecules 2008;9:1088.

[30] Temenoff JS, Kasper, F.K., Mikos, A.G. Fumarate-based macromers as scaffolds for tissue engineering. Top Tissue Eng 2007;3:16.

[31] Platzer M, Ozegowski JH, Neubert RH. Quantification of hyaluronan in pharmaceutical formulations using high performance capillary electrophoresis and the modified uronic acid carbazole reaction. J Pharm Biomed Anal 1999;21:491.

CHAPTER 7

Hydrolytically Degradable Hyaluronic Acid Hydrogels to Assess the Influence of Temporal Mechanical Support on Left Ventricular Remodeling

(Adapted from: **E Tous**, JL Ifkovits, KJ Koomalsingh, T Shuto, T Soeda, N Kondo, JH Gorman, III, RC Gorman, JA Burdick, "Influence of Injectable Hyaluronic Acid Hydrogel Degradation Behavior on Infarction Induced Ventricular Remodeling," Biomacromolecules, 2011, 12:4127-4135.)

7.1 Introduction

As reviewed in Chapter 1, myocardial infarction (MI) results from the occlusion of a coronary artery, leading to the depletion of oxygen and nutrients and resulting in cardiomyocyte necrosis and extracellular matrix (ECM) break down. As the ECM is disrupted, the myocardium is susceptible to geometric changes that subsequently increase stress throughout the injured and healthy regions of the heart [1-4]. These maladaptive responses lead to a series of biological and mechanical changes that cause further cell death and increase myocardial instability, which contribute to contractile dysfunction and can progress into a positive feedback loop that ultimately leads to heart failure (HF) [5-8]. The strategy in this investigation was to target these initial geometric alterations, which have been identified as the initiator of the maladaptive events associated with adverse post-MI remodeling [9-11].

7.1.1 Injectable Biomaterials for Myocardial Infarction (MI)

As has been discussed throughout this dissertation, numerous theoretical [2, 12, 13] and experimental models [14-32] have shown that limiting infarct expansion with the introduction of injectable materials into the infarct can attenuate the remodeling process, primarily through bulking (thickening) and stabilizing (stiffening) the infarct zone. While these reports have demonstrated the benefits of these injectable agents, the materials tested to date have had a wide range of properties, including the method of gelation, bulk mechanical properties and degradation behavior [14-16, 18-32]; consequently the mechanism behind their efficacy is unclear. Few studies have been performed to determine the optimal mechanical and degradation properties of the injected material; although, based on theoretical analyses both parameters should affect their efficacy [12, 13]. (Refer to Chapter 5 for theoretical assessment on the influence of mechanical factors).

7.1.2 Injectable Biomaterials for MI: Tunable Systems

Tunable hydrogel systems provide an important experimental tool to help identify optimal material properties of the injectate, since material properties (gelation, stiffness, and degradation) can be independently manipulated and examined. Ifkovits et al. recently used a mechanically tunable injectable material system where the influence of a mechanics on negative remodeling could independently be assessed [17]. Chapters 3, 4 and 5 already thoroughly discussed and referred to the mechanically tunable methacrylated hyaluronic acid (MeHA) hydrogels employed in that work. Briefly, two variations of MeHA were explored, where crosslink density (i.e., mechanics) was adjusted by varying the amount of methacrylation (low and high), yet gelation behavior and mass loss were similar [17]. This work concluded that high MeHA was more

effective in attenuating LV remodeling and motivated the importance of material mechanical properties in bulking agents and in stabilizing the myocardial wall post-MI. In this case both hydrogels were stable and still present after 8 weeks in an ovine MI model.

This chapter will further discuss properties for injectable hydrogels, with a focus on the timing of the material degradation. HA was functionalized with hydroxyethyl methacrylate (HeMA), to yield a macromer (HeMA-HA) that crosslinks similar to MeHA, yet has additional ester bonds that provide further control over hydrogel degradation. Initial HeMA-HA hydrogel characterization (gel onset, mechanics, and degradation) was performed in Chapter 6, and demonstrated that these properties could be tailored based on HeMA modification in a controlled manner. Here, we specifically compare the previous experimental work [17] of two versions of MeHA hydrogels (low and high mechanics) with the newly synthesized HeMA-HA hydrogels, where initial mechanics are matched and degradation timing was varied to evaluate the influence of temporal changes with HeMA-HA hydrogels. This system is the first to examine the temporal dependency of mechanical stabilization during the progression of LV remodeling, and provides insight into how long mechanical support must be applied to attenuate the aftermath of MI.

7.2 Materials and Methodology

The animals studied in this investigation received care in compliance with the protocols from the University of Pennsylvania that were approved by the Institutional Animal Care and Use Committee in accordance with the guidelines for humane care (National Institutes of Health Publication 85-23, revised 1996). All materials were purchased from Sigma-Aldrich unless otherwise indicated.

7.2.1 Synthesis of Hydroxyethyl Methacrylated Hyaluronic Acid (HeMA-HA) Macromer

Variations of HeMA-HA were synthesized by coupling HA-tetrabutylammonium salt (HA-TBA) with HeMA-COOH as discussed in Chapter 6. (For a more detailed description on HeMA-HA synthesis and purification refer to Sections 6.2.1 and 6.3.2, respectively). Briefly, HA-TBA coupling to HeMA-COOH was performed in di-methyl sulfoxide (DMSO) (Acros) for 20 hours and purified overnight by dialysis against deionized water at 4 °C, precipitation in acetone, and dialysis for 3 additional days against deionized water at 4 °C. Methacrylation was adjusted by varying the amount of HeMA-COOH and di-*tert*-butyl dicarbonate (BOC_2O) and all products were assessed with ^1H NMR (Bruker, 360 MHz). More details on tuning coupling are described in Section 6.3.3.

7.2.2 Synthesis of Methacrylated Hyaluronic Acid (MeHA) Macromer

MeHA was synthesized as described in Section 4.2.1 through the reaction of HA with methacrylic anhydride (Sigma) at pH 8.0 for 24 hours followed by dialysis and lyophilization [33]. Methacrylation was altered by varying the amount of methacrylic anhydride relative to HA and was assessed with ^1H NMR.

7.2.3 Formation, Characterization, and Selection of HeMA-HA Hydrogels

HeMA-HA hydrogel characterization was performed in Chapter 6 to examine the influence of varying degrees of HeMA functionalization on material properties (gel onset, initial mechanics and degradation). To compare HeMA-HA efficacy to that of MeHA in attenuating LV remodeling, two HeMA-HA variations (low and high) were selected based on this initial characterization. The chosen formulations were normalized to their respective MeHA (low and high) initial mechanics and gel dispersion by adjusting the

efficiency of crosslinking via alteration of the concentration of the oxidation-reduction (redox) initiators ammonium persulfate (APS, low: 8 mM, high: 7 mM) and N,N,N,N',N'-tetramethylethylenediamine (TEMED, low: 4 mM, high: 7 mM) (Table 7.1).

As described in Section 6.2.4, 4 wt% hydrogels were formed through a redox radical polymerization reaction with APS and TEMED [34]. Gelation was assessed, as in Section 6.2.4, by monitoring the storage (G') and loss (G'') moduli using an AR2000ex Rheometer (TA Instruments) at 37 °C under 1% strain and a frequency of 1 Hz in a cone and plate geometry (1°, 20 mm diameter). Gel dispersion was also evaluated in ovine explants by injecting 0.3 mL at either 2 or 3 minutes (depending on gel onset rheology data) to evaluate time dependent influences in high HeMA-HA compared to low HeMA-HA hydrogels.

To evaluate mechanics and degradation, hydrogels were formed between two glass slides within a teflon mold sealed with vacuum grease by mixing macromer and initiator solutions. To assess temporal mechanics, compression testing was performed on samples immediately after gelation (Day 0) or at desired time points throughout degradation (as in Section 6.2.4) with a Dynamic Mechanical Analyzer (DMA) (Q800 TA Instruments) at a strain rate of 10%/ min; moduli were calculated as the slope of the stress-strain curve at 10-20% strain. For degradation assessment, gels were incubated in phosphate buffered saline (PBS) at 37 °C and samples were collected at various time points and percent mass loss was quantified using a uronic acid assay [35].

7.2.4 In Vivo Evaluation in MI Model

Low and high HeMA-HA macromers were sterilized under germicidal ultraviolet (UV) light for 30 minutes on each side, and all solutions were filter sterilized. An established reproducible *in vivo* ovine MI model was employed to assess their efficacy in

limiting LV remodeling [28]. Twenty-one adult male Dorset sheep (35-40 kg) (n=6 low HeMA-HA, n=8 high HeMA-HA, n=7 infarct control) were anesthetized, underwent a left thoracotomy to expose the heart, and were monitored for arterial, ventricular, and pulmonary artery pressure and electrocardiogram throughout the surgery. Baseline echocardiographic and hemodynamic data were first obtained and then followed by infarction, induced via ligation of the left anterior descending (LAD) and second diagonal coronary artery to create an infarct that was ~40% of the distance from the apex to the base of the heart and included ~20% of the LV mass at the anteroapex [36].

Thirty minutes post-MI, HeMA-HA treatment sheep received 20 0.3 mL injections in the infarct area of the pre-polymer solution that was mixed for 2 to 3 minutes, depending on the polymer, before injection and gelation. Hemodynamic data and real-time three-dimensional echocardiographs (3DE) were collected before infarction, 30 minutes post-MI, 30 minutes post-injection, and 2 and 8 weeks after therapy. 3DE was used to quantify the extent of global LV remodeling by measuring LV end diastolic and systolic volumes at each time point. All volume measurements were normalized to pre-infarction values [17]. Functional outcomes were analyzed by evaluating ejection fraction (EF) at 2 and 8 weeks and with dobutamine (DoB) (2.5 and 5.0 mg kg^{-1} min^{-1}) stress testing. EF was evaluated by comparing baseline values to outcomes at 2 and 8 weeks post-MI and values under stress to no stress at 8 weeks. Animals were sacrificed at 8 weeks, and morphometric and histologic evaluations were performed on the excised hearts. Results were compared to controls consisting of infarct controls and previously published MeHA work (low MeHA (n=5) and high MeHA (n=7)) [17] to determine the efficacy of this system in limiting global LV remodeling.

7.2.4.1 In Vivo Evaluation in MI Model: Immunohistochemistry

Due to the potential influences of degradation on biological activity, both vessel formation and inflammation were evaluated in all groups in paraffin embedded sections at the 8 week time point. Vessels were stained with anti-α-smooth muscle actin (α-SMA, mouse anti-human, Dako, MO851), and examined at the apical, middle, and basilar infarct regions (one section per animal for each region). Vessel density was calculated in three fields of view at 20X magnification at the apical and basilar infarct regions and in nine magnification views in the middle infarct area of each section. Vessels were identified by positive α-SMA staining and were quantified in three ways: 1) all vessels greater than 10 μm, 2) all vessels with visible lumen greater than 10 μm, and 3) all thick vessels (vessels with more than one cell layer comprising the lumen) greater than 10 μm.

The inflammatory response was investigated by performing immunohistochemical (IHC) staining with major histocompatibility complex (MHC) class II (mouse anti-sheep, Serotec, MCA901). Staining was evaluated both near the biomaterial and in the surrounding tissue. Briefly, for IHC staining, paraffin sections were deparaffinized, hydrated and quenched for endogenous peroxidase activity for 5 minutes in 4% H_2O_2 in deionized water. After quenching, samples were washed 3X in Dako 1X wash buffer and primary antibody was applied at appropriate dilutions in Dako diluent (α-SMA: 1:500, MHC class II: 1:10) at room temperature (RT) for 30 minutes in a humidified chamber. After incubation, 3 washes in wash buffer were performed and samples were incubated with HRP labeled polymer (Dako, K4000) for 30 min at RT in a humidified chamber. After washing 3X in wash buffer, sections were incubated in diaminobenzadine substrate (Vector, SK-4100) at RT. Samples were then washed in

deionized water to stop the reaction, counterstained in hematoxylin stain, dehydrated and cover slipped.

7.2.5 Statistical Analysis

Data is presented as either mean ± SD (standard deviation) or mean ± SEM (standard error of the mean) as indicated in figure legends. All changes in data were assessed using a one-way ANOVA with Tukey's post hoc evaluation to account for differences between groups or time points. $p<0.05$ was considered statistically significant for all comparisons.

7.3 Results and Discussion

7.3.1 Selection and Characterization of HeMA-HA Hydrogels: Mechanics and Gelation

We previously synthesized MeHA macromer and injected two hydrogel formulations with varying mechanics *in vivo* into infarcted myocardium and observed mechanically-dependent outcomes [17]. Here, we address another property, degradation, by employing a new HA macromer that contains additional ester bonds between the HA backbone and reactive methacrylate that are susceptible to hydrolysis; similar to MeHA, HeMA-HA modification (percent) was assessed by ^{1}H NMR (Section 6.3.3).

HeMA-HA was reacted into hydrogels using redox initiation by mixing solutions of HeMA-HA containing either APS or TEMED to form kinetic chains and generate a network with bulk properties (e.g., mechanics) dependent on the crosslink density, which was influenced by factors including modification. Unlike MeHA hydrogels, HeMA-HA hydrogels are susceptible to both enzymatic degradation of the HA backbone and

hydrolysis of the side groups; thus, as demonstrated in Section 6.3.5, in addition to mechanical tunability, HeMA-HA also allows for enhanced tunability of degradation.

To address how both mechanics and degradation influence adverse LV remodeling, we investigated two variations (low and high) of two different macromers (HeMA-HA and MeHA) (four hydrogel groups in total), where two hydrogels with low mechanics were compared and two hydrogels with high mechanics were compared, each having variable degradation behavior. Specifically, the HeMA-HA tunability was used to identify two formulations for direct comparison to low and high MeHA from a previous study [17], where the initial material properties (i.e., initial mechanics and gel onset) were similar, but degradation was more rapid than their respective MeHA counterpart (i.e., low HeMA-HA vs. low MeHA and high HeMA-HA vs. high MeHA) (Table 7.1).

Table 7.1 Summary of the material properties of HeMA-HA and MeHA formulations evaluated in an *in vivo* ovine MI model.

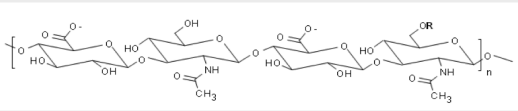		**Wt%**	**APS (A) and TEMED (T) Concentrations**	**Initial Mechanics**	**Degradation Time**
R= (MeHA) 	Low	4	A: 5 mM T: 5 mM	7.73 ± 1.05 kPa	Stable
	High	4	A: 5 mM T: 5 mM	43.00 ± 12.40 kPa	Stable
R= (HeMA-HA) 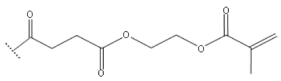	Low	4	A: 8 mM T: 4 mM	7.75 ± 2.44 kPa	~3 weeks
	High	4	A: 7 mM T: 7 mM	33.46 ± 0.84 kPa	~10 weeks

As demonstrated in Chapter 6, HeMA-HA material properties including mechanics and gelation behavior are both dependent on methacrylation; conversely, other work has shown that, while MeHA hydrogel mechanics are influenced by modification, gel onset properties (evaluated via rheometry) are not significantly affected [17]. To compensate for this discrepancy, initiator concentrations were tailored for HeMA-HA formulations (Table 7.1) to achieve gelation and mechanical properties that were similar to MeHA hydrogels. Previous work by Ifkovits et al., as well as data in Sections 5.3.1, have shown that material properties such as gel dispersion and bulk mechanics can be tuned by varying initiator concentrations [17]. While altering the initiator concentration was sufficient to normalize low HeMA-HA gelation to that of MeHA, high HeMA-HA gelation was more accelerated, according to rheometry assessment, despite adjustments of initiator concentration (Figure 7.1A). This was accounted for in *in vivo* work by injecting high HeMA-HA at 2 minutes, while low HeMA-HA and low and high MeHA were injected at 3 minutes. Gel dispersion of HeMA-HA was additionally examined in myocardial explants before *in vivo* work was performed to confirm that the delay in injection resulted in similar gel dispersion (Figure 7.1B).

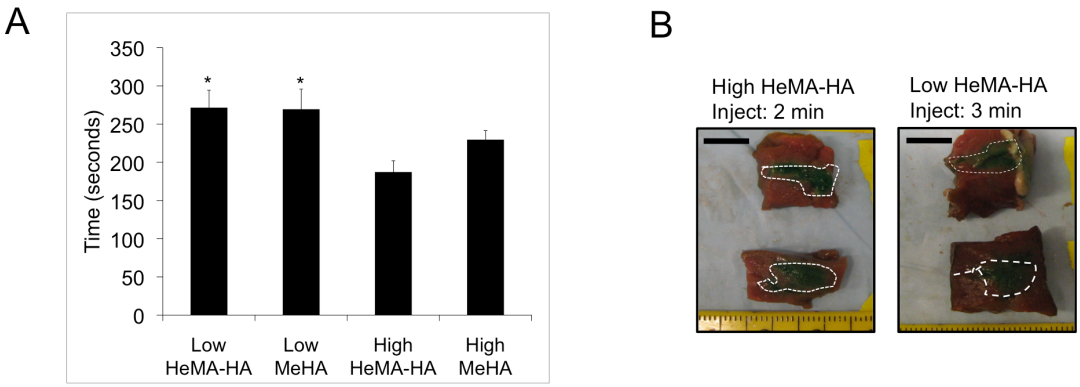

Figure 7.1 Gel onset time evaluated via rheometry for all four hydrogel formulations studied in *in vivo* MI work (n=3) (A) and representative images of low and high HeMA-HA dispersion in ovine explanted myocardial samples to validate similar dispersion at injected times (B). Data presented as mean ± SD. *p<0.05 vs. high HeMA-HA. Scale bar= 10 mm.

7.3.2 Characterization of HeMA-HA Hydrogels: Degradation

As previously discussed, HA is enzymatically degradable at its backbone; however, this is dependent on the availability of hyaluronidases [33, 37, 38]. Although MeHA does have an ester bond where the methacrylate attaches to HA, accessibility to this bond is sterically hindered and hydrolytic degradation is minimal; therefore, MeHA degradation is primarily dependent on an enzymatic mechanism and will be referred to as having stable degradation for the remainder of this chapter. HeMA-HA, however, has additional ester bonds that are accessible for hydrolytic degradation. Thus, in addition to the enzymatic mechanism of the HA backbone, HeMA-HA hydrogels undergo hydrolytic bulk degradation due to the availability of water throughout the gels. As seen in the degradation profiles (Figure 7.2A), both MeHA formulations lose little mass throughout the 8 week period, while both HeMA-HA formulations degraded within 8-10 weeks,

depending on the extent of modification. Since the HA is reacted via many groups into the kinetic chains, there is minimal mass loss at early time periods even with crosslink hydrolysis, which accelerates at late times when the HA chains can be released from the network, and eventually completely converts to soluble products.

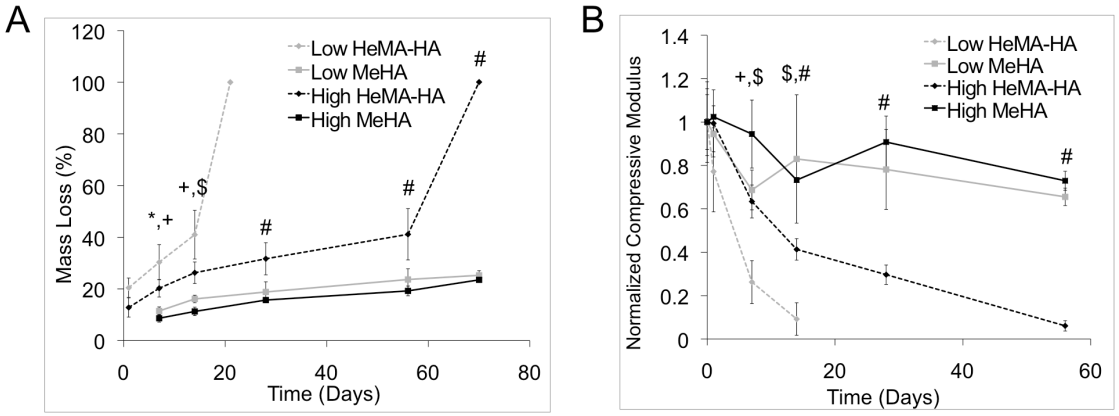

Figure 7.2 MeHA and HeMA-HA degradation, n=3-4, (A) and temporal mechanics profiles, n=3-4 (B). Data are presented as mean ± SD. *p<0.05 low HeMA-HA vs. low MeHA, +p<0.05 high HeMA-HA vs. high MeHA, $p<0.05 low HeMA-HA vs. all treatments, #p<0.05 high HeMA-HA vs. all treatments.

This hydrolysis also leads to exponential decreases in HeMA-HA mechanics, even more rapidly than mass loss, since hydrolysis can cleave the crosslinks and lead to decreases in mechanics prior to releasing mass into the surroundings (Figure 7.2B) [39-43]. MeHA hydrogel degradation profiles showed an initial minimal burst response that is commonly observed in hydrogels due to a soluble fraction, followed by stable, or minimal, degradation. Slight mechanical decreases in MeHA hydrogels were observed over this period. Overall, it is evident from degradation and mechanical temporal profiles that hydrolytic degradation was more influential in HeMA-HA hydrogels compared to

MeHA hydrogels. Importantly, release of HA may also have some biological function; as discussed in Section 6.1.2, HA plays an active role in wound healing by promoting cell migration and differentiation and angiogenesis and is involved in heart morphogenesis and development [44-48]. The influence of all treatment groups on local vessel density and inflammation will be discussed in more detailed in the *in vivo* portion of this chapter (i.e., Sections 7.3.3.4).

7.3.3 In Vivo Evaluation in MI Model

As previously discussed, LV remodeling refers to the complex series of events that occur post-MI. Briefly, initial ECM break down triggers infarct dilation that propagates throughout the borderzone (BZ) and remote region of the myocardium [1-4] leading to thinning of the myocardial wall and in global geometric changes that cause the heart to be susceptible to increased stress [5-7, 9, 10]. Although bulking agents are becoming an attractive therapy to stabilize the myocardium and deter geometric changes [14-32], there is still a lot that remains to be elucidated towards optimal properties of the injected material. Towards the importance of degradation, LV remodeling is a time sensitive process that can be broken down into three main periods of necrosis and acute inflammation, fibrosis, and remodeling. In humans, necrosis and acute inflammation occur within the first week, followed by fibrosis for approximately three additional weeks and finally by remodeling for approximately four more weeks [1]. Thus, it is of great importance to understand how the material presence during these various periods after infarction plays a role in the progression of LV remodeling; this is performed here with four material formulations.

7.3.3.1 In Vivo Evaluation in MI Model: Thickness

Thinning of the infarct region is an important contributor to increased wall stress both within the infarct and in the perfused regions of the heart and has been identified as a precipitating and sustaining phenomenon that drives adverse remodeling after MI. Infarct thickness was analyzed to evaluate the efficacy of the four treatment groups in preventing remodeling. Specifically, thicknesses in the apical infarct, basilar infarct, BZ, and in the remote myocardium were measured for each treatment group, normal (non-infarcted) and for infarct controls (Figure 7.3A, B). As expected, 8 weeks post-MI, infarct control animals displayed a significantly thinner myocardial wall in the apical and basilar infarct (apical: 2.2 mm, basilar: 4.6 mm) regions compared to normal non-infarct animals measured at areas corresponding to infarct regions in treatment animals (apical: 6.1 mm, basilar: 8.5 mm). As previously shown, MeHA treatment was able to maintain thicknesses in the apical and basilar infarct at levels similar to normal tissue (low MeHA: apical: 6.5 mm, basilar: 7.0 mm, high MeHA: apical: 7.0 mm, basilar: 7.2 mm) [17]; this is likely due to the stability and minimal degradation behavior of these polymers. Interestingly, despite their susceptibility to hydrolytic degradation, treatment with both HeMA-HA polymers increased the myocardium thickness compared to infarct controls, with significant increases observed in high HeMA-HA treatments in the apical infarct region but no significant increases in either polymer in the basilar infarct region (low HeMA-HA: apical: 3.5 mm, basilar: 6.0 mm, high HeMA-HA: apical: 4.1 mm, basilar 6.1 mm). The mechanism behind HeMA-HA thickness increases, particularly for low HeMA-HA, are not completely understood, but are thought to be due to a biological role of the material and degradation products (including vessel formation and inflammation) [24]. Similar increases in myocardial thickness relative to infarct controls have been observed following injection of fibrin, which also degrades in several weeks [14, 21].

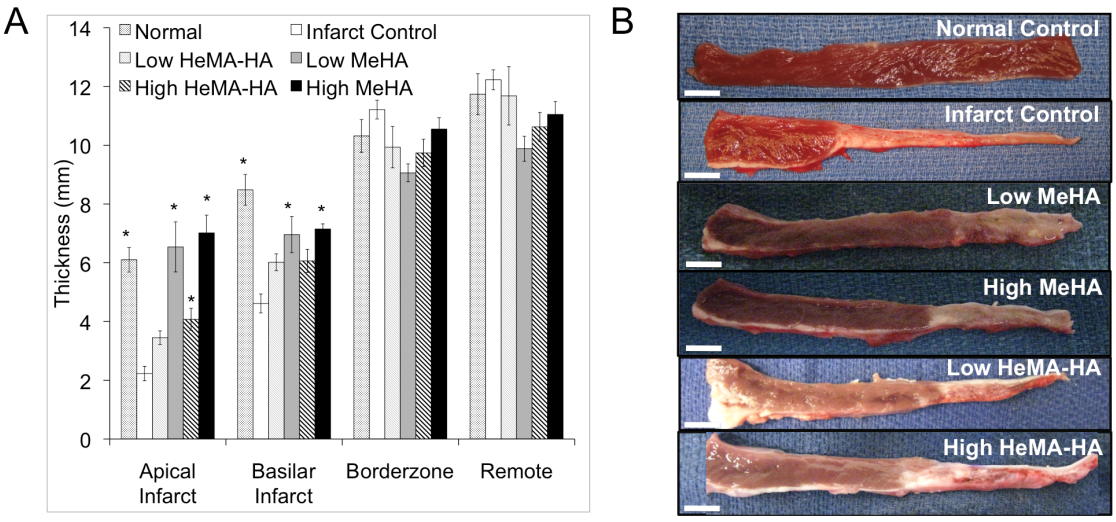

Figure 7.3 Myocardium thickness of normal myocardium, infarct controls, and HA treatment groups (A: quantified, B: images) 8 weeks post-MI. Data are presented as mean ± SEM. *p<0.05 vs. infarct control. Scale bar= 10 mm.

Histological analysis of the tissue at 8 weeks provided insight into the amount of remaining gel at this time post-MI (Figure 7.4). As expected from the *in vitro* degradation assays, hydrogel was present in both MeHA formulations and to a minimal extent in the high HeMA-HA treatment group, primarily in the apical infarct regions. In contrast, no gel was observed at all locations at 8 weeks for the low HeMA-HA groups. This observation supports *in vitro* trends as well as the limited enzymatic degradation that occurs to break down the MeHA hydrogels. Generally, extensive collagen staining was observed in all groups, with more prominent staining in the low HeMA-HA formulations, potentially due to the released degradation products and changes in the inflammatory response.

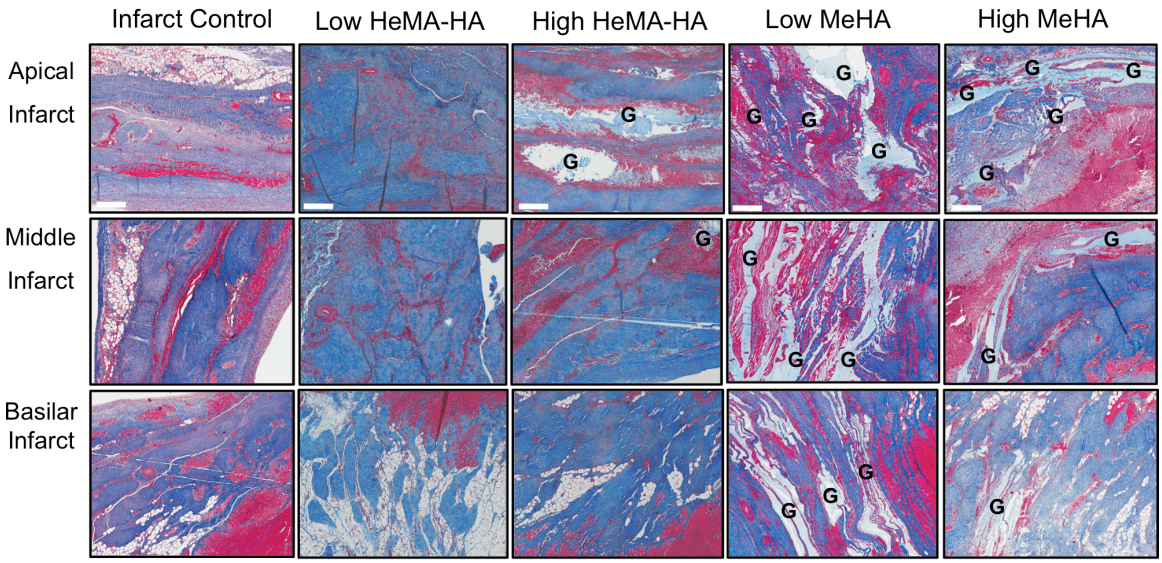

Figure 7.4 Histological evaluation (Masson's Trichrome stain) and representative images of treatment groups at the apical, middle, and basilar infarct regions 8 weeks post-MI. Scale bar= 500 μm. G= Gel.

7.3.3.2 In Vivo Evaluation in MI Model: End Diastolic and Systolic Volume

In addition to thickness increases, the extent of LV dilation in treatment groups was compared to infarct control data by quantifying normalized end diastolic and systolic volumes (NEDV and NESV) from 3DE data 2 and 8 weeks post-MI. As expected from previous studies [17] both low polymers were ineffective in preventing volume increases (Figure 7.5). Conversely, treatment with high polymers revealed promising results at 2 weeks where both high polymers limited LV increases to similar degrees (high HeMA-HA: NEDV: 1.61 and NESV: 1.96, and high MeHA: NEDV: 1.62 and NESV: 1.89); however, at 8 weeks it was evident that the high MeHA was more effective (high HeMA-HA: NEDV: 1.98 and NESV: 2.46, and high MeHA: NEDV: 1.70 and NESV: 1.98). *In vitro* mechanical data supported these findings; while both high polymers had higher

mechanics than myocardial tissue (~6 kPa) at 2 weeks [17], high HeMA-HA mechanics were reduced to values lower than initial low values (~2 kPa) by 8 weeks. This finding supports the importance of the timing of mechanical support and suggests that myocardium stabilization is required for a longer period of time (at least 8 weeks) to be most effective in attenuating LV dilation.

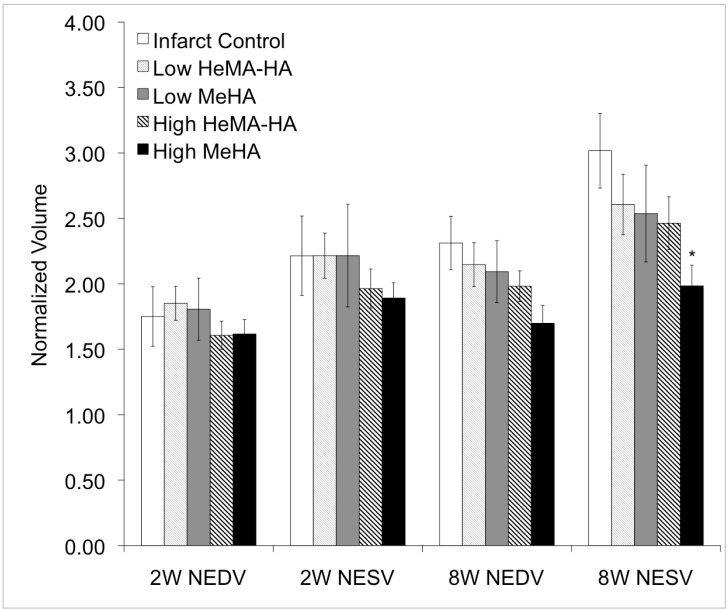

Figure 7.5 End diastolic and systolic volumes normalized to each treatment's respective baseline (NEDV and NESV) 8 weeks post-MI. Data presented as mean ± SEM. *p<0.05 vs. infarct control.

7.3.3.3 In Vivo Evaluation in MI Model: Infarct Area

As discussed, post-MI the ischemic infarcted region can spread and further the progression of maladaptive LV remodeling. Treatment with both HeMA-HA polymers significantly decreased the infarct area compared to infarct controls (Figure 7.6). These improvements could be due to the biological role of soluble HA, which has shown to

promote wound healing as well as angiogenesis [24, 49]. While biological factors are thought to contribute to this finding, Ifkovits et al. demonstrated that mechanical factors also play a role in decreasing infarct area [17]. It is, thus, likely that both these factors influence remodeling; additional investigation (e.g., on the biological role of HA in MI) would be beneficial to fully elucidate the mechanism behind this finding.

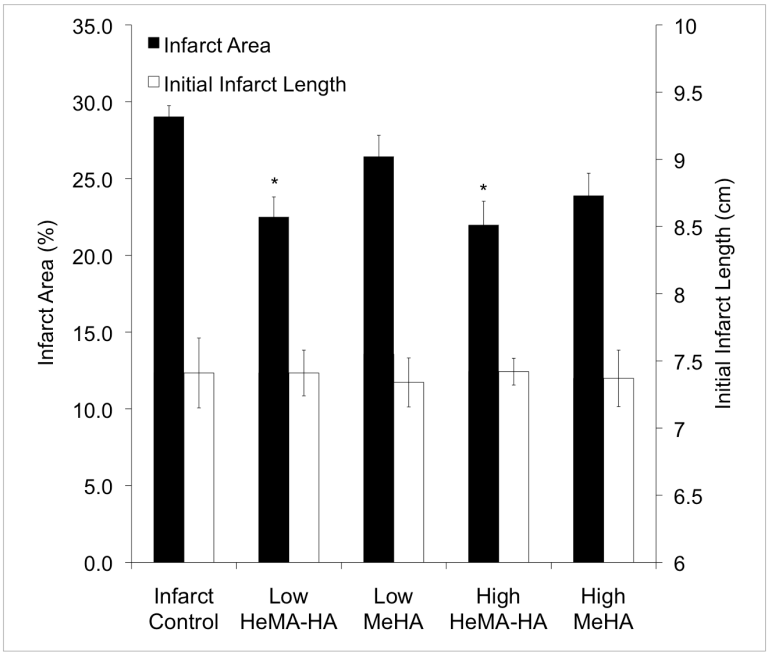

Figure 7.6 Infarct area of each group along side their respective initial infarct length compared to infarct control. Data are presented as mean ± SEM. *p<0.05 vs. infarct control.

7.3.3.4 In Vivo Evaluation in MI Model: Immunohistochemistry

Vessel Formation: α-SMA

MI results from the occlusion of an artery and leads to the depletion of oxygen and nutrients to the heart. To remedy this and salvage viable myocardium, groups have

focused on restoring blood flow to ischemic tissue by stimulating vessel formation. While this has been successful via delivery of pro-angiogenic growth factors such as FGF [50-53], VEGF [54, 55] and PDGF [54], and molecules such as pleiotrophin [56], other groups have also shown that biomaterials without angiogenic stimulants also hold the potential to promote neovascularization [57]. In this investigation, IHC staining for α-SMA was performed to assess the ability of our HA hydrogels to induce vessel formation.

At 8 weeks post-MI, treatment with all four HA hydrogel groups resulted in an increase in vessel density in the apical, middle, and basilar infarct regions of the heart compared to infarct controls (Figure 7.7), suggesting a role of HA hydrogel treatment in stimulating neovascularization. Significant improvements were observed when evaluating all vessels (Figure 7.7C) and thick vessels greater than 10 μm (Figure 7.7E) between HeMA-HA hydrogel groups and infarct controls in the middle region of the infarct. In addition, both high mechanics hydrogel groups demonstrated significant increases in vessel density in the basilar infarct region compared to infarct controls. No significant differences were observed when examining vessels with visible lumen (Figure 7.7D). In general, vessel quantification showed that HA treatment resulted in a similar degree of vessel formation in degradable and stable gels. α-SMA positive staining in non-vessel forming cells was also observed, potentially indicative of myofibroblasts. While all treatment groups demonstrated more positive staining than infarct controls, groups with hydrogel remaining 8 weeks post-MI (high HeMA-HA, low MeHA, and high MeHA), particularly MeHA hydrogels, exhibited more pronounced staining around biomaterial implants (Figure 7.7A).

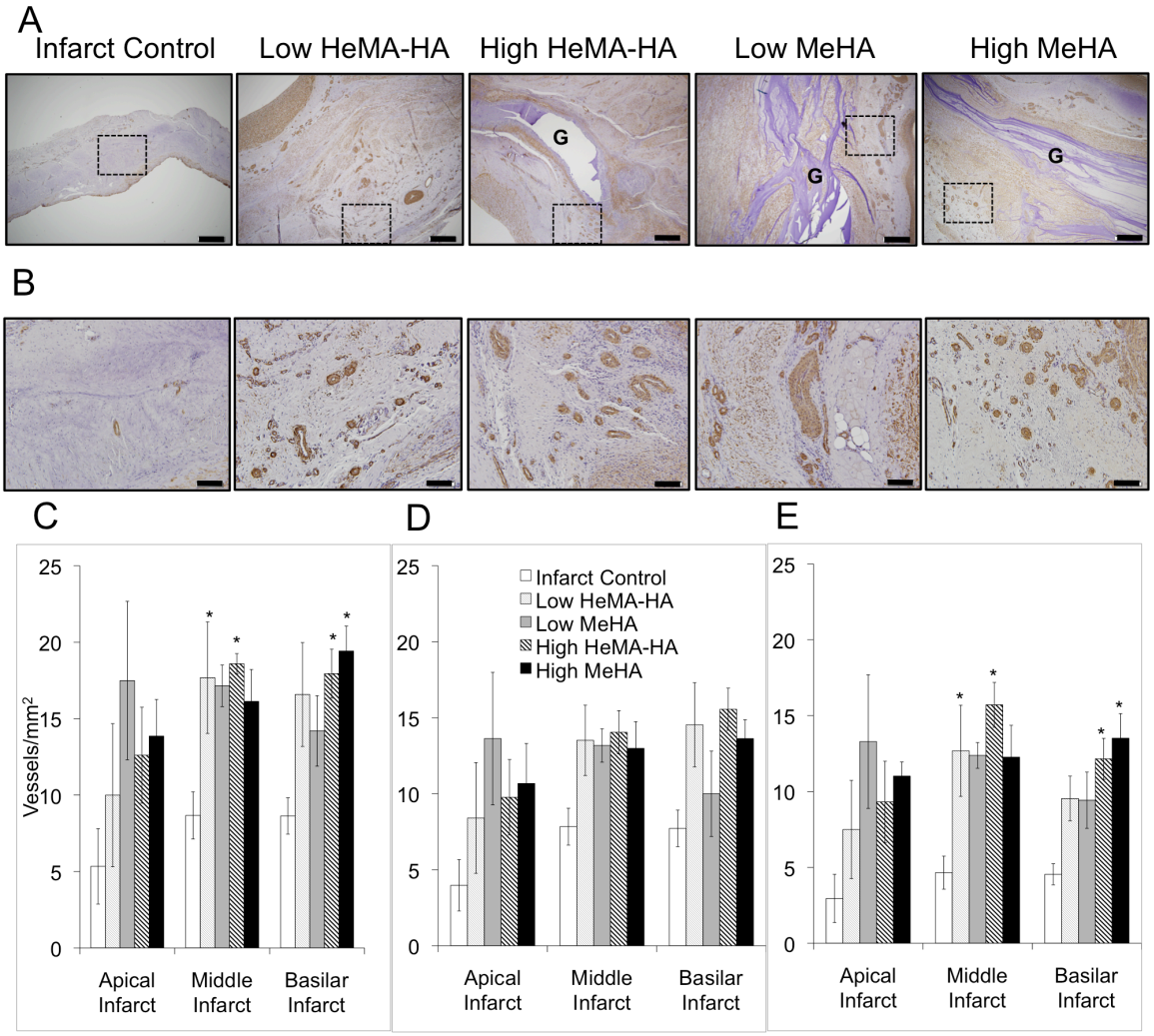

Figure 7.7 Immunohistochemical evaluation of α-SMA for vessel formation. Representative images of myocardium cross-section in middle region of infarct (scale bar= 500 μm) (A), and zoomed in representative images of vessels (scale bar= 100 μm) (B) in each group. Quantified vessel density of all vessels over 10 μm (C), all vessels with lumen over 10 μm (D), and all thick vessels over 10 μm (E). Data are presented as mean ± SEM. *p<0.05 vs. infarct control. G= Gel.

Inflammation: MHC Class II

Inflammatory responses play a large role in tissue remodeling, which is important in the context of biomaterials for cardiac repair [58, 59]. To address this, an IHC evaluation with anti-MHC class II was performed to assess the degree of inflammation resulting from degradable and stable HA hydrogel treatments. MHC class II proteins are expressed on antigen presenting cells, which include macrophages, dendritic cells and B lymphocytes. These cells present digested fragments of foreign extracellular antigens on their surface and are able to interact with helper T cells to stimulate an adaptive immune response [60, 61]. Examination of MHC class II expressing cells, thus, provides a general idea of the inflammatory response to various hydrogels.

MHC class II staining was analyzed in both the surrounding tissue and at the biomaterial interface, in groups where biomaterial was still present at 8 weeks. Staining in the surrounding tissue was generally limited to areas with vessels and as a result, all treatment groups displayed more positive MHC class II staining in this region (Figure 7.8). Although all groups exhibited more staining, treatment with both HeMA-HA groups, particularly high HeMA-HA, appeared to result in more prevalent staining in the surrounding tissue (Figure 7.8A). A similar observation was observed at the biomaterial interface, where high HeMA-HA resulted in more positive MHC class II staining around the hydrogel compared to stable degrading MeHA hydrogels (Figure 7.8B). According to *in vitro* work, high HeMA-HA hydrogels degrade within approximately 10 weeks; thus, it is expected that they are undergoing degradation and release degradation products, which stimulate MHC class II expression, compared to MeHA gels, which have limited degradation at 8 weeks.

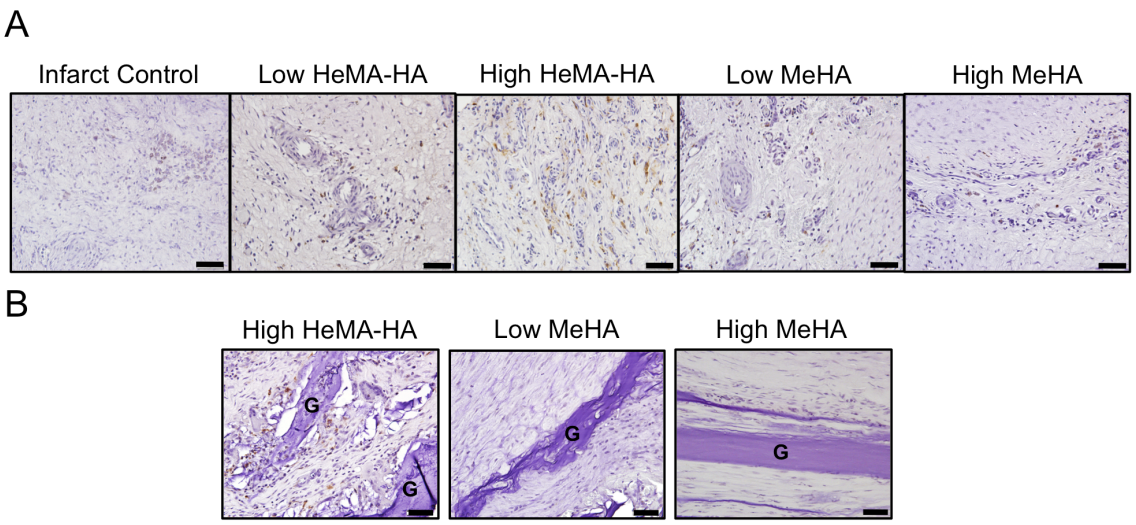

Figure 7.8 Immunohistochemical examination of inflammation with MHC class II. Representative images in surrounding tissue in all groups (A) and representative images at biomaterial interface in all groups with biomaterial present at 8 weeks (B). Scale bar= 50 μm. G=Gel.

7.3.3.5 In Vivo Evaluation in MI Model: Ejection Fraction

Functional improvements of ejection fraction (EF) were evaluated by comparing baseline to 2 and 8 weeks post-MI. All groups displayed lower EF at 2 and 8 weeks post-MI compared to baseline; however, all treatment groups resulted in smaller decreases in EF than infarct controls (Figure 7.9A). In addition to comparing EF at 2 and 8 weeks, EF was also evaluated during stress testing. Stress testing, which can be implemented via exercise or intravenous pharmacological simulation [62, 63], is often used for diagnostic purposes to evaluate how the heart responds to external stress by comparing blood flow before and after exertion. Examining the heart during exertion allows clinicians to better pinpoint any abnormalities and determine the patient's prognosis that may not have been obvious before testing. Stress testing was used in

this study as a more sensitive technique to detect functional improvements from treatments. Cardiac function was evaluated upon stress testing with dobutamine (DoB) (2.5 and 5.0 $mg \cdot kg^{-1}min^{-1}$), which was conducted before sacrifice at 8 weeks. EF values of all groups increased with stress compared to no stress at 8 weeks (Figure 7.9B), with most improvement in the high MeHA hydrogel treatment group (Figure 7.9B). These EF trends verify previous work [17], in that that highest mechanical support did result in the largest functional improvement under stress. While some improved trends were also observed in the high HeMA-HA treated group, they were lower than high MeHA. These findings suggest that while HeMA-HA initial support at 2 weeks did provide subtle improvements seen under stress, treatment with the high MeHA is more effective in promoting functional improvements under stress. Further functional evaluation at longer time points may provide more information on the observed trends as well as more insight into long-term improvements.

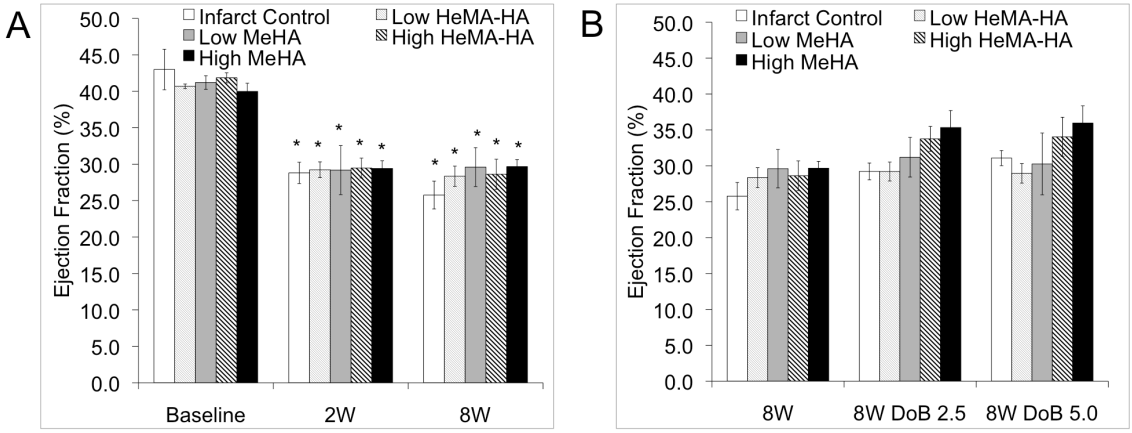

Figure 7.9 Ejection fraction of treatment groups compared to their respective baseline values (A) and under dobutamine stress testing compared to no stress at 8 weeks (B). Data are presented as mean ± SEM. *$p<0.05$ vs. respective baseline.

As previously discussed, hydrogels were injected 30 minutes post-MI and evaluated at 2 and 8 weeks. Treatment was employed early to reduce the number of surgical interventions to limit animal mortality. Other studies have injected materials as early as immediately after MI [25] and as late as two months [18]; most have shown improvement, with earlier injections before potential irreversible processes resulting in more effective attenuation in LV remodeling [18]. Despite this, the appropriate time for injection it is still not clear. The average time between MI symptom onset to hospital prevention is 2-6 hours [64, 65], thus, a 30 minute injection time is not clinically feasible. Another implication to consider is the progression of the remodeling process; in this report, hydrogels were injected during the onset of necrosis and acute inflammation. The specific stage during which the hydrogel is injected, as well as the temporal properties from that injection point, may play a role in the overall outcomes.

7.4 Conclusions

The overall goal of this chapter was to gain a better understanding on the significance of the duration of mechanical support in attenuating LV remodeling. This was achieved by employing hydrolytically degradable hydrogels (HeMA-HA) with tunable degradation and temporal mechanics. Specifically, two formulations of HeMA-HA hydrogels were selected to compare to two MeHA hydrogels, with similar initial mechanics and gel dispersion, in their efficacy to limit negative remodeling. When injected into early infarct tissue in an ovine model, HeMA-HA hydrogels demonstrated a similar vascular response to their MeHA gel counterpart; however, they also induced a stronger inflammatory response that may be associated with their degradation. Along similar lines, HeMA-HA hydrogels also revealed that HA may play a biological role in limiting spreading of ischemic tissue. Most interestingly, however, studies with HeMA-

HA revealed that geometrical improvements (e.g., limited chamber dilation) are dependent on the duration of mechanical support with best outcomes resulting from high MeHA treatment. High MeHA treatment also showed the most improved trends in EF under stress testing. Overall, these results demonstrate the utility of tunable hydrogel systems in probing the influence of material properties on adverse remodeling outcomes after infarction. Specifically, they implicate a significant role in the duration of mechanical support (e.g., temporal mechanics) and the potential biological function of HA.

References:

[1] Holmes JW, Borg TK, Covell JW. Structure and mechanics of healing myocardial infarcts. Annu Rev Biomed Eng 2005;7:223.

[2] Pilla JJ, Gorman JH, 3rd, Gorman RC. Theoretic impact of infarct compliance on left ventricular function. Ann Thorac Surg 2009;87:803.

[3] Kelley ST, Malekan R, Gorman JH, 3rd, Jackson BM, Gorman RC, Suzuki Y, Plappert T, Bogen DK, Sutton MG, Edmunds LH, Jr. Restraining infarct expansion preserves left ventricular geometry and function after acute anteroapical infarction. Circulation 1999;99:135.

[4] Jackson BM, Gorman JH, 3rd, Salgo IS, Moainie SL, Plappert T, St John-Sutton M, Edmunds LH, Jr., Gorman RC. Border zone geometry increases wall stress after myocardial infarction: contrast echocardiographic assessment. Am J Physiol Heart Circ Physiol 2003;284:H475.

[5] Epstein FH, Yang Z, Gilson WD, Berr SS, Kramer CM, French BA. MR tagging early after myocardial infarction in mice demonstrates contractile dysfunction in adjacent and remote regions. Magn Reson Med 2002;48:399.

[6] Frangogiannis NG, Smith CW, Entman ML. The inflammatory response in myocardial infarction. Cardiovasc Res 2002;53:31.

[7] Dobaczewski M, Gonzalez-Quesada C, Frangogiannis NG. The extracellular matrix as a modulator of the inflammatory and reparative response following myocardial infarction. J Mol Cell Cardiol 2010;48:504.

[8] Dang AB, Guccione JM, Mishell JM, Zhang P, Wallace AW, Gorman RC, Gorman JH, 3rd, Ratcliffe MB. Akinetic myocardial infarcts must contain contracting myocytes: finite-element model study. Am J Physiol Heart Circ Physiol 2005;288:H1844.

[9] Pfeffer MA, Braunwald E. Ventricular remodeling after myocardial infarction. Experimental observations and clinical implications. Circulation 1990;81:1161.

[10] Pfeffer MA, Pfeffer JM. Ventricular enlargement and reduced survival after myocardial infarction. Circulation 1987;75:IV93.

[11] Erlebacher JA, Weiss JL, Weisfeldt ML, Bulkley BH. Early dilation of the infarcted segment in acute transmural myocardial infarction: role of infarct expansion in acute left ventricular enlargement. J Am Coll Cardiol 1984;4:201.

[12] Wall ST, Walker JC, Healy KE, Ratcliffe MB, Guccione JM. Theoretical impact of the injection of material into the myocardium: a finite element model simulation. Circulation 2006;114:2627.

[13] Wenk JF, Wall ST, Peterson RC, Helgerson SL, Sabbah HN, Burger M, Stander N, Ratcliffe MB, Guccione JM. A method for automatically optimizing medical devices for treating heart failure: designing polymeric injection patterns. J Biomech Eng 2009;131:121011.

[14] Christman KL, Fok HH, Sievers RE, Fang Q, Lee RJ. Fibrin glue alone and skeletal myoblasts in a fibrin scaffold preserve cardiac function after myocardial infarction. Tissue Eng 2004;10:403.

[15] Christman KL, Vardanian AJ, Fang Q, Sievers RE, Fok HH, Lee RJ. Injectable fibrin scaffold improves cell transplant survival, reduces infarct expansion, and induces neovasculature formation in ischemic myocardium. J Am Coll Cardiol 2004;44:654.

[16] Dai W, Wold LE, Dow JS, Kloner RA. Thickening of the infarcted wall by collagen injection improves left ventricular function in rats: a novel approach to preserve cardiac function after myocardial infarction. J Am Coll Cardiol 2005;46:714.

[17] Ifkovits JL, Tous E, Minakawa M, Morita M, Robb JD, Koomalsingh KJ, Gorman JH, 3rd, Gorman RC, Burdick JA. Injectable hydrogel properties influence infarct

expansion and extent of postinfarction left ventricular remodeling in an ovine model. Proc Natl Acad Sci U S A 2010;107:11507.

[18] Landa N, Miller L, Feinberg MS, Holbova R, Shachar M, Freeman I, Cohen S, Leor J. Effect of injectable alginate implant on cardiac remodeling and function after recent and old infarcts in rat. Circulation 2008;117:1388.

[19] Nelson DM, Ma Z, Fujimoto KL, Hashizume R, Wagner WR. Intra-myocardial biomaterial injection therapy in the treatment of heart failure: Materials, outcomes and challenges. Acta Biomater 2011;7:1.

[20] Tsur-Gang O, Ruvinov E, Landa N, Holbova R, Feinberg MS, Leor J, Cohen S. The effects of peptide-based modification of alginate on left ventricular remodeling and function after myocardial infarction. Biomaterials 2009;30:189.

[21] Yu J, Christman KL, Chin E, Sievers RE, Saeed M, Lee RJ. Restoration of left ventricular geometry and improvement of left ventricular function in a rodent model of chronic ischemic cardiomyopathy. J Thorac Cardiovasc Surg 2009;137:180.

[22] Mukherjee R, Zavadzkas JA, Saunders SM, McLean JE, Jeffords LB, Beck C, Stroud RE, Leone AM, Koval CN, Rivers WT, Basu S, Sheehy A, Michal G, Spinale FG. Targeted myocardial microinjections of a biocomposite material reduces infarct expansion in pigs. Ann Thorac Surg 2008;86:1268.

[23] Huang NF, Yu J, Sievers R, Li S, Lee RJ. Injectable biopolymers enhance angiogenesis after myocardial infarction. Tissue Eng 2005;11:1860.

[24] Yoon SJ, Fang YH, Lim CH, Kim BS, Son HS, Park Y, Sun K. Regeneration of ischemic heart using hyaluronic acid-based injectable hydrogel. J Biomed Mater Res B: Appl Biomater 2009;91:163.

[25] Kofidis T, Lebl DR, Martinez EC, Hoyt G, Tanaka M, Robbins RC. Novel injectable bioartificial tissue facilitates targeted, less invasive, large-scale tissue restoration on the beating heart after myocardial injury. Circulation 2005;112:I173.

[26] Yu J, Gu Y, Du KT, Mihardja S, Sievers RE, Lee RJ. The effect of injected RGD modified alginate on angiogenesis and left ventricular function in a chronic rat infarct model. Biomaterials 2009;30:751.

[27] Leor J, Tuvia S, Guetta V, Manczur F, Castel D, Willenz U, Petnehazy O, Landa N, Feinberg MS, Konen E, Goitein O, Tsur-Gang O, Shaul M, Klapper L, Cohen S. Intracoronary injection of in situ forming alginate hydrogel reverses left ventricular remodeling after myocardial infarction in swine. J Am Coll Cardiol 2009;54:1014.

[28] Ryan LP, Matsuzaki K, Noma M, Jackson BM, Eperjesi TJ, Plappert TJ, St John-Sutton MG, Gorman JH, 3rd, Gorman RC. Dermal filler injection: a novel approach for limiting infarct expansion. Ann Thorac Surg 2009;87:148.

[29] Fujimoto KL, Ma Z, Nelson DM, Hashizume R, Guan J, Tobita K, Wagner WR. Synthesis, characterization and therapeutic efficacy of a biodegradable, thermoresponsive hydrogel designed for application in chronic infarcted myocardium. Biomaterials 2009;30:4357.

[30] Jiang XJ, Wang T, Li XY, Wu DQ, Zheng ZB, Zhang JF, Chen JL, Peng B, Jiang H, Huang C, Zhang XZ. Injection of a novel synthetic hydrogel preserves left ventricle function after myocardial infarction. J Biomed Mater Res A 2009;90:472.

[31] Wang T, Jiang XJ, Lin T, Ren S, Li XY, Zhang XZ, Tang QZ. The inhibition of postinfarct ventricle remodeling without polycythaemia following local sustained intramyocardial delivery of erythropoietin within a supramolecular hydrogel. Biomaterials 2009;30:4161.

[32] Wang T, Wu DQ, Jiang XJ, Zhang XZ, Li XY, Zhang JF, Zheng ZB, Zhuo R, Jiang H, Huang C. Novel thermosensitive hydrogel injection inhibits post-infarct ventricle remodelling. Eur J Heart Fail 2009;11:14.

[33] Burdick JA, Chung C, Jia X, Randolph MA, Langer R. Controlled degradation and mechanical behavior of photopolymerized hyaluronic acid networks. Biomacromolecules 2005;6:386.

[34] Temenoff JS, Kasper FK, Mikos AG. Fumarate-based macromers as scaffolds for tissue engineering. Top Tissue Eng 2007;3:16.

[35] Platzer M, Ozegowski JH, Neubert RH. Quantification of hyaluronan in pharmaceutical formulations using high performance capillary electrophoresis and the modified uronic acid carbazole reaction. J Pharm Biomed Anal 1999;21:491.

[36] Markovitz LJ, Savage EB, Ratcliffe MB, Bavaria JE, Kreiner G, Iozzo RV, Hargrove WC, 3rd, Bogen DK, Edmunds LH, Jr. Large animal model of left ventricular aneurysm. Ann Thorac Surg 1989;48:838.

[37] Ernst S, Langer R, Cooney CL, Sasisekharan R. Enzymatic degradation of glycosaminoglycans. Crit Rev Biochem Mol Biol 1995;30:387.

[38] Sahoo S CC, Khetan S, Burdick J. Hydrolytically degradable hyraluronic acid hydrogels with controlled temporal structures. Biomacromolecules 2008;8:5.

[39] Langer R, Peppas, N. Chemical and physical structure of polymers as carriers for controlled release of bioactive agents: a review. J Macromol Sci-Rev Macromol Chem Phys 1983;C23:65.

[40] Metters AT, Bowman CN, Anseth KS. A statistical kinetic model for the bulk degradation of PLA-b-PEG-b-PLA hydrogel networks. J Phys Chem B 2000;104:7.

[41] Metters AT, Anseth KS, Bowman CN. Fundamental studies of biodegradable hydrogels as cartilage replacement materials. Biomed Sci Instrum 1999;35:33.

[42] Sawhney AS, Hubbell JA. Poly(ethylene oxide)-graft-poly(L-lysine) copolymers to enhance the biocompatibility of poly(L-lysine)-alginate microcapsule membranes. Biomaterials 1992;13:863.

[43] von Burkersroda F, Schedl L, Gopferich A. Why degradable polymers undergo surface erosion or bulk erosion. Biomaterials 2002;23:4221.

[44] Camenisch TD, Spicer AP, Brehm-Gibson T, Biesterfeldt J, Augustine ML, Calabro A, Jr., Kubalak S, Klewer SE, McDonald JA. Disruption of hyaluronan synthase-2 abrogates normal cardiac morphogenesis and hyaluronan-mediated transformation of epithelium to mesenchyme. J Clin Invest 2000;106:349.

[45] Chen WY, Abatangelo G. Functions of hyaluronan in wound repair. Wound Repair Regen 1999;7:79.

[46] Laurent TC, Fraser JR. Hyaluronan. FASEB J 1992;6:2397.

[47] Mataveli FD, Han SW, Nader HB, Mendes A, Kanishiro R, Tucci P, Lopes AC, Baptista-Silva JC, Marolla AP, de Carvalho LP, Denapoli PM, Pinhal MA. Long-term effects for acute phase myocardial infarct VEGF165 gene transfer cardiac extracellular matrix remodeling. Growth Factors 2009;27:22.

[48] Rodgers LS, Lalani S, Hardy KM, Xiang X, Broka D, Antin PB, Camenisch TD. Depolymerized hyaluronan induces vascular endothelial growth factor, a negative regulator of developmental epithelial-to-mesenchymal transformation. Circ Res 2006;99:583.

[49] Kang SW, Cho ER, Kim BS. PLGA microspheres in hyaluronic acid gel as a potential bulking agent for urologic and dermatologic injection therapies. Journal Microbiol Biotechnol 2004;15:9.

[50] Yamamoto T, Suto N, Okubo T, Mikuniya A, Hanada H, Yagihashi S, Fujita M, Okumura K. Intramyocardial delivery of basic fibroblast growth factor-impregnated

gelatin hydrogel microspheres enhances collateral circulation to infarcted canine myocardium. Jpn Circ J 2001;65:439.

[51] Iwakura A, Fujita M, Kataoka K, Tambara K, Sakakibara Y, Komeda M, Tabata Y. Intramyocardial sustained delivery of basic fibroblast growth factor improves angiogenesis and ventricular function in a rat infarct model. Heart Vessels 2003;18:93.

[52] Liu Y, Sun L, Huan Y, Zhao H, Deng J. Effects of basic fibroblast growth factor microspheres on angiogenesis in ischemic myocardium and cardiac function: analysis with dobutamine cardiovascular magnetic resonance tagging. Eur J Cardiothorac Surg 2006;30:103.

[53] Fujita M, Ishihara M, Morimoto Y, Simizu M, Saito Y, Yura H, Matsui T, Takase B, Hattori H, Kanatani Y, Kikuchi M, Maehara T. Efficacy of photocrosslinkable chitosan hydrogel containing fibroblast growth factor-2 in a rabbit model of chronic myocardial infarction. J Surg Res 2005;126:27.

[54] Hao X, Silva EA, Mansson-Broberg A, Grinnemo KH, Siddiqui AJ, Dellgren G, Wardell E, Brodin LA, Mooney DJ, Sylven C. Angiogenic effects of sequential release of VEGF-A165 and PDGF-BB with alginate hydrogels after myocardial infarction. Cardiovasc Res 2007;75:178.

[55] Wu J, Zeng F, Huang XP, Chung JC, Konecny F, Weisel RD, Li RK. Infarct stabilization and cardiac repair with a VEGF-conjugated, injectable hydrogel. Biomaterials 2011;32:579.

[56] Christman KL, Fang Q, Yee MS, Johnson KR, Sievers RE, Lee RJ. Enhanced neovasculature formation in ischemic myocardium following delivery of pleiotrophin plasmid in a biopolymer. Biomaterials 2005;26:1139.

[57] Tous E, Purcell B, Ifkovits JL, Burdick JA. Injectable acellular hydrogels for cardiac repair. J Cardiovasc Transl Res 2011;4:528.

[58] Anderson JM. Biological responses to materials. Annu Rev Mater Res 2001;31:20.

[59] Anderson JM, Rodriguez A, Chang DT. Foreign body reaction to biomaterials. Semin Immunol 2008;20:86.

[60] Alberts B, Johnson A, Lewis J, Raff M, Roberts K, Walter P. T cells and MHC proteins. Molecular Biology of The Cell, vol. 4. New York: Garland Science, 2002. p.18.

[61] Mitchell RN. Innate and adaptive immunity: the immune response to foreign materials. In: Ratner BD, Hoffman AS, Schoen FJ, Lemons JE, editor. Biomaterials Science, vol. 2. San Diego: Elsevier Acadmic Press, 2004. p.304.

[62] Elhendy A, van Domburg RT, Poldermans D, Bax JJ, Nierop PR, Geleijnse ML, Roelandt JR. Safety and feasibility of dobutamine-atropine stress echocardiography for the diagnosis of coronary artery disease in diabetic patients unable to perform an exercise stress test. Diabetes Care 1998;21:1797.

[63] Penfornis A, Zimmermann C, Boumal D, Sabbah A, Meneveau N, Gaultier-Bourgeois S, Bassand JP, Bernard Y. Use of dobutamine stress echocardiography in detecting silent myocardial ischaemia in asymptomatic diabetic patients: a comparison with thallium scintigraphy and exercise testing. Diabet Med 2001;18:900.

[64] Jneid H, Fonarow GC, Cannon CP, Palacios IF, Kilic T, Moukarbel GV, Maree AO, LaBresh KA, Liang L, Newby LK, Fletcher G, Wexler L, Peterson E. Impact of time of presentation on the care and outcomes of acute myocardial infarction. Circulation 2008;117:2502.

[65] Miura T, Miki T. Limitation of myocardial infarct size in the clinical setting: current status and challenges in translating animal experiments into clinical therapy. Basic Res Cardiol 2008;103:501.

CHAPTER 8

Attenuation of Left Ventricular Remodeling via Natural Bulking with Hyaluronic Acid Hydrogel and Poly(lactide-co-glycolide) Microsphere Composites

(Adapted from: **E Tous**, HM Weber, MH Lee, KJ Koomalsingh, T Shuto, N Kondo, JH Gorman, III, D Lee, RC Gorman, JA Burdick, **"**Tunable Hydrogel-Microsphere Composites that Modulate Local Inflammation and Collagen Bulking," Acta Biomater, 2012, in press.)

8.1 Introduction

Chapter 7 employed a hydrolytically degradable hydrogel system to evaluate the relevance of temporal mechanics in limiting left ventricular (LV) remodeling. This study demonstrated that treatment with longer-lasting stiff hydrogels is most effective in limiting LV remodeling (i.e., limiting myocardial wall thinning and ventricle dilation). The benefits in this system, as well as most injectable acellular materials, are related to the stability directly provided by the injected material; consequently, after material degradation, support may be minimized and LV remodeling may continue its course. This chapter will explore an alternative strategy to temporally target LV remodeling; instead of enhancing myocardial stability with only the injected material, in this case, stability will also be provided by collagen bulking induced as a result of the body's natural foreign body response (FBR) to a stimulatory composite material. The goal is that collagen production will provide enhanced natural long-lasting support during and after material degradation.

These types of composite systems are commonly used for various biomedical and cosmetic applications and are referred to as dermal fillers [1-5]. Originally, most fillers, as with most injectable biomaterial approaches for myocardial infarction (MI) repair, were volumizing replacements; however, these approaches have evolved beyond this towards the design of stimulatory composites that promote a transient tissue filling effect by inducing a FBR. This promotes collagen production and a gradual increase in tissue bulking, resulting in a natural filling effect over time [1-5]. Most stimulatory fillers are comprised of two main components: 1) a particle that determines the type of FBR and bulking that is endured and 2) a carrier material that delivers the particle and is subsequently resorbed [1-5]. The mechanism behind this response relies on the activation and "crosstalk" between macrophages and fibroblasts, which is mediated by particle and carrier design.

8.1.1 The Foreign Body Response: Pro-inflammatory versus Pro-Healing Responses

When a foreign object is implanted into the body, proteins immediately adsorb to its surface and activate an inflammatory cascade that determines the cellular response and extent of tissue remodeling [6-10]. This entails an initial innate response comprised of neutrophil infiltration and macrophage phagocytosis, followed by a more specialized response that relies on macrophage plasticity [11, 12]. Macrophages have recently been loosely characterized as having M1 (pro-inflammatory) and M2 (pro-healing) phenotypes [13-17]. Classically activated (M1) macrophages are induced by IFN-γ, LPS, and TNF-α, and play a dominant role in the initial inflammation, and are characterized as inducing a chronic inflammatory response [14, 15]. Alternatively activated (M2) macrophages are stimulated by Il-4, Il-10, and Il-13 cytokines and are anti-inflammatory

because of their ability to facilitate tissue remodeling [13-15]. It is thought that these macrophages, in particular, play a large role in secreting TGF-βs to stimulate fibroblasts to produce collagen for constructive tissue repair [8, 14, 18-22]. One approach to mediate a specific biomaterial response is to direct this macrophage response by controlling the initial protein adsorption to the biomaterial [23-25]; however, there is overlap and switching between the M1 and M2 pathways, making it difficult to clearly distinguish and selectively activate one or the other [13]. Regardless, advances have been made in understanding tissue responses to materials and have led to the improved design of dermal fillers for constructive remodeling.

8.1.2 Design Criterion for Induction of Pro-Healing (M2) Responses

Towards strategies to induce a constructive healing response via particle design, specific focus has been placed on particle chemistry, geometry, and size. Hydrophilicity [4, 13], crosslinking [26], and biodegradability [4] all influence the degree of inflammation, and have impacted the material selection for particle stimuli. Particle geometry and size have also been extensively studied; generally, smooth surfaces and a smaller area for a given volume induce a macrophage mediated constructive collagen bulking. Although irregularly shaped particles do induce inflammation, they elicit a macrophage mediated chronic healing response leading to inconsistent collagen distribution [4, 27, 28]. Microsphere size is also an important design parameter; particles should be small enough for injectable delivery and to prevent fibrous capsule isolation (typically < ~100 μm), but large enough to avoid macrophage phagocytosis (> ~10 μm), which can amplify an undesired chronic inflammatory response [5-7, 27, 29].

8.1.3 Dermal Fillers as Bulking Agents for Myocardial Infarction (MI)

Dermal fillers have been studied as bulking agents to prevent maladaptive LV remodeling post-MI [30, 31]. Specifically, Radiesse is an FDA approved stimulatory dermal filler comprised of a suspension of 30% calcium hydroxyapatite (CaHA) microspheres (25-45 μm) in a 70% aqueous gel carrier of water, glycerin, and carboxymethylcellulose [1-5]. As a stimulatory filler, Radiesse induces cells to infiltrate the carrier portion and fibroblasts to produce collagen around the microspheres. Morita et al. recently demonstrated that Radiesse injection into the infarcted myocardium thickened the myocardium and resulted in geometric and functional improvements [30]. Here we strive to further understand and improve on work such as this by investigating how material design parameters within a composite system influence tissue outcomes.

In this investigation, we developed a tunable and biodegradable composite comprised of a hyaluronic acid (HA) hydrogel carrier containing poly(lactide-co-glycolide) (PLGA) microspheres. Previous work by Kang et al. demonstrated successful bulking via delivery of a suspension of PLGA microspheres in high-molecular-weight HA [32]; motivated by their work, this crosslinkable system will provide the addition of tunable control over microsphere presentation through an actual HA hydrogel with controlled degradation. Due to its natural benefits *in vivo* [33], HA is commonly used in dermal fillers [1-5] and, furthermore, can be functionalized to form hydrogels with controlled properties [34, 35]. As in the preceding chapters (Chapters 6 and 7) [35], HA was modified with a hydroxyethyl methacrylate (HeMA) group to tailor hydrogel gelation, degradation, and mechanics, as well as microsphere temporal presentation via crosslinking. PLGA particles have been used extensively in tissue engineering [36-38] and, as briefly discussed, even to promote bulking [32]. Here, smooth PLGA

microspheres (20-60 μm) were fabricated and encapsulated at varying concentrations (0, 10, 75, 300 mg/mL) in two formulations of the HeMA-HA (low and high percent modified) carrier to examine material design considerations on local and temporal bulking. Composites were evaluated *in vivo* in a subcutaneous murine model and, similar to the work of Morita et al. [30], in an ovine MI model to determine how controlled microsphere presentation influences collagen bulking and attenuates negative remodeling, respectively.

8.2 Materials and Methodology

All animals studied in this work received care in compliance with protocols from the University of Pennsylvania that were approved by the Institutional Animal Care and Use Committee according to the guidelines for humane care. Materials and reagents were purchased from Sigma Aldrich and used without further purification unless otherwise specified.

8.2.1 Synthesis of Hydroxyethyl Methacrylated Hyaluronic Acid (HeMA-HA) Macromer

The two same formulations of HeMA-HA (low and high, Table 7.1) used in Chapter 7 were synthesized as previously described [35]. For a more detailed explanation on HeMA-HA synthesis and purification, refer to Sections 6.2.1 and 6.3.2, and for more details on the specific HeMA-HA formulations employed in this chapter refer to Sections 7.3.1 and 7.3.2. Briefly, HA-sodium salt (HA-Na, Lifecore, 66 kDa) was converted to HA-tetrabutylammonium salt (HA-TBA) and coupled to HeMA-COOH by reacting at 45 °C for 20 hours. The product was dialyzed, purified by acetone precipitation, and further dialyzed. Methacrylation (percent) was adjusted by varying the

ratio of HeMA-COOH and di-*tert*-butyl dicarbonate (BOC_2O) and assessed with ^1H NMR (Bruker, 360 MHz) (Section 6.3.3).

8.2.2 Fabrication of Poly(lactide-co-glycolide) (PLGA) Microspheres

8.2.2.1 Fabrication via Homogenization

PLGA (Lactel Absorbable, 50:50, 0.41dL/g) microspheres were initially fabricated using conventional homogenization to form oil-in-water emulations (O/W). One mL of 10 wt% PLGA in dichloromethane (DCM) (Fisher) was slowly dripped into a solution of 100 mL of 0.5 wt% polyvinyl alcohol (PVA) with stirring. After complete addition of PLGA, the mixture was homogenized for 15 min at 1000 rpm. The solvent was evaporated by stirring 2 hours, microspheres were washed 3X in deionized water, lyophilized, and stored at -20 °C until use. Microspheres were imaged with an upright microscope (Olympus BX51) and a scanning electron microscope (SEM, JEOL 7500F HRSEM, Penn Regional Nanotechnology Facility). Light micrographs were used to evaluate microsphere size using ImageJ software.

8.2.2.2 Fabrication via Microfluidic Device

PLGA microspheres between 20-60 μm were fabricated by forming oil-in-water (O/W) single emulsions in a glass microfluidic device [39]. The inner phase (O) was 4 wt% PLGA (Lactel Absorbable Polymers, 75:25, 0.71 dL/g) in dichloromethane (DCM) and the outer phase (W) was a 2 wt% polyvinyl alcohol (PVA, 13,000-23,000 g/mol) aqueous solution. The outer phase hydrodynamically focused the inner fluid stream into the collection channel, leading to the formation of single emulsions. DCM was removed by rotovap at 37 °C and 398 mbar, microspheres were washed 3X in deionized water and then lyophilized for storage. Emulsion formation was monitored on a Nikon Diaphot

300 and a Nikon TMD/TME automated stage microscope with Vision Research Phantom V7.1. Microsphere size was quantified using light micrographs and ImageJ software. For morphological evaluation with degradation, microspheres (75 mg/mL) were incubated in phosphate buffered saline (PBS) at 37 °C, and samples were removed at pre-defined time points and imaged under SEM. In addition to topography, SEM images also provided information on the size of microspheres with time via analysis using ImageJ software. Degradation was also assessed by monitoring the pH of microsphere/PBS solutions (75 mg/mL) incubated at 37 °C at the same time points as morphology studies.

8.2.3 Formation and Characterization of Hydrogel Composites

Microspheres were mixed (0, 10, 75, 300 mg/mL) and crosslinked within the HA hydrogels (either low or high HeMA-HA, 4wt%) via oxidation-reduction (redox) reactions with ammonium persulfate (APS, low: 8 mM, high: 7 mM) and N,N,N,N',N'-tetramethylethylenediamine (TEMED, low: 4mM, high: 7 mM) to form hydrogel/microsphere composites. Hydrogels without microspheres will be referred to as empty hydrogels throughout this chapter and were formed similar to those used in Chapters 6 and 7 (described in Section 6.2.4). For *in vitro* characterization and *in vivo* subcutaneous evaluation, hydrogel composites were formed between two glass slides within a Teflon mold sealed with vacuum grease at 37 °C for 30 minutes.

Gelation was evaluated by monitoring the storage (G') and loss (G'') moduli after mixing using an AR2000ex Rheometer (TA Instruments) at 37 °C under 1% strain and a frequency of 1 Hz in a parallel plate geometry (20 mm diameter). A parallel plate geometry was employed due to microsphere addition, and thus, the need for a larger geometry gap for testing. Gelation onset time of composites was normalized to empty

hydrogels (i.e., composite gel onset time was divided by empty hydrogel gel onset time) to determine the influence of microsphere addition on polymerization. Degradation of the hydrogel portion of the composites was examined at 37 °C in PBS with a uronic acid assay [40]. Hydrogel and composite mechanical properties were assessed initially and with degradation (PBS at 37 °C) via compressive testing using a Dynamic Mechanical Analyzer (DMA) (Q800 TA Instruments) at a strain rate of 10%/ min and moduli were calculated between 10-20% strain.

8.2.4 In Vivo Evaluation in Subcutaneous Model

Microsphere/PBS solutions were sterilized under germicidal ultraviolet (UV) light for 1 hour. HeMA-HA macromer was similarly sterilized for 30 minutes on each side, and all solutions were filter sterilized. Hydrogel composites (~50 μL, n=3 per group) were formed *ex vivo,* sterilized under germicidal UV light for 30 minutes on each side, and implanted subcutaneously into dorsal pockets of rats. The animals were euthanized and explants were collected at 1, 2, and 4 weeks, fixed in 4% formalin overnight and paraffin embedded using standard histological techniques. Samples were processed into 7 μm sections and stained with hematoxylin and eosin (H&E) and Masson's Trichrome (MT) to evaluate the extent of tissue (primarily collagen) integration.

8.2.4.1 In Vivo Evaluation in Subcutaneous Model: Immunohistochemistry

For immunohistochemical (IHC) analysis, all PBS was filtered and all washes were 2 minutes. IHC staining was performed on low HeMA-HA composites at the 4 week time point to evaluate the phenotypic macrophage response by targeting surface markers: CD68 (general), CCR7 (pro-inflammatory, M1), and CD163 (pro-healing, M2).

Primary antibodies used were mouse anti-rat CD68 (Serotec, MCA341R) at 1:100, rabbit anti-CCR7 (Cell Applications Inc., CA0710) at 1:200, and mouse anti-rat CD163 (Serotec, MCA342R) at 1:50; all were incubated with 1% normal horse serum (Vector, S-2000) (CD68 and CD163) or 1% goat serum (Vector, S-1000) (CCR7). Secondary antibodies used were biotinylated horse anti-mouse IgG (CD68 and CD163, Vector, BA-2000) at 1:100 and goat anti-rabbit IgG (CCR7, BA-1000) at 1:200, all incubated with 1.5% normal horse serum (CD68 and CD163) or 1.5% goat serum (CCR7).

Sections were deparaffinized with citrisolv and hydrated with a graded series of ethanol solutions ranging from 100% to 50%. Slides were immersed in boiling antigen retrieval buffer (10 mM citric acid monohydrate, pH 6) for 20 minutes and allowed to cool in the buffer. They were washed 2X in tris buffer (tris buffered saline/ tween 20, pH 7.4) and 3X in PBS. Samples were blocked in 1.5% normal horse serum (CD68 and CD163) or 1.5% normal goat serum (CCR7) for 45 minutes at room temperature (RT). After removing blocking solution, samples were directly incubated with primary antibody (CD68, CCR7, or CD163) for 15 minutes at RT and overnight at 4 ˚C in a humidified chamber. Following primary incubation, samples were washed 3X in PBS, quenched in 3% H_2O_2 in methanol for 30 minutes, and washed again 3X in PBS. Secondary antibody incubation was performed for 30 minutes at either RT (CD68) or at 37 ˚C (CCR7 and CD163). Samples were washed 3X with PBS (CD68 and CD163) or 7X (CCR7) and incubated with Vectastain ABC reagent (Vector) for 1 hr (CD68 and CD163) or 30 min (CCR7) in a humidified chamber at 37 ˚C. Samples were washed 3X with PBS and incubated with diaminobenzadine substrate for 1 minute (Dab, Vector, SK-4100) at RT. The reaction was stopped by washing 3X with deionized water. Slides were counterstained with hematoxylin (Gill No. 2) for 2 minutes, dehydrated and cover slipped.

The phenotypic macrophage response due to microsphere concentration was analyzed in low HeMA-HA composites at week 4 by counting positively stained cells for each marker (CD68, CCR7, CD163) in each explant of each group (0, 10, 75, and 300 mg/mL, n= 3). Six fields of view (FOV) at 400X magnification were analyzed; three FOV were counted at the biomaterial/tissue interface and in the surrounding tissue, with the latter defined as tissue >25 μm from the biomaterial. In samples where the composite was no longer present, six FOV of the tissue representing the area where the material was implanted were counted. Tissue area in each FOV was calculated by excluding microsphere and hydrogel area using ImageJ software, and cell number in each FOV was normalized by tissue area (mm^2).

8.2.5 In Vivo Evaluation in MI Model

Microspheres, macromer, and all solutions were sterilized as described in the subcutaneous studies. The same established *in vivo* ovine MI model used in Chapter 7 was used to evaluate the efficacy of the selected composite in attenuating LV remodeling [31]. For a more detailed description refer to section 7.2.4 in this dissertation. Thirty minutes post-MI, six adult male Dorset sheep (30-50 kg) underwent composite treatment; the composite (macromer/ microsphere) pre-polymer solution was mixed for 3 minutes and injected into the infarct (20 0.3 mL injections). Hemodynamic data and real time three-dimensional echocardiographs (3DE) were collected, animals were sacrificed at 8 weeks, and histological evaluation was performed (H&E and MT staining). Wall thicknesses in the apical infarct, basilar infarct, and borderzone (BZ) regions were normalized to remote myocardium. Ejection fraction (EF) as a functional outcome was assessed at 2 and 8 weeks by comparing to baseline values, and also by comparing before and after dobutamine (DoB) (2.5 and 5.0 mg kg^{-1} min^{-1}) stress testing.

Composite treated sheep were compared to infarct and low HeMA-HA controls (e.g., empty hydrogel) from the study described in Chapter 7 [35].

Vessel density and inflammation were both evaluated by staining for anti-α-smooth muscle actin (α–SMA) and major histocompatibility complex (MHC) class II, respectively. For details on the IHC staining that was performed refer to Section 7.2.4.1.

8.2.6 Statistical Analysis

Data is presented as either mean ± SD (standard deviation) or mean ± SEM (standard error of the mean) as indicated in the figure captions. All changes were assessed using a one-way ANOVA with Tukey's post hoc evaluation to account for differences between groups. $p \leq 0.05$ was considered statistically significant for all comparisons.

8.3 Results and Discussion

8.3.1 Fabrication and Characterization of PLGA Microspheres

PLGA microspheres were fabricated with a glass capillary microfluidic device to guarantee a smooth surface and high uniformity in size (Figure 8.1C, D) [39], as opposed to standard homogenization techniques that resulted in undesired variations in size and topography (Figure 8.1A, B). To form microspheres, the dispersed phase (4 wt% PLGA) and continuous phase (2% PVA) were delivered from opposite sides of the square outer capillary at adjusted flow rates until solutions formed a cone at the orifice of the collection tube and pinched off to form microspheres. The majority of microspheres obtained after solvent removal, were smooth and between 20-60 μm, meeting the criteria for bulking agents (Figure 8.1D) [5, 27-29].

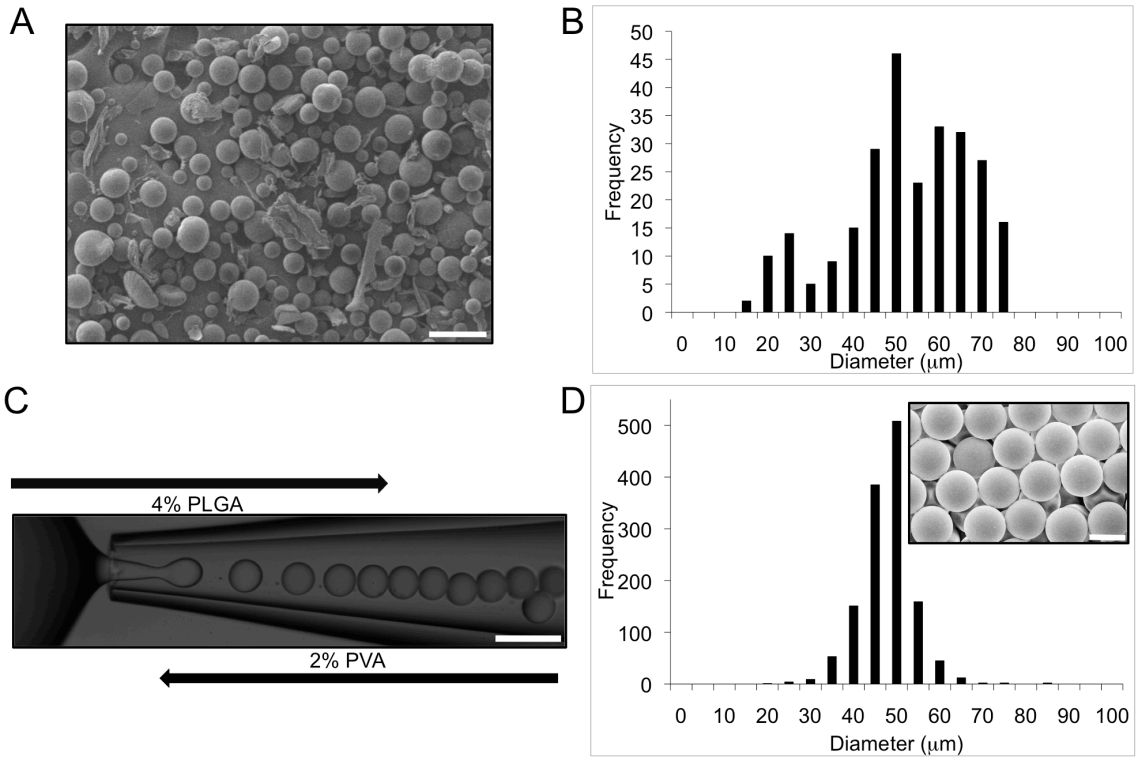

Figure 8.1 PLGA microsphere fabrication using standard homogenization techniques, representative SEM image (A) and microsphere size distribution (B). PLGA microsphere fabrication in glass capillary microfluidic device (C), post-purification microsphere size distribution, and SEM image (inset) (D). In panel A, scale bar= 150 μm. Scale bar= 250 μm in C and scale bar= 40 μm in D.

In addition to being FDA approved and used for numerous tissue engineering applications [36-38], PLGA was selected because of its biodegradable nature. While it is desirable for microspheres to eventually degrade, it is also important that they remain stable and maintain a smooth geometry to promote constructive collagen remodeling. PLGA microsphere surfaces and diameters remained unchanged after 8 weeks (Figure 8.2A, B) and minimal changes in pH were observed during degradation (~7.4 to 7.2) (Figure 8.2C) suggesting insignificant degradation throughout the 8 weeks. In addition

to this work, others have shown that while the molecular weight (MW) of PLGA decreases in 8 weeks, the mass of the microspheres changes very little [41]. Thus, there is likely little release of acidic byproducts during the span of 8 weeks.

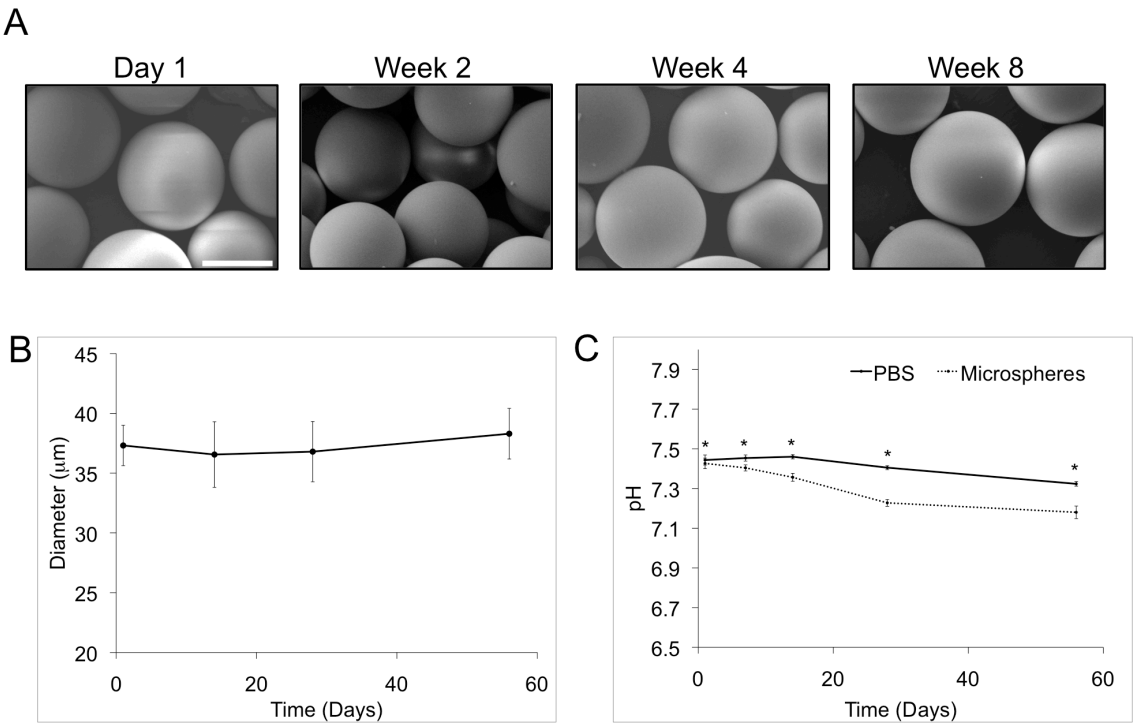

Figure 8.2 Microsphere SEM images after incubation in PBS up to 8 weeks (A). Microsphere diameter quantification (B) and variation in pH (C) to investigate degradation with time (8 weeks). Data are presented as mean ± SD. *p<0.05 vs. PBS. Scale bar= 40 μm.

8.3.2 Formation and Characterization of Composites

HeMA-HA was synthesized as described in Sections 6.3.1-6.3.3 to yield macromers with a low (~10%) or high degree (~30%) of modification. HeMA-HA undergoes a radical polymerization via the redox initiators APS and TEMED at the

methacrylate groups to form hydrogels that undergo either enzymatic degradation through the HA backbone or hydrolytic degradation through the esters on the HeMA groups [35]. Variation in the extent of modification leads to changes in the crosslinking density, which alters the gelation, mechanics, and degradation behavior of these hydrogels. In this work, the rate of degradation also alters how fast the microspheres are released from the carrier hydrogel.

Composites were formed by crosslinking HeMA-HA formulations (low or high) in the presence of 0, 10, 75, or 300 mg/mL of PLGA microspheres (Figure 8.3). As discussed in Methods, gel onset time was defined as the intersection of G' and G''. Rheometry showed that microspheres did not affect gel onset in most composites with only the gelation of low HeMA-HA at 300 mg/mL significantly increased (~40% slower than empty hydrogels, Figure 8.4).

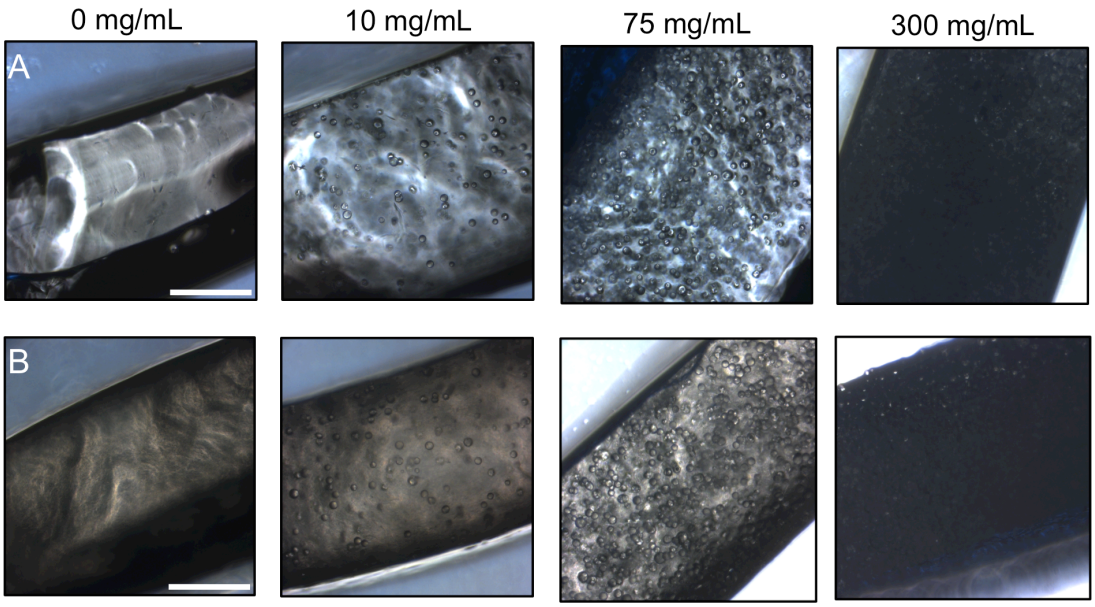

Figure 8.3 Cross-sectional views of low (A) and high (B) HeMA-HA composites at the four microspheres concentrations. Scale bar= 500 μm.

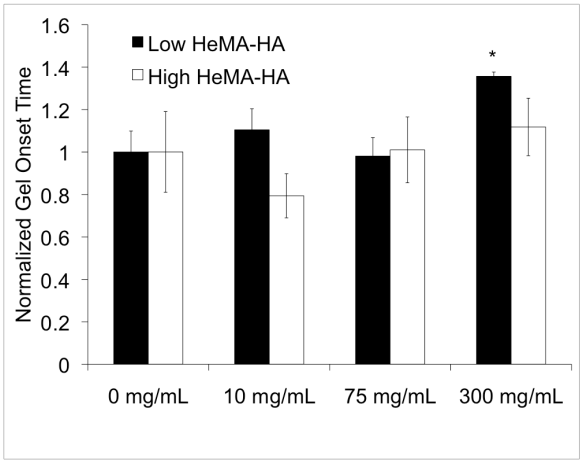

Figure 8.4 Gel onset for composites normalized to low or high HeMA-HA, 0 mg/mL formulations. Data are presented as mean ± SD. *p<0.05 vs. low HeMA-HA 0 mg/mL.

Composite hydrogel mass loss in both low and high HeMA-HA hydrogels were influenced slightly by microsphere concentration; however, degradation trends remained generally comparable (Figure 8.5A, B). In low HeMA-HA hydrogels, concentrations of 10 and 75 mg/mL significantly decreased the amount of mass loss compared to empty hydrogels; yet, their degradation rate was similar until the final week when they accelerated to compensate for initial lower mass losses (Figure 8.5A). While these results indicate that a concentration of 300 mg/mL did not affect mass loss, this is likely due to incomplete gelation as suggested by slower gel onset. High HeMA-HA hydrogel mass loss was predominantly influenced at 10 and 300 mg/mL, being significantly lower at all time points compared to empty hydrogels except for at week 8 where only 10 mg/mL was affected (Figure 8.5B). Significant differences in degradation rates were only observed at 7 days (300 mg/mL) and at 8 and 10 weeks (10 mg/mL), as in low hydrogels.

The presence of microspheres only increased the compressive modulus of hydrogels at the initial time points (Figure 8.5C, D). Specifically, significant increases in moduli were observed at 75 and 300 mg/mL in low HeMA-HA composites at day 0 compared to empty hydrogels (Figure 8.5C) and at days 0 and 1 for 300 mg/mL in high HeMA-HA composites (Figure 8.5D). Thus, *in vitro* characterization demonstrated that microspheres had minimal influences on composite material properties (particularly degradation and mechanics) and that differences are likely due to initial changes in the gelation around the microspheres. Nonetheless, composite material properties should be characterized when selecting a formulation for implantation.

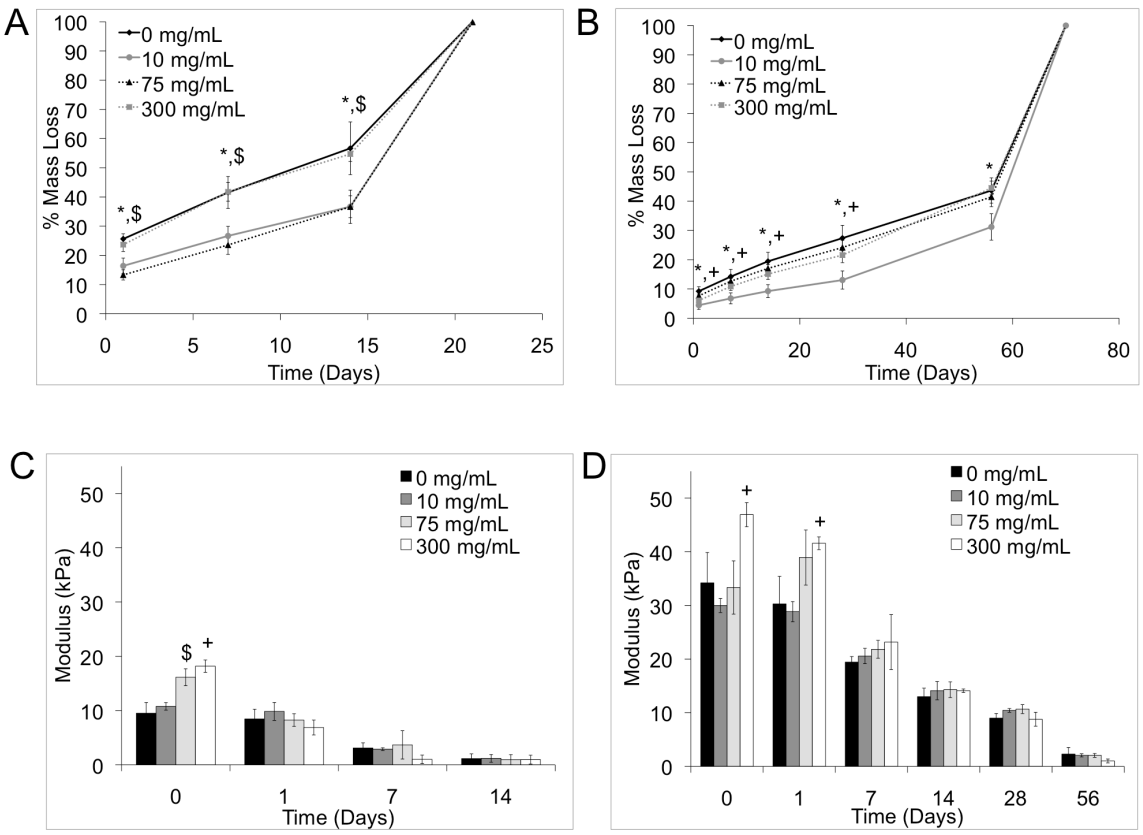

Figure 8.5 *In vitro* characterization of low HeMA-HA (A) and high HeMA-HA (B) hydrogel composite degradation and low HeMA-HA (C) and high HeMA-HA (D) hydrogel composite mechanics with degradation. Data are presented as mean ± SD. *p<0.05 for 10 mg/mL vs. 0 mg/mL, $p<0.05 for 75 mg/mL vs. 0 mg/mL, +p<0.05 for 300 mg/mL vs. 0 mg/mL.

8.3.3 In Vivo Evaluation in Subcutaneous Model

8.3.3.1 Macroscopic and Histological Evaluation

Macroscopic evaluation of subcutaneous explants demonstrated a temporal correlation in bulking with hydrogel formulation (low HeMA-HA vs. high HeMA-HA composites). Differences in explants were observed 1 week post-treatment, with tissue

integration beginning in low HeMA-HA composites and delayed in high HeMA-HA composites until week 2. Furthermore, at 4 weeks, low HeMA-HA hydrogels were explanted as a mass of tissue, whereas the more slowly degrading high HeMA-HA hydrogels remained primarily as hydrogel disks, surrounded by tissue (Figure 8.6). This is likely due to the slower hydrogel degradation behavior in the high formulations, limiting initial interactions of the material and microspheres with local tissue; in contrast, the low formulation degrades within a few weeks, allowing cells and tissue to interact more quickly with the microspheres. While gross evaluation revealed distinct differences in bulking with polymer modification (low vs. high), there did not appear to be a macroscopic response based on the microsphere introduction or concentration.

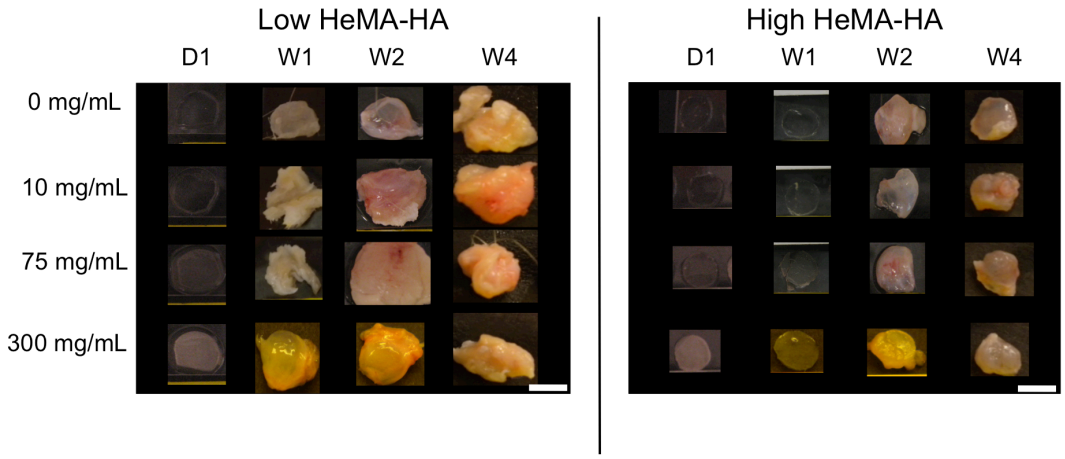

Figure 8.6 Gross evaluation of bulking in low and high HeMA-HA hydrogel composites at 1 day (D1), 1 week (W1), 2 weeks (W2) and 4 weeks (W4) after subcutaneous implantation and containing 0, 10, 75, or 300 mg/mL of microspheres. Scale bar= 5 mm.

MT staining was performed to validate macromer influences and address microsphere effects on bulking by assessing collagen infiltration within and surrounding

each composite (Figure 8.7). Collagen integrated at the edge of low HeMA-HA composites by 1 week and into composites by 2 weeks; in contrast, minimal collagen was observed within the slowly degrading high HeMA-HA composites and was limited to the edge of the hydrogel. In contrast to low HeMA-HA, which showed tissue integration within the composite, slower degradation of the high HeMA-HA composites resulted in the formation of a fibrous capsule at 4 weeks, limiting microsphere presentation. Due to negligible microsphere exposure in high HeMA-HA, the effects of microsphere incorporation on collagen bulking could only be assessed in low HeMA-HA composites. This highlights the importance of the design of the carrier material when designing bulking formulations. At week 4 in the low formulations, it was evident that microsphere concentration influenced the tissue response with increasing collagen integration from 0 to 75 mg/mL in low HeMA-HA composites (Figure 8.7) with primarily adipose tissue (determined by pathological assessment) in the 0 and 10 mg/mL groups. The high concentration of 300 mg/mL microsphere composites presented primarily aggregates of microspheres throughout the gel, limiting tissue and cellular interactions in some areas.

Interestingly, in contrast to *in vitro* degradation results, while empty hydrogels and 10 mg/mL composites appeared completely degraded by week 4, 75 and 300 mg/mL composites still had remnants of hydrogel composite present between infiltrated tissue. This observation may be due to a combination of the influence of the local tissue response on degradation and the suspected microsphere hydrophobic interactions. Staining showed that as tissue infiltrated the edge of the hydrogel, the hydrogel broke into smaller pieces. Composites with more microspheres may further decrease the rate of tissue infiltration due to additional hydrophobic interactions.

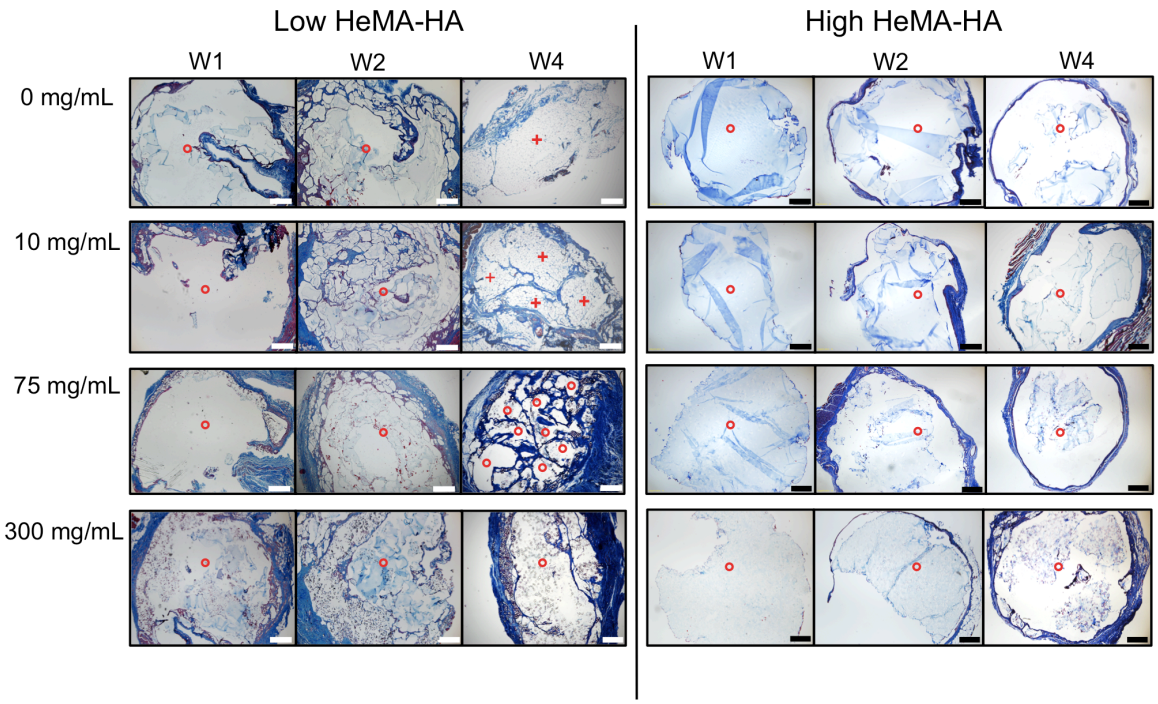

Figure 8.7 Masson's Trichrome staining of explants 1 week (W1), 2 weeks (W2) and 4 weeks (W4) after subcutaneous implantation and containing 0, 10, 75, or 300 mg/mL of microspheres. Scale bar= 500 μm. Red circles and red positive signs represent gel and adipose tissue respectively.

8.3.3.2 Immunohistochemical Macrophage Evaluation

IHC staining for general, M1 (pro-inflammatory), and M2 (pro-healing) macrophages was performed to determine the influence of hydrogel/microsphere composites on the type of inflammatory response (Figure 8.8). As an overall trend, staining for all markers indicated that macrophage presence was highest in the 75 and 300 mg/mL formulations, suggesting that macrophage infiltration is dependent on microsphere concentration. 75 mg/mL composites elicited the largest response, with a statistically significant increase in general macrophage response compared to empty hydrogels (641 ± 113 vs. 93 ± 28 macrophages/ mm^2) (Figure 8.9A). Lower numbers in

300 mg/mL composites could be due to observed microsphere aggregation limiting their cellular interactions. In contrast, in 75 mg/mL composites, cells and tissue were able to penetrate the hydrogel and readily access microspheres (Figure 8.8).

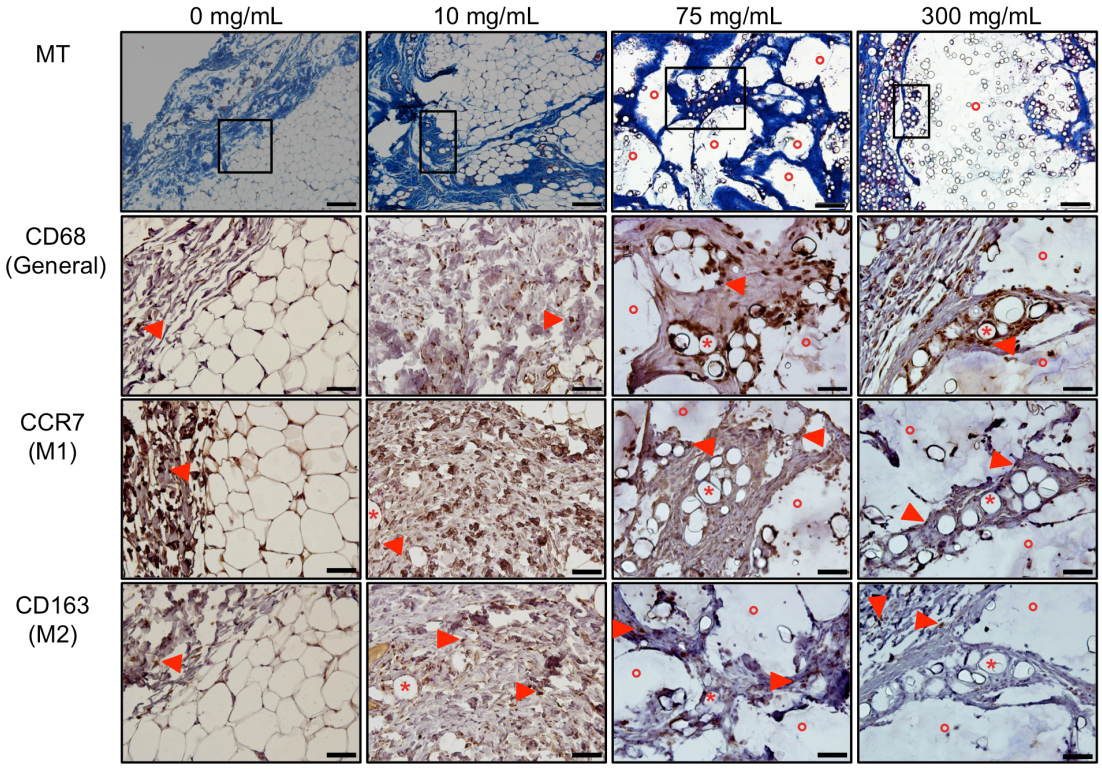

Figure 8.8 Immunohistochemical evaluation of macrophage phenotype in composites at week 4. Top row is Masson's Trichrome stain, scale bar= 200 μm. Other rows are general (CD68) and M1 (CCR7) and M2 (CD163) macrophage stains, scale bar= 50 μm. Red circles represent gel. Red stars and red arrows indicate representative microspheres and macrophages respectively.

Treatment with composites of 75 mg/mL microspheres resulted in greater M1 (0 mg/mL: 41 ± 10, 10 mg/mL: 61 ± 6, 75 mg/mL: 171 ± 55 macrophages/mm^2) and M2 (0 mg/mL: 25 ± 14, 10 mg/mL: 24 ± 14, 75 mg/mL: 80 ± 16 macrophages/mm^2) responses

compared to the less concentrated composites (Figure 8.9B, C). The presence of fewer macrophages in empty hydrogel and 10 mg/mL composites is likely due to complete hydrogel degradation by week 4, suggesting that they do not stimulate a sufficient inflammatory response to bulk. Low HeMA-HA 300 mg/mL composites elicited the largest M2 response (300 mg/mL: 130 ± 25 macrophages/mm^2) with statistically significant higher numbers than empty hydrogels and resulted in a slightly greater M2 responses compared to their respective M1 (300 mg/mL: 99 ± 20 macrophages/mm^2) response (Figure 8.9B, C). This finding is not completely understood; however, it could be attributed to the plasticity of M2 macrophages [13], the time point investigated, and the nature of collagen distribution at the implant. As a general observation, more M2 macrophages were observed in the surrounding tissue, while M1 macrophages were more prominent in areas with tissue and biomaterial contact. It is speculated that this may be because M1 macrophages initiate a response with the composite as it is degrading; HA fragments have also been shown to induce a strong pro-inflammatory response [42]. Following material degradation and acute inflammatory activity, M2 macrophages may also play a role in remodeling [20]. As discussed, in 300 mg/mL composites, there was a tendency to wall off composites and limit tissue penetration. Consequently, this restricted analysis in most samples to tissue interaction at the edge as opposed to within composites of infiltrated tissue regions. Prolonging this study may provide more information on long-term macrophage polarization with time after complete hydrogel degradation. However, this analysis supports a phenotypic dependence on composite design and the presence of microspheres. Due to the above results, we chose the low HeMA-HA containing 75 mg/mL composite formulation for application as a bulking agent in cardiac repair.

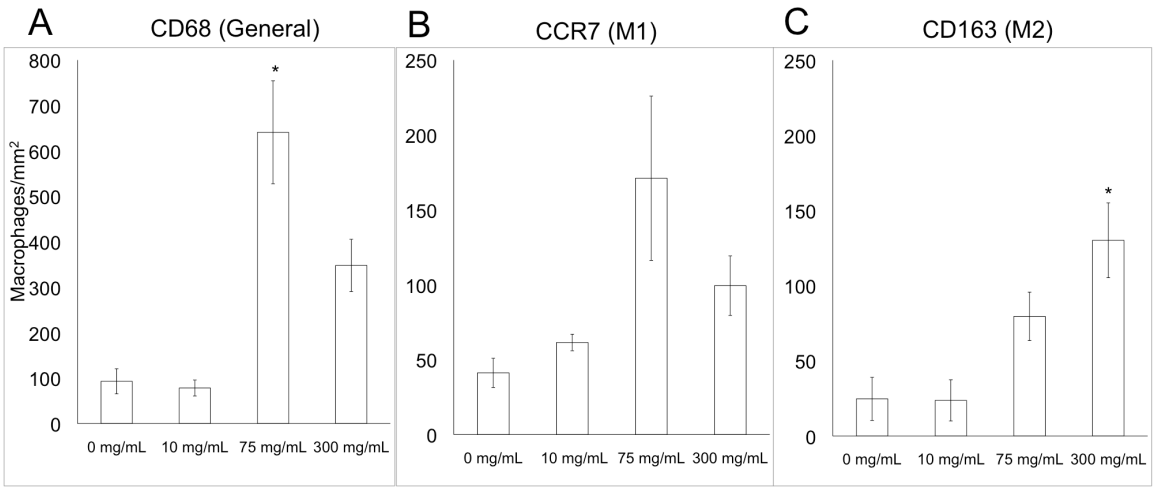

Figure 8.9 Quantification of general (A), M1 (B) and M2 (C) macrophage phenotype in low HeMA-HA composites at week 4 from immunohistochemistry. Data are presented as mean ± SEM. *p<0.05 vs. 0 mg/mL.

8.3.4 In Vivo Evaluation in MI Model

Subcutaneous work validated the ability of composites to temporally and locally control remodeling by varying hydrogel crosslinking and microsphere concentration, respectively. Exploiting these tunable properties may be beneficial in treatment of injuries, such as MI, where bulking may improve outcomes, but where more control is necessary to effectively attenuate maladaptive geometric changes that occur [43]. In particular, the timing of treatment is critical due to the time dependent remodeling observed in MI where necrosis dominates for the first week and the overall process can extend for 8 weeks and beyond [44]. Previous work described in Chapter 7 with the empty low HeMA-HA hydrogel formulation revealed that compared to the empty high HeMA-HA group it did not provide sufficient stability to attenuate long-term negative remodeling, which was attributed to its accelerated degradation and subsequent

decrease in mechanics with time [35]. Other agents that have been investigated range from synthetic and natural materials; however, most of their bulking capacity relies on their ability to physically support the damaged myocardium, and few directly stimulate and control natural thickening [43]. As discussed, Morita et al. applied the FDA approved dermal filler, Radiesse, to induce bulking in the myocardium post-MI and demonstrated its efficacy in limiting geometric changes [30]. This study and the temporal nature of MI remodeling provide motivation to improve on our previous approach by implementing low HeMA-HA composites, where hydrogels carry microsphere stimuli to control delivery (avoiding prime necrosis 1 week post-MI) and potentially induce natural bulking for enhanced stability during (as the tissue penetrates the hydrogel) and after hydrogel degradation.

The low HeMA-HA, 75 mg/mL composite formulation was selected for this work because of its similar material properties (gelation, degradation and compressive moduli trends) to empty hydrogels and its ability to induce collagen bulking and a macrophage response in subcutaneous studies. At this formulation, material properties can for the most part be decoupled from microsphere effects enabling direct evaluation of microsphere presentation (e.g., composite vs. empty low HeMA-HA treatments) in attenuating LV remodeling.

8.3.4.1 In Vivo Evaluation in MI Model: Thickness

LV remodeling leads to a series of adverse changes (thinning of the myocardial wall, dilation and infarct expansion) that can negatively affect function and lead to heart failure [45-48]. When analyzing normalized thickness, both composite and hydrogel alone treatments significantly thickened the apical infarct region compared to infarct controls (composite: 0.40, empty: 0.29, infarct control: 0.18, normal: 0.52) (Figure

8.10A); however, the composite also resulted in a statistically significant increase in thickness compared to empty hydrogels. Increased thicknesses were also observed within the basilar infarct region for both hydrogel groups (composite: 0.51, empty: 0.51, infarct control: 0.38, normal: 0.72). All groups were similar in the BZ region. MT staining in the apical, middle, and basilar infarct regions demonstrated cellular infiltration around microspheres surrounded by a collagen network (Figure 8.10B).

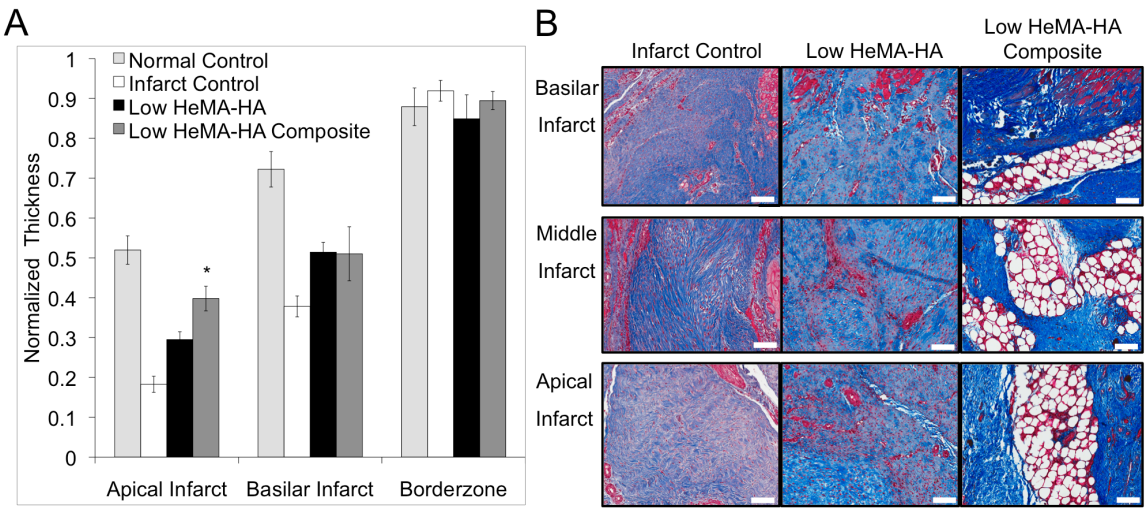

Figure 8.10 Myocardial wall thickness in apical infarct, basilar infarct, and borderzone (BZ) regions normalized to remote healthy myocardium (A) and Masson's Trichrome staining in the basilar, middle, and apical infarct regions (B). Data presented as mean ± SEM. All groups are significantly different from normal control in apical and basilar infarct regions and from infarct control in the apical infarct region. *$p<0.05$ vs. empty low HeMA-HA. Scale bar= 100 μm.

8.3.4.2 In Vivo Evaluation in MI Model: End Diastolic and Systolic Volume

LV volumes were measured to assess the extent of their dilation with and without treatment; composite hydrogels showed trends in decreasing normalized end diastolic volume (NEDV) and normalized end systolic volume (NESV) at 2 and 8 weeks compared to infarct controls and empty hydrogels, particularly at 2 weeks (composite 2W NEDV: 1.63, composite 2W NESV: 1.94, composite 8W NEDV: 1.98, composite 8W NESV: 2.50 vs. empty 2W NEDV: 1.85, empty 2W NESV: 2.22, empty 8W NEDV: 2.15, empty 8W NESV: 2.61 vs. infarct 2W NEDV: 1.75, infarct 2W NESV: 2.21, infarct 8W NEDV: 2.31, infarct 8W NESV: 3.02) (Figure 8.11). This suggests that, compared to empty hydrogels, composites were more effective in attenuating geometric changes associated with MI, specifically by enhanced bulking and stabilizing the myocardial wall.

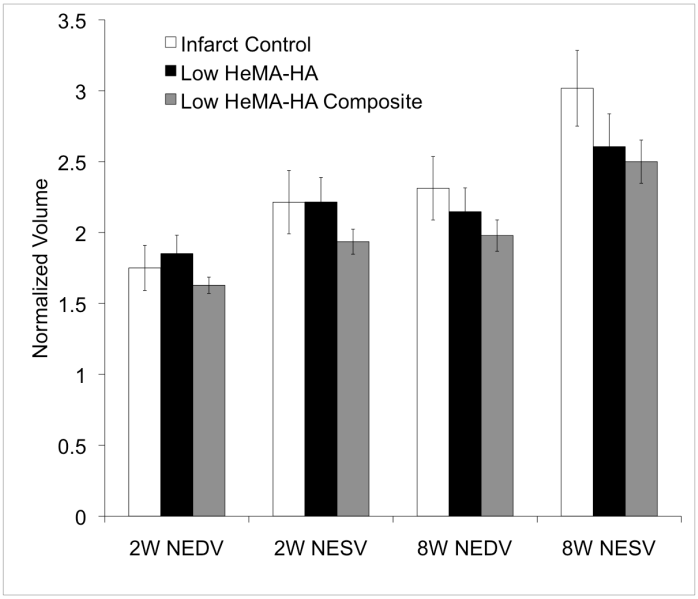

Figure 8.11 Normalized end diastolic volume (NEDV) and normalized end systolic volume (NESV) at 2 and 8 weeks (2W NEDV and NESV and 8W NEDV and NESV). Data presented as mean ± SEM.

8.3.4.3 In Vivo Evaluation in MI Model: Infarct Area

Post-MI, the area of non-viable myocardium increases as remodeling progresses; consequently, several groups have used infarct area as a metric to evaluate treatment efficacy [42]. In our case, infarct area was statistically significantly decreased by both composite and empty low HeMA-HA treatment compared to infarct controls (composite: 22.9%, empty: 22.5%, infarct control: 29.0%) (Figure 8.12); yet there was no statistically significant difference between hydrogel groups. As reported in Chapter 7, both degradable systems prevented the spreading of the infarct region, suggesting a beneficial biological influence from HA; however, further investigation is needed to confirm this hypothesis.

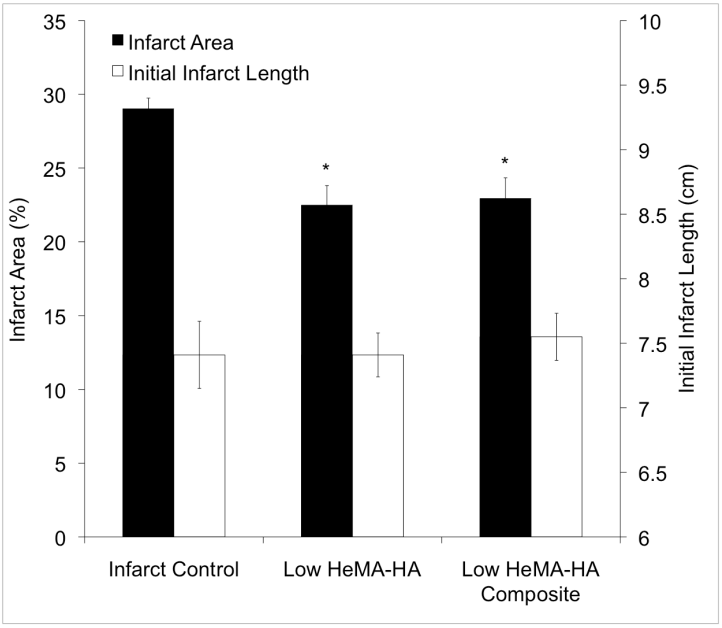

Figure 8.12 Initial infarct length and infarct area at week 8. Data presented as mean ± SEM. *p<0.05 vs. infarct control.

8.3.4.4 In Vivo Evaluation in MI Model: Immunohistochemistry

Vessel Formation: α-SMA

Another important parameter in infarct remodeling and repair is the supply of nutrients to myocardium through vessel growth in ischemic tissue [49-55]. In this study, infarct control (Figure 8.13A), empty hydrogel (Figure 8.13B) and composite (Figure 8.13C) treated infarct tissues were stained for α-SMA to identify vessels. Quantification revealed increases in all vessels over 10 μm (Figure 8.13D), with lumen (Figure 8.13E), and thick vessels (Figure 8.13F) in both composite and empty cohorts. Overall, treatment with composites tended to result in the highest vessel number, with significant increases in thicker vessels compared to infarct controls; however, there were no significant differences compared to empty hydrogels. Interestingly, composite stimulated vessel development was prominent at the apex region, agreeing with thickness data that indicated that composite therapy significantly bulked this region. Overall, vessel assessment suggests that both biological and mechanical factors play a role in attenuating LV remodeling. In particular, increased vessel density could be due to a combination of the mechanical support provided by composites and the biological effects of HA, which may affect vessel development and be the contributing stimulator in both treatments [32, 33, 56].

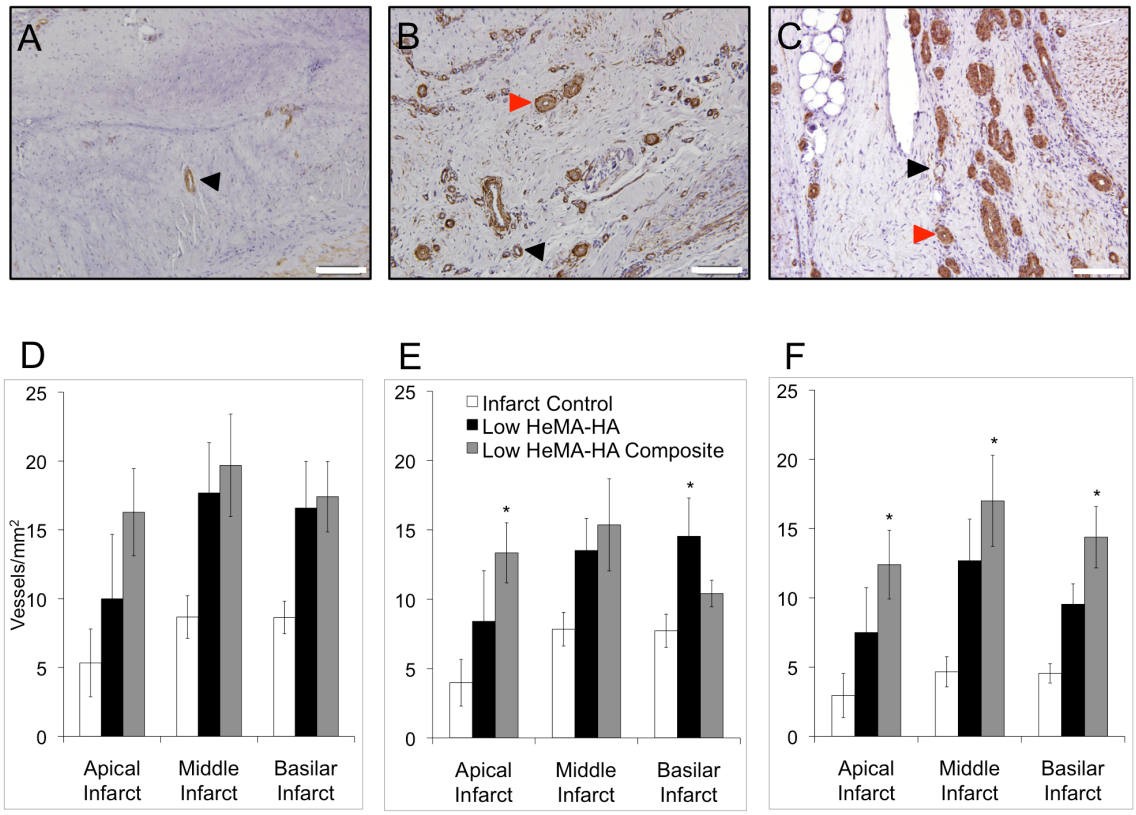

Figure 8.13 Staining for α-SMA to identify vessels in infarct controls (A) and empty (B) and composite hydrogels (C). Quantification of all vessels greater than 10 μm (D), all vessels greater than 10 μm with lumen (E), and all thick vessels greater than 10 μm (F). Scale bar= 100 μm. Data are presented as mean ± SEM. *p<0.05 vs. infarct control. Red arrows= representative thick-walled vessels. Black arrows= representative thin-walled vessels.

Inflammation: MHC Class II

MHC class II was performed to assess inflammation at 8 weeks post-MI, particularly in empty and composite hydrogel treatment to assess inflammation after hydrogel degradation. MHC class II proteins are expressed on antigen presenting cells

such as macrophages, dendritic cells, and B lymphocytes, which later present foreign digested fragments to stimulate an adaptive immune response [57, 58]. Thus, investigating MHC class II expressing cells provides a general view of the degree of inflammation induced by each group. As shown in staining in Chapter 7, both treatments resulted in more positive staining for MHC class II compared to infarct controls. While a few samples displayed positive staining around microspheres, empty and composite hydrogels generally induced a similar inflammatory response (Figure 8.14).

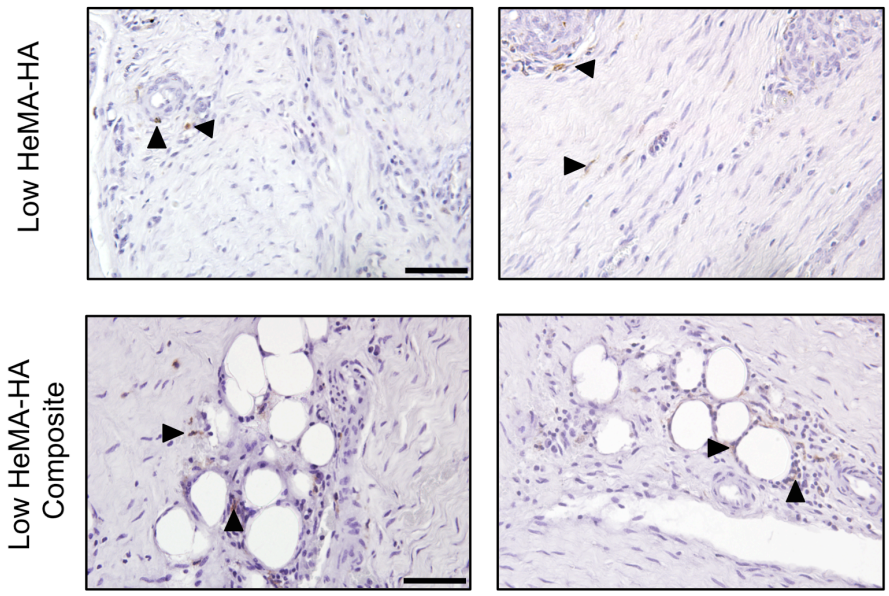

Figure 8.14 Representative images for MHC class II staining to evaluate inflammation at 8 weeks in empty hydrogel and composite treated cohorts. Scale bar= 50 μm. Black arrows= representative positive staining.

8.3.4.5 In Vivo Evaluation in MI Model: Ejection Fraction

Ejection fraction (EF) was evaluated to assess the performance of heart contraction. EF at 2 and 8 weeks decreased less relative to infarct controls in both

treatments; however, no noteworthy improvements were observed between treatments (Figure 8.15A). EF after stress testing did not improve with either treatment relative to infarct controls (Figure 8.15B). This may be because the functional benefits come over time or after myocardial wall stabilization from composite treatment. To further explore this it would be valuable to perform a functional evaluation at a time point after 8 weeks.

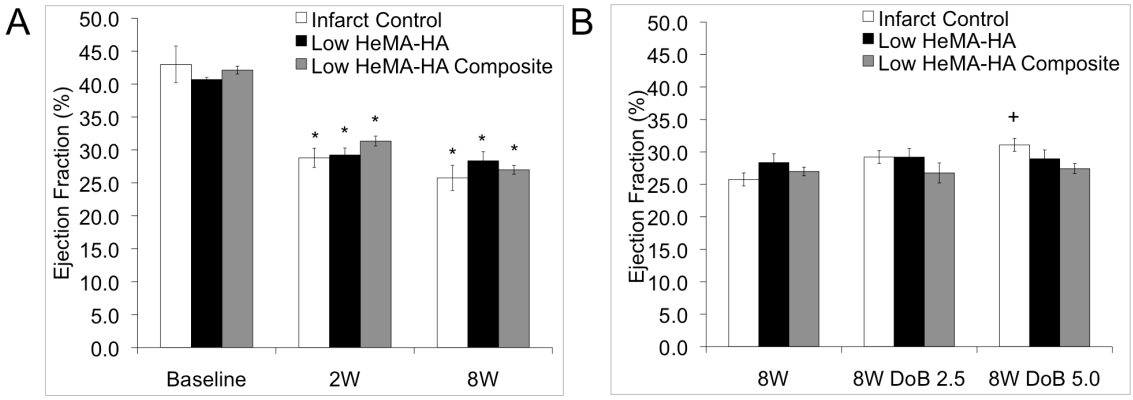

Figure 8.15 Functional assessment for MI work. Ejection fraction at 2 weeks (2W) and 8 weeks (8W) compared to baseline (A) and at 8W following dobutamine stress (2.5 and 5.0 mg kg^{-1} min^{-1}) echocardiographic testing compared to no stress (B). Data are presented as mean ± SEM. *$p<0.05$ vs. baseline, +$p<0.05$ vs. 8W no stress.

MI work agrees with Radiesse studies by Morita et al., confirming similar geometric trends [30]. While composite design enhanced low HeMA-HA treatment, it is important to place this work in perspective with the rest of the field, and note that other stable agents (e.g., high MeHA, as discussed in Chapter 7) with proven high mechanics have provided higher degrees of prolonged support in MI [34]. As previously discussed, the benefits from treatment with hydrogel/microsphere composites could potentially be improved upon by tailoring composite design (e.g., microsphere concentration and HA

crosslinking) and material properties to alter the degree of bulking and presentation of microsphere in the progression of remodeling. These modifications could lead to further material myocardial wall stability and possible functional improvements with time.

8.4 Conclusions

A composite hydrogel microsphere system was developed with tunable material properties (gelation, degradation, and mechanics) to adjust the extent and timing of collagen bulking to treat negative LV remodeling. Subcutaneous *in vivo* work demonstrated a temporal dependence of tissue response on macromer functionalization and a local dependence on microsphere concentration. Composites improved on the design of empty low HeMA-HA hydrogel (evaluated in Chapter 7) for MI repair by stimulating myocardial bulking and providing enhanced stability to attenuate maladaptive geometric changes. This investigation with tunable HeMA-HA/PLGA microsphere composites demonstrated the ability to present stimulatory bulking agents in a controlled manner after MI and showed promise for the application of stimulatory fillers as an alternative natural treatment for MI repair.

References:

[1] Carruthers J. Review of long-lasting dermal fillers. A Continueing Medical Education Program, vol. 2. Aliso, Viejo, CA: Medical Insight Inc. , 2006. p.27.

[2] Goldberg DJ. Breakthroughs in US dermal fillers for facial soft-tissue augmentation. J Cosmet Laser Ther 2009;11:240.

[3] Jones DH. Semipermanent and permanent injectable fillers. Dermatol Clin 2009;27:433.

[4] Nicolau PJ. Long-lasting and permanent fillers: biomaterial influence over host tissue response. Plast Reconstr Surg 2007;119:2271.

[5] Kusin S, Lippitz J. Skin fillers. Dis Mon 2009;55:236.

[6] Anderson JM. Biological responses to materials. Annu Rev Mater Res 2001;31:20.

[7] Anderson JM, Rodriguez A, Chang DT. Foreign body reaction to biomaterials. Semin Immunol 2008;20:86.

[8] Badylak SF, Gilbert TW. Immune response to biologic scaffold materials. Semin Immunol 2008;20:109.

[9] Madden LR, Mortisen DJ, Sussman EM, Dupras SK, Fugate JA, Cuy JL, Hauch KD, Laflamme MA, Murry CE, Ratner BD. Proangiogenic scaffolds as functional templates for cardiac tissue engineering. Proc Natl Acad Sci U S A 2010;107:15211.

[10] Mikos AG, McIntire LV, Anderson JM, Babensee JE. Host response to tissue engineered devices. Adv Drug Deliv Rev 1998;33:111.

[11] Mills CD, Kincaid K, Alt JM, Heilman MJ, Hill AM. M-1/M-2 macrophages and the Th1/Th2 paradigm. J Immunol 2000;164:6166.

[12] Stout RD, Jiang C, Matta B, Tietzel I, Watkins SK, Suttles J. Macrophages sequentially change their functional phenotype in response to changes in microenvironmental influences. J Immunol 2005;175:342.

[13] Kou PM, Babensee JE. Macrophage and dendritic cell phenotypic diversity in the context of biomaterials. J Biomed Mater Res A 2011;96:239.

[14] Mantovani A, Sica A, Sozzani S, Allavena P, Vecchi A, Locati M. The chemokine system in diverse forms of macrophage activation and polarization. Trends Immunol 2004;25:677.

[15] Martinez FO, Sica A, Mantovani A, Locati M. Macrophage activation and polarization. Front Biosci 2008;13:453.

[16] Wang W, Wang J, Dong SF, Liu CH, Italiani P, Sun SH, Xu J, Boraschi D, Ma SP, Qu D. Immunomodulatory activity of andrographolide on macrophage activation and specific antibody response. Acta Pharmacol Sin 2010;31:191.

[17] Mosser DM, Edwards JP. Exploring the full spectrum of macrophage activation. Nat Rev Immunol 2008;8:958.

[18] Badylak SF, Valentin JE, Ravindra AK, McCabe GP, Stewart-Akers AM. Macrophage phenotype as a determinant of biologic scaffold remodeling. Tissue Eng Part A 2008;14:1835.

[19] Brown BN, Valentin JE, Stewart-Akers AM, McCabe GP, Badylak SF. Macrophage phenotype and remodeling outcomes in response to biologic scaffolds with and without a cellular component. Biomaterials 2009;30:1482.

[20] Duffield JS. The inflammatory macrophage: a story of Jekyll and Hyde. Clin Sci (Lond) 2003;104:27.

[21] Mosser DM. The many faces of macrophage activation. J Leukoc Biol 2003;73:209.

[22] Song E, Ouyang N, Horbelt M, Antus B, Wang M, Exton MS. Influence of alternatively and classically activated macrophages on fibrogenic activities of human fibroblasts. Cell Immunol 2000;204:19.

[23] Kao WJ, Hubbell JA, Anderson JM. Protein-mediated macrophage adhesion and activation on biomaterials: a model for modulating cell behavior. J Mater Sci Mater Med 1999;10:601.

[24] McNally AK, Anderson JM. Complement C3 participation in monocyte adhesion to different surfaces. Proc Natl Acad Sci U S A 1994;91:10119.

[25] Wilson CJ, Clegg RE, Leavesley DI, Pearcy MJ. Mediation of biomaterial-cell interactions by adsorbed proteins: a review. Tissue Eng 2005;11:1.

[26] Brown BN, Barnes CA, Kasick RT, Michel R, Gilbert TW, Beer-Stolz D, Castner DG, Ratner BD, Badylak SF. Surface characterization of extracellular matrix scaffolds. Biomaterials 2010;31:428.

[27] Gelb H, Schumacher HR, Cuckler J, Ducheyne P, Baker DG. In vivo inflammatory response to polymethylmethacrylate particulate debris: effect of size, morphology, and surface area. J Orthop Res 1994;12:83.

[28] Ziats NP, Miller KM, Anderson JM. In vitro and in vivo interactions of cells with biomaterials. Biomaterials 1988;9:5.

[29] Lemperle G, Morhenn VB, Pestonjamasp V, Gallo RL. Migration studies and histology of injectable microspheres of different sizes in mice. Plast Reconstr Surg 2004;113:1380.

[30] Morita M, Eckert CE, Matsuzaki K, Noma M, Ryan LP, Burdick JA, Jackson BM, Gorman JH, 3rd, Sacks MS, Gorman RC. Modification of infarct material properties limits adverse ventricular remodeling. Ann Thorac Surg 2011;92:617.

[31] Ryan LP, Matsuzaki K, Noma M, Jackson BM, Eperjesi TJ, Plappert TJ, St John-Sutton MG, Gorman JH, 3rd, Gorman RC. Dermal filler injection: a novel approach for limiting infarct expansion. Ann Thorac Surg 2009;87:148.

[32] Kang SW, Cho ER, Kim BS. PLGA microspheres in hyaluronic acid gel as a potential bulking agent for urologic and dermatologic injection therapies. J Microbiol Biotechnol 2005;15:510.

[33] Toole BP. Hyaluronan in morphogenesis. Semin Cell Dev Biol 2001;12:79.

[34] Ifkovits JL, Tous E, Minakawa M, Morita M, Robb JD, Koomalsingh KJ, Gorman JH, 3rd, Gorman RC, Burdick JA. Injectable hydrogel properties influence infarct expansion and extent of postinfarction left ventricular remodeling in an ovine model. Proc Natl Acad Sci U S A 2010;107:11507.

[35] Tous E, Ifkovits JL, Koomalsingh KJ, Shuto T, Soeda T, Kondo N, Gorman JH, 3rd, Gorman RC, Burdick JA. Influence of injectable hyaluronic acid hydrogel degradation behavior on infarction-induced ventricular remodeling. Biomacromolecules 2011;12:4127.

[36] Cohen S, Yoshioka T, Lucarelli M, Hwang LH, Langer R. Controlled delivery systems for proteins based on poly(lactic/glycolic acid) microspheres. Pharm Res 1991;8:713.

[37] Newman KD, McBurney MW. Poly(D,L lactic-co-glycolic acid) microspheres as biodegradable microcarriers for pluripotent stem cells. Biomaterials 2004;25:5763.

[38] Oldham JB, Lu L, Zhu X, Porter BD, Hefferan TE, Larson DR, Currier BL, Mikos AG, Yaszemski MJ. Biological activity of rhBMP-2 released from PLGA microspheres. J Biomech Eng 2000;122:289.

[39] Shah RK, Shum HC, Rowat AC, Lee D, Agresti JJ, Utada AS, Chu L, Kim J, Fernandez A, Martinez CJ, Weitz DA. Designer emulsions using microfluidic. Materialstoday 2008;11:10.

[40] Platzer M, Ozegowski JH, Neubert RH. Quantification of hyaluronan in pharmaceutical formulations using high performance capillary electrophoresis and the modified uronic acid carbazole reaction. J Pharm Biomed Anal 1999;21:491.

[41] Kang SW, Cho ER, Jeon O, Kim BS. The effect of microsphere degradation rate on the efficacy of polymeric microspheres as bulking agents: an 18-month follow-up study. J Biomed Mater Res B Appl Biomater 2007;80:253.

[42] Zhang X, Mosser DM. Macrophage activation by endogenous danger signals. J Pathol 2008;214:161.

[43] Tous E, Purcell B, Ifkovits JL, Burdick JA. Injectable acellular hydrogels for cardiac repair. J Cardiovasc Transl Res 2011;4:528.

[44] Holmes JW, Borg TK, Covell JW. Structure and mechanics of healing myocardial infarcts. Annu Rev Biomed Eng 2005;7:223.

[45] Jackson BM, Gorman JH, 3rd, Salgo IS, Moainie SL, Plappert T, St John-Sutton M, Edmunds LH, Jr., Gorman RC. Border zone geometry increases wall stress after myocardial infarction: contrast echocardiographic assessment. Am J Physiol Heart Circ Physiol 2003;284:H475.

[46] Pfeffer MA, Braunwald E. Ventricular remodeling after myocardial infarction. Experimental observations and clinical implications. Circulation 1990;81:1161.

[47] Pfeffer MA, Pfeffer JM. Ventricular enlargement and reduced survival after myocardial infarction. Circulation 1987;75:IV93.

[48] Pilla JJ, Gorman JH, 3rd, Gorman RC. Theoretic impact of infarct compliance on left ventricular function. Ann Thorac Surg 2009;87:803.

[49] Christman KL, Fang Q, Yee MS, Johnson KR, Sievers RE, Lee RJ. Enhanced neovasculature formation in ischemic myocardium following delivery of pleiotrophin plasmid in a biopolymer. Biomaterials 2005;26:1139.

[50] Fujita M, Ishihara M, Morimoto Y, Simizu M, Saito Y, Yura H, Matsui T, Takase B, Hattori H, Kanatani Y, Kikuchi M, Maehara T. Efficacy of photocrosslinkable chitosan hydrogel containing fibroblast growth factor-2 in a rabbit model of chronic myocardial infarction. J Surg Res 2005;126:27.

[51] Hao X, Silva EA, Mansson-Broberg A, Grinnemo KH, Siddiqui AJ, Dellgren G, Wardell E, Brodin LA, Mooney DJ, Sylven C. Angiogenic effects of sequential release of VEGF-A165 and PDGF-BB with alginate hydrogels after myocardial infarction. Cardiovasc Res 2007;75:178.

[52] Iwakura A, Fujita M, Kataoka K, Tambara K, Sakakibara Y, Komeda M, Tabata Y. Intramyocardial sustained delivery of basic fibroblast growth factor improves angiogenesis and ventricular function in a rat infarct model. Heart Vessels 2003;18:93.

[53] Liu Y, Sun L, Huan Y, Zhao H, Deng J. Effects of basic fibroblast growth factor microspheres on angiogenesis in ischemic myocardium and cardiac function: analysis with dobutamine cardiovascular magnetic resonance tagging. Eur J Cardiothorac Surg 2006;30:103.

[54] Wu J, Zeng F, Huang XP, Chung JC, Konecny F, Weisel RD, Li RK. Infarct stabilization and cardiac repair with a VEGF-conjugated, injectable hydrogel. Biomaterials 2011;32:579.

[55] Yamamoto T, Suto N, Okubo T, Mikuniya A, Hanada H, Yagihashi S, Fujita M, Okumura K. Intramyocardial delivery of basic fibroblast growth factor-impregnated gelatin hydrogel microspheres enhances collateral circulation to infarcted canine myocardium. Jpn Circ J 2001;65:439.

[56] Yoon SJ, Fang YH, Lim CH, Kim BS, Son HS, Park Y, Sun K. Regeneration of ischemic heart using hyaluronic acid-based injectable hydrogel. J Biomed Mater Res B Appl Biomater 2009:91:163.

[57] Alberts B, Johnson A, Lewis J, Raff M, Roberts K, Walter P. T Cells and MHC Proteins. Molecular Biology of The Cell, vol. 4. New York: Garland Science, 2002. p.18.

[58] Mitchell RN. Innate and adaptive immunity: the immune response to foreign materials. In: Ratner BD, Hoffman AS, Schoen FJ, Lemons JE, editor. Biomaterials Science, vol. 2. San Diego: Elsevier Acadmic Press, 2004. p.304.

CHAPTER 9

Limitations, Future Directions, and Conclusions

9.1 Summary

Myocardial infarction (MI) initiates left ventricular (LV) remodeling which is associated with a series of subsequent maladaptive alterations that can compromise heart function and result in heart failure (HF). Chapter 1 described the pathological alterations that occur due to LV remodeling both on the cellular and tissue scale. Current clinical treatments for MI are often either invasive or insufficient to limit its repercussions, and while numerous cellular-based tissue engineering (TE) strategies have demonstrated a degree of efficacy in animal models, they are limited by concerns including optimal delivery for cell survival and engraftment, cell source, and "cell dosage" to impart function.

Consequently, the use of acellular materials has become a more attractive approach to treat MI; the goal is to impart stability to counteract geometric changes rather than direct regeneration of the infarct. Injectable biomaterials offer a minimally invasive alternative to physical restraints, since the material may be delivered directly to the myocardial tissue to provide mechanical support and limit LV remodeling. Chapter 3 summarized a range of natural and synthetic hydrogels that have been investigated for this purpose, and concluded that while treatment with many of these materials has attenuated LV remodeling, the mechanism behind their success is not clear. This dissertation aimed to elaborate on the work of Ifkovits et al., which addressed these

concerns by employing a tunable methacrylated hyaluronic acid (MeHA) hydrogel to limit LV remodeling [1].

The overall goal of Chapters 4 and 5 was to assess stress reduction in the dilated LV due to treatment with various MeHA hydrogel formulations formed via oxidation-reduction (redox) initiation. Hydrogels had low or high macromer modification (percent) and low or high initiator concentration (ammonium persulfate (APS, A) and N,N,N,N',N'-tetramethylethylenediamine (TEMED, T)) (e.g., low MeHA, low A/T, high MeHA, low A/T, low MeHA, high A/T, high MeHA, high A/T). An established finite element (FE) model developed by our collaborator, Dr. Jonathan Wenk, that allowed variation of the hydrogel/myocardial tissue composite mechanical properties, volume, and injection distribution was implemented. To acquire data for FE model analysis *in vitro* assessment of both hydrogel volume and hydrogel/tissue mechanical properties were performed. In Chapter 4, the volume of each MeHA hydrogel formulation in myocardial explant tissue was quantified via non-contrast magnetic resonance imaging (MRI); data indicated that volume distribution was especially dependent on initiator concentration, and to a lesser degree, on macromer modification (at lower percent modifications). Higher initiator concentration and higher macromer modification (at low initiator concentration) resulted in larger volumes.

In Chapter 5, biaxial testing was performed on each MeHA/tissue formulation; composites generally exhibited stiffer moduli in the longitudinal direction compared to control tissue (myocardium alone) and mechanics generally increased directly with macromer modification and initiator concentration. Composite anisotropy decreased compared to normal myocardium controls. These mechanical data (i.e., tissue stress/strain curves) were used to generate diastolic myocardial material parameters for each composite formulation. Mechanical and volume data were incorporated into a FE

model to simulate treatment with each formulation in a dilated LV. Comparisons between the low A/T formulations previously studied by Ifkovits et al. revealed that global and regional stresses in the fiber direction generally decreased most with the stiffer hydrogel (i.e., high MeHA), which correlated with previously reported *in vivo* geometric outcomes [1]. Relative comparisons between all MeHA formulations revealed that stress in the fiber direction was generally dependent on the mechanics and volume of the injections with the greatest stress reductions observed as both were increased.

Two approaches were explored to evaluate the temporal significance of mechanical support in attenuating LV remodeling. Chapter 6 introduced the hydrolytically degradable HA hydrogel system that would be employed for both strategies. Macromers with a range of modification extents were synthesized by coupling hydroxyethyl methacrylate (HeMA) to HA. The material properties of HeMA-HA hydrogels formed by redox initiation were altered by varying the modification percent; in particular, higher modification resulted in faster gelation, higher mechanics, and slower degradation. In Chapter 7, to assess the importance of degradation, two HeMA-HA modification percentages were selected, and by varying APS and TEMED initiator concentrations, low and high mechanics HeMA-HA hydrogels were designed with similar gelation and mechanics, but differing degradation kinetics as those of low and high mechanics MeHA hydrogels investigated by Ifkovits et al. [1]. In an *in vivo* ovine MI model, HeMA-HA hydrogel treatment (particularly the high formulation) increased the thickness of the myocardium compared to infarct control, though to a lesser extent than either MeHA treatment. Volume data provided the most interesting information; at 2 weeks, high HeMA-HA and MeHA treatment were most effective in preventing normalized end diastolic (NEDV) and normalized end systolic volume (NESV) increases; however, by 8 weeks, only high MeHA limited volume dilation. This was attributed to the

decreased mechanics (from *in vitro* data) of high HeMA-HA hydrogels at 8 weeks and suggests that the duration of mechanical support is significant in treating LV remodeling. Despite the lack of mechanical support, treatment with both HeMA-HA formulations was effective in limiting expansion of the infarct area compared to controls. This finding may have to do with the biological role of soluble HA released from degraded HeMA-HA.

Chapter 8 introduced an alternative system to assess temporal mechanical support on LV remodeling; here, the weakened infarct wall was stabilized by natural collagen produced as a result of a controlled foreign body response (FBR) to a stimulatory composite material. The same low and high HeMA-HA formulations employed in Chapter 7 were implemented as the carriers for poly(lactide-co-glycolide) (PLGA) microsphere stimuli. Macromers were mixed with microspheres (0, 10, 75, or 300 mg/mL) and hydrogel composites were formed similarly to Chapter 7 via redox initiation. Composites were characterized for mechanics, gelation, and degradation to assess microsphere influences on hydrogel material properties. An *in vivo* subcutaneous assessment was performed to determine the type of tissue response each composite elicited; a histological evaluation via Masson's Trichrome (MT) staining demonstrated that the timing and extent of collagen bulking induced by composites was dependent on macromer formulation (i.e., degree of crosslinking), which influenced the presentation of microspheres to the *in vivo* environment, and microsphere concentration, respectively. An immunohistochemical (IHC) assessment was performed only on low HeMA-HA composite explants due to minimal tissue infiltration into the slowly degrading high HeMA-HA composites. A macrophage dependent response was observed in composites with higher concentrations of microspheres; the largest general and M1 macrophage response was induced by 75 mg/mL composites and largest M2 response was induced by 300 mg/mL composites. Based on these findings, the low HeMA-HA, 75

mg/mL composite was selected for assessment in an *in vivo* ovine MI model. Composite treatment data was compared to a previously studied treatment with empty low HeMA-HA hydrogels to determine if microsphere incorporation prolonged the lack of stability imparted by empty low HeMA-HA and attenuated LV remodeling. Composite treatment increased the thickness of the apical infarct region and decreased ventricle dilation, particularly at 2 weeks when compared to empty low HeMA-HA hydrogels. These data suggest that prolonging mechanical support by natural collagen bulking enhances treatment. Infarct area was statistically significantly decreased to a similar extent by both low HeMA-HA and composite treatment and may be due in part to the bioactive role of HA.

When comparing *in vivo* outcomes (Table 9.1) between all five hydrogel treatments discussed in this dissertation, this work demonstrates that stiffer, longer lasting biomaterials are most effective in attenuating LV remodeling. Interestingly, although not as effective in limiting geometric changes, degradable HA systems (i.e., low and high HeMA-HA and low HeMA composites) are more effective in limiting infarct size, suggesting an additional biological mechanism in HA injectable materials. Overall, this work supports that material design criterion is important to consider when developing treatments to attenuate LV remodeling.

Table 9.1 Summary of *in vivo* outcomes for infarct control and all five hydrogel treatments: normalized thickness (to remote myocardium) at 8 weeks (8W) post-MI, infarct area at 8W post-MI, normalized end diastolic and end systolic volumes (to baseline volumes, NEDV and NESV) at 2W and 8W post-MI, and ejection fraction (EF) at baseline, 2W, and 8W and after dobutamine (DoB, 2.5 and 5.0 mg kg^{-1} min^{-1}) stress testing post-MI. Data are presented as mean ± SEM.

	Infarct Control	Low HeMA-HA	Low HeMA-HA Composite	Low MeHA	High HeMA-HA	High MeHA
Normalized Thickness						
Apical Infarct	0.18 ± 0.02	0.30 ± 0.02	0.40 ± 0.03	0.66 ± 0.09	0.38 ± 0.04	0.63 ± 0.06
Basilar Infarct	0.38 ± 0.03	0.51 ± 0.3	0.51 ± 0.07	0.70 ± 0.06	0.57 ± 0.04	0.64 ± 0.02
Borderzone	0.92 ± 0.03	0.85 ± 0.06	0.89 ± 0.02	0.92 ± 0.03	0.92 ± 0.04	0.95 ± 0.04
Infarct Area						
Initial Length (cm)	7.23 ± 0.26	7.41 ± 0.17	7.55 ± 0.18	7.34 ± 0.10	7.42 ± 0.21	7.37 ± 0.19
Infarct Area (%)	29.0 ± 0.7	22.5 ± 1.3	22.9 ± 1.4	26.4 ± 1.66	22.0 ± 1.48	23.9 ± 0.94
Normalized End Diastolic and End Systolic Volume						
2W NEDV	1.75 ± 0.16	1.85 ± 0.13	1.63 ± 0.06	1.81 ± 0.24	1.61 ± 0.11	1.62 ± 0.11
2W NESV	2.21 ± 0.22	2.22 ± 0.17	1.94 ± 0.09	2.22 ± 0.39	1.96 ± 0.15	1.89 ± 0.12
8W NEDV	2.31 ± 0.22	2.15 ± 0.17	1.98 ± 0.11	2.09 ± 0.24	1.98 ± 0.12	1.70 ± 0.14
8W NESV	3.02 ± 0.27	2.61 ± 0.23	2.50 ± 0.15	2.54 ± 0.37	2.46 ± 0.20	1.98 ± 0.16
Ejection Fraction						
Baseline EF (%)	42.99 ± 2.78	40.68 ± 0.32	42.13 ± 0.60	41.21 ± 0.93	41.85 ± 0.69	39.98 ± 1.12
2W EF (%)	28.80 ± 1.46	29.23 ± 1.07	31.35 ± 0.75	29.18 ± 3.36	29.47 ± 1.36	29.41 ± 0.03
8W EF (%)	25.76 ± 1.91	28.35 ± 1.38	26.99 ± 0.664	29.60 ± 2.67	28.61 ± 2.07	29.66 ± 0.96
8W EF DoB 2.5 (%)	29.21 ± 1.17	29.20 ± 1.31	26.76 ± 1.55	31.20 ± 2.76	33.75 ± 1.73	35.33 ± 2.37
8W EF DoB 5.0 (%)	31.08 ± 1.05	28.94 ± 1.36	27.42 ± 0.76	30.26 ± 4.30	34.04 ± 2.73	35.95 ± 2.41

9.2 Limitations and Future Directions

9.2.1 Specific Aim 1

To theoretically examine different formulations of MeHA hydrogels with various mechanics and volume distributions to determine their influence on stress reduction in a FE model of the dilated LV.

9.2.1.1 Limitations

Limitations in *In Vitro* Data Acquisition

A general limitation to the explant work performed in this dissertation was that explant myocardial tissue used was 1) from normal myocardium (not infarct) and 2) thawed from frozen explants. Studies have shown that infarcted tissue has different mechanical properties than normal myocardium [2-5]; thus, the tissue used could influence FE input values. Additionally, most biaxial testing on myocardium uses fresh tissue [4, 6, 7]. While to our knowledge a direct comparison between the mechanical properties of thawed and fresh myocardium has not been performed, comparisons with other tissues have shown that freezing and thawing may alter mechanical properties [8, 9]. Ideally, to circumvent these limitations, biaxial testing should be performed by injecting MeHA formulations into an infarcted heart *in vivo* and later sacrificing the animal and performing biaxial testing on the tissue

In this work, samples were only subjected to equibiaxial testing; typically, biaxial testing is performed at numerous ratios to generate several sets of data to fit the constitutive equation to generate a unique set of parameters. While this would have been ideal, the diastole passive mechanical parameters reported here for control myocardium are similar to parameters that have been previously reported for large animals [10-12]. Another limitation concerning biaxial testing was that grip strains did not completely match with tissue strains, possibly due to the heterogeneous nature of injection throughout the tissue and to the transmurally dependent changes in fiber orientation.

Limitations in Finite Element Model

As discussed in the previous section, normal myocardial explant tissue rather than infarcted tissue was used in this work. Consequently, to maintain consistency with the acquired material parameters it was assumed that contraction at the injection sites was similar to normal myocardium and active systole parameters were selected to simulate these properties. Another limitation in the FE model was its inability to replicate the exact geometry of injections; thus, an ellipse was selected as the best approximation to represent all formulations (depending on their volume).

Finally, the FE model itself was limited in that it could not accommodate 20 injections at the calculated average volumes for most groups (i.e., high MeHA, low A/T, low MeHA, high A/T, high MeHA, high A/T). As discussed in Section 5.2.3.2, volumes were decreased systematically for initial FE analysis to make relative comparisons between groups. Despite these adjustments, this data may not accurately reflect specific stress reductions from modeling with the average calculated volumes. Related to the aforementioned limitation, the distribution of injections was modeled as a 5 by 4 grid, and, while a good approximation, is not completely representative of the pattern employed in *in vivo* studies, which follows more of a tapering of injections as they approach the apex of the heart [1].

9.2.1.2 Future Directions

To better understand stress reduction due to hydrogel treatment, the FE model should be adjusted to incorporate larger volumes and an injection distribution that more closely matches previous *in vivo* work [1]. Simulations should be performed using the calculated average injection volumes to achieve stress data that corresponds to the

exact formulations studied. These stress data would provide valuable insight on future hydrogel formulations to implement and test *in vivo.*

Future work should also evaluate the influence of hydrogel volume, in hydrogels with similar mechanics, on stress reductions. This would be accomplished by varying hydrogel properties by altering initiator concentration, macromer percent modification, and weight percent to design different hydrogel formulations with similar volumes and different mechanics. Similar *in vitro* characterization (i.e., MRI imaging and biaxial testing) would be performed to acquire hydrogel volume and mechanical data for FE model simulation to determine stress reductions.

Overall, in addition to stress, global pump function should also be theoretically assessed. Others have demonstrated (via theoretical modeling) that reductions in stress do not necessarily translate to improvements in global functionality (e.g., stroke volume/end diastolic pressure relationship) [13]; thus, the influence of material treatment on these functional metrics should be further assessed (pending the appropriate model).

9.2.2 Specific Aim 2

To synthesize and characterize hydrolytically degradable HA hydrogels and select formulations to assess the temporal role of mechanical support in attenuating LV remodeling in an *in viv*o ovine MI model.

9.2.2.1 Limitations

Limitations in *In Vitro* Characterization

In this section, the distribution of HeMA-HA hydrogels was normalized to MeHA hydrogels by altering APS and TEMED concentrations to achieve a similar gel onset time (assessed via rheometry) as MeHA hydrogels. While gel onset has been assessed

this way in previous reports [1], MRI studies from Chapter 4 demonstrated that despite exhibiting similar gel onset times, hydrogels of differing methacrylation may not distribute similarly. This was particularly seen in formulations with low modification and low initiator concentrations; however, gel onset trends seemed to correlate well with MRI data when comparing between hydrogels with higher macromer modifications and initiator combinations. MRI imaging may be a better assessment of material distribution in tissue. Yet, the work in this Aim was performed before MRI data was used for volume calculations.

Limitations in *In Vivo* MI Model Assessment

The extent of remodeling in this study was evaluated by injecting the hydrogel treatment into the infarct region 30 minutes post-MI in an *in vivo* ovine MI model. While this model has been used in several previous studies to evaluate the efficacy of material treatment in limiting LV remodeling, this time-frame is not necessarily clinically relevant [1, 14-16]. Material delivery to the infarct region should be evaluated at other time points. Furthermore, most *in vivo* metrics were assessed utilizing three-dimensional (3-D) echocardiography, which was unable to provide data on resulting myocardial strain in infarct control and hydrogel treatment cohorts; hence, employment of other tools (i.e., imaging modalities) should be considered to provide more information with regard to tissue properties.

Studies have demonstrated that treatment with HA can increase angiogenesis, and in a MI model it has shown regenerative capabilities [17, 18]. However, in this work, the delivery of HA is coupled to mechanical and degradation behavior. In order to completely understand the role of HA in this study, biological and mechanical influences would need to be decoupled; this could be done by assessing treatment with a non-

bioactive hydrogel with tunable mechanics and degradation that matched HeMA-HA formulations.

9.2.2.2 Future Directions

To determine the optimal duration of mechanical support that is required to limit LV dilation, future investigation should entail designing HeMA-HA hydrogels with higher mechanics and longer degradation times. This may be accomplished by varying macromer modification, macromer weight percent, and initiator concentrations. In addition to improving material design, future studies should be performed in an *in vivo* model where geometric and functional outcomes can be measured via MRI instead of echocardiography. This type of assessment has been performed in the past and would provide more informative outcomes for this work including strain data that could be directly input into a FE model to determine stresses without the need for additional biaxial testing [19]. In addition to being a more efficient model for data acquisition at any given time point, MRI assessment allows for strain data acquisition throughout the study. Thus, temporal stress profiles could be acquired and directly correlated to geometric and functional improvements using this type of method.

9.2.3 Specific Aim 3

To design various hydrogel/microsphere composites to evaluate their influence on collagen production and macrophage response in a subcutaneous model, and to identify an optimal composite formulation to attenuate LV remodeling in an *in vivo* ovine MI model.

9.2.3.1 Limitations

Limitations in *In Vitro* Characterization

The same limitations concerning the correlation of gel onset and gel distribution are relevant to this Aim and should be addressed as discussed in Aim 2.

Limitations in *In Vivo* Subcutaneous Model Assessment

While subcutaneous results indicated a clear dependence of bulking on microsphere concentration and macromer modification, the macrophage phenotypic response was only investigated at a single time point. Specifically, subcutaneous work was only assessed for 4 weeks, because hydrogels degraded *in vitro* by 3 weeks. Longer implantation could provide more information on general composite degradation and on macrophage phenotype with time.

Limitations in *In Vivo* MI Model Assessment

As in Aim 2, the efficacy of the selected composite to attenuate LV remodeling was assessed in an *in vivo* ovine MI model via 3-D echocardiography. Thus, the same concerns regarding injection 30 minutes post-MI and limitations with the employed imaging modality remain for this Aim. IHC for specific macrophage phenotypes was not performed in this study because, to our knowledge, anti-M1 macrophage antibodies for sheep are not available. To better characterize macrophage phenotypic responses to composite treatment in MI, an alternative animal model could be explored. Similar limitations to Aim 2 regarding the biological role of HA also apply here.

9.2.3.2 Future Directions

Future work should entail performing studies to better understand the FBR induced by composites and to further increase the induced collagen bulking to enhance stability following MI. The former could be accomplished by prolonging the *in vivo* subcutaneous studies to at least 8 weeks; tissue responses could then be directly compared to results observed at 8 weeks in the employed MI model. MT staining would be performed to assess collagen infiltration and IHC for general, M1 and M2 macrophages should be performed to gain insight on the macrophage-phenotypic-specific response.

To further understand the FBR and determine if the observed responses in these studies are PLGA-dependent, alternative microsphere stimuli (i.e., of similar size and concentration but synthesized from a different polymer) could be incorporated into HeMA-HA hydrogel carriers. Examples of alternative microsphere candidates include less degradable poly-lactic acid or polymethylmethacrylate microspheres, which have already been extensively used in dermal fillers [20]. Induced tissue responses could be assessed in a subcutaneous *in vivo* model and explants analyzed via MT and IHC (e.g., general, M1 and M2 macrophage) staining.

To further enhance bulking, alternative concentrations of PLGA microspheres within HeMA-HA hydrogels could be evaluated. A concentration of 300 mg/mL was originally selected as the extreme case for this work to match the concentration of calcium hydroxyapatite microspheres that comprise Radiesse (the dermal filler employed by Morita et al. to treat LV remodeling [14]). A microsphere concentration between 75 and 300 mg/mL was not assessed in this work; it is possible that an intermediate composite may provide optimal bulking both subcutaneously and after MI. Tissue responses could be initially assessed in an *in vivo* subcutaneous model and evaluated

via MT and IHC staining on explants. Following validation of bulking in the subcutaneous model, the composite treatment could be evaluated in an *in vivo* ovine MI model to assess its ability to attenuate LV remodeling with evaluation metrics including thickness, chamber volume, and infarct area.

In addition to adjusting the type and concentration of particle stimuli, stimulatory proteins and/or cytokines including TGF-β, Il-10, and Il-4 could be encapsulated within microspheres to induce the desired M2 inflammatory response. ELISA would be performed to optimize factor release from microspheres for *in vivo* application. Subsequently, composites with stimulatory factors could be implanted subcutaneously to examine their induced biological response by performing MT staining and IHC for general, M1 and M2 macrophages.

9.3 Conclusions

Geometric alterations in LV remodeling are thought to be the main contributor in the onset of HF, but are not adequately addressed by current therapies. The goal of this dissertation was to understand the influence of material properties of acellular injectable biomaterials as a minimally invasive strategy to stabilize the myocardial wall and limit LV remodeling. This was accomplished by employing tunable HA-based hydrogels that were formed via redox initiation. Overall, in addition to the importance of higher initial mechanical support for stress reduction in the dilated LV, the data presented in this dissertation indicates that temporal considerations are critically important in material design and that longer mechanical support results in the largest benefits towards attenuating LV remodeling. The findings of this dissertation represent advancements in material design and will be beneficial in developing more effective injectable material treatments to better target LV remodeling and prevent the onset of HF.

References:

[1] Ifkovits JL, Tous E, Minakawa M, Morita M, Robb JD, Koomalsingh KJ, Gorman JH, 3rd, Gorman RC, Burdick JA. Injectable hydrogel properties influence infarct expansion and extent of postinfarction left ventricular remodeling in an ovine model. Proc Natl Acad Sci U S A 2010;107:11507.

[2] Fomovsky GM, Holmes JW. Evolution of scar structure, mechanics, and ventricular function after myocardial infarction in the rat. Am J Physiol Heart Circ Physiol 2010;298:H221.

[3] Fomovsky GM, Macadangdang JR, Ailawadi G, Holmes JW. Model-based design of mechanical therapies for myocardial infarction. J Cardiovasc Transl Res 2011;4:82.

[4] Gupta KB, Ratcliffe MB, Fallert MA, Edmunds LH, Jr., Bogen DK. Changes in passive mechanical stiffness of myocardial tissue with aneurysm formation. Circulation 1994;89:2315.

[5] Holmes JW, Nunez JA, Covell JW. Functional implications of myocardial scar structure. Am J Physiol 1997;272:H2123.

[6] Sacks M. Biaxial mechanical evaluation of planar and biological materials. J Elast 2001;61:199.

[7] Demer LL, Yin FC. Passive biaxial mechanical properties of isolated canine myocardium. J Physiol 1983;339:615.

[8] Chow MJ, Zhang Y. Changes in the mechanical and biochemical properties of aortic tissue due to cold storage. J Surg Res 2011;171:434.

[9] Santago AC. Characterizing the biomechanical response of the liver. Biomedical Engineering, Master of Science. Blacksburg: Virginia Polytechnic Institute and State University, 2010. p.62.

[10] Guccione JM, Costa KD, McCulloch AD. Finite element stress analysis of left ventricular mechanics in the beating dog heart. J Biomech 1995;28:1167.

[11] Jhun CS, Wenk JF, Zhang Z, Wall ST, Sun K, Sabbah HN, Ratcliffe MB, Guccione JM. Effect of adjustable passive constraint on the failing left ventricle: a finite-element model study. Ann Thorac Surg 2010;89:132.

[12] Guccione JM, Moonly SM, Moustakidis P, Costa KD, Moulton MJ, Ratcliffe MB, Pasque MK. Mechanism underlying mechanical dysfunction in the border zone of left ventricular aneurysm: a finite element model study. Ann Thorac Surg 2001;71:654.

[13] Wall ST, Walker JC, Healy KE, Ratcliffe MB, Guccione JM. Theoretical impact of the injection of material into the myocardium: a finite element model simulation. Circulation 2006;114:2627.

[14] Morita M, Eckert CE, Matsuzaki K, Noma M, Ryan LP, Burdick JA, Jackson BM, Gorman JH, 3rd, Sacks MS, Gorman RC. Modification of infarct material properties limits adverse ventricular remodeling. Ann Thorac Surg 2011;92:617.

[15] Jneid H, Fonarow GC, Cannon CP, Palacios IF, Kilic T, Moukarbel GV, Maree AO, LaBresh KA, Liang L, Newby LK, Fletcher G, Wexler L, Peterson E. Impact of time of presentation on the care and outcomes of acute myocardial infarction. Circulation 2008;117:2502.

[16] Miura T, Miki T. Limitation of myocardial infarct size in the clinical setting: current status and challenges in translating animal experiments into clinical therapy. Basic Res Cardiol 2008;103:501.

[17] Kang SW, Cho ER, Kim BS. PLGA microspheres in hyaluronic acid gel as a potential bulking agent for urologic and dermatologic injection therapies. J Microbiol Biotechnol 2005;15:510.

[18] Yoon SJ, Fang YH, Lim CH, Kim BS, Son HS, Park Y, Sun K. Regeneration of ischemic heart using hyaluronic acid-based injectable hydrogel. J Biomed Mater Res B Appl Biomater 2009;91:163.

[19] Witschey WR, Pilla JJ, Ferrari G, Koomalsingh K, Haris M, Hinmon R, Zsido G, Gorman JH, 3rd, Gorman RC, Reddy R. Rotating frame spin lattice relaxation in a swine model of chronic, left ventricular myocardial infarction. Magn Reson Med 2010;64:1453.

[20] Carruthers J. Review of long-lasting dermal fillers. A Continueing Medical Education Program, vol. 2. Aliso, Viejo, CA: Medical Insight Inc., 2006. p.27.